Wood/Polymeric Isocyante Resin Interactions: Species dependence

by

Sudipto Das

A dissertation submitted to the Faculty of
Virginia Polytechnic Institute and State University
in partial fulfillment of the requirements for the degree of

Doctor of Philosophy

in

Macromolecular Science and Engineering

Approved by

Dr. Charles E. Frazier
Chairman

Dr. Wolfgang G. Glasser

Dr. Garth L. Wilkes

Dr. Audrey Zink-Sharp

Dr. Maren Roman

July 18, 2005
Blacksburg, Virginia

Keywords: Isocyanate resin, Wood species, Solid-state nuclear magnetic resonance, Differential scanning calorimetry, Dynamic mechanical analysis, Creep, Thermogravimetric analysis

WOOD/POLYMERIC ISOCYANTE RESIN INTERACTIONS: SPECIES DEPENDENCE

Sudipto Das

ABSTRACT

The performance of polymeric diphenylmethane diisocyanate (PMDI) resin is known to be highly dependent on the wood species. This species dependence may be due to differences in: cure chemistry, interphase morphology, or both of these factors. This study addresses aspects of the cure chemistry and interphase morphology of wood/PMDI bondlines; specifically these effects are compared using two woods: yellow-poplar and southern pine.

In this study, the cure chemistry of wood-PMDI system was analyzed with solid state NMR (SSNMR) using wood samples cured with doubly labeled (^{15}N,^{13}C) PMDI resin. The kinetics of PMDI cure in the presence of wood was analyzed with differential scanning calorimetry. Thermogravimetric analysis was used to analyze the effect of resin impregnation on the degradation patterns of wood. The wood-PMDI bond morphology was probed with dynamic and static (creep) mechanical analyses in both dry and plasticized conditions. The effect of resin on wood polymer relaxations was quantitatively analyzed by both the time-temperature superposition principle and the Kohlrausch-Williams-Watts equation.

The presence of a small but statistically significant species effect was observed on both the cure chemistry and bond morphology of wood-PMDI system at low cure temperatures. The cure of PMDI resin was found to be significantly faster in pine relative to corresponding poplar samples. Resin impregnation showed a significant species

dependent effect on the wood mechanical properties; the resinated pine samples showed increase in compliance while the corresponding poplar samples became stiffer.

The in situ lignin relaxation was studied with both dynamic and static modes, using plasticized wood samples. Results showed that the lignin relaxation was slightly affected by resin impregnation in both woods, but the effect was relatively larger in pine. Static experiments of dry wood samples showed a significant reduction in the interchain interactions of wood polymers in pine samples, exclusively. Investigation of plasticized pine samples, which focuses on the in situ lignin relaxations, showed only minor changes with resin impregnation. This led us to hypothesize that the large changes observed in dry samples, were due to the in situ amorphous polysaccharides. The wood-PMDI interactions were significantly reduced upon acetylation of wood. This study also discusses three new and highly sensitive methods for the analysis of wood-resin interactions.

Acknowledgements

At the end of my work, I would like to take the opportunity to thank the people, without whose assistance this work would not have seen the light of day. This list is not exhaustive and I would beg my forgiveness to those, whose names have been left out, unintentionally.

First and foremost I would like to thank my advisor Dr. C.E. Frazier. He played one of the most important roles in completing this project. His patience (which I'm afraid I have severely tested several time over the course of the last few months), guidance and support have been invaluable. The numerous discussion we had made it possible to for me to grow and think scientifically. I hope I learned some of his work ethic and attention to details and accuracy. I feel honored and lucky for the opportunity to work for him,

I would also like to thank my committee members: Dr. Wolfgang G. Glasser. Dr. Garth L. Wilkes, Dr. Audrey Zink-Sharp and Dr. Maren Roman; for taking the time from their busy schedules to serve on my committee. Their suggestions and help during my research and their probing questions during my defense helped me a lot.

I would like to thank Tom Glass, Analytical Chemistry Supervisor in the Chemistry department for his immense help with my solid-state NMR work. Without his constant help and guidance, the solid-state work would not have been completed in time. I would also like to thank David Jones, Wood Shop manager in the department of Wood Science and Forest Products, for making the huge volume of wood samples for the dynamic mechanical analysis.

I would also like to acknowledge the people who the made few years in Blacksburg enjoyable: Brian Einsla, Ann Fornoff and Debayan Sen, My heartfelt thanks to all the past and present members of the Wood Adhesion (the best !!) Group (Dr. Jun Zheng, Dr. Nanjin Sun, Dr. Christian Heinemenn, Darren Ridlinger, Mike Malmberg, Dr. Nichole Brown and Dr. Marie-Pierre Laborie). I would also like to thank Dr. Scott Renecker for all his help during my research at Virginia Tech. Last, but not the least, Francisco Lopez-Suevos (Fuco), for the invigorating discussion and all the beers, wines and Spanish foods.

I would also like to thanks my parents, Chanchal Das aand Kabita Das, for their love, support and blessings, which made it possible for me to come to this country and pursue higher studies. I am eternally grateful to them and nothing I do could repay my debt towards them.

Finally, this work would not have been completed without the loving support and immense sacrifices from my wife, Rituparna Paul. This work is as much hers as mine. I do thank you from the bottom of my heart for being with me in the hardest times of time life.

Dedicated to my parents:

Chanchal and Kabita Das

Table of Contents

List of Figures

List of Tables

2. Background and Research Proposal

Polymeric methylene-bis(phenyl isocyanate) (PMDI) resin is a mixture of methylenediphenyldiisocyanate (MDI) monomer (~50%) and oligomeric polyisocyanates (degree of polymerization ~ 1 to 12) [1]. The majority of the monomer fraction is the 4,4'-MDI isomer (~90%), with 5-10% of the 2,4'-isomer and traces of the 2,2'-isomer [2]. The average functionality of commercial PMDI is ~2.8, which corresponds to an isocyanate content of ~30 - 32%.

PMDI is used primarily in the polyurethane industry for the production of foams, fibers, coatings and adhesives [3, 4], and its application in the wood products industry constitutes a small fraction of the total PMDI market. But its use in the wood products industry has increased tremendously in recent years. In 1992, PMDI constituted 25% of all resins used in the oriented strandboard (OSB) industry [4]. 160 million pounds of PMDI was used in the wood industry in 1997[3]. Presently, it is one of the major adhesives used in the manufacture of particulate-based wood composites such as OSB and laminated strand lumber. This is due to numerous advantages that PMDI provides over other adhesives, for example: faster press times, no formaldehyde emission, higher moisture tolerance and superior mechanical properties at low resin loading [5-9]. Studies [1] have also shown that PMDI cures faster than phenol-formaldehyde (PF) resins, which are the principle competition to PMDI. Panels bonded with PMDI resin also exhibit higher strength and stiffness, higher wet and dry internal bond strength and lower thickness swell [6, 7]. The cure chemistry of PMDI in wood is different from other conventional wood adhesives in that it reacts with wood moisture to form a tough crosslinked polyurea network. Liquid PMDI is also water insoluble; this and the fact that it reacts with water

makes PMDI highly moisture tolerant (resistant to the effects of steam during panel hotpressing). It has been reported that PMDI enables wood composite hotpressing at wood moisture contents as high as 18% [10, 11]. In contrast, PF resins require much lower wood moisture contents, on the order of 4-8%. These advantages could enable lower energy consumption and VOC emissions during wood drying.

OSB is a layered particle panel comprised of strand-type flakes (2”-4” long, 0.50”-2.0” wide and 0.01”-0.025” thick) [12] aligned in perpendicular directions in successive layers to strengthen, stiffen, and improve the dimensional stability of the panel. Each board is made up of an odd number of layers (3 or 5 typically) which are bound together with a thermosetting adhesive such as PF and/or PMDI in most cases. In OSB manufacture, the adhesive is sprayed on the flakes, which are then arranged into a mat and pressed to form the final board. The wood used in OSB manufacture is commonly obtained from local forests, which may often be a mixture of both hardwoods and softwoods. In the southern United States, OSB is commonly produced from southern yellow pine (*Pinus sp.*) and yellow-poplar (*Liriodendron tulipifera*), among other woods. OSB manufacturers generally have little or no control over the composition of the wood species mixture, which changes daily due to the supply. The variation of this wood species mixture is associated with significant variations in OSB properties. This OSB property variation could be caused by a number of complex interactions that arise during panel hotpressing. It is believed that one important factor is the adhesive performance which differs as a function of wood species.

The above mentioned species dependent performance of PMDI has been observed in previous studies [10, 13-15]. Phanopolous *et al.* [13] studied the effect using static contact

angle and resin penetration measurements on Scots pine and aspen woods. They correlated their results to thickness swell (TS) and internal bond strength (IB) measurements on OSB boards bonded with 6% resin. Their results showed that the resin wetting and penetration was greater in aspen, which was correlated with slightly better IB and TS results. Boa *et al*. [14] studied the PMDI performance differences observed between southern yellow pine and aspen; they used solid-state NMR to reveal moisture and wood species effects on PMDI cure. Johns *et al.* [10] also observed the species-dependent performance of PMDI, by performing IB measurements of flakeboards made from five different wood species (Douglas-fir, white fir, red oak, hickory and loblolly pine).

Recently, Malmberg studied the wood species related performance of PMDI with fracture testing in Mode-I cleavage [16]. Two different wood species were tested: southern yellow pine (SYP) and yellow-poplar (YP).

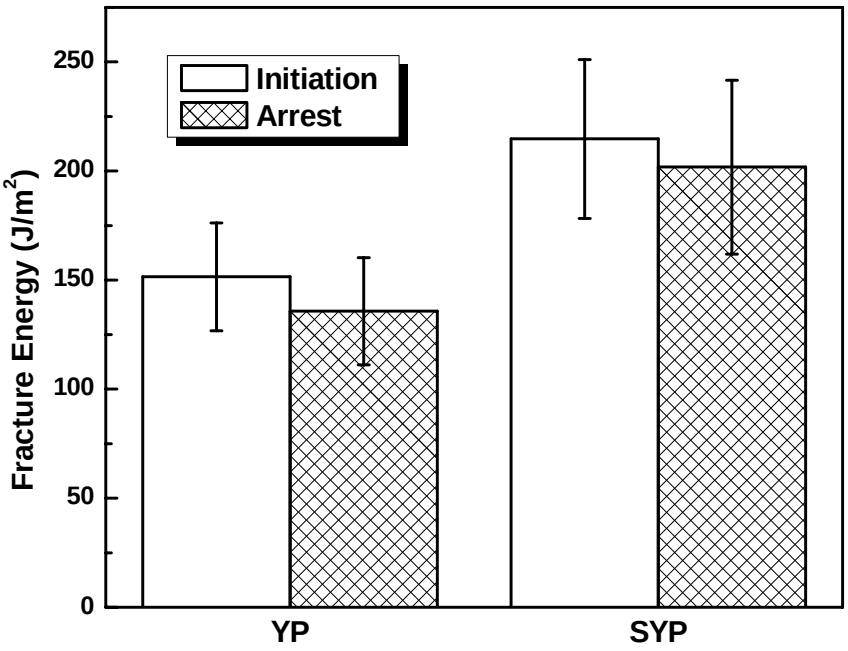

Figure 2.1. Effect of wood species on the mode I fracture energy of wood bonded with PMDI resin. (Adapted from[16])

The results (Figure 2.1) demonstrated that pine/PMDI bonds were tougher than poplar/PMDI bonds. These fracture results were obtained using a corrected compliance method from standard beam theory [17], which factors the stiffness of the individual specimens into the calculation of the fracture energy [18]. Consequently, the results obtained were independent of bulk wood stiffness or density.

This species-dependent performance of PMDI resin may be due to differences in

- Heat and mass transfer differences arising from morphological differences
- Cure-chemistry
- Bond-morphology
- Or a combination of the above two factors.

This study addresses aspects of the cure chemistry and interphase morphology of wood/PMDI bondlines; specifically these effects are compared using two woods: yellow-poplar and southern pine. The cure chemistry has been evaluated using solid-state NMR of wood samples cured with magnetically labeled PMDI resin. The wood species dependence of the cure kinetics has been studied with differential scanning calorimetry. Aspects of interphase morphology have been analyzed with thermomechanical analysis, in dynamic and static modes. Finally, the species dependence of PMDI has also been studied using high-resolution thermogravimetry.

In the following sections, the different characterization techniques used in this study will be discussed, with special emphasis on the use of the respective techniques to characterize wood and/or wood-resin systems.

References

1. Frink, J. W.; Sachs, H. I., Isocyanate Binders for Wood Composite Boards. In *Urethane Chemistry and Applications*, 1981; p 285.
2. Twitchett, H. J. *Chem. Soc. Rev, London Chem. Soc.* **1974,** 3, (2), 209.
3. McCoy, M. *Chemical & Engineering News* **1998,** 37, 76.
4. Galbraith, C. J.; Newman, W. H. In *Reaction Mechanisms and Effects with MDI Isocyanate Binders for Wood Composites*, Pacific Rim Bio-based Composites Symposium, Rotorua, New Zealand, 1992; Rotorua, New Zealand, 1992; p 130.
5. Hawke, R. N.; Sun, B. C. H.; Gale, M. R. *Forest Products Journal* **1992,** 42, (11/12), 61-68.
6. Hawke, R. N.; Sun, B. C. H.; Gale, M. R. *Forest Products Journal* **1993,** 43, (1), 15-20.
7. Hawke, R. N.; Sun, B. C. H.; Gale, M. R. *Forest Products Journal* **1994,** 44, (3), 34-40.
8. Hawke, R. N.; Sun, B. C. H.; Gale, M. R. *Forest Products Journal* **1994,** 44, (4), 53-58.
9. Johns, W. E., In *Wood Adhesives Chemistry and Technology*, Marcel Dekker Inc.: New York, 1989; Vol. 2, pp 75-96.
10. Johns, W. E.; Maloney, T. M.; Saunders, J. B.; Huffaker, E. M.; Lentz, M. T. In *The effect of Species and Moisture Content on the bonding Efficiency of Polymeric MDI Isocyanate*, 16th W.S.U. Particleboard Symposium, 1982; 1982; p 71.
11. Owens, N. L.; Banks, W. B.; West, H. *Journal of Molec. Struc.* **1988,** 175, 389-394.
12. Marra, A. A., *Technology of Wood Bonding: Principles in Practice*. Van Nostrand Reinhold: New York, 1992.
13. Phanopoulos, C.; Bosch, C. V. D.; Ecker, J. V. In *Penetration of isocyanate (MDI) into wood and how this influences wood composite: some initial findings.*
14. Bao, S.; Daunch, W. A.; Sun, Y.; Rinaldi, P. L.; Marcinko, J. J.; Phanopoulos, C. *Journal of Adhesion* **1999,** 71, 377-394.
15. Ball, G. W. In *New opportunities in manufacturing Conventional Particleboard using Isocyanate Binders*, 15th W.S.U. Symp. Particleboard, 1981; 1981; p 265.
16. Malmberg, M. *Species dependence of PMDI/Wood Adhesion*. MS Thesis, 2000 Virginia Polytechnic Institute and State University, Blacksburg, VA.
17. Blackman, B.; Dear, J. P.; Kinloch, J.; Osiyemi, S. *Journal of Material Science Letters* **1991,** 10, 253.
18. Rakestraw, M. D.; Taylor, M. W.; Dillard, D. A.; Chang, T. *Journal of Adhesion* **1995,** 55, 123.

3.1. PMDI Synthesis

Since its introduction into the wood products industry in the late 1960's [1], Polymeric Diphenylmethane Diisocyanate (PMDI) has become one of the most important wood binders, primarily for the bonding of oriented strand boards (OSB) and similar particulate wood-based composites. In 2001, PMDI accounted for ~20% of the total resin solids used in the OSB manufacturing industry in North America [2]. It offers several advantages over other available binders including:

- Cure at high moisture conditions.
- Superior mechanical performance.
- Weather durability.
- No formaldehyde emission.

PMDI resins are expensive relative to the other commercially available wood adhesives. But, faster production rates that can be achieved by using lower resin loading and lower press temperatures compensate for the high resin cost. There are some significant disadvantages associated with PMDI resins:

- Adhesion of the panels to the cauls or press platens necessitates the use of release agents.
- The acute toxicity of isocyanates.
- Requires special storage conditions in order to avoid premature cure of the resin with ambient moisture.

The PMDI that is used in the wood composite industry is a mixture of methylenebis(phenyl isocyanate) (MDI) monomers (~50%) and oligomers. The average

functionality of commercial PMDI is ~2.8 and the resin has an isocyanate content of ~30 - 32% [3,4].

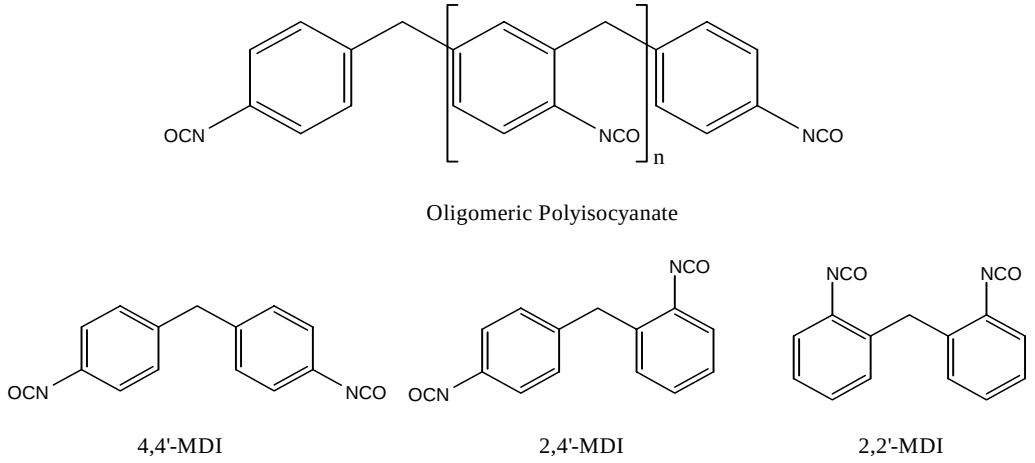

Figure 3.1.1. Molecular structure of the components of commercial PMDI resin.

The monomer fraction is mostly comprised of 4,4'-MDI (>90% of monomer fraction), with a small amount of 2,4'-MDI (2-7% of monomer fraction) and traces of the 2,2'-isomer (fig. 3.1.1).

3.1.1. PMDI Synthesis

There are different laboratory routes for the synthesis of isocyanates. Isocyanates can be synthesized by the Curtis, Hoffman and Lossen rearrangement reactions, all of which involve the nitrene ($RCON^-$) intermediate (fig 3.1.2).

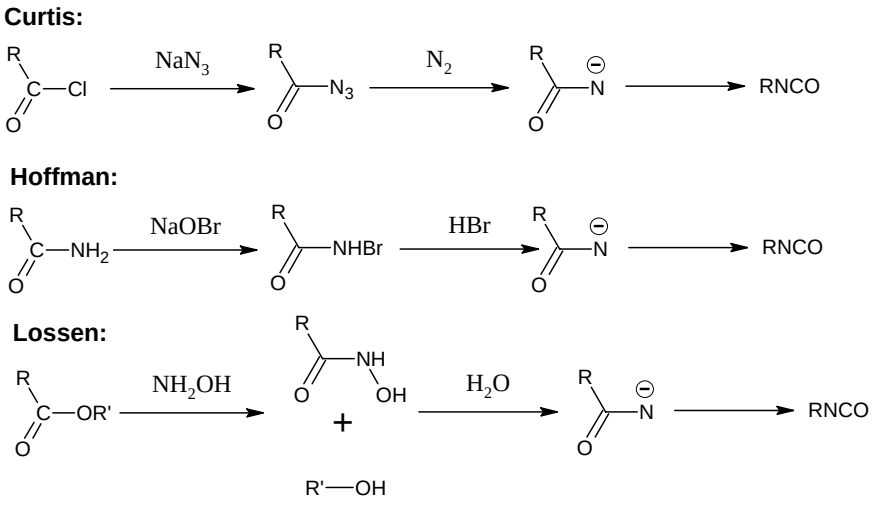

Figure 3.1.2. Curtis, Hoffman and Lossen rearrangement reactions.

But these reactions have certain disadvantages which make them unsuitable for large-scale industrial operation. For example, the Curtis reaction involves the use of hazardous azides (NaN_3).

In 1884, Hentschel [5] discovered a synthetic route for the synthesis of various aliphatic and aromatic isocyanates by phosgenation of the corresponding primary amines. Siefken [6] also used this method to synthesize numerous isocyanates in the laboratory scale and at present, practically all commercial operations are based on this procedure. This process consists of two different steps:

- Polyamine synthesis.
- Phosgenation of the polyamine.

3.1.1.1. Polyamine Synthesis

The aromatic polyamine is prepared from the acid-catalyzed condensation of aniline and formaldehyde. In the presence of acid, formaldehyde adds to aniline to form the iminium ion (fig 3.1.3).

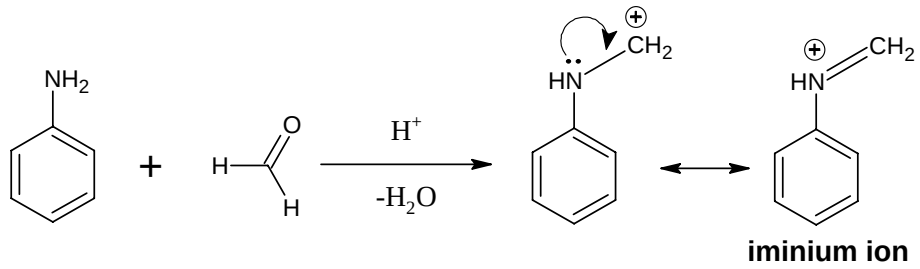

Figure 3.1.3. Formation of Iminium ion.

The iminium electrophile subsequently reacts with aniline to form *o*-/*p*-aminobenzylanilines (secondary amine) (fig 3.1.4); this is an electrophilic aromatic substitution reaction.

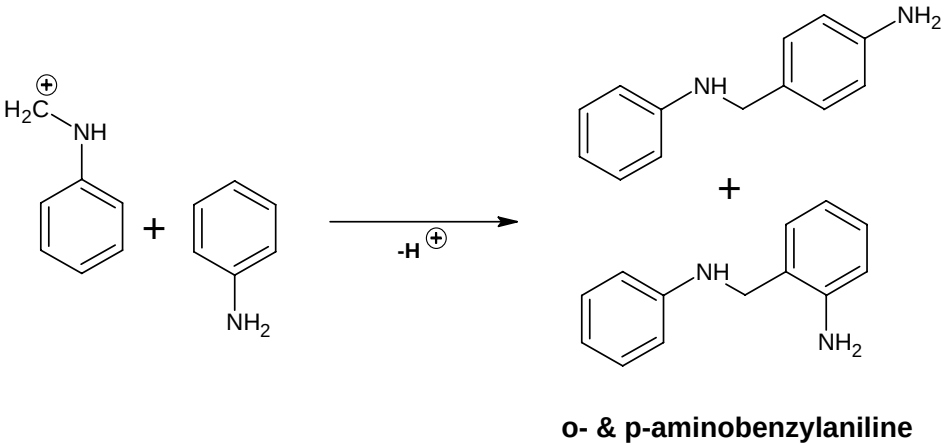

Figure 3.1.4. Formation of aminobenzylanilines (secondary amines).

Similarly, a diamine may attack the protonated aminobenzylanilines to form triamine and subsequently poly(aminobenzylanilines) (fig. 3.1.5).

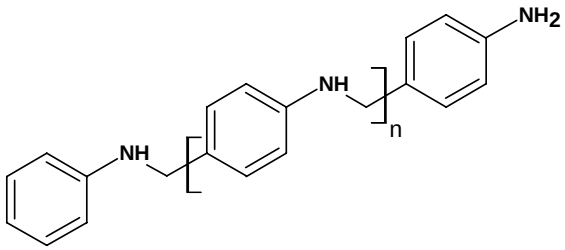

Figure 3.1.5. Structure of a typical poly(aminobenzylanilines).

The next step is an “isomerization” step in which the secondary amine is converted to a primary amine by an intermolecular reaction between the protonated secondary amine and a non-protonated primary amine. This step is pH-sensitive and is accelerated by heating the reaction mixture to 95° - 100°C. The following figure (3.1.6) shows the isomerization step involving a protonated secondary polyamine and aniline to form 4,4’-MDI and a lower polymeric secondary amine.

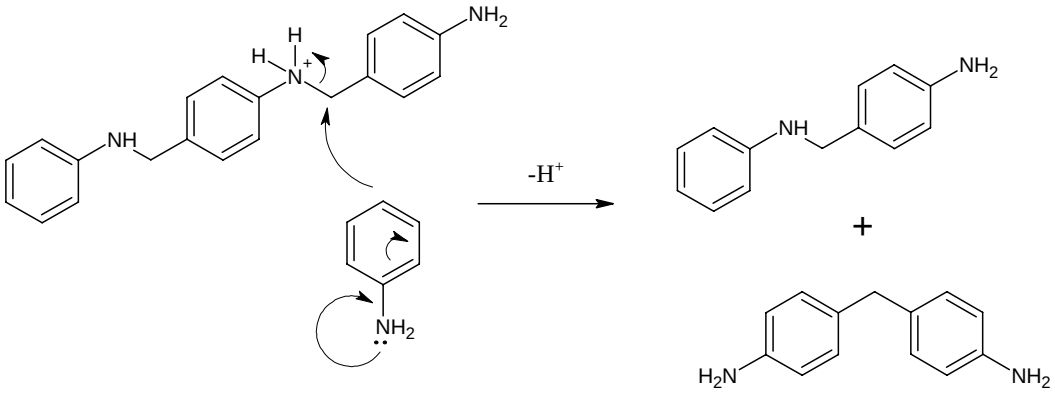

Figure 3.1.6. Isomerization of secondary amine to primary amine.

Similarly 2,4’-diaminodiphenylmethane may be formed by substitution of the iminium ion into an aromatic nucleus ortho to the amino group. Apart from the diamine, different tri-, tetra- and poly-amines may also be formed.

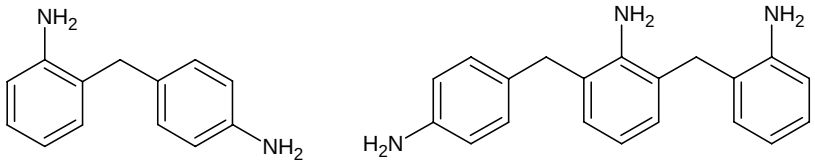

2,4’-diaminodiphenylmethane **Triamine**

Figure 3.1.7. Other products from the acid-catalyzed isomerization reaction.

The rate of the isomerization reaction is controlled by the initial acid-to-aniline ratio and also the reaction temperature. Studies have shown that as the molar ratio of acid-to-

aniline exceeds unity, the isomerization rate decreases, due to the decrease in the concentration of free amines. After the isomerization step, the polyamine is purified to remove water and excess aniline.

3.1.1.2. Phosgenation of polyamine

The phosgenation of polyamine may be carried out in different ways. The most common practice is to phosgenate the polyamine which is dissolved in an inert high boiling solvent such as ortho-dichlorobenzene. Another process involves phosgenation of the polyamine salt suspension, which is formed by passing dry HCl gas into the polyamine solution [7,8]. But, the phosgenation of the pre-formed salts is relatively slower than the dissolved amine process. Another method, known as the "interfacial phosgenation", involves reaction between an aqueous solution of primary amine and an acid acceptor (e.g. inorganic alkali, tertiary amine) and phosgene in an organic solvent [8]. The isocyanate is formed in the organic layer. This process is particularly suitable for phosgenation of unsaturated primary amines, but unsuitable for synthesis of aromatic isocyanates.

Regarding the typical process in inert solvent, phosgene and the polyamine initially react to form carbamoyl chloride and amine hydrochloride (figure 3.1.8i). At ~50°C, carbamoyl chloride dissociates into isocyanate with the release of HCl gas (fig. 3.1.8ii).

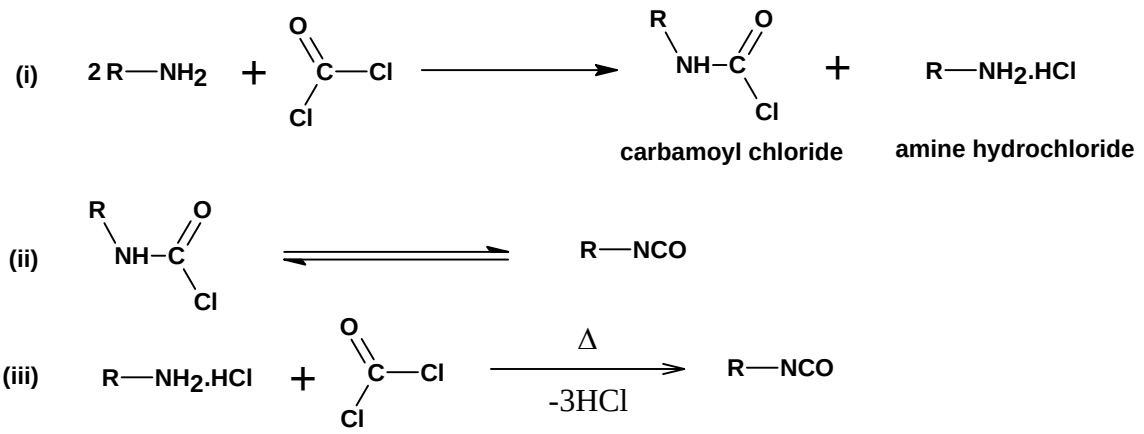

Figure 3.1.8. Phosgenation of a primary amine.

The phosgenation of the amine chloride occurs above 100°C (fig 3.8.iii).

Many undesirable products are formed during the phosgenation reaction. The primary amines may react with the isocyanate to form urea, which in turn reacts with more isocyanate to form biurets and polyurets (fig. 3.1.9).

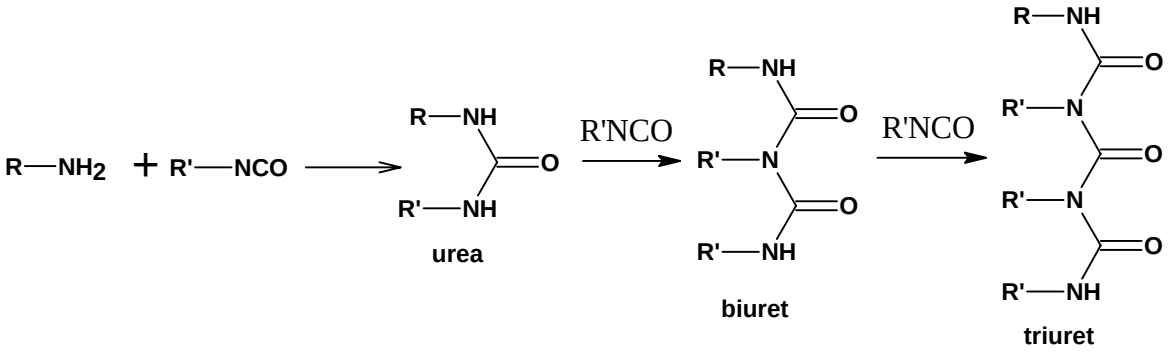

Figure 3.1.9. Formation of ureas and biurets during the phosgenation reaction.

These ureas react readily with phosgene to give rise to chlorine-containing impurities e.g. isocyanide dichloride (fig. 3.1.10i). These compounds have boiling points similar to that of the isocyanates and hence cannot be readily separated by distillation and are present in the final product as contaminants.

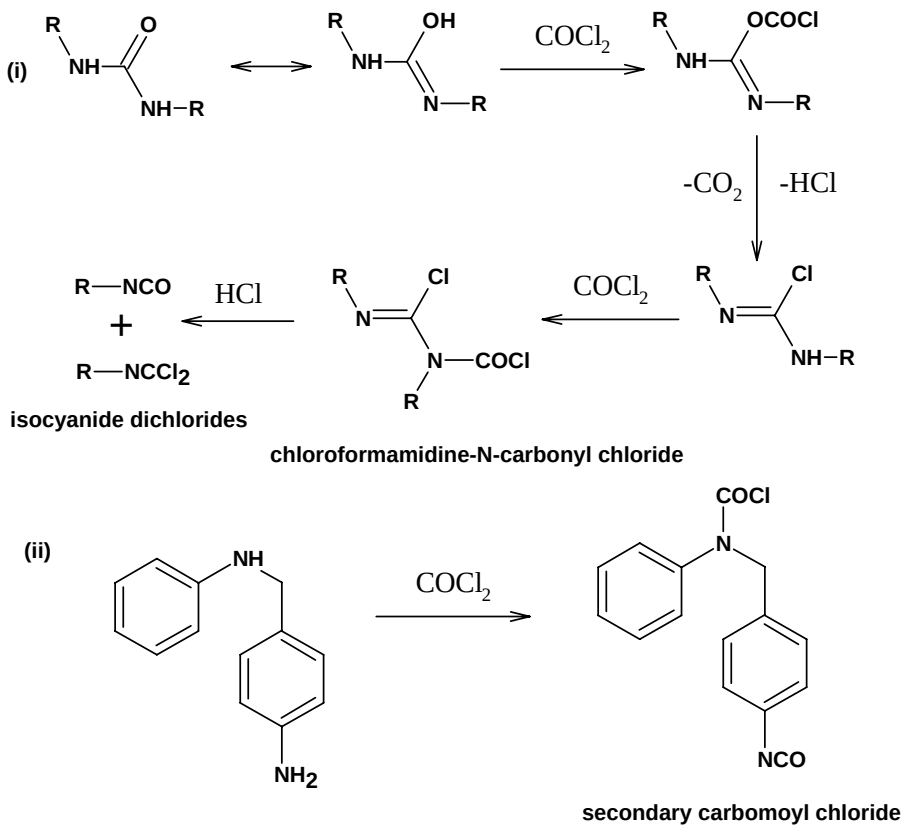

Figure 3.1.10. Formation of different chlorine containing impurities during phosgenation.

The formation of these contaminants may be avoided by carefully suppressing the formation of ureas during phosgenation, by using excess phosgene, dilute solutions and efficient agitation in the reactor [3]. Chlorine containing impurities may also be formed by the phosgenation of secondary amines (fig. 3.1.10ii).

These chlorine containing impurities may be reduced by treating the PMDI at a high temperature under specialized conditions [8,9]. During the treatment, the chloroformamidine-*N*-carbonyl chloride (fig 3.10i), which is formed by the phosgenation of urea, decomposes to carbodi-imide along with the evolution of phosgene and HCl (fig. 3.1.11).

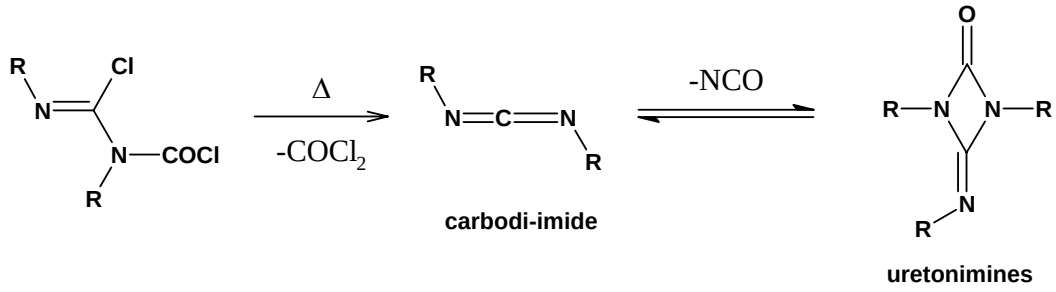

Figure 3.1.11. Formation of uretonimines.

On cooling, the carbodi-imide reacts reversibly with isocyanate to form uretonimines (fig. 3.1.11). The presence of uretonimines in PMDI results in viscosity increase at low temperatures and hence decreases the processibility of the resin.

During the heat treatment, an insoluble sediment is often formed, due to the dimerization of the isocyanates, to form uretidione (fig 3.1.12) [10].

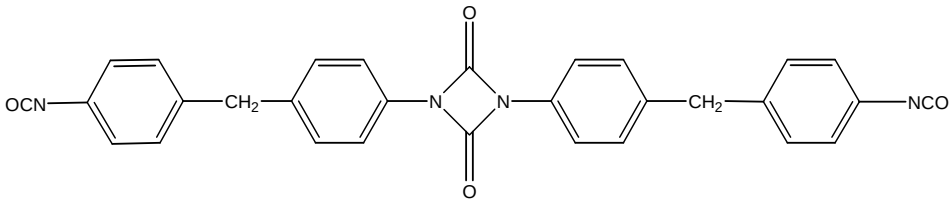

Uretidione

Figure 3.1.12. Structure of uretidione.

Though the dimerization is reversible and the rate of formation of the dimer, uretidione, at room temperature is extremely slow, appreciable amounts of uretidione are formed since it is thermodynamically stable under ambient conditions. The dimerization may be prevented by heat treatment at 200°C followed by rapid cooling to freeze the equilibrium.

3.1.2. Factors controlling the composition of PMDI

The different factors that control the composition of PMDI are

- Ratio of aniline-to-formaldehyde (A:F)

- Ratio of aniline-to-HCl acid (A:H)
- Temperature
- Rate of addition of formaldehyde

The composition of the polyamines formed at different reaction conditions are shown in table 3.1.1. The formation of 4,4'-isomer is favored in the presence of a large excess of aniline [3,11]. On the other hand, use of large amounts of formaldehyde (A:F ≈ 1) results in the formation of higher functionality polyamine. Use of higher A:H ratio (i.e. lower acid content) leads to PMDI with higher 2,4'-isomer along with larger proportions of the higher methylene-bridged polyamines. The catalyzed high-temperature pressure process produces PMDI having more 2,4'- and 2,2'-isomers, due to lower selectivity under the extreme reaction conditions, relative to the aqueous HCl route [12,13].

Table 3.1.1. Composition of PMDI resin under different reaction conditions [3]

Reaction Process	Diamine (%)			Polyamines
	4,4'	2,4'	2,2'	
Aqueous HCl	60	5	traces	35%
Catalytic high temperature	18.3	18.6	4.7	58%

Another process [14] uses heterogeneous catalysis (activated montmorillonite clay) and higher reaction pressures, to synthesize PMDI having predominately 2,4'-isomer (2,4': 2,2' : 4,4' = 64 : 9 : 27).

3.1.3. Reactions of Isocyanates

Isocyanates are susceptible to attack by nucleophiles, because of the highly electrophilic isocyanate carbon atom, as demonstrated by the isocyanate resonance structures below (fig 3.1.13).

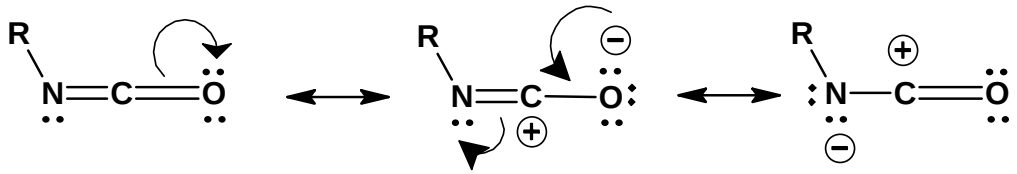

Figure 3.1.13. Resonance structures of isocyanates.

Electron-withdrawing substituents attached to the isocyanate group increase reactivity; electron-donating groups reduce reactivity. Thus, aromatic isocyanates are more reactive than aliphatic isocyanates because of the greater electronegativity of sp^2 hybridized aromatic carbons, as compared to the sp^3 hybridized aliphatic carbon atoms.

Isocyanates react readily with compounds having active hydrogen (i.e. hydrogen atoms bonded to electronegative atoms) e.g. amines, alcohols, water, carboxylic acids etc. The relative reactivity of isocyanates with different active hydrogen compounds is as follows [10]:

1° aliphatic amine > 2° aliphatic amine > 1° aromatic amine > 1° hydroxyl > water > carboxylic acid > 2° hydroxyl > urea > 3° hydroxyl > urethane > amide

The reaction between isocyanate and an active hydrogen compound may be described as an addition of a nucleophile to the carbon-nitrogen double bond. The reaction starts with attack of the electrophilic carbon of isocyanate group by the nucleophilic center of the active hydrogen compound, which is followed by addition of the active hydrogen atom to the isocyanate nitrogen atom (fig 3.1.14).

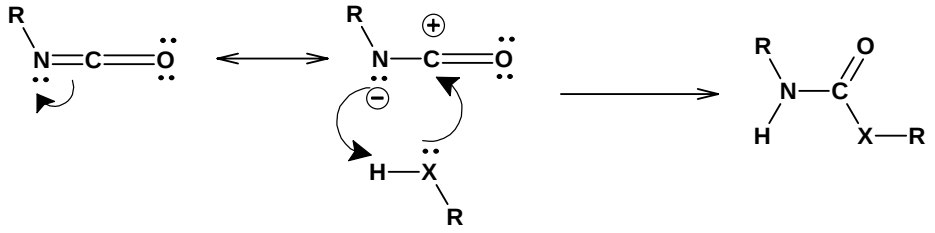

Figure 3.1.14. Schematic diagram showing the reaction of isocyanate with an active hydrogen compound.

Wood contains a substantial amount of adsorbed water. The isocyanate reacts with water to form carbamic acid. The carbamic acid being thermally unstable, spontaneously decomposes to form a primary amine and CO_2, with the evolution of heat. The amine, being an active hydrogen-containing compound, in turn reacts with additional isocyanate to form urea. Due to the presence of active hydrogen in urea, the reaction continues, with the formation of biuret, triuret and finally polyuret structures (fig. 3.1.15). Thus, in the presence of water, isocyanate resin forms a tough crosslinked polyurea network that is known to promote adhesion through hydrogen bonding and mechanical interlocking with the wood surface [15].

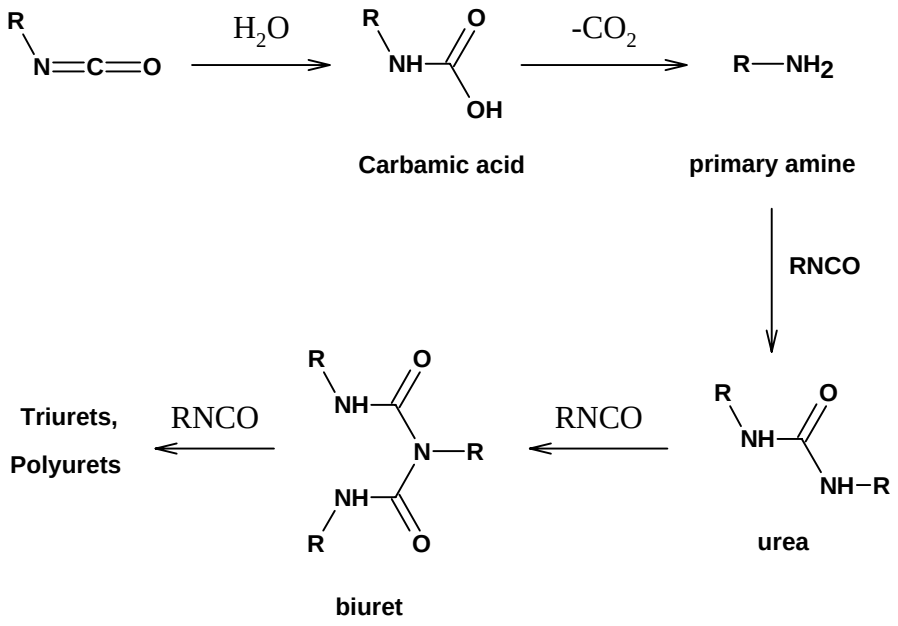

Figure 3.1.15. Reaction of isocyanate with water

Wood also contains various active hydrogen compounds (such as aliphatic alcohol, phenol, etc.), which may react with isocyanate to form carbamate or urethane linkages. Urethanes contains active hydrogen, which may further react with additional isocyanate to form allophanates (fig. 3.1.16)

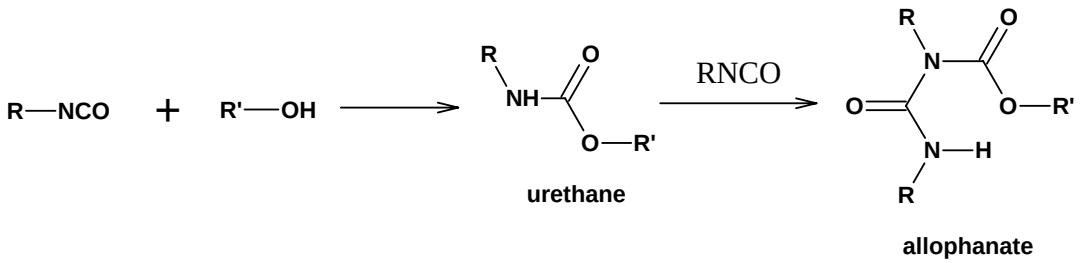

Figure 3.1.16. Reaction of isocyanate with compounds containing hydroxyl functional groups

Various characterization techniques have been used to analyze the reaction of PMDI resin with wood and isolated wood polymers. Studies have shown that PMDI resin reacts more readily with lignin than any sugar derivatives [16]. Other studies used techniques like infrared spectroscopy and differential scanning calorimetry to show that

polyurea structures dominate the wood-PMDI bondline in the presence of moisture [17,18]. But the reaction between PMDI and water has been shown to be catalytically activated in the presence of wood [19]. Urethane bonds were observed in the wood-PMDI bondline under specialized conditions e.g. anhydrous conditions and in the presence of excess resin [20-22]. The excellent performance of particleboard bonded with PMDI resins has often been attributed to the formation of this covalent bond between the resin and wood [23].

References

(1) Marra, A. A. *Technology of Wood Bonding: Principles in Practice*; Van Nostrand Reinhold: New York, 1992.
(2) Sellers, T. *Forest Products Journal* **2001**, *51*, 12-22.
(3) Twitchett, H. J. *Chemical Society Reviews* **1974**, *3*, 209-230.
(4) Moriarty, C. In *Proceedings of 33rd International particleboard/composite materials symposium*; M.P.Wolcoot, Ed.: Pullman, WA, 1999; pp 159-164.
(5) Hentschel, W. *Ber.* **1884**, *17*, 1284.
(6) Siefken, W. *Annalen.* **1949**, *562*, 75.
(7) Bayer. U.S.
(8) ICI. British.
(9) DuPont. England.
(10) Arnold, R. G.; Nelson, J. A.; Verbanc, J. J. In *American Chemical Society*: Cleveland, Ohio, 1956; pp 47-76.
(11) Dombrow, B. A. *Polyurethanes*, 2nd ed.; Reinhold Publishing Corp.: New York, 1965.
(12) Bentley, F. E., 1978.
(13) Laszlo, P. *Surfactant Science Ser.* **1991**, *38*, 437.
(14) Ni, J.; Frazier, C. E. *Journal of Adhesion* **1998**, *66*, 89-116.
(15) Chelak, W.; Newmann, W. H. In *International Particleboard/Composite Materials Symposium*; T.M.Maloney, Ed.: Pullman, washington, 1991; pp 205-229.
(16) Weaver, F. W.; Owen, N. L. *Applied Spectroscopy* **1995**, *49*, 171-176.
(17) Weaver, F. W.; Owen, N. L. In *Pacific Rim Bio-based Composites Syposium*, FRI Bulletin No. 177 ed.: Rotorua, New Zealand, 1992; Vol. 143.
(18) Steiner, P. R.; Chow, S.; Vadja, S. *Forest Products Journal* **1980**, *30*, 21.
(19) Pizzi, A.; Owen, N. A. *Holzforschung* **1995**, *49*, 269-272.
(20) Rowell, R. M.; Ellis, E. M. *Wood Science* **1979**, *12*, 52.
(21) Rowell, R. M.; Ellis, E. M. *Urethane Chemistry and Applications*; American Chemical Society: Washington D.C., 1981.
(22) Rowell, R. M.; Feist, W. C.; Ellis, E. M. *Wood Science* **1981**, *13*, 202.
(23) Johns, W. E. *Journal of Adhesion* **1982**, *15*, 59-67.

3.2. Characteristic differences between Yellow-poplar and Pine

In this study, the species dependent performance of PMDI resins is studied with a softwood, southern yellow pine (*Pinus sp.*) and a hardwood, yellow-poplar (*Liriodendron tulipifera*). Hereafter the woods will simply be referred to as pine and poplar. In the following section, the anatomical and chemical differences of these woods will be discussed.

3.2.1. Anatomical Differences

A number of species are marketed as pine, of which the four major species are longleaf pine (*Pinus palustris),* shortleaf pine (*Pinus echinata*), loblolly pine (*Pinus taeda*) and slash pine (*Pinus elliottii*) [1]. The anatomy of these species is so similar that they cannot be differentiated by most classical methods. Pine has a simple anatomical structure and consistent radial alignment of cells (fig 3.2.1). In pine, the major cell type which occupies 90% of the wood volume is known as the tracheid [2]. These cells provide fluid conduction and also mechanical support to the tree. The other different cell types present in pines are parenchyma (storage and transverse conduction of fluids) and epithelial cells (secretion of resin into the lateral and transverse resin canals).

In contrast, poplar has a more complex structure, typical of hardwoods, with multiple cell types that lack radial alignment (fig 3.2.2). The four major cell types in poplar are fiber tracheids, vessel elements, longitudinal parenchyma and ray parenchyma. Unlike pine, poplar contains specialized conducting cells called vessels, which are characterized by a large diameter (~70 microns), and thin walled tube-like structures. Poplar vessels are evenly distributed throughout the annual growth ring, a characteristic

which is described as diffuse porosity; poplar is a diffuse porous wood. Poplar also contains fibers tracheids, which provide mechanical support to the plant; but they are different from those observed in pine.

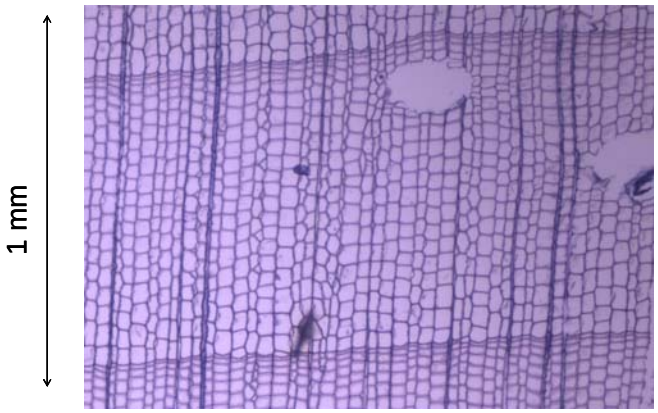

Figure 3.2.1. Light microscopic image of southern pine (40 × magnification)

Poplar fibers tracheids are thick-walled, circular in cross section and are dispersed randomly among the vessels. In contrast, the pine tracheids (35-45 microns in diameter) have rectangular cross sections, are two to three times larger than the corresponding poplar fiber tracheids (6-15 microns in diameter) and are aligned in fairly straight radial rows. Pines have no vessels, but, they do have resin canals for the transport of resinous materials.

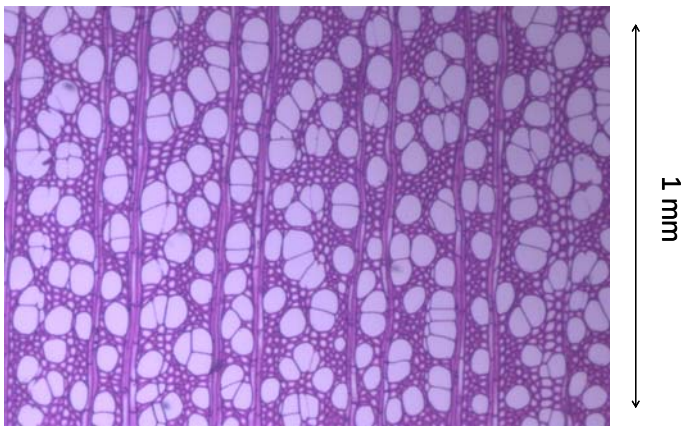

Figure 3.2.2. Light microscopic image of yellow-poplar (40 × magnification)

Thus, the major anatomical differences between pine and poplar are those typical of the comparison of softwoods and hardwoods. Poplar is more complex and because of its even distribution of vessel cells, it is relatively more porous than pine.

3.2.2. Chemical Differences

Wood is composed of different chemical substances, which are produced near the cambium (growing layer between the xylem and phloem) of a living tree. The wood chemically contains approximately 50% carbon, 44% oxygen and 6% hydrogen with ~0.1% nitrogen and 0.2-0.3% ash (mineral constituents like calcium and magnesium carbonates, and silica crystals) [3].

The organic wood constituents may be broadly divided into two components: the polymeric cell wall components and the extractives. There are three main polymeric cell wall components: cellulose, hemicellulose and lignin

The following table (table 3.2.1) shows the variation of the different organic components in the wood species.

Table 3.2.1. Variation of organic wood components in pine and poplar

Chemical Components	Southern Pine [4] (%)	Yellow-poplar [5] (%)
Cellulose	43 ± 2	39.1
Hemicellulose	24 ± 3	28
Lignin	25-30	~ 24
Extractives	3-9	2-4
Inorganics	<1	0.3

Cellulose is the principal constituent of the cell wall and is the most abundant naturally occurring organic substance on earth. Cellulose is comprised of anhydroglucose

units (1.03 nm in length [6]) (fig 3.2.3); however the actual repeat unit is the dimer cellobiose.

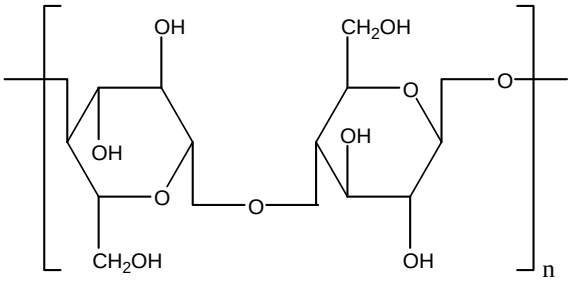

Figure 3.2.3. Structure of cellobiose repeating unit of cellulose

The major portion of cellulose (60-70%) is present in tightly packed crystalline bundles (called elementary fibrils), which are inaccessible to moisture and other chemicals. Each of these elementary fibrils contains parallel arrays of 36 cellulose chains, aligned predominantly along the fibril axis [3]. These elementary fibrils aggregate into larger microfibrils (3.5×10 nm) through hydrogen-bonding [7].

Hemicelluloses are heteropolysaccharides which are crudely subclassified into two different polysaccharides, xylans and glucomannans. The xylan backbone contains xylose units, whereas the glucomannan backbone consists of glucose and mannose. Most hemicelluloses have a degree of polymerization of about 200 [8]. These polysaccharides are extensively branched and are soluble in water and/or aqueous NaOH solutions. Hemicellulose is amorphous due to the presence of abundant side groups, which hinder the formation of crystalline structures. It is believed that there are no covalent linkages between the cellulose microfibrils and hemicellulose molecules, but significant interactions occur through hydrogen bonds and Van der Waal's forces [3]. Numerous studies have shown the existence of covalent linkages between lignin and hemicellulose. Eriksson *et al.* [9] proved the existence of these covalent linkages by separating lignin-

carbohydrate complexes (LCC), where the hemicellulose components are covalently linked to the lignin through arabinose, xylose and galactose moieties. The composition and structure of hemicellulose in pine is distinctly different from those present in poplar. The principal hemicellulose components in pine are galactoglucomannans (~20%), arabinoglucuronoxylans (5-10%) and arabinogalactan. On the other hand, poplar hemicellulose is mostly composed of glucuronoxylan (15-30% of dry wood) and glucomannan (2-5%) [3]. The xylans and mannans are also chemically different between the two wood species. Poplar glucomannans are characterized by a slightly branched heteropolymer backbone consisting of mannose and glucose units (ratio of 1.5:2.1 [2]) linked together by β-(1-4)-glycosidic bonds. Pine glucomannans are similar but contain acetyl groups and galactose units. Pine xylans also differ from the corresponding poplar xylans by the lack of acetyl groups and by the presence of arabinofuranose units linked by α-(1-3)-glycosidic bonds to the xylan backbone.

Lignin is a highly branched and/or network heteropolymer containing phenylpropane repeating units; it constitutes 20-30% of the total weight of wood. It is an amorphous material, which primarily functions as a binding and stiffening agent for the cellulose microfibrils. Lignin is formed by free-radical polymerization of three closely related phenolic compounds i.e. *p*-coumaryl alcohol, coniferyl alcohol and sinapyl alcohol, which are shown in figure 3.2.4 [8].

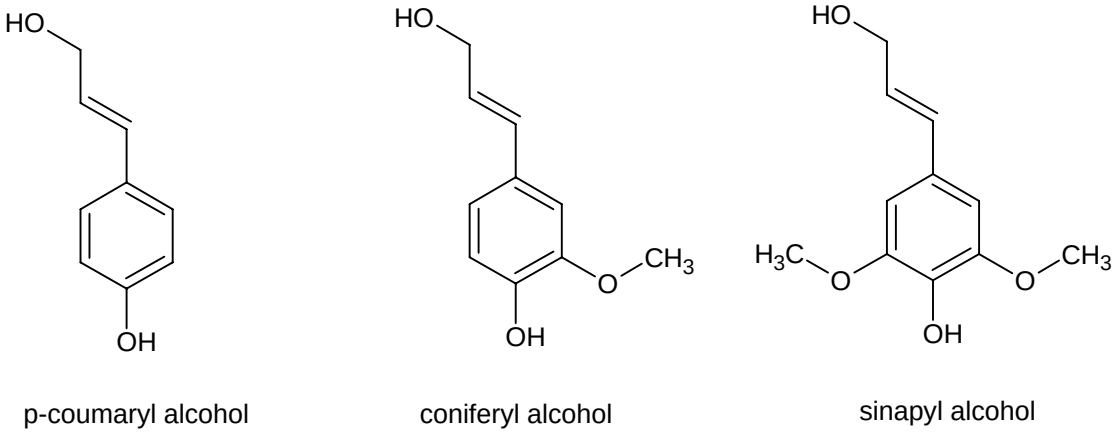

Figure 3.2.4. Different Lignin monomeric units

The nature of the lignin in the different wood species is different. In pines, lignin is formed by the polymerization of coniferyl alcohol, while in poplar, it is mostly a copolymer of coniferyl and sinapyl alcohol (copolymer ratio: 4:1 to 1:2) [8]. The functional groups (methoxyl, phenolic hydroxyl, benzylic hydroxyl and carbonyl groups) which have a major effect on the reactivity of lignin are also different in different wood species (table 3.2.2).

Table 3.2.2. Lignin functional groups per 100 C_6C_3 units [10]

Functional groups	Southern Pine lignin	Yellow-poplar lignin
Methoxyl	90-95	140-160
Phenolic hydroxyl	20-30	10-20
Aliphatic hydroxyl	115-120	110-115
Carbonyl	20	15

Extractives are natural products extraneous to the lignocellulosic cell walls which can be extracted by means of various polar and non-polar solvents. These are mainly concentrated in the resin canals and ray parenchyma cells [2], but smaller amounts are also found in the middle lamellae and cell walls of tracheids and libriform fibers. They

function as energy reserves, tree metabolism intermediates and as a defense mechanism against microbial attack. The three main extractives are described below:

a) Short-chain carbohydrates: these are water-soluble compounds and include sugars, cyclitols, gums, starch, pectins etc.

b) Phenolic compounds: these are acetone-soluble compounds found in bark and heartwoods like hydrolysable tannins, flavonoids, lignans, stilbenes and tropolones.

c) Resins: these include terpenes, resin acids, fatty acids and esters, various alcohols, hydrocarbons which are soluble in neutral non-polar solvents e.g ether.

The following table shows the variation of these extractives in poplar and pine.

Table 3.2.3. Variation of different extractives in pine and poplar [11]

Extractives	Southern pine	Yellow-poplar
Carbohydrates	3	2
Phenolics	4	1
Resin	3.3	0.2

Thus, pine and poplar have very different chemical and anatomical properties that could affect their interaction with PMDI resin. Anatomical differences affect the penetration of resin into the wood structure. The diffuse porous structure of poplar (many large vessels distributed uniformly) causes liquid PMDI to penetrate poplar more effectively than pine. However, PMDI penetration into pine is also quite facile because of the low viscosity and low surface tension of PMDI.

Chemically, the proportions of the different cell wall components vary in pine and poplar. Hemicelluloses are different between the two different wood species: poplar

hemicelluloses are predominantly xylans (15-30%) with smaller amounts of glucomannans (2-5%), while pine hemicelluloses are predominantly glucomannans (~20%) with smaller amounts of xylans (5-10%). Glucomannans contain primary hydroxyl groups, which are known to be highly reactive towards isocyanate resins. Thus, pine hemicelluloses might be more reactive towards the PMDI. Pine lignin is also significantly different from poplar lignin; the latter contains lower amounts of free phenolic hydroxyl groups and substantially higher amounts of methoxyl groups. Phenolic hydroxyl groups are known to be one of the most reactive sites in lignin [12]. Thus, higher amounts of phenolic hydroxyl groups in pine would make it more reactive towards the resin. Thus, we might expect that pine and poplar would exhibit different degrees of reactivity with PMDI. Of course this implies that the reactivity is the addition of alcohols to the isocyanate group. The isocyanate reaction with adsorbed wood water is also very important and may dominate the chemical differences between pine and poplar.

Extractives constitute only a very small fraction of the total wood mass (4-10%), but they have significant influence on wood adhesion. Extractives are known to decrease the hygroscopicity and permeability of wood [3]. Since extractives are deposits in the cell wall or lumens, they can easily migrate to the wood surface (by diffusion) and reduce its surface energy and thus resin wettability. This movement may occur due to thermal and moisture gradients and also due to capillary and surface forces [3]. Studies have shown that extractive removal results in a significant increase in wood surface energy [13]. The amount of extractives in pine is almost double than poplar; thus the interference to wood-resin interactions due to extractives would be more significant in pine woods.

References

(1) Miller, R. B. In *Wood Handbook*.
(2) Fengel, D.; Wegner, G. *Wood: Chemistry, Ultrastructure, Reactions*; Walter de Gruyter: Berlin, 1983.
(3) Marra, A. A. *Technology of Wood Bonding: Principles in Practice*; Van Nostrand Reinhold: New York, 1992.
(4) Koch, P. In *Agricultural Handbook*, 1972; p 420.
(5) Koch, P. In *Agricultural Handbook*, 1985; p 605.
(6) Siau, J. F. *Wood: Influence of moisture on physical properties*; Department of Wood Science and Forest products, VPI & SU: Blacksburg, VA, 1995.
(7) Bodig, J.; Jayne, B. A. *Mechanics of Wood and Wood Composites*; Krieger Publishing Company: Malabar, Florida, 1993.
(8) Sjostrom, E. *Wood Chemistry: Fundamentals and Applications*; Academic Press Inc.: New York, 1981.
(9) Eriksson, O.; Lindgren, B. O. *Sven. Papperstidn.* **1977**, *80*, 59-63.
(10) Stenius, P. *Papermaking Science and Technology: Forest Products Chemistry*; Fapat Oy: Helsinki, Finland, 2000.
(11) Hillis, W. E. *Wood Extractives*; Academic Press: New York, 1962.
(12) Alder, E. *Wood Sci. Technol.* **1977**, *11*, 169.
(13) Chen, C. M. *Forest Products Journal* **1970**, *20*, 36-41.

3.3. Solid-state NMR

Nuclear magnetic resonance (NMR) spectroscopy has been a valuable characterization tool for chemists. However, most work on NMR was traditionally done with samples in solution rather than in solids. The solution NMR spectrum provides a wealth of well resolved resonances, analysis of which leads to chemical shift and J-coupling values that can be used to obtain information about the chemical environment of the resonating nuclei. Thus, solution NMR had been successfully used in the past years for chemical identification, studies of chemical kinetics and for the determination of chemical or structural changes at specific molecular sites. The well resolved resonances in a solution NMR spectrum also allow the determination of molecular dynamics of the sample in solution through measurements of different relaxation times e.g. T_1, T_2 and $T_{1\rho}$.

In the solution state, the sample nuclei are in rapid isotropic motion; thus, all dipolar and quadrupolar interactions are averaged to zero. This averaging of local fields, leads to well resolved lines/resonances in the NMR spectra of solutions. In contrast, the nuclei of solid samples are either rigid relative to the NMR time scale or possess limited anisotropic motions. The absence of isotropic averaging in solids leads to broad resonances in the corresponding NMR spectrum.

There are two major interactions, which contribute to the broad line widths in NMR spectra of solids. They are

- Chemical shift anisotropy
- Dipolar interactions

3.3.1. Chemical Shift Anisotropy (CSA)

CSA may be defined as the chemical shift difference with the orientation of the bond in the static magnetic field. One of the major anisotropic interactions present in solids is due to chemical shielding of nuclei from the applied magnetic field by the surrounding electron cloud. In most chemical bonds, the electron clouds do not have a spherical symmetry and hence is anisotropic in nature. Due to this anisotropic shielding, the resonance shift of nuclei depends on the orientation of the electron cloud with the applied magnetic field, which in turn determines the shape of the resonance lines. In solution NMR, due to the fast and random motion of the molecules (in the NMR time scale), all interactions between the nuclei and the magnetic field (which is anisotropic in nature) are averaged to their isotropic values. But in solids, since the molecules are rigid in the NMR timescale, the interactions remain anisotropic and manifest themselves as broad resonances.

3.3.2. Dipolar Interactions

Dipolar interactions are defined as the interaction between the magnetic moments of nuclei with non-zero nuclear spin. The interaction of nuclei with similar spins (H_d) may be represented as follows:

$$H_d = \frac{c\left(1-3\cos^2\theta\right)}{r_0^{\,3}} \tag{3.3.1}$$

where, r_0 is the internuclear distance,

c is a constant,

θ is the angle between the internuclear vector and the direction of the external magnetic field.

In solids, due to the absence of motion, these interactions are not averaged out , as a result of which a given nucleus experiences dipolar interactions with several neighboring nuclei. This in turn results in a variety of internuclear vectors and hence overlapping resonances.

3.3.3. Cross-Polarization / Magic Angle Spinning (CP / MAS) experiment

The dipolar interaction and chemical shift anisotropy may be supressed in solid samples by performing the CP/MAS experiment.

The main reason for the appearance of broad resonances in the solid state NMR spectra is the restricted motion of molecules in the solid state. Studies [1-3] have shown that the rapid motion of molecules in solution may be emulated in the solid state by rapidly spinning the solid sample at 54.7° (*the magic angle*). Under such conditions, each nucleus experiences a continuous series of orientations relative to the applied magnetic field, which in turn results in isotropic averaging of the chemical shifts similar to those observed in liquid samples [4]. The anisotropic chemical shift (σ_a) may be written as follows:

$$\sigma_a = \frac{1}{3}\left\{\sigma_1 - \sigma_2\left(3\cos^2\theta - 1\right)\right\} \qquad (3.3.2)$$

Thus, if the sample is rotated at the magic angle, σ_a, becomes zero. Thus, the chemical shift anisotropy may be removed by MAS of the solid sample.

One complication observed in spectra obtained with MAS, is the appearance of rotational echoes as spinning side-bands that flank the isotropic peak, when the sample spinning speed is less than the CSA. The side-band spacing is inversely dependent upon

the spinning frequency. Thus, with the increase in spinning rate, the rotational spinning side-bands move further out and become weaker. At very high spinning rates, the side-band intensities become negligible and the spectrum consists of a well resolved central resonance at the Larmor frequency, ω_0.

The setting of the spinning angle in a MAS experiment is also critical. Studies have shown that an error of 0.1° in the magic angle setting for a shielding anisotropy of 200 ppm, results in a line broadening of 1.02 ppm [5].

Cross-polarization is an useful technique, developed by Pines, Gibby and Waugh [6], for observing non abundant spins such as ^{13}C, ^{14}N etc. in the presence of more abundant spin species such as ^{1}H. It leads to enhancement of the observed signal and faster data acquisition rates. Heteronuclear decoupling of the abundant spins may also be achieved by leaving the high-powered spin locking on during data acquisition.

Cross-polarization is a double-resonance experiment in which the energy levels of proton and any non abundant species are matched to the Hartman-Hahn condition, which leads to the transfer of energy from protons to the less abundant species. The result of the experiment is the enhancement of the magnetization of the less abundant species at the expense of ^{1}H magnetization.

The Hartmann-Hahn match is obtained when

$$\gamma_H B_{1H} = \gamma_C B_{1C} \tag{3.3.3}$$

where, γ_i is the magnetogyric ratio of nucleus i,

B_{1H} & B_{1C} are the field strength of the rf pulse for proton and rare C spin reservoirs respectively.

Under these conditions, the proton and the carbon nuclei precess at equal frequencies in their respective rotating reference frames and their energies in the rotating frames are also comparable. This allows the rapid transfer of magnetization between protons and C nuclei, which is known as cross-polarization. This transfer of energy from the abundant proton spin reservoir to the rare C-spin occurs during the so-called contact time. The time constant for the transfer of polarization under these conditions is known as the T_{CH} relaxation time. T_{CH} is a spin-spin relaxation process and has values in the range of 100 μsec [4]. In the final step of the experiment, the ^{13}C pulse is terminated and the FID is observed while the proton channel is used for decoupling.

The transfer of magnetization by cross-polarization (CP) is a common relaxation phenomena observed in organic polymers. The rate of CP, T_{CH}, depends upon several factors as discussed below.

- CP varies inversely with the C-H internuclear distance. Thus, carbons which are directly bonded to protons cross-polarize more rapidly relative to carbons which do not have any attached protons.

- CP is much more effective in rigid systems relative to mobile systems. Due to extensive motion, the C-H dipolar interactions decreases which in turn results in lower CP rates. Thus, for mobile systems, it is often difficult to perform CP experiments, due to the fact that the proton magnetization gets depleted due to $T_{1\rho}$ relaxation before it can be transferred to the rare spin system.

- The enhancement of magnetization of a rare spin due to CP also depends on the phase of the polymer. The CP enhancement in disordered systems is smaller due to extensive molecular motion, which shortens $T_{1\rho}$ and increases T_{CH}. Studies have shown

that in polyethylene, the CP enhancement factor is 3.5 ± 0.2 in crystalline regions, whereas 2.4 – 3.0 in amorphous systems [7].

Studies have shown that perfect transfer of energy from the protons to ^{13}C, can improve the signal of the less abundant species i.e. ^{13}C, by a factor of 4 [4]. Further signal enhancement may be accomplished by signal averaging through the coaddition of different FIDs (by a factor of $\sqrt{\frac{^{C}T_1}{^{H}T_1}}$).

Figure 3.3.1 shows the variation of ^{13}C magnetization (shown in relative signal area) with contact time in CP/MAS variable contact time experiment.

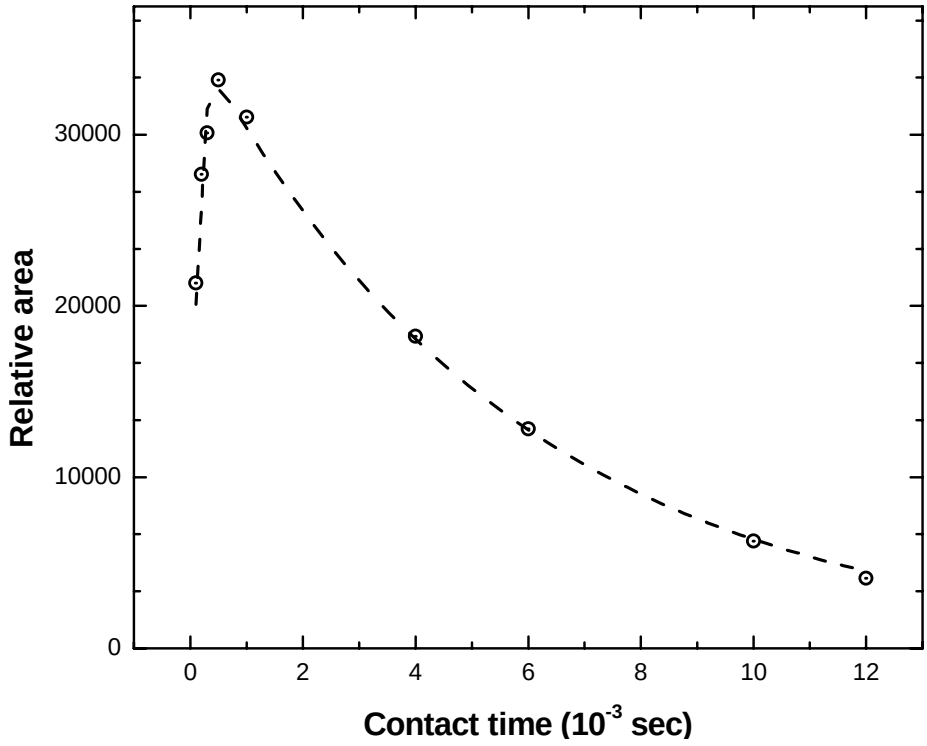

Figure 3.3.1. Variation of carbon magnetization with contact time in a CP/MAS experiment.

In CP/MAS variable contact time (VCT) experiments, two opposing relaxation processes are simultaneously active. With increase in contact time, the amount of energy

transferred from the abundant proton spin-reservoir to the rare C-spin system increases. At the same time, as the contact time is increased, the proton magnetization is lost due to the $T_{1\rho}$ relaxation process. At shorter τ, the process is dominated by T_{CH} and hence the ^{13}C magnetization increases exponentially. But at longer τ, $T_{1\rho}$ dominates and the rare spin magnetization decreases exponentially. Thus, the initial rate of magnetization growth is inversely proportional to T_{CH} and the final magnetization decay is proportional to the inverse of $T_{1\rho}$.

The relaxation parameters ($T_{1\rho}$ & T_{CH}) may be determined by fitting the raw data from a VC-CP/MAS experiment into the following equation [8].

$$I(\tau) = I^* \frac{T_{1\rho H}}{T_{1\rho H} - T_{CH}} \left(e^{-\frac{\tau}{T_{1\rho H}}} - e^{-\frac{\tau}{T_{CH}}} \right) \qquad (3.3.4)$$

where, $I(\tau)$ is the signal intensity at contact time, τ,

I^* is the ^{13}C magnetization, when the cross-polarization is instantaneous and the rotating frame relaxation is infinitely slow. It is the corrected intensity, which is obtained by dividing the corrected intensity of a desired peak by the sum of all the corrected intensity. Thus, I^* gives us a *semi-quantitative idea* of the relative concentration of each chemical species present in the sample.

3.3.4. Application of CP/MAS on wood-based systems

Recently, a number of studies have shown the utility of CP/MAS NMR experiments for the *in situ* characterization of wood. Most studies have dealt with the investigation of relaxation parameters in order to gain insight into the wood morphology. This section will discuss various CP/MAS NMR studies conducted on wood in order to

determine the effects of various chemical treatments on the *in situ* morphology of wood-adhesive bond-lines.

Due to numerous studies, the assignments of wood ^{13}C chemical shifts are well established [9]. Figure 3.3.2 shows a ^{13}C CP/MAS NMR spectrum of yellow-poplar wood.

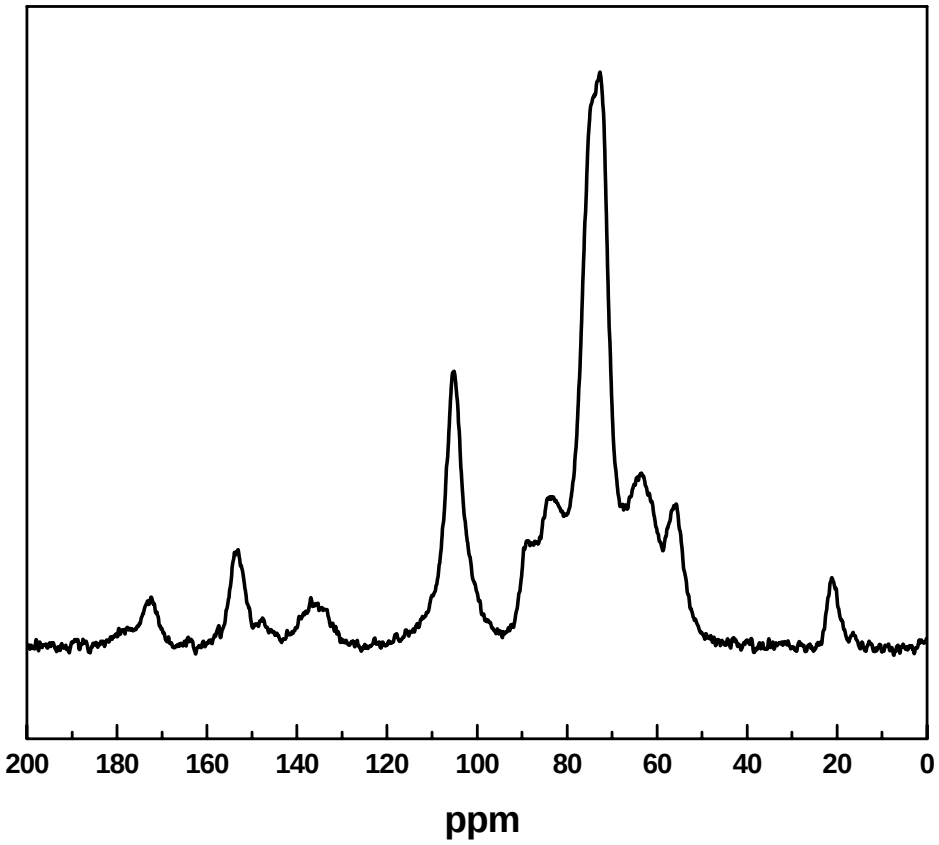

Figure 3.3.2. ^{13}C CP/MAS spectrum of yellow-poplar wood.

The ^{13}C spectrum is dominated by carbohydrate signals. Carbohydrate C_2, C_3 and C_5 signals are present in the 72-74 ppm region. Carbohydrate C_4 and C_6 signals appear at 85-90 ppm and 63-66 ppm respectively. The resonances of both C_4 and C_6 consist of a sharp peak and a broad shoulder. The sharp peak is due to the crystalline regions of cellulose while the shoulder is due to the disordered amorphous regions [10]. The resonance of cellulose C_1 appears at ~105 ppm which overlaps with the hemicellulose C_1 signal at 103

ppm. The hemicellulose acetyl resonances are present at 22 ppm (methyl carbon) and 175 (carbonyl carbon). The other hemicellulose carbons are present as broad background signals. The lignin signals are present at 56 (methoxyl group), 122 (unsubstituted aromatic carbon), 135 (alkylated aromatic carbon) and 153 (oxygen substituted aromatic carbon) ppm. Thus, CP/MAS NMR may be used to obtain reasonably well-resolved resonances of different wood polymers, allowing one to probe the morphology and molecular dynamics of wood.

In the past, nuclear spin relaxation experiments have been utilized widely for the characterization of wood morphology. These studies have shown that the amorphous matrix and the crystalline cellulose microfibrils in wood are present in phase separated domains. This was concluded by observing the presence of distinct proton $T_{1\rho}$s [11] and T_1s [12] for the mobile (lignin and hemicellulose) and rigid (cellulose) components of wood. While $T_{1\rho}$ suggested phase separation at a scale of nanometers, T_1 studies imply that phase heterogeneity exists on a scale greater than 30 nanometers.

CP/MAS studies also showed the effect of moisture on the different wood relaxations. Studies [13] have shown that the $T_{1\rho}$ relaxation of lignin decreases with increase in wood moisture content due to the enhancement of spin diffusion. On the other hand, with increase in moisture content, $T_{1\rho}$ of cellulose increases due to the change in cellulose microstructure into a more ordered state by increased hydrogen bonding [14].

CP/MAS NMR studies have also been used extensively to determine the effect of various treatments e.g. steam explosion, sulphonation, methylation, heat treatments etc., on wood morphology. Using this technique, Kosikova *et al.* [15] studied the effect of heat

treatment on the structure of different cell wall polymers. They showed that due to heat treatment, the following structural changes occur in the different wood polymers:

- The crystallinity of the cellulose component increases with steam treatment due to various reasons e.g. conversion of amorphous cellulose to the more ordered crystalline state, preferential degradation of amorphous cellulose, or splitting of hydrogen bonds [16].
- The main hemicellulose component of the treated wood, glucuronoxylan is partially removed by steam treatment.
- Steam treatment also chemically modifies the lignin component e.g. demethoxylation of phenylpropane units, depolymerization of lignin.
- Formation of lignin-cellulose linkages.

They also showed the utility of proton $T_{1\rho}$ relaxation measurements for the detection of lignin-cellulose linkages during thermal treatment.

Ahvazi *et al.* [17] studied the effect of pH on the proton spin-lattice relaxation times, T_{1H}, of black spruce cellulose and lignin. He found that the T_{1H} of both lignin and cellulose shows a strikingly similar variation with pH, suggesting some type of molecular connectivity between these two cell wall components [18,19].

Larsson *et al.* [20] showed that solid state CP/MAS ^{13}C NMR can be used in conjunction with spectral fitting to monitor changes in the cellulose structure due to different chemical, mechanical and thermal treatments. They also used this technique to successfully determine the interactions between cellulose present at the fibril surfaces and hemicellulose.

Teckley *et al.* [21] studied the effect of steam explosion on the morphology of wood at the molecular level. Steam explosion is a process in which wood chips are contacted with superheated steam under high pressure for a brief period of time, after which the pressure is released, resulting in explosive difibrilation. They demonstrated that upon steam explosion, the molecular mixing of the different wood polymers was reduced as evidenced by the distinct $T_{1\rho}$ of the different wood components.

Other studies [22,23] have shown the utility of using cross-polarization relaxation data to study morphological heterogeneities in polymers. Marcinko *et al.* [24,25] have also shown that T_{CH} relaxation times can be correlated with the dynamic storage modulus, E', for many synthetic polymers.

Thus, by measuring different relaxation parameter e.g. T_1, $T_{1\rho}$ and T_{CH}, we can successfully probe the morphology and dynamics of different wood systems. In fact, these techniques are increasingly used to gain insight on different wood-adhesive interphases. These studies may broadly be divided into two types: one dealing with the changes in the bondline with respect to the adhesive and the other dealings with the changes in the wood polymer relaxations due to adhesive interactions.

Marcinko *et al.* [26-28] studied the effect of adhesive on the molecular motions of wood in different wood composites. They showed that liquid isocyanate resin decreased wood component $T_{1\rho H}$ in Aspen wood due to the achievement of intimate contact between the resin and wood polymers through plasticization [26]. The same group studied the changes in the molecular and bulk dynamics of southern pine wood polymers in PMDI and UF wood composites [27]. The results showed that the $T_{1\rho H}$ values of the different wood polymers in UF/pine composites were similar to that of the neat wood

polymers, while those in PMDI/pine wood composites were significantly different from the neat wood polymers. As in Aspen wood, PMDI significantly decreased the $T_{1\rho H}$ relaxations in Southern Pine. The different $T_{1\rho H}$ relaxations in pine and PMDI/pine composite were due to penetration and intimate association of PMDI with wood polymers (in the range of 1-3 nm), which lead to changes in the packing of the wood polymers. In contrast, UF-coated wood exhibited no change in $T_{1\rho H}$ and hence there was no interaction between the UF resin and wood polymers.

In another study, Marcinko *et al.* [28] used solid state inversion recovery cross polarization (IRCP) NMR experiments to probe the near static motions of aspen wood polymers (by monitoring changes in T_{CH}) in the presence and absence of cured PMDI adhesive. Results showed that PMDI modified the physical nature of wood by decreasing the molecular mobility of lignin and hemicellulose carbons. These changes were ascribed to the ability of PMDI to achieve intimate contact with the wood polymers through plasticization. Frazier *et al.* [29] studied the effect of PMDI resin on yellow poplar $T_{1\rho}$s. They found that PMDI had no effect on the relaxations of the different components of yellow poplar, which was ascribed to the inability of the PMDI resin to penetrate and come into intimate contact with the wood polymers within the time-scale of the experiment.

Numerous studies have shown that the in-situ wood adhesion mechanisms can be directly investigated by probing the wood-adhesive bondline with solid state CP/MAS NMR. Fine structural and morphological information of the bondline may be obtained by enriching the adhesive with magnetically active nuclei. This technique has been

extensively used to probe the chemistry and morphology of wood-isocyanate bond lines [30-35].

The wood-isocyanate bondline chemistry had been analyzed with ^{13}C CP/MAS experiments [9] and the signals due to the different wood components and that of the resin is well established. Figure 3.3.3 shows the ^{13}C CP/MAS spectra of yellow-poplar wood bonded with a ^{13}C-labeled PMDI resin.

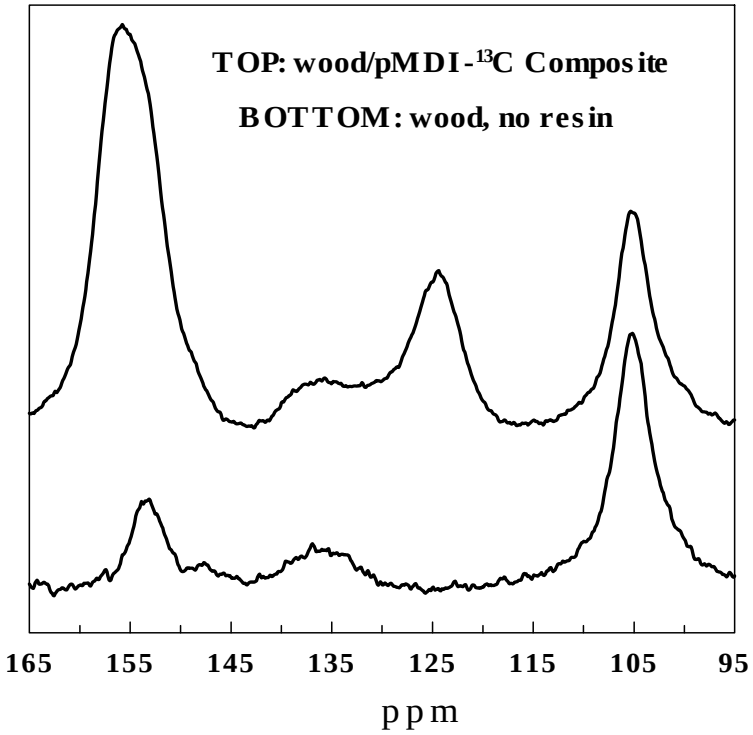

Figure 3.3.3. ^{13}C CP/MAS spectra of neat yellow poplar and yellow poplar bonded with ^{13}C-PMDI resin

The figure shows that due to the strong signals from labeled carbons, overlap of wood resin signals are of little concern. In comparison, ^{15}N NMR spectra lack contributions from wood signals, allowing the direct observation of resin chemistry for nitrogenous adhesives such as PMDI. Thus, fewer signals coupled with broader spectral width make the interpretation of ^{15}N spectra relatively easier than the corresponding ^{13}C spectra.

Several studies [36-39] have shown the advantages of ^{15}N CP/MAS over similar ^{13}C experiments. The resonances arising from the resin in the wood-PMDI system are well studied and are shown in the following table (3.3.1).

Table 3.3.1. Chemical Shifts of different chemical species in wood-PMDI^{15}N bondline

Chemical species	Chemical Shift (ppm)
Isocyanate	44
Urea	104
Biuret Amide	111
Biuret Imide	138

Wendler and Frazier [30-32] used ^{15}N CP/MAS experiments to study the effect of cure temperature, cure time and wood moisture content on the cure chemistry and bond morphology of the wood-PMDI-^{15}N bondline. They showed that at lower cure temperatures, the bondline is dominated by polyurea with lesser amounts of biurets; but as the cure temperature is increased, a clear shift from polyurea to biuret type structures was observed. With increase in cure time, the concentration of urea increased significantly with a slight increase in biuret imide. The increase in urea was attributed to the thermal degradation of biuret producing urea and isocyanate [40]. Wendler and Frazier [30] also showed that wood moisture has a significant effect on the wood-PMDI cure chemistry. The bondline was dominated by biuret-type structures at low moisture conditions, but at higher moisture content (>6%), there was a significant formation of polyurea-type structures. Similar results were also reported by Bao *et al.* [33]. Ni and Frazier[34] studied the effects of resin molecular weight and structural isomerism in PMDI on the cure chemistry of the wood-PMDI bondline by similar techniques. Their results showed that the cure chemistry of wood with lower molecular weight resins were similar to those with relatively higher molecular resins, but the formation of biuret-type

structures was less prevalent with lower molecular weight resins. They also showed that the cured network formed by resins high in 2,4'-MDI was more mobile in the mid-kilohertz frequency range than the 4,4'-PMDI network. But all the work with the singly labeled resin failed to detect any significant urethane formation due to the overlap of the urea and urethane signals [29-32].

In 2001, Zhou and Frazier [35] claimed to show the presence of covalent urethane linkages in the wood-PMDI bondline by solid state NMR. In their study they used a doubly labeled PMDI resin, having ^{15}N and ^{13}C labels in the isocyanate functional groups.

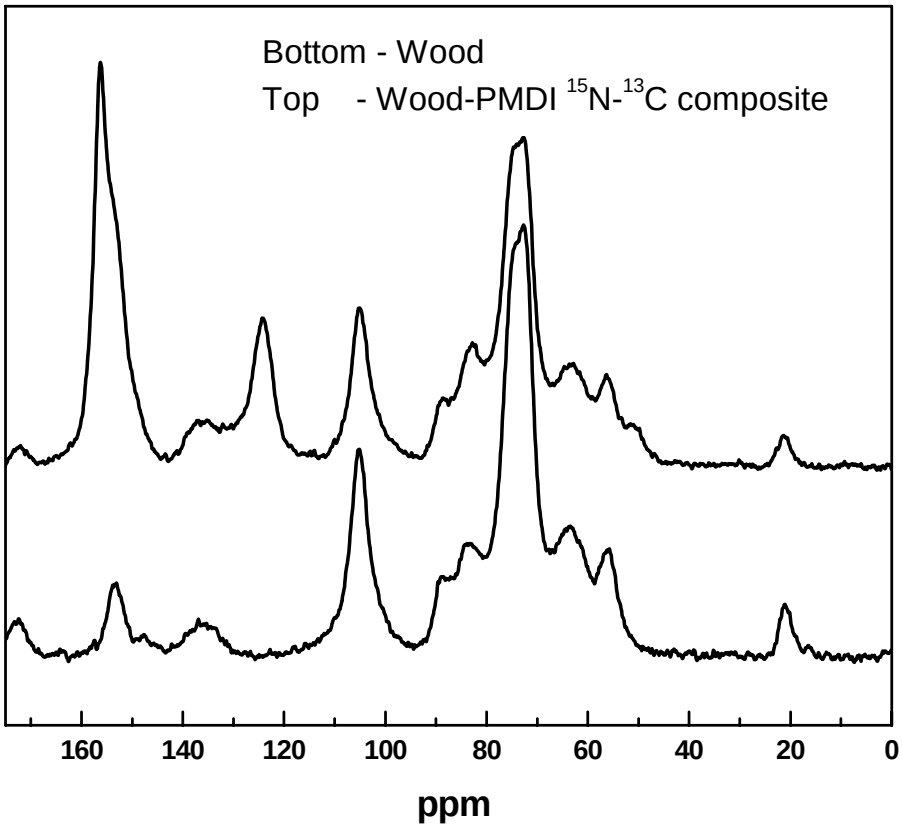

Figure 3.3.4. ^{13}C CP/MAS NMR spectra of yellow poplar and wood composite bonded with doubly labeled PMDI resin.

The double label served two purposes:

- Firstly, the ^{15}N nucleus significantly decreased the carbon broadening (0.7-1.3 ppm), thereby providing partial resolution of the urea and urethane carbonyl signals in the carbon spectra.
- Secondly, the double label provided complementary carbon and nitrogen spectra that helped in the interpretation of the spectra.

The authors claimed that the 156 and 154 ppm peaks in the carbon spectra were due to urethane and urea respectively. Similarly the urea and urethane signals in the nitrogen spectra occurred at 104 and 102 ppm respectively.

Thus, the authors successfully showed the utility of solid state CP/MAS NMR coupled with doubly labeled PMDI in the study of the adhesive mechanism in wood-PMDI systems. In addition, the relaxation parameters ($T_{1\rho}$ and T_{CH}) may be utilized to study the morphology of the bondlines at a molecular scale.

References

(1) Andrew, E. R.; Bradbury, A.; Eades, R. G. *Nature (London)* **1959**, *182*, 1659.
(2) Andrew, E. R.; Eades, R. G. *Discuss. Faraday Soc.* **1972**, *34*, 38.
(3) Lowe, I. J. *Physical Review Letters* **1959**, *2*, 285.
(4) Koenig, J. L. *Spectroscopy of Polymers*; American Chemical Society: Washington D.C., 1992.
(5) Gerstein, B. C. *Analytical Chemistry* **1983**, *55*, 899A.
(6) Pines, A.; Gibby, M. G.; Waugh, J. S. *Jour. of Chem. Phys.* **1973**, *59*, 569-590.
(7) VanderHart, D. L.; Khoury, F. *Polymer* **1984**, *25*, 1589.
(8) Mehring, M. *High-Resolution NMR Spectroscopy of Solid Polymers*; Springer-Verlag: Berlin, 1983.
(9) Kolodziejski, V.; Frye, J. S.; Maciel, G. E. *Analytical Chemistry* **1982**, *54*, 1419.
(10) Gil, A. M.; Pascoal, C. *Annual Reports on NMR Spectroscopy* **1999**, *37*, 76.
(11) Newmann, R. H. *Viscoelasticity of Biomaterials*; American Chemical Society: Washington D.C., 1992.
(12) Tekely, P.; Vignon, M. R. *Journal of Polymer Science: Part C: Polymer Letters* **1995**, *29*, 19.
(13) Newmann, R. H. *Holzforschung* **1996**, *46*, 205.
(14) Willis, J. M.; Herring, F. G. *Macromolecules* **1987**, *20*, 1554.
(15) Kosikova, B.; Hricovini, M.; Cosentini, C. *Wood Science and Technology* **1999**, *33*, 373-380.
(16) Kosikova, B.; Hricovini, M.; Simonutti, R. *Cellulose Chem. Technol.* **1995**, *29*, 683-690.
(17) Ahvazi, B.; Argyropoulos, D. S. *Wood Science and Technology* **2000**, *34*, 45-53.
(18) Argyropoulus, D. S.; Morin, F. G. *Wood Science and Technology* **1995**, *29*, 19-30.
(19) Argyropoulus, D. S.; Morin, F. G.; Lapcik, l. *Holzforschung* **1995**, *49*, 115-118.
(20) Larsson, P. T.; Hult, E.; Wickholm, K.; Pettersson, E.; Iversen, T. *Solid State Nuclear Magnetic Resonance* **1999**, *15*, 31-40.
(21) Tekely, P.; Vignon, M. R. *Journal of Chemistry and Technology* **1987**, *7*, 215.
(22) Cory, D. G.; Ritchey, W. M. *Macromolecules* **1989**, *22*, 1611-1615.
(23) Parker, A. A.; Marcinko, J. J.; Sheih, Y. T.; Sheilds, C.; Hedrick, D. P.; Ritchey, W. M. *Polymer Bulletin* **1989**, *21*, 229-234.
(24) Marcinko, J. J.; Parker, A. A.; Rinaldi, P. L.; Ritchey, W. M. *Journal of Applied Polymer Science* **1994**, *51*, 1777-1780.
(25) Marcinko, J. J.; Parker, A. A.; Sheih, Y. T.; Ritchey, W. M. *Journal of Applied Polymer Science* **1992**, *45*, 391-398.
(26) Marcinko, J. J.; Newmann, W. H.; Phanopoulos, C. In *Proc. Second Bio-based Composites Symposium*: University of British Columbia, Vancouver, British Columbia, Canada, 1994; pp 286-293.
(27) Marcinko, J. J.; Devathala, S.; Rinaldi, P. L.; Bao, S. *Forest Products Journal* **1998**, *48*, 81-84.
(28) Marcinko, J. J.; Rinaldi, P. L.; Bao, S. *Forest Products Journal* **1999**, *49*, 75-78.
(29) Frazier, C. E.; Ni, J. *International Journal of Adhesion and Adhesives* **1998**, *18*, 81-87.

(30) Wendler, S. L.; Frazier, C. E. *Journal of Adhesion* **1995**, *50*, 135-153.
(31) Wendler, S. L.; Frazier, C. E. *International Journal of Adhesion and Adhesives* **1996**, *16*, 179-186.
(32) Wendler, S. L.; Frazier, C. E. *Journal of Applied Polymer Science* **1996**, *61*, 775-782.
(33) Bao, S.; Daunch, W. A.; Sun, Y.; Rinaldi, P. L.; Marcinko, J. J.; Phanopoulos, C. *Journal of Adhesion* **1999**, *71*, 377-394.
(34) Ni, J.; Frazier, C. E. *Journal of Adhesion* **1998**, *66*, 89-116.
(35) Zhou, X.; Frazier, C. E. *International Journal of Adhesion and Adhesives* **2001**, *21*, 259-264.
(36) Duff, D. W.; Maciel, G. E. *Macromolecules* **1990**, *23*, 3069.
(37) Duff, D. W.; Maciel, G. E. *Macromolecules* **1990**, *23*, 4367.
(38) Duff, D. W.; Maciel, G. E. *Macromolecules* **1991**, *24*, 387.
(39) Duff, D. W.; Maciel, G. E. *Macromolecules* **1991**, *24*, 651.
(40) Fabris, H. J. *Advances Ureth. Sci., Technol.* **1976**, *4*, 89.

3.4. Differential Scanning Calorimetry

Differential Scanning Calorimetry (DSC) is a technique in which heat flow changes are measured as a sample is exposed to a controlled thermal profile. It provides both qualitative and quantitative information about material transitions such as glass transition (T_g), crystallization, curing, melting, decomposition, oxidation and phase changes as a function of temperature and time.

DSC has been used extensively in analyzing the cure of various thermosetting resins. This is because it provides quantitative measurements of the heat associated with the process, thus revealing the reaction kinetics. Thermoset cure can be broadly divided into two typical models: n^{th} order and autocatalytic reactions [1].

Thermosets obeying n^{th} order kinetics show a maximum rate of heat evolution at t=0 [1], i.e. during isothermal cure, the cure exotherm peak for these thermosets occur almost at the start of the experiment. The conversion rate of a thermoset cure following n^{th} order kinetics may be expressed as

$$\frac{d\alpha}{dt} = k(1-\alpha)^n \qquad (3.4.1)$$

where, $d\alpha/dt$ is the reaction rate,

α is the fractional reaction conversion,

k is the specific rate constant

n is the reaction order.

In an autocatalyzed cure, one of the reaction products acts as a catalyst for further reaction. During isothermal cure, these systems show maximum heat evolution at 30-40% of the reaction[1]. The kinetics of such a thermoset cure may be expressed as

$$\frac{d\alpha}{dt} = k\alpha^{m}(1-\alpha)^{n} \qquad (3.4.2)$$

where, k is the rate constant

m and n are the reaction orders.

The cure kinetics of most systems may be analyzed by three methods: single heating rate method (Borchardt-Daniels), multiple heating rates (Ozawa) and the isothermal method [2]. The isothermal method provides the most reliable and accurate description of a cure reaction [2]. Single heating rate methods are attractive because of the wealth of information they provide from a single DSC experiment. But in general, this method is inconsistent in its ability to reproduce isothermal kinetic parameters. But it can be used for comparative studies, for example for evaluating the effectiveness of different catalysts. Multiple heating rate methods provide reliable estimates of E_{act} for most reactions without detailed knowledge of the reaction mechanisms. They are also effective in estimating kinetic information for systems that cannot be studied easily by other methods. These include systems having multiple reactions, irregular baselines and residual solvents [2].

3.4.1. Isothermal method

This method is used for the complete characterization and modeling of any cure reaction. It is applicable for both n^{th} order and autocatalytic reactions. But it is not applied for endothermic reactions or crystallization kinetics [3].

Two basic parameters have to be determined from the DSC experiments in order to characterize any reaction with this technique. They are the reaction rate $\left(\frac{d\alpha}{dt}\right)$ and

fractional reaction conversion (α). The reaction rate is determined by dividing the peak height $\left(\frac{dH}{dt}\right)$ at time t by the total heat of the reaction (ΔH_0).

$$\frac{d\alpha}{dt} = \frac{\left(dH/dt\right)}{\Delta H_0} \tag{3.4.3}$$

α is determined by dividing the partial heat of reaction (ΔH_t) at time t by the total reaction heat.

$$\alpha = \frac{\Delta H_t}{\Delta H_o} \tag{3.4.4}$$

For n^{th} order reactions, n and k can be determined from the slope and intercept of the plot of $\ln\left(\frac{d\alpha}{dt}\right)$ vs. (1-α) respectively. For autocatalyzed reactions, k and n may be calculated from the slope and intercept of the plot of $\ln\left(\frac{d\alpha}{dt}\right)$ vs. $\ln \alpha^{\frac{m}{n}}(1-\alpha)$. The second reaction order, m, may be calculated by substituting the values of k and n and solving equation 2.

3.4.2. Single heating rate (Borchardt and Daniels) method:

This method allows the calculation of activation energy (E_{act}), pre-exponential factor (Z), heat of reaction (ΔH), *n* and k from a single DSC experiment. This approach [3] assumes that the cure reaction follows the n^{th} order kinetics and the temperature dependence of the cure reaction follows the Arrhenius relationship as

$$k = Ze^{-\frac{E_{act}}{RT}} \tag{3.4.5}$$

where, Z is the pre-exponential factor or Arrhenius factor (1/sec),

E_{act} is the activation energy (J/mol)

R is the universal gas constant (8.314 J/mol°K)

Combining equation 3.4.1 and 3.4.5,

$$\frac{d\alpha}{dt} = Ze^{-\frac{E_{act}}{RT}}(1-\alpha)^n \qquad (3.4.6)$$

Taking the logarithm, we get

$$\ln\left(\frac{d\alpha}{dt}\right) = \ln Z - \frac{E_{act}}{RT} + n\ln(1-\alpha) \qquad (3.4.7)$$

Equation 4 may be solved by a multiple linear regression (z = a + bx + cy). E_{act} and Z may be determined from the slope and intercept of the regression line. This method is attractive because it provides a great deal of information from a single DSC experiment. It is fairly rapid and works reasonably well for simple first order reactions. But previous studies have shown that, for most thermoset cure reactions, this method consistently overestimates E_{act} and Z compared to parameters obtained from isothermal experiments [1]. This method is not consistently reliable for predicting cure reactions over a wide time-temperature range [2]. It is also not applicable for autocatalyzed reactions and reactions having overlapping cure peaks [4-6].

3.4.3. Multiple heating rate (Ozawa) method:

This ASTM [7] (E698-79) recommended method requires three or more DSC experiments at different heating rates (β), usually between 1° and 10°C/min. The different assumptions of this model are

- First-order kinetics
- Arrhenius temperature-dependence

- Isoconversion, i.e. the extent of reaction at peak exotherm is constant and independent of heating rate

Combining equation 3.4.1 and 3.4.5 yields

$$\frac{d\alpha}{dt} = Ze^{-\frac{E_{act}}{RT}}(1-\alpha) \tag{3.4.8}$$

Incorporation of heating rate, β $\left(=\frac{dT}{dt}\right)$ in the above equation and rearranging,

$$\frac{d\alpha}{dT} = \frac{Z}{\beta}e^{-\frac{E_{act}}{RT}}(1-\alpha) \tag{3.4.9}$$

Kissinger [8] showed that the pre-exponential factor may be expressed as

$$Z = \frac{\beta E_{act} e^{\frac{E_{act}}{RT_p}}}{RT_p^2} \tag{3.4.10}$$

where, T_p is the temperature of the exotherm peak.

Rearranging and taking logarithm of the above equation yields,

$$-\ln\left(\frac{\beta}{T_p^2}\right) = \frac{E_{act}}{RT_p} - \ln\left(\frac{ZR}{E_{act}}\right) \tag{3.4.11}$$

Thus, E_{act} and Z may be calculated from the slope and intercept of a plot of $-\ln\left(\frac{\beta}{T_p^2}\right)$ vs. $\frac{1}{T_p}$.

Studies have shown that this method gives accurate (relative to isothermal experiments) estimation of E_{act}, Z and k for n^{th} order reactions [9]. For autocatalyzed systems, this method gives accurate estimation of E_{act} and good estimation of Z [2]. The

error in estimation of Z is due to the assumption of n^{th} order reaction kinetics [3]. This method is not applicable to systems that do not follow n^{th} order kinetics and Arrhenius behavior. Systems where isomerzation occurs at the reaction temperature or decomposition occurs during melting cannot be modeled by this method [9]. These systems should instead be modeled by isothermal methods.

3.4.4. Past studies on the characterization of PMDI cure by DSC

Review of literature over the last decade reveals only a few studies which deal with the characterization of wood-PMDI cure by DSC [10-15]. Marcinko *et al.* compared the reaction of Phenol-formaldehyde (PF) and PMDI resins in the presence of wood [13]. Results showed that while a cure exotherm (~105°C) was observed for the reaction between PMDI resin and wood, none was observed for the PF and wood samples. This led the authors to conclude that the reinforcing of wood by PMDI resin results from the combination of deep penetration of the resin and formation of chemical bonds (primary or secondary) after curing.

Vadja *et al.*[15] also showed that the PMDI-wood and PF-wood reactions are different. They also studied the PMDI-wood reactions with water and wood flour equilibrated at different moisture contents (MC). For the PMDI-water reaction, the authors found an endothermic (110°C) and an exothermic (150°C) peak; the latter was attributed to the formation of urea and polyurea. The reaction of PMDI with wood was found to be different from that with water. At low MC (5%), an exothermic peak (40° - 50°C) was obtained, which increased with the PMDI content (up to ~28% PMDI). The presence of this low temperature peak suggested a rapid reaction between PMDI and

wood. A broad endothermic peak (similar to that observed in PMDI-water reaction) was also observed at 70°-90°C. With increase in MC, the intensity of the exothermic peak at 40°C decreased, while the endothermic peak intensity increased. The latter peak also shifted to higher temperatures with increase in PMDI content (from 80°C at 0% PMDI to 95°C at 28% PMDI). Additional degradation peaks (endothermic at 240°C and exothermic at 280°C) were observed in the PMDI-wood thermograms that were absent in the neat wood thermograms. This led the authors to conclude that the thermal stability of PMDI-wood system was less than that of neat wood.

Pizzi *et al.* [14] studied the curing reaction of MDI with water, cellulose and wood. MDI was found to react with water in the temperature range of 87°-99°C (E_{act} ~ 430 kJ/mol). Dry cellulose- and wood-MDI systems showed two exothermic peaks in the temperature ranges of 128°-177 and 241°-295°C. These reactions were attributed to the formation of covalent bonds between wood and resin. These reactions were found to be catalytically activated in the presence of lignocellulosic substrates (lower E_{act} ~ 50 kJ/mol).

Harper *et al.*[10, 11] conducted extensive studies on the cure kinetics of wood-PMDI system with DSC and micro-dielectric analysis (μDEA). They initially studied the PMDI-wood reaction using the ASTM E698-79 (Multiple-heating rate/Ozawa) method. But they observed that the assumptions of the ASTM model (i.e. the exothermic peak occurs at a constant cure and it follows n^{th} order kinetics) are violated in the wood-PMDI system [10]. So they modified the ASTM method to fit the autocatalyzed PMDI-wood reaction. The modified ASTM method predicted slightly higher E_{act} than the ASTM method. The authors also characterized the PMDI-wood reaction in saturated steam environments by

μDEA. E_{act} and Z values obtained from μDEA were found to be higher than those obtained by DSC. This led the authors to conclude that DSC was more sensitive to the onset of cure while μDEA was more sensitive to changes occurring during the formation of the network.

Recently, He *et al.* [12] studied the effect of moisture on the cure kinetics of the wood-PMDI system. The curing reaction for the resin was significantly different between oven-dried wood and wood with moisture. In the absence of moisture, the resin was thought to react with the wood hydroxyl groups, which was diffusion controlled. But in the presence of moisture, the dominant reaction was that between resin and water. The kinetic parameters (E_{act}, k) were found to be significantly lower in the absence of moisture.

References

1. Park, B.-D.; Rield, B.; Hsu, E. W.; Shields, J. *Polymer* **1999,** 40, 1689-1699.
2. Prime, R. B., In *Thermal Characterization of Polymeric Materials*, Turi, E. A., Ed. Academic Press: New York, 1997; Vol. 2, pp 1380-1744.
3. Instruments, T. A. A Review of DSC Kinetics Methods. www.tainst.com
4. Prime, R. B.; Sacher, E. *Polymer* **1972,** 12, 455.
5. Prime, R. B. *Polymer Eng. Sci.* **1973,** 4, 155.
6. Taylor, L. J.; Watson, S. W. *Analytical Chemistry* **1970,** 42, 297.
7. ASTM-E-698, Philadelphia, PA, 1988; Vol. 14.02.
8. Kissinger, H. E. *Analytical Chemistry* **1957,** 29, 1702.
9. Duswalt, A. A. *Thermochemica Acta* **1974,** 8, 57-68.
10. Harper, D. P.; Walcott, M. P.; Rials, T. G. *International Journal of Adhesion and Adhesives* **2001,** 21, 137-144.
11. Harper, D. P.; Walcott, M. P.; Rials, T. G. *Journal of Adhesion* **2001,** 76, 55-74.
12. He, G.; Yan, N. *International Journal of Adhesion and Adhesives* **2005,** 25, 450-455.
13. Marcinko, J. J.; Newman, W. H.; Phanopoulos, C. In 29th International Particleboard/composite Materials Symposium, Pullman, Washington, 1995; pp 175-183.
14. Pizzi, A.; Owens, N. A. *Holzforchung* **1995,** 49, 269-272.
15. Steiner, P. R.; Chow, S.; Vadja, S. *Forest Products Journal* **1980,** 30, (7), 21-27.

3.5. Dynamic & Static Mechanical Analysis

3.5.1. Dynamic Mechanical Analysis

Dynamic mechanical analysis (DMA) is invaluable for the determination of mechanical properties of polymeric materials over a range of time (frequency) and temperature, and also plasticizer content. The thermal transitions detected with DMA are a manifestation of various molecular motions (both short and long range) as well as primary and secondary interactions. Consequently, DMA is useful for conducting structure-property relationships and for developing an improved understanding of polymer morphology. In DMA, an oscillating sinusoidal stress (σ) is applied at a specific frequency and the material response (strain,ε) is measured. The phase lag (δ) between the response (ε) and the applied deformation (σ) depends on the nature of the material tested. For a perfectly elastic material, there is no phase lag between σ and ε ($\delta = 0°$). In a purely viscous material, the phase lag is 90°, whereas, in a viscoelastic material, the phase lag is somewhere between 0° and 90°. The stress in a dynamic experiment is referred to as a complex stress (σ^*) with two separate components (elastic stress, σ', and viscous stress, σ") as shown in the following equation:

$$\sigma^* = \sigma' + i\sigma'' \tag{3.5.1}$$

The elastic stress is in phase with the strain ($\sigma' = \sigma^* cos\delta$) and represents the degree to which the material behaves as an elastic solid. The viscous stress, on the other hand, represents the viscous response of the material.

The modulus measured by DMA is called the complex modulus, E^*, and is different from the Young's modulus, which is measured from the slope of the initial

linear portion of a stress-strain curve [1]. *E** is comprised of two independent viscoelastic properties:

- The real part, which is in phase with E^*, is known as the Storage Modulus ($E' = E^* cos\delta$) and measures the elasticity of the material i.e. the ability of the material to store energy.
- The imaginary part, representing the out of phase component of E^*, is known as the Loss Modulus ($E'' = E^* sin\delta$) and measures the ability of the material to dissipate energy.

The ratio of the loss and storage modulus is the tangent of the phase angle ($tan\delta$) and measures the material damping. The following figure (fig. 3.5.1) shows the vector representation of the relationships between the various dynamic viscoelastic parameters.

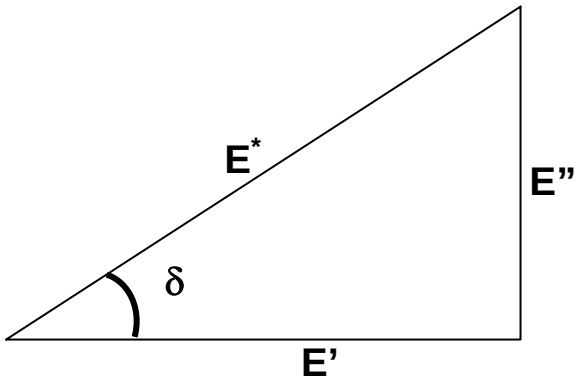

Figure 3.5.1. Vectorial representation of dynamic viscoelastic properties

One of the most important requirements of DMA is that the material should be deformed at an amplitude (or strain %) within the linear viscoelastic region (LVR) of the material. The linear viscoelastic region may be defined as the region in which the material stiffness (*E*) is independent of the strain, or a region where the stress-strain curve has a constant slope, as shown in the following figure (fig. 3.5.2).

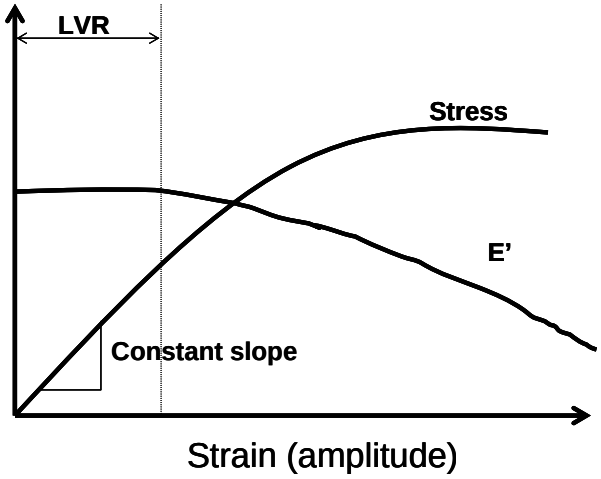

Figure 3.5.2 Determination of the linear viscoelastic region of a material

In the LVR, the response of the material is independent of the amount of deformation of the sample and the structure (packing order) of the material remains intact. Thus, the differences in the dynamic mechanical responses can be directly related to the differences in the material structure. This in turn yields a characteristic "fingerprint" of the material structure [2].

3.5.1.1. Thermal Analysis by DMA

Dynamic mechanical analysis is an important tool for thermal analysis. It is found to be much more sensitive (10 to 100) to polymeric thermal transitions than Differential Scanning Calorimetry (DSC) or Differential Thermal Analysis (DTA) [1].

The main thermal transition in an amorphous polymer is the glass transition temperature (T_g) or α-transition, which is associated with the onset of long-range cooperative segmental motions. It is the temperature at which a polymer changes from a glassy to a rubbery state, accompanied by a drastic change in its mechanical properties. In most polymers, the modulus drops by a factor of ~10^3 in a range of 20°-30°C [3]. It is also

known as a second order transition. This is because the second derivative of free energy e.g. heat capacity, C_p $\left(=\left(\frac{dH}{dT}\right)_P\right)$ and coefficient of thermal expansion, α $\left(=\frac{1}{V}\frac{d}{dT}\left\{\left(\frac{dG}{dP}\right)_T\right\}_P\right)$ undergo discontinuities at T_g as shown in figure 3.5.3.

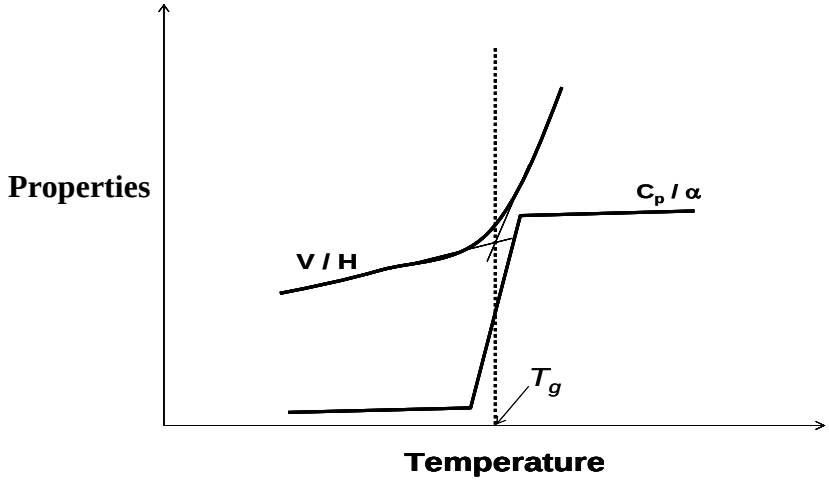

Figure 3.5.3. Variation of different material properties with temperature

The figure also shows that at T_g, the specific volume (V) and enthalpy (H) undergo a change in slope, instead of a sharp change or discontinuity [4].

In DMA, T_g is assigned as the onset of decrease in *E'* and as peaks in *E"* or *tanδ*. For the same T_g, the *tanδ* peak occurs at the highest temperature, followed by the *E"* peak, while the onset of *E'* decrease occurs at the lowest temperature. It is a common practice to assign T_g as the *tanδ* peak. The shape and height of the *tanδ* peak also gives an idea of the amorphous content of the polymer [5].

Below T_g, the long-range cooperative chain movements cease, but there are still motions in the polymer chains, known as sub-T_g transitions. The different sub-T_g transitions are due to small scale motions such as:

- Intramolecular rotation of main chain segments (4 – 6 atoms in length)

- Cooperative motion of side groups with the main chain
- Side-chain motions independent of the main chain
- Motion of small molecules (diluents, plasticizers etc.)

These motions are sometimes too weak to be determined by DSC or DTA, but can easily be observed by DMA or Dielectric Analysis (DEA). The main difference between T_g and the sub-T_g transitions is the degree of coordination required among the chains during the respective relaxations. Side group motions give rise to a β-transition and are sometimes related to the toughness of polymers. The movement of small molecules due to free volume effects gives rise to γ-transitions. The approximate activation energies for the different transitions are shown in the following table (3.5.1).

Table 3.5.1 Activation energies of different thermal transitions [1]

Transitions	Activation Energy (kJ/mol)
α	300 - 400
β	20 - 30
γ	3-4

The activation energy (E_a) of a transition may be determined by performing a temperature scan at different frequencies (f). With increase in frequency, T_g shifts to higher temperatures. The frequency-dependence of T_g may be described by an Arrhenius type equation

$$f = f_0 e^{-\frac{E_a}{RT}} \qquad (3.5.2)$$

where, f_o is a pre-exponential factor

T is the peak temperature at a certain frequency f.

Thus, the activation energy may be determined from the slope of the plot of ln$f$ vs. $(T)^{-1}$.

The following figure (fig 3.5.4) shows the variation of *E'* with change in temperature as determined by DMA.

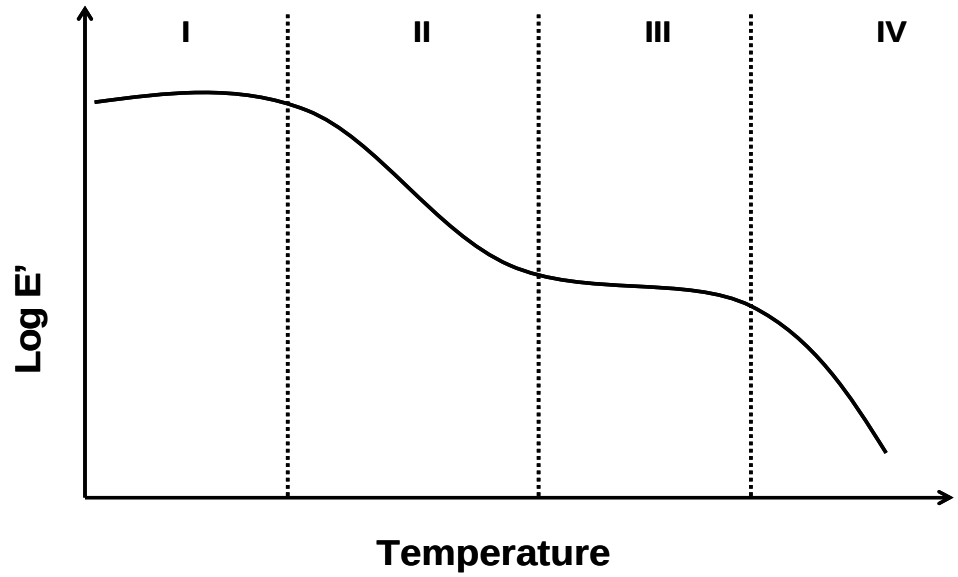

Figure 3.5.4 Hypothetical dynamic temperature scan showing the different viscoelastic regions of a polymer.

The figure shows four distinct viscoelastic regions. In **region I**, the polymer is in the glassy state and is mostly brittle. Only β- and γ-transitions can occur in this region which are uncoordinated with large-scale segmental motions. The modulus of most polymers are in the region of ~3×10^9 Pa [3]. **Region II** is the glass transition region, where the free volume increases with increasing temperature, and large segments of the polymer chain (cooperative movements) start moving. For most polymers, T_g represents the upper operating range, while for rubbery materials it is the lower operating temperature. T_g is dependent on the molecular weight of the polymer up to a critical value (T_c) above which it is independent of molecular weight. The critical molecular weight may be defined as the upper molecular weight at which molecular entanglements occur. **Region III** is

known as the rubbery plateau. Here the modulus is almost constant (~2×10^6 Pa) [3]. The length of the rubbery plateau depends on the molecular weight between entanglements (M_e) or crosslinks [1]. The modulus in this region may be increased by increasing the crosslink density or crystallinity of the material [1]. Polymers in this region exhibit the property of rubber elasticity, where the material can be stretched to a high degree without damaging the polymer structure; the material reverts back to its original dimensions when the stress is removed. **Region IV** is the terminal or liquid flow region. In this region, the kinetic energy of the polymer chains and the material free volume increases, allowing the chains to free themselves from molecular entanglements and slide past each other leading to viscous flow. The modulus again drops drastically in this region due to the disentanglement of the polymer chains or in severe cases thermal degradation. In some polymers, the modulus in this region may rise again due to crosslinking reactions.

The thermal transitions of polymers are dependent on the test frequency of a DMA experiment. With increase in test frequency, polymers become more elastic and hence are stiffer at higher frequencies. Thus, with increase in frequency the transitions shift to higher temperatures.

3.5.2. Static Mechanical Analysis (Creep)

Creep experiments involve the instantaneous application of a constant stress followed by monitoring of the resultant deformation as a function of time. The creep response of a viscoelastic material consists of three different components [6,7], namely

- Elastic deformation, which is instantaneous and recoverable
- Delayed elastic deformation, which is time-dependent and recoverable and
- Viscous deformation, which is permanent and non-recoverable.

Creep testing may be used to analyze the response of a material under service conditions. Experiments may also be conducted within the linear viscoelastic region (LVR) of the material to determine equilibrium values for viscosity, modulus and compliance [1]. The latter may be defined as the ease with which a material can be deformed and is the inverse of the modulus for an elastic material. The LVR of a material may be determined by conducting a series of creep experiments with increasing stresses. According to the Boltzmann superposition principle, the applied stress and resultant strains are linear in the LVR [1]. Thus, the linear viscoelastic limit may be defined as the stress at which the relationship between the stress and strain become non-linear [1].

Figure 3.5.5 shows a typical creep curve for a polymeric material.

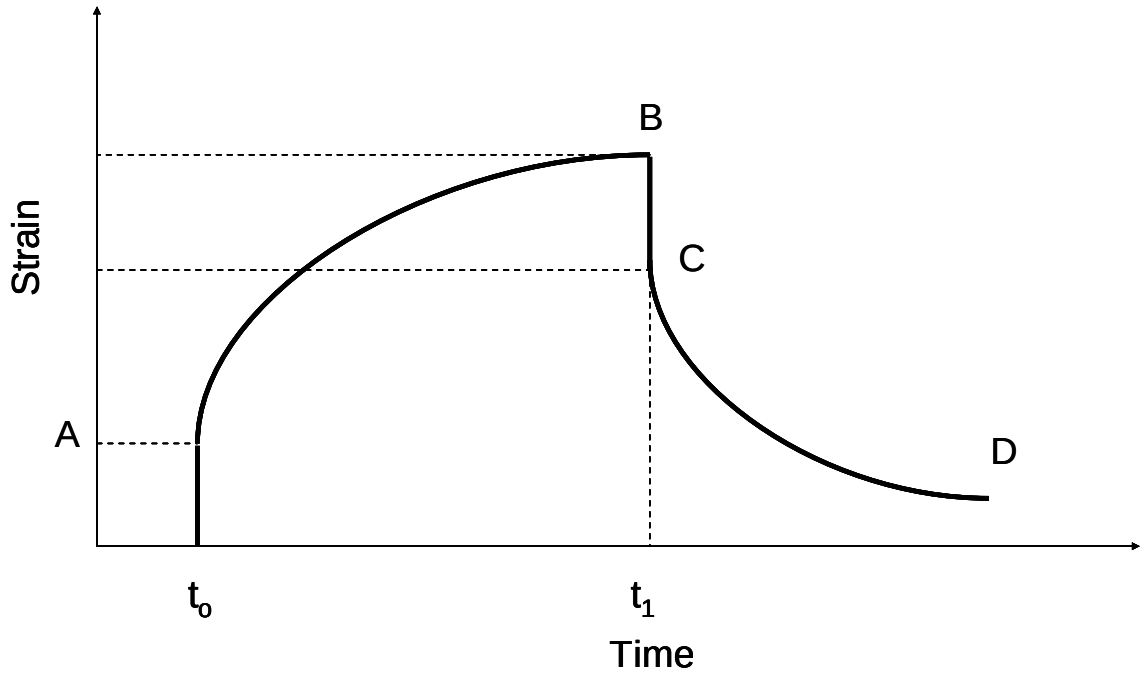

Figure 3.5.5. Typical creep curve of a viscoelastic material.

Application of the load results in an instantaneous deformation (g_1) due to the elastic component of the material. This is followed by a period of retarded deformation up to the time t_1, when the load is removed. Removal of the load also results in an instantaneous

partial recovery, followed by a time dependent recovery. After a long time, some materials exhibit a permanent deformation due to viscous flow within the sample. Thus, in a creep experiment, the viscous and elastic responses are coupled so that the material deforms gradually and in a non-linear fashion with time.

3.5.3. Time-Temperature Superposition Principle (TTSP)

The deformation and flow behavior of polymeric materials is dependent on both temperature and time (frequency). For example, modulus measurements performed at a higher frequency (i.e. lower time scales), give rise to higher values compared to measurements done over a longer time span (i.e. lower frequency). When loaded at a higher rate (i.e. smaller time-scale), the material does not have the time to rearrange; it reacts to the stress by distortion of interatomic bonds and bond-angles. These distortions require high energy and hence result in high modulus. At longer times, the chains have ample time to reorient themselves and relax to their lower energy conformations, resulting in a decrease in modulus. Thus, in order to verify material performance for any application, the material must be tested under the exact service conditions.

The difficulty of extrapolating limited laboratory test results to realistic service conditions may be overcome by the fact that the change in material properties due to temperature increase may be reproduced by decreasing the experimental time-scale and *vice versa*. Thus, there is a direct correspondence between the temperature and time-scale (frequency) of an experiment for viscoelastic materials. This is called the Time-Temperature Superposition Principle (TTSP) that was comprehensively described by the work of Williams, Landel and Ferry [8]. TTSP is also known as the “method of reduced variables” [9].

TTSP theory suggests that modulus curves of viscoelastic materials, determined at different temperatures can be exactly superimposed by shifting them horizontally along the frequency axis to generate a *mastercurve*. In most cases, the shifting is performed relative to a selected reference temperature (T_{ref}). The master curve helps us to determine material properties over a much greater frequency range than can be obtained experimentally. The amount each curve is shifted to form the mastercurve is known as the shift factor, $log\ a_T$. It may also be expressed as the ratio of relaxation times, τ, at a certain temperature to that at the reference temperature, T_{ref}.

$$a_T = \frac{\tau(T)}{\tau(T_{ref})} \tag{3.5.3}$$

where, $\tau(T_i)$ represents the relaxation time at temperature T_i.

The relaxation times are related to molecular diffusional motions that are responsible for the material's viscoelastic characteristics and are a function of the viscosity and modulus of the material [3].

The master curve may be fitted into an empirical equation developed by Williams, Landel and Ferry, known as the WLF equation [8].

$$\log a_T = \frac{-C_1\left(T - T_{ref}\right)}{C_2 + \left(T - T_{ref}\right)} \tag{3.5.4}$$

where, C_1 and C_2 are the constants obtained from curve fitting.

When $T_{ref} = T_g$, the constants are known as the universal constants and for most linear amorphous polymers $C_1 = 17.44$ and $C_2 = 51.6$. Initially, these constants were thought to be universal, but later studies showed that different polymers have different constants. For most polymers, C_1 was found to be approximately constant, but C_2 was found to vary

[10]. The constants may be determined from the intercept and slope of the plot of $\frac{1}{\log a_T}$ vs. $\frac{1}{T - T_{ref}}$.

TTSP is applicable for amorphous polymers within a temperature range of T_g to $T_g + 100$ [1,2]. For TTSP to work, the polymer should also be *thermorheologically simple*, which implies that all molecular relaxations have a similar temperature dependence; a change in temperature shifts the time/frequency scale of all relaxations by the same amount [9,11]. Thus, in thermorheologically simple materials, the entire viscoelastic spectrum at a certain temperature may be related to that at another temperature by a change in time scale only. TTSP also assumes that within the temperature range in which TTSP is performed, the five different polymer parameters, i.e. chemical composition, morphology, topology, molecular weight distribution (MWD) and stereochemistry of the polymer remain the same and only a single relaxation mechanism is involved in that temperature range.

The WLF equation was derived on the basis of two basic assumptions: firstly, the viscosity is an exponential function of the reciprocal fractional free volume (Doolittle theory) and the fractional free volume is a linear function of temperature [8,9]. Thus, the WLF equation may also be derived from the semi-empirical Doolittle equation (Equ. 3.5.5), which describes the viscosity of non-associated liquids based on the free volume concepts [12].

$$\ln \eta = \ln A + B\left(\frac{v_0}{v_f}\right) \tag{3.5.5}$$

where, A and B are constants

v_0 & v_f are the occupied and free volumes, respectively.

It was shown that the WLF constants are related to the fractional free volume at T_g (f_g) and the coefficient of thermal expansion of the free volume (α_f) as

$$C_1 = \frac{B}{2.303 f_g} \tag{3.5.6}$$

$$C_2 = \frac{f_g}{\alpha_f} \tag{3.5.7}$$

where, B is a constant and equal to unity [8].

The empirical Arrhenius equation (equ. 3.5.8) may also be used for time-temperature superposition.

$$\log a_T = \frac{E_{act}}{2.303R}\left(\frac{1}{T} - \frac{1}{T_{ref}}\right) \tag{3.5.8}$$

Both Arrhenius and WLF equations are based on the same assumptions, but in some cases, the former equation was found to fit the experimental curve-shifting data better than the WLF equation. The Arrhenius equation is generally found to fit the shift factor data better at temperatures below T_g and above T_g + 100°C [2].

3.5.4. Kohlrausch-Williams-Watts (KWW) equation and the coupling parameter (*n*)

Significant deviations from the Arrhenius behavior around T_g are commonly observed; and this is attributed to intermolecular coupling between neighboring non-bonded chain segments. The concept of molecular cooperativity was first introduced by Adam and Gibbs, with their model of glass relaxation in 1965 [13]. The Adam-Gibbs (AG) model is based on the transition state theory for molecular relaxation, which states that molecular relaxations from one state to another involve an energy barrier, where the population of each state is governed by the Boltzmann distribution [9]. In the AG model, it

was assumed that cooperative regions (having z^* molecules in each cooperative domain) simultaneously exceeded the individual energy barriers (activation energy),$\Delta\mu$, that hinder their cooperative rearrangements and these transitions were independent of temperature. This led the authors to describe a single characteristic relaxation time, $\tau(T)$, as

$$\tau(T) = \tau_\infty e^{\frac{z^*\Delta\mu}{kT}} \tag{3.5.9}$$

where, τ_∞ is the relaxation time at infinite temperature,

k is the Boltzmann constant.

The main drawback of the AG theory was its assumption that all the cooperative rearrangements were identical and occur with the same relaxation time, which in turn is a linear relaxation function. But, in most glass-forming liquids, the relaxation near T_g departs from the linear exponential behavior and may be well approximated by the Kohlrausch-Williams-Watts (KWW) function [14,15], which describes the distribution of characteristic relaxation times (τ^*) near T_g as a stretched decay function, $\phi(t)$, as follows [16],

$$\phi(t) = \exp\left[-\left(\frac{t}{\tau}\right)\right]^\beta \tag{3.5.10}$$

where, τ is the mean relaxation time,

β is the KWW-parameter, which controls the breadth of the α-relaxation in the frequency domain. The β-parameter has value between 0 and 1. β is equal to 1, when the α-transition is described by a single relaxation time. The value of β decreases with increase in the complexity of the α-relaxation process, which is exemplified by a wider

distribution of the relaxation times. The KWW function has been shown to hold only in the short-time range of the glass-rubber transition [7].

Ngai and Rendell proposed a model known as the coupling model [11,17,18], which (in the glassy state) has a similar form as that of the KWW model:

$$\phi(t) = \exp\left[-\left(\frac{t}{\tau^*}\right)^{1-n}\right] \qquad (3.5.11)$$

where, τ^* is the characteristic relaxation time of chain segments restricted by intermolecular coupling ,

n is the coupling parameter that measures the magnitude of intermolecular interactions and has magnitude between 0 and 1. Comparison of equation 10 and 11 gives,

$$n = 1-\beta \qquad (3.5.12)$$

Thus, an increase in intermolecular cooperativity will increase in the breadth of relaxation times.

Numerous studies have shown the dependence of the coupling factor, *n*, on the chemical structure of polymers [19-22]. Generally, polymers with smoother, less polar, more compact, symmetric or flexible backbones have smaller *n* values; while polymers with sterically-hindering pendent groups have larger *n* values [20]. For example, epoxidation of polyisoprene enhances the intermolecular cooperativity (higher *n*) due to steric interactions promoted by oxirane functional groups [19]. Intermolecular cooperativity of polymers was found to increase with the number of phenyl rings in the repeating units [11]. Roland *et al.* [21] also found that increases in vinyl content (inflexible pendent functional groups) of polybutadiene leads to increases in the intermolecular coupling parameter, *n*,

which was manifested as broadening of the loss modulus peak and steepening of the plot of log a_T vs. T_g/T.

3.5.5. Viscoelastic Properties of Wood

Wood is a composite of three different polymers: cellulose, hemicellulose and lignin, each of which displays characteristic viscoelastic properties due to their chemical structures, morphology and distribution in the different regions of the cell-wall. The study of the viscoelastic properties of wood may be divided into two parts: study of the isolated wood polymers and study of the in situ wood polymers.

3.5.5.1. Dynamic viscoelastic properties of isolated wood polymers

The viscoelastic properties of cellulose have been extensively studied due to its industrial importance. In wood, cellulose is present as semi-crystalline microfibrils. The melting of cellulose cannot be observed in a DMA scan because the thermal degradation temperature of cellulose is lower than its melting point. Thus, only the T_g and some characteristic secondary relaxations of cellulose can be observed by DMA. The T_g of dry isolated cellulose was shown to be ~230°C by DSC and DMA [23,24]. Studies have shown that water plays a critical effect on the cellulose T_g. The cellulose T_g was found to decrease from 220°C to sub-ambient temperatures with increase in moisture content [25]. The T_g was also found to be dependent on the cellulose crystallinity; Yano *et al.* [26] showed that with increase in crystallinity, the cellulose T_g increased from 200°C to 236°C. Apart from T_g, isolated celluloses also show two sub-ambient transitions, γ and β, at -120° and -50°C, respectively [27]. By comparing DMA and DEA data obtained from various polysaccharides e.g. cellulose, dextran, pullulan and amylose, the γ-transition was

attributed to the localized non-coupled rotational motions of the hydroxymethyl groups of cellulose [27]. Montes *et al.* [28] showed that the activation energy of γ-transitions are essentially due to enthalpic contributions. The molecular interpretation of the β-transition is still controversial. While some authors suggest that the origin of the β-relaxation is due to the motion of the hydroxymethyl groups interacting with the water molecules [27], others believe the β-relaxation process to be due to localized motions of the main chain segments [29,30]. Montes [31] showed that the β-transition was critically dependent on the moisture content and nearly disappears in dry cellulose samples. They [32] showed that the β-relaxation involves cooperative but localized chain motions and the activation energy has mainly entropic contributions. Recently, Obataya *et al.* [33] attributed the β-relaxation to the motion of adsorbed water molecules.

Hemicellulose is a low molecular weight branched heteropolysaccharide but it has a molecular structure which is similar to cellulose. Thus, like cellulose it also shows the characteristic sub-ambient γ and β transitions [33]. But the T_g of hemicellulose is lower than the cellulose: around 165°-225°C under dry conditions [34] and ~0°C under wet conditions [35]. Olsson *et al.* [36] used a new DMA technique for studying the hemicellulose softening in which the relative humidity (RH) and hence the moisture content and the temperature was precisely controlled with the help of a humidity generator. Two transitions were observed; one weak transition at 20-40% RH and another major relaxation at 50-90% RH [37]. The apparent activation energy of the major xylan transition (500kJ/mol at 16% moisture content) showed that it was due to main chain motion [37]. They showed that for isolated xylans the T_g occurred at a higher RH (76% RH) relative to glucomannan (65% RH). This was attributed to differences in the backbone structures of these

hemicelluloses. Through similar experiments they were also able to show that the xylans were closely associated with the amorphous lignin components while the galactoglucomannans were intimately associated with the crystalline cellulose microfibrils [38].

Lignin is an amorphous, highly branched, polymer containing phenylpropane repeating units. Lignin softening had been extensively studied due to its importance in the pulp and paper manufacturing process [24]. Dry isolated lignin softens around 205°C [23,24], while the presence of moisture reduces its T_g to ~100°C [35].

Thus, the various studies conducted on the viscoelastic properties of different isolated wood polymers, point to the fact that all the polymers have similar T_g's under dry conditions, which makes their study difficult. But moisture decreases the T_gs to varied degrees depending upon the hydrophilicity of the different wood polymers and hence makes it possible to study the different *in situ* wood transitions separately by varying the wood moisture content.

3.5.5.2. Dynamic *in situ* viscoelastic properties of Wood Polymers

Dynamic thermal scans of dry wood show a secondary tan δ peak ~100°C (γ-transition). Similar relaxations (by dielectric analysis) were also observed in cellulose, amylose and mannans, but not in dextran and xylans [33]. This analogous relaxation in cellulose was found to disappear completely when the methylol groups were selectively substituted with triphenylmethyl groups [39]. This suggested that the γ-relaxation was due

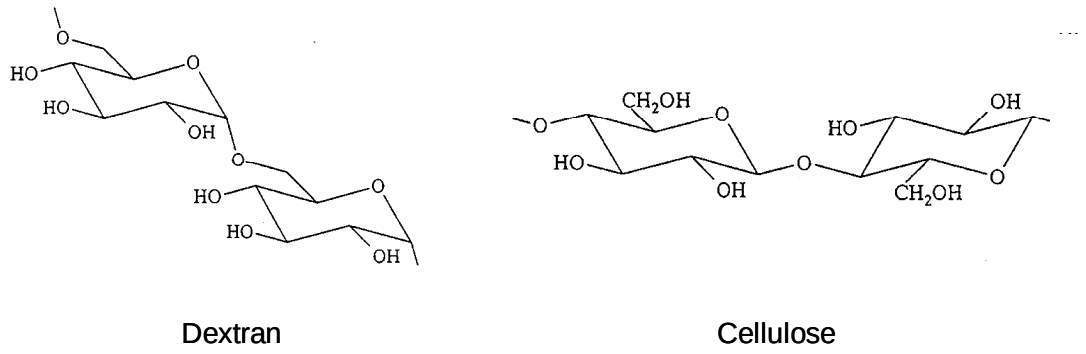

Figure 3.5.6. Chemical structures of dextran and cellulose.

to the motion of methyol groups of the cell wall amorphous polymers [33,40,41]. Chemical modification of wood was found to affect this transition significantly. The intensity of the γ-relaxation was found to decrease and its peak shifted to higher temperatures upon acetylation [33,41]. The relaxation was not affected by formaldehyde- treatment, but was found to shift to lower temperatures upon polyethylene glycol impregnation [33].

Another secondary relaxation (β-relaxation) was observed in the dynamic thermal spectra of wood at ~40°C, in the presence of adsorbed moisture. This relaxation was found to shift to lower temperatures and its activation energy was found to decrease with increase in wood moisture content (upto 15%). Formalization had no effect on this relaxation which suggested that the β-relaxation was not due to segmental motions of the main chains. The β-relaxation was attributed to the motion of adsorbed water molecules [33,40,41].

The dynamic mechanical behavior of dry wood samples was found to depend on the grain orientation of the wood samples. Backman *et al.* [40] compared the dynamic thermal spectra of dry wood in radial and tangential direction in tension mode. Though both samples had similar dynamic spectra (i.e. both showed γ- and β-relaxations), the intensity of the relaxations were found to be relatively smaller in the radial samples. The

relaxations were also found to occur at relatively higher temperatures in the tangential wood samples.

Due to its importance in the wood industry, most of the early research was focused on determining the viscoelastic properties of wood plasticized by water. Irvine [34] studied the softening of wood as a function of moisture content and found a main secondary transition around 60°-90°C, which was postulated to be due to the lignin T_g. Salmen [35] studied the viscoelastic properties of wood under water-saturated conditions in the temperature range of 20° to 140°C and demonstrated that within the studied temperature range, the major transition was due to the T_g of *in situ* lignin. He also studied the applicability of TTSP to the viscoelastic behavior of *in situ* lignin and found that the WLF equation is applicable to this system in the range of T_g (72°C) to T_g + 55°C, which was narrower than for normal synthetic polymers (T_g to T_g+100°C). He determined the WLF constants for this system to be C_1 = -18.18 and C_2 = 77.19. He also determined the activation energy for the *in situ* lignin transition to be 450 kJ/mol. In the same study, he determined the softening behavior of *in situ* lignin along and across the grain and found small differences, which were attributed to the stiffening effects of cellulose microfibrils, which are aligned preferentially along the fiber axis.

Olsson *et al.* [42] studied the effect of the structural differences in hardwood and softwood lignins on the viscoelastic properties of *in-situ* lignin. Their results showed that hardwood lignins softened at lower temperatures relative to the softwood lignins; this was attributed to the higher degree of crosslinking in the softwood lignins relative to the hardwood lignins. They also successfully applied TTSP on the different systems and determined the activation energies of the hardwood (~340 kJ/mol) and softwood (~430

kJ/mol) lignins. They also studied the effect of lignin structure on the softening behavior of different hardwoods [43]. Their results showed that lignin softening temperature decreased with an increase in the lignin methoxyl content. They attributed this due to the increase in mobility of the lignin macromolecules due to decreased crosslink density.

Kelley *et al.* [44] studied the viscoelastic response of wood over a wide range of moisture contents and over a wide temperature range (-150°C to +150°C). They observed two distinct transitions due to hemicellulose and lignin which pointed to the existence of a phase-separated incompatible blend morphology in the wood cell wall. They also found the plasticization effect of moisture on the different transitions, whereby the transitions were shifted to lower temperatures with the increase in wood moisture content. The effect of moisture on the lignin and hemicellulose transitions was found to fit the Kwei model:

$$T_g = \frac{W_1 T_{g1} + kW_2 T_{g2}}{W_1 + kW_2} + qW_1 W_2 \qquad (3.5.13)$$

where, W_i is the weight fraction of the i-th component,

T_{gi} is the glass transition temperature of the i-th component,

k is an adjustable parameter derived from free-volume considerations

q is an adjustable parameter derived from secondary interaction effects.

They also applied TTSP on the *in situ* lignin transition of wood plasticized by ethyl formamide. The WLF equation was found to be applicable over the temperature range of T_g to T_g+85°C, with WLF constants C_1 = 17.7 and C_2 = 52.1.

Wennerblom *et al.* [45] studied the viscoelastic properties of early and latewood saturated with ethylene glycol and water. Though they didn't find any significant differences between the softening behaviors of diluent-saturated earlywood and latewood, they showed the utility of using ethylene glycol as a wood plasticizer for wood DMA

studies. The depression of different *in situ* transitions was found to be significantly higher with ethylene glycol than water [46]. Studies [35,44] have shown that the William-Landel-Ferry (WLF) equation [47] can be used to study the viscoelastic properties of plasticized wood above the lignin T_g.

Several studies have also been conducted to determine the effect of different chemical treatments on the glass transitions of different wood polymers [42,48-53]. The introduction of diluents e.g. propylene oxide, methyl methacrylate, low molecular weight polyethylene glycol, and bulky groups like acyl groups was found to cause depression of the *in situ* T_g of different wood polymers. On the other hand, chemical crosslinking treatments like formalization increase the softening temperatures of the wood components. A similar result was also shown by Olsson *et al.* [42], where the T_g of *in-situ* spruce lignin was found to increase from 88°C to 113°C (at 0.5 Hz) due to the introduction of crosslinks.

Marcinko *et al.* [54,55] used DMA to compare the effects of UF and PMDI adhesives on the softening behavior of *in situ* lignin. The tan δ peaks of neat wood and wood coated with UF resin were found to be similar; but the tan δ peak of wood coated with PMDI resin was found to be broader and at a lower temperature relative to the neat wood. The broadening of the tan δ peak was attributed to a broader distribution of polymer chain dynamics in the PMDI-wood system as a result of deep adhesive penetration and intimate molecular associations. In contrast UF-coated wood did not exhibit any change in molecular level dynamics relative to the neat wood.

Recently, Laborie *et al.*[56] used cooperativity analysis to probe the *in situ* T_g of lignin in ethylene glycol plasticized wood. Though they didn't find significant differences

between hardwood and softwood species with this analysis, the utility of this technique for characterization of *in situ* transitions and wood morphology was well established.

Thus, the above discussion showed the versatility of DMA to probe the viscoelastic responses of different wood polymers. TTSP and cooperativity analysis was found to be applicable for the *in-situ* lignin and hemicellulose transitions.

3.5.5.3. Static viscoelastic properties of wood

Extensive research has been conducted on the creep behavior of wood. Most studies have been conducted in bending mode. But bending tests give information about the structural element properties and not material properties. During tests in bending mode, the stresses and strains are known to vary throughout the cross section of the sample which in turn tends to mask the true time-dependent material response [57].

Studies have shown that creep is more sensitive to temperature, moisture content and physical aging than various elastic properties [58]. The creep deformation is found to increase with increase in temperature. Bach [59] showed that the tensile creep parallel to grain of hard maple was proportional to the square of the temperature in the range of 30°-70°C. Davidson [60] performed creep and creep recovery tests in bending mode on three different wood species in the temperature range of 20°-60°C. Results showed small increase in the slopes of the recovery curves upto 50°C, followed by a large change in the temperature range of 50°-60°C, which was attributed to the scission of hydrogen bonds between the cellulose chains. Wood grain orientation also affects the creep behavior of wood; creep in shear mode was found to be less than creep perpendicular to the grain [61].

Moisture acts as a plasticizer for wood, as a result of which creep is found to increase with moisture content. Studies [59] have shown that the tensile creep compliance is

proportional to the square of the wood moisture content in the range of 4-12%. A significant increase in the creep rate and the total creep was observed, when the sample moisture content changed during test e.g. the relative creep of a loaded beam, which was allowed to dry was found to be twice than that observed under constant moisture conditions- this is referred to as the mechanosorptive effect [62]. This acceleration of creep was found to be more pronounced under cyclic moisture changes [63]. The relationship between mechanosorptive creep and the change in moisture content was found to be linear in nature [64].

Several studies [65-68] utilized the time-temperature superposition principle to predict long-term responses of wood. This was achieved by performing short-term isothermal creep experiments at different temperatures, followed by shifting of the creep isotherms with respect to a reference temperature to generate a mastercurve. The mastercurve described the long-term response of the material at the reference temperature. Bond [67] used TTSP to develop long-term creep models for different woods (Douglas-fir, southern pine, yellow-poplar) in both tension and compression modes. Short-term creep experiments (6 hr) were conducted on wood samples in the temperature range of 20° to 80°C, which were then used to construct mastercurves by both horizontal and vertical shifting at 20°C reference temperature. The shift-factor plot was linear and thus showed Arrhenius behavior; the activation energies of all wood tested were ~17 – 35 kcal/mol. The validity of the long-term creep models generated by TTSP was also successfully tested with a long-term (105 days) creep on yellow-poplar and pine samples in both tension and compression modes. Similar results were also obtained by

Samarasinghe *et al.*[68], who used TTSP to develop long-term compression creep models for southern pine.

References

(1) Menard, K. P. *Dynamic Mechanical Analysis: A Practical Introduction*; CRC Press: Washington D.C., 1999.
(2) Turi, E. A. *Thermal Characterization of Polymeric Materials*, 2nd ed.; Academic Press: New York, 1997; Vol. 1.
(3) Chanda, M. *Advanced Polymer Chemistry: A Problem solving Guide*; Marcel Dekker Inc.: New York, 2000.
(4) Ghosh, P. *Polymer Science and Technology of Plastics and Rubbers*; Tata McGraw-Hill Publishing Company Ltd.: New Delhi, 1995.
(5) Instruments, T., 2001.
(6) Bodig, J.; Jayne, B. A. *Mechnaics of Wood and Wood Composites*; Krieger Publishing Company: Malabar, Florida, 1993.
(7) Strobl, G. *The Physics of Polymers*, 2nd ed.; Springer: Berlin, 1997.
(8) Williams, M. L.; Landel, R. F.; Ferry, J. D. *Journal of American Chemical Society* **1955**, *77*, 3701.
(9) Ferry, J. D. *Viscoelastic Properties of Polymers*; John Wiley & Sons Inc.: New York, 1969.
(10) Aklonis, J. J.; Macknight, W. J. *Introduction to Polymer Viscoelasticity*, 2nd ed.; John Wiley & Sons Inc.: New York.
(11) Ngai, K. L.; Plazeck, D. J. *Rubber Chemistry and Technology Rubb. Rev.* **1995**, *68*, 376-434.
(12) Doolittle, A. K. *Journal of Applied Physics* **1951**, *22*, 1471.
(13) Adams, G.; Gibbs, J. H. *Journal of Chemical Physics* **1965**, *43*, 139.
(14) Williams, G.; Watts, D. C. *Trans. Faraday Soc.* **1970**, *66*, 80.
(15) Kohlrausch, R. *Pogg. Ann. Phys.* **1847**, *12*, 393.
(16) Riande, E.; Diaz-Calleja, R.; Prolonga, M. G.; Masegosa, R. M.; Salom, C. *Polymer Viscoelasticity: Stress and Strain in Practice*; Marcel Dekker Inc.: New York, 2000.
(17) Ngai, K. L. *Journal of Physical Chemistry B* **1999**, *103*, 5895-5902.
(18) Ngai, K. L.; Rendell, R. W. *Journal of Non-Crystalline Solids* **1991**, *131-133*, 942-948.
(19) Roland, C. M. *Macromolecules* **1992**, *25*, 7031-7036.
(20) Ngai, K. L.; Roland, C. M. *Macromolecules* **1993**, *26*, 6824-6830.
(21) Roland, C. M.; K.L.Ngai. *Macromolecules* **1991**, *24*, 5315-5319.
(22) Ngai, K. L.; Roland, C. M. *Macromolecules* **1992**, *25*, 1844.
(23) Goring, D. A. I. *Pulp Paper Mag. Can.* **1986**, *64*, T-51.
(24) Salmen, N. L. *Pulp Paper Can. Trans Techn. Sec.* **1979**, *5*, TR-45.
(25) Salmen, N. L.; Back, E. L. *TAPPI* **1984**, *60*, 137.
(26) Yano, S.; Hatakeyama, H.; T.Hatakeyama. *Journal of Applied Polymer Science* **1996**, *20*, 3221.
(27) Bradley, S. A.; Carr, S. H. *Journal of Polymer Science: Phys. Ed.* **1976**, *14*, 111.

(28) Montes, H.; Mazeau, K.; Cavaille, J. Y. *Macromolecules* **1997**, *30*, 6977-6984.
(29) Nishinari, K.; Tsutsumi, A. *Journal of Polymer Science: Phys. Ed.* **1984**, *22*, 95.
(30) Nishinari, K.; Shibuya, N.; Kainuma, K. *Makromol. Chem.* **1985**, *186*, 433.
(31) Montes, H.; Cavaille, J. Y. *Polymer* **1999**, *40*, 2649.
(32) Montes, H.; Mazeau, K.; Cavaille, J. Y. *Journal of Non-Crystalline Solids* **1998**, *235-237*, 416-421.
(33) Obataya, E.; Norimoto, M.; Tomita, B. *Journal of Applied Polymer Science* **2001**, *81*, 3338-3347.
(34) Irvine, G. M. *Tappi Journal* **1984**, *67*, 118.
(35) Salmen, L. *Journal of Materials Science* **1984**, *19*, 3090-3096.
(36) Olsson, A.-M.; Salmen, L. In *International Conference of COST Action E8*: Copenhagen, Denmark, 1997; pp 269-279.
(37) Olsson, A.-M.; Salmen, L. In *Hemicellulose: Science and Technology*; Gatenholm, P.; Tenkanen, M., Eds.; American Chemical Society: Washington D.C., 2004; pp 184-196.
(38) Salmen, L.; Olsson, A.-M. *Journal of Pulp and Paper Science* **1998**, *24*, 99-103.
(39) Hagiwara, I.; Shiraishi, N.; Yokota, T.; Norimoto, M.; Hayashi, Y. *Journal of Wood Chemistry and Technology* **1981**, *1*, 93.
(40) Backman, A. C.; Lindberg, K. A. H. *Journal of Materials Science* **2001**, *36*, 3777-3783.
(41) Sugiyama, M.; Obataya, E.; Norimoto, M. *Journal of Materials Science* **1998**, *33*, 3505-3510.
(42) Olsson, A.-M.; Salmen, L. In *Viscoelasticity of Biomaterials*, ACS Symposium Series 489 ed.; Glasser, W. G.; Hatakeyama, H., Eds.; American Chemical Society: Washington D.C., 1992; pp 133-143.
(43) Olsson, A.-M.; Salmen, L. *Nordic Pulp and Paper Research Journal* **1997**, *12*, 140-144.
(44) Kelly, S. S.; Rials, T. G.; Glasser, W. G. *Journal of Materials Science* **1987**, *22*, 617-624.
(45) Wennerblom, M.; Frovi, A. D.; Olsson, A.-M.; Salmen, L. *Nordic Pulp and Paper Research Journal* **1996**, *4*, 279-280.
(46) Sadoh, T. *Wood Science and Technology* **1981**, *15*, 57-66.
(47) William, M. L.; Landel, R. F.; Ferry, J. D. *Journal of American Chemical Society* **1955**, *77*, 3701-3707.
(48) Sugiyama, M.; Norimoto, M. *Mokuzai Gakkaishi* **1996**, *42*, 1049.
(49) Nakano, T.; Nakamura, H. *Mokuzai Gakkaishi* **1988**, *33*, 472.
(50) Olsson, A.-M.; Salmen, L. In *Cellulosics: Chemical, Biomedical and Material Aspects*; Kennedy, J. F.; Phillips, G. O.; Williams, P. A., Eds.; Ellis Horwood: New York pp 257-262.
(51) Bjorkman, A.; Salmen, L. *Cellulose Chemistry and Technology* **2000**, *37*, 7-20.
(52) Bjorkman, A. *Cellulose Chemistry and Technology* **2002**, *36*, 3-35.
(53) Bjorkman, A. In *IAWS*: Beijing, China, 2002; pp 25-36.
(54) Marcinko, J. J.; Devathala, S.; Rinaldi, P. L.; Bao, S. *Forest Products Journal* **1998**, *48*, 81-84.
(55) Marcinko, J. J.; Rinaldi, P. L.; Bao, S. *Forest Products Journal* **1999**, *49*, 75-78.
(56) Laborie, M.-P. G.; Salmen, L.; Frazier, C. E. *Holzforschung* **2004**, *58*, 129-133.

(57) Holzer, S. M.; Loferski, J. R.; Dillard, D. A. *Wood and Fiber Science* **1989**, *21*, 376-392.
(58) Bodig, J.; B.A.Jayne. *Mechanics of Wood and Wood Composites*; Van Nostrand Reinhold: New York, 1982.
(59) Bach, L.; Syracuse University: Syracuse, NY, 1965.
(60) Davidson, R. W. *Forest Products Journal* **1962**, *12*, 377-381.
(61) Schniewind, A. P.; Barrett, J. D. *Wood Science and Technology* **1972**, *6*, 43-57.
(62) Armstrong, L. D.; Kingston, R. S. T. *Nature* **1960**, *185*, 862-863.
(63) Armstorng, L. D.; Christensen, G. N. *Nature* **1961**, *191*, 869-870.
(64) Hearmon, R. F. S.; Paton, J. M. *Forest Products Journal* **1964**, *14*, 357-359.
(65) Findley, W. N.; Peterson, D. B. *Proceedings ASTM* **1958**, *58*, 841-861.
(66) Gressel, P. *Holz Roh-werks* **1984**, *42*, 379-397.
(67) Bond, B. H. In *Wood Science and Forest Products*; Virginia Tech: Blacksburg, VA, 1993.
(68) Samarasinghe, S.; Loferski, J. R.; Holzer, S. M. *Wood and Fiber Science* **1994**, *26*, 122-130.

3.6. Thermogravimetric Analysis

The foundation for modern thermogravimetric analysis (TGA) was laid by Honda in 1915, who used a "thermo-balance" to investigate the mass change in different metal salts (e.g. $MnSO_4.H_2O$, $CaCO_3$ and CrO_3) [1]. In 1963, Duval developed an automated analytical method based on thermogravimetry to study the stability of various gold precipitates [2] and the pyrolysis of filter paper [3]. In the last few decades, improvements in instrumentation, techniques and data interpretation has made TGA a common characterization technique especially in the field of polymer thermal stability

The amount and rate of change of the sample mass is continuously monitored during dynamic or isothermal heating in a controlled atmosphere. This eliminates the tedious techniques associated with classical gravimetric analysis. The TGA response is influenced by several factors, which are discussed below [4].

- **Heating rate:** Sample decomposition is found to increase proportionally with the heating rate. This leads to significant temperature lag between the sample and furnace temperature.
- **Sample size:** More accurate results are obtained with smaller samples. Erroneous results are generated with larger samples due to the presence of a thermal gradient within the sample. Moreover, thinner samples degrade faster than thicker samples and the decomposition of samples increase with increase in sample particle size.
- **Degradation atmosphere:** The atmosphere in which sample degradation is monitored should be carefully selected. The degradation study may be performed in various atmosphere e.g. air, oxygen, nitrogen, helium etc.

This technique is used in various applications such as in the determination of weight change, drying rate, reactivity in different atmospheres, oxidative degradation, reaction kinetics, volatilization analysis, sample composition, stabilizer effectiveness and measuring inorganic (noncombustible) fillers in polymer or composite materials. TGA may also be coupled with infrared spectroscopy or mass spectroscopy for the identification of evolved gases.

A significant volume of work has been conducted on the thermogravimetric behavior of wood. Wood is composed of three structural polymers: cellulose, hemicellulose and lignin. The amount and nature of each component is considerably different between different wood species. Thermal treatment causes numerous structural, chemical and physical changes in wood. In the following sections, some of the past works on thermogravimetric analysis of wood will be reviewed.

3.6.1. Thermal degradation of wood

When wood is subjected to treatments at elevated temperatures, significant changes occur, the extent of which depends on a number of factors such as atmosphere, pressure, treatment time, water content and sample geometry [5]. Permanent reduction in strength may occur due to thermal treatments both below and above 100°C, which is mostly ascribed to depolymerization reactions, the rate of which increases with treatment temperature. Noncombustible products such as CO_2, traces of organic compounds and water vapor are released between 100°C and 200°C [6]. Pyrolysis of wood begins at temperatures above 270°C [5]. The amount of gaseous products released increases with further increase in temperature.

The thermal degradation reaction of wood is different from its isolated individual components (i.e. cellulose, hemicellulose and lignin). A study was conducted to determine the thermal degradation of Douglas fir and its components by TGA [6]. Results showed that the holocellulose components closely followed the degradation pattern of the wood, although it started degrading at a lower temperature than the wood. Lignin degraded at the slowest rate and produced the largest amount of char among the different wood components. The rate of degradation of cellulose and wood were similar, but cellulose degradation temperature was higher than that of wood.

Studies have been conducted to analyze the effect of degradation environment on the thermal degradation profile to wood. Marcovich *et al*. [7] studied the degradation of wood in nitrogen atmosphere. They found that in the temperature range of 25° to 170°C, there was negligible mass loss which was mainly attributed to the loss of moisture. Significant mass loss starts around 170°C, due to the onset of lignin and hemicellulose degradations. The low-molecular weight protolignins starts degrading at this temperature, but at a rate considerably slower than that of the other constituents. The rate of hemicellulose degradation was found to be slow until it reaches the onset temperature of cellulose degradation (~270°C), after which it degraded at a rate approaching that of cellulose. The hemicellulose degradation at this temperature involved the splitting of side-groups to evolve organic acids (e.g. acetic acid), followed by decomposition. Cellulose decomposed in two major stages which constituted the loss of hydroxyl groups and the depolymerization of anhydroglucose units. Cellulose decomposition occurred at a very narrow temperature range (270° to 400°C) which constituted the bulk of the mass loss. Major changes of lignin occurred at the temperature range of 450° - 500°C. The

weight change of the sample was insignificant at higher temperatures. Significant char (~15%) formation was observed, the majority of which came from the lignin component of the wood. Similar results were also obtained by Chauvette *et al.* [8], who also studied the degradation profiles of wood in air and oxygen. In oxygen environment, the degradation of wood showed a single weight loss between 200° and 360°C. The weight loss during the thermal degradation of wood in air showed three distinct stages. The first stage (200° to 316°C) overlapped with the second stage (316° to 360°C) and was attributed to the decomposition of hemicellulose and cellulose respectively. Lignin decomposition occurred between 360° and 480°C. Thus, separation of the degradation of different wood constituents can be achieved by conducting TGA analysis of wood in a dynamic air atmosphere. Kumagai *et al.* [9] compared the degradation pattern of wood flour in air and nitrogen (20°-600°C). Their results showed that significant weight loss started at 185°-205°C in air and 193°-225°C in nitrogen. Active pyrolysis of the wood flour commenced at 320°-330°C in air and 350°-370°C in nitrogen. They also reported a three-stage thermal degradation pattern in the temperature range of 240°-330° in air and a corresponding four stage degradation in the temperature range of 250°-380°C in nitrogen.

Gronli *et al.* [10] studied the thermal degradation profiles of various hardwoods and softwoods in nitrogen atmosphere. The time derivative of the mass fraction (DTG) curves of both hardwoods and softwoods were qualitatively similar to each other. Both of them showed two main regions of weight losses for hemicellulose and cellulose degradation respectively. But hemicellulose decomposition appeared as a shoulder on the cellulose peak. Due to the rapid decomposition of cellulose, it showed a narrow peak followed by a rapid decay and a long tail. Since lignin degrades over a wide range of temperatures, it

did not show a characteristic peak. Comparison of the DTG curves of hardwoods and softwoods revealed the following observations:

- There was a higher degree of overlap between the hemicellulose and cellulose degradation zones in softwoods, while hardwoods showed a well defined shoulder for the hemicellulose degradation.
- Softwoods showed relatively lower hemicellulose reactivity (degradation).
- The char yield of softwoods (20-26.5%) was relatively larger than hardwoods (14-23%).

One study [11] compared the activation energies (E_{act}) for the thermal degradation of hardwoods and softwoods, in both nitrogen and oxygen atmospheres. E_{act} for hardwoods were larger than softwoods in both atmospheres. For both wood species, it was found to increase when the atmosphere was changed from nitrogen to air. Similar results were also observed in another study [9], which was analyzing the degradation of wood flour at different atmospheres. They reported that E_{act} ranged from 16-30 kcal/mol at 250°-285°C to 42-89 kcal/mol at 340°-370°C in nitrogen. But it increased to 22-38 kcal/mol at 240°-270°C and 54-82 kcal/mol at 300°-330°C in air.

3.6.2. Thermal degradation of PMDI resin

Lin et al. [12] studied the thermal degradation behavior of air-dried (105°C for >3h) PMDI resin in nitrogen with TGA and TGA-IR. Results showed that PMDI degradation started at 247°C. The derivative (DTG) curve showed three peaks at 297°, 514° and 547°C. The char yield at 850°C was 20.61%. The volatiles evolved during degradation were analyzed with IR spectroscopy. Results showed the evolution of CO_2 occurred in

the temperature range of 207°-567°C and degradation of O=N=C groups started at ~327°C.

Umemura *et al.* [13-16] did extensive studies on the durability of isocyanate adhesives under different thermal conditions. They used an aqueous emulsion-type PMDI resin, which was cured with water (PMDI-W). The mechanical properties of the cured PMDI-W was monitored with dynamic mechanical analysis (DMA), while the chemical and mass changes occurring in the cured resin with temperature was monitored with Fourier transform IR (FTIR) and TGA[13]. This allowed the authors to relate changes in mechanical properties of the system to chemical changes and thermal degradation. DMA results showed that the modulus of PMDI-W decreased slowly with temperature until 200°C. A sudden drop of modulus was observed at 200°C, after which the modulus decreased rapidly. FTIR of the samples showed that the chemical structure of the cured resin was stable until 200°C, except for the evidence of some hydrogen-bond cleavage. The sudden drop at 200°C was attributed to the inception of resin segmental motion. Rapid decrease in modulus above 200°C was attributed to degradation reactions as evidenced by the appearance of carbodiimide (-N=C=N-) peak (2100 cm^{-1}), which is formed by condensation of two isocyanate groups [13]. The thermal stability of the resin was improved by the addition of a small amount (5%) of a low molecular weight (400 g/mol) polyol during moisture-curing (PMDI-P-W) [14]. The sudden modulus drop observed in the DMA was found to shift to a higher temperature (280°C) with the incorporation of the polyols.

The authors also studied the durability of both PMDI-W and PMDI-P-W under dry [15] and steam [16] heating conditions. Isothermal TGA experiments [15] at 160°C showed

that the time required for 1% weight loss in PMDI-W and PMDI-P-W systems, were 4.3 & 22.3 hours respectively. In order to monitor the chemical changes occurring in these systems due to the dry heat treatment, the treated samples were analyzed with IR spectroscopy [15]. IR results showed that both the untreated resins contained considerable amounts of unreacted isocyanate groups. The amount of unreacted isocyanate was found to decrease with the increase in treatment time (after-cure). Other than the decrease in isocyanate absorption with increase in treatment time, the IR spectra of both systems did not change significantly. This led the authors to conclude that under dry heating conditions, after-cure of the resin was more dominant than resin degradation. The resin durability was also examined under constant steam heating (160°C at 0.63 MPa) [16]. TGA experiments showed that the onset temperature (T^*) of weight loss for untreated PMDI-P-W resins were higher than PMDI-W systems. For the PMDI-P-W systems, increase in steam treatment time was the thermal stability of PMDI-P-W systems decreased after steam treatment. But for PMDI-W systems, a significant increase in T^* was observed initially (1 hour), followed by slow decrease with the steam treatment time. The initial increase in T^* was attributed to the after-cure of the PMDI-W resin with water.

Vadja *et al.* [17] were studying the cure-kinetics of PMDI resin with wood with dynamic scanning calorimetry (DSC). They observed degradation peaks (endothermic at 240°C and exothermic at 280°C) in the PMDI-wood thermograms that were absent in the neat wood thermograms. This led the authors to conclude that the thermal stability of PMDI-wood system was less than that of neat wood.

References

(1) Honda, K. *Thermal analysis*; Dowen Hutchinson & Ross, 1976.
(2) Gallager, P. A. *Thermal Characterization of Polymeric Materials*, 2nd ed.; Academic Press: San Deigo, CA; Vol. 1.
(3) Duval, C. *Anal. Chim. Acta* **1948**, *2*, 92.
(4) T. Nguyen, E. Z., E. M. Barrall. *Journal of Macromolecular Science: Reviews in Macromolecular Chemistry* **1981**, *C(20)*, 1-65.
(5) D. Fengel, G. W. *Wood: Chemistry, Ultrastructure, teactions*; Walter de Gruyter: Berlin, 1989.
(6) LeVan, S. L. In *Concise Encyclopedia of Wood and Wood-based Materials*, 1st ed.; Schniewind, A. P., Ed.; Pergamon Press: Elmsford, NY, 1989; pp 271-272.
(7) N. E. Marcovich, M. M. R., M. I. Aranguren. *Thermochemica Acta* **2001**, *372*, 45-57.
(8) G. Chauvette, M. H., M. Rubio, J. Khorami, E. Chornet, H. Menard. *Thermochemica Acta* **1985**, *84*, 1-5.
(9) Kumagai, Y.; Ohuchi, T.; Ono, M. *Mokuzai Gakkaishi* **1973**, *19*, 273.
(10) M. G. Gronli, G. V., C. D. Blasi. *Industrial and Engineering Chemistry Research* **2002**, *41*, 4201-4208.
(11) Beall, F. C. In *Encyclopedia of Materials Science and Engineering*, 1st ed.; Bever, M. B., Ed.; Pergamon Press: Oxford, 1986; Vol. 7, pp 4933-4935.
(12) Lin, H. C.; Ohuchi, T.; murase, Y. *Journal of the Faculty of Agriculture, Kyushu University* **2004**, *49*, 449-459.
(13) Umemura, K.; Takahashi, A.; Kawai, S. *Journal of Wood Science* **1998**, *44*, 204-210.
(14) Umemura, K.; Takahashi, A.; Kawai, S. *Journal of Applied Polymer Science* **1999**, *74*, 1807-1814.
(15) Umemura, K.; Takahashi, A.; Kawai, S. *Journal of Wood Science* **2002**, *48*, 380-386.
(16) Umemura, K.; Takahashi, A.; Kawai, S. *Journal of Wood Science* **2002**, *48*, 387-393.
(17) Steiner, P. R.; Chow, S.; Vadja, S. *Forest Products Journal* **1980**, *30*, 21-27.

4.1. Solid-state NMR Analysis of Wood-PMDI Cure Chemistry

The results and discussion for this study are presented in the form of a paper to be submitted to “International Journal of Adhesives and Adhesion”.

The study was conducted with doubly labeled PMDI resin. Two batches of resin were synthesized; first batch was synthesized by M.J. Malmberg, while the second batch was synthesized by the author. The resins were used to prepare wood flake NMR samples. The NMR experiments and data analysis were conducted by the author.

The fracture testing was conducted by M.J. Malmberg.

Results that were not shown in this paper, are presented in the appendix (6.1 and 6.2)

Cure Chemistry of Wood/Polymeric Isocyanate (PMDI) Bonds: Effect of Wood Species

Sudipto Das, Michael J. Malmberg, Charles E. Frazier
Wood-Based Composites Center, Department of Wood Science and Forest Products, Virginia Polytechnic Institute and State University, Blacksburg, VA 24061-0323

Abstract

The wood-species dependent performance of polymeric isocyanate resin was investigated by fracture analysis and solid-state NMR. The fracture energy of two different wood species (yellow-poplar and southern yellow pine) bonded with PMDI resin was evaluated using mode-I cleavage with double cantilever beam specimens. The fracture toughness of pine samples was significantly greater than the corresponding yellow-poplar samples. The effect of wood species on the cure of wood/PMDI bondlines was also evaluated by solid-state NMR with doubly-labeled (^{15}N-^{13}C) PMDI resin. Results showed the existence of a small but statistically significant species effect on both the cure chemistry and morphology of wood/PMDI bondlines. But at higher cure temperatures the differences in chemistry between the wood species disappears and the bond morphology becomes more homogeneous. Acetylation was found to alter the wood-PMDI cure chemistry as expected.

4.1.1. Introduction

Polymeric diphenylmethane diisocyanate (PMDI) is an important adhesive for the manufacture of oriented strand board (OSB) and similar particulate wood-based composites. This wood binder polymerizes into a polyurea/polybiuret network through a rapid reaction with adsorbed wood moisture [1]. The adhesive is also capable of forming covalent urethane bonds with wood [2], which serve to enhance bondline durability. The general nature of PMDI cure chemistry with wood is depicted in Figure 4.1.1.

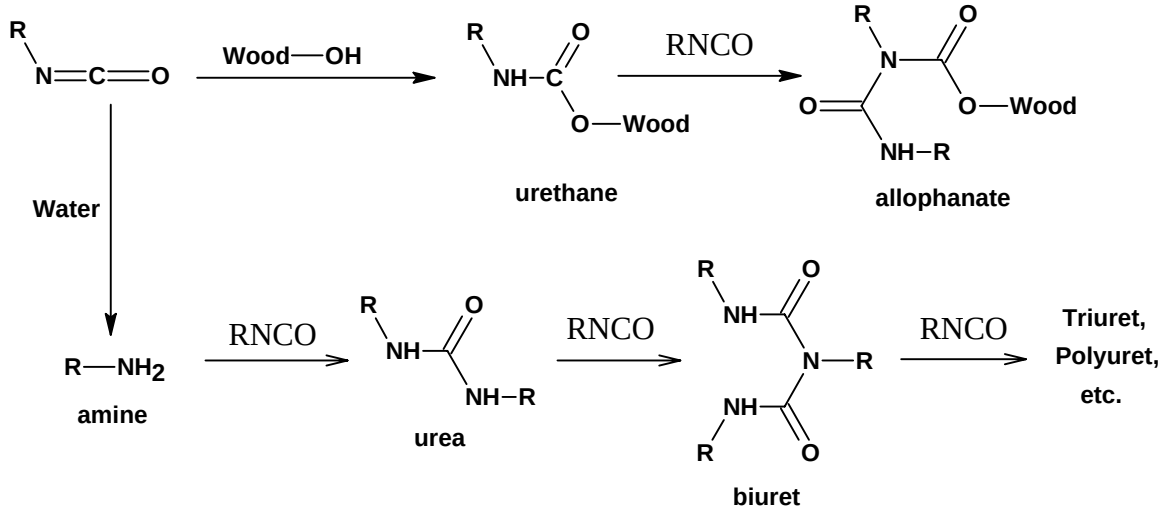

Figure 4.1.1. Reaction of PMDI resin with wood.

PMDI resins are known to exhibit a wood species dependent performance[3-5]. This is of great practical significance because the wood species mixture in OSB manufacture will vary daily as a function of timber availability; resin performance and composite properties will vary accordingly. This work attempts to reveal the nature of the species dependent performance of PMDI resins. In this case, resin performance is compared using mode-I fracture testing of southern yellow pine and yellow-poplar, two woods which are commonly used for OSB manufacture in the southeastern United States. Aspects of the cure chemistry and morphology of pine and poplar bondlines are

compared using solid-state NMR of magnetically labeled PMDI resins cured with these two woods.

4.1.2. Experimental

4.1.2.1 Materials

Commercial PMDI resin (Huntsman Rubinate 1840) was obtained from Hunstman Polyurethanes and was used as received.

^{13}C-Carbon monoxide (99% ^{13}C) and ^{15}N-aniline (98% ^{15}N) were purchased from Cambridge Isotopes Laboratories and used as received. All other chemicals were purchased from Aldrich Chemical Company and used as received.

Two different wood species were tested: yellow-poplar (*Liriodendren tulipifera*) & southern yellow pine *(Pinus* spp.). Blocks of yellow-poplar (YP) and southern yellow pine (SYP) were softened by soaking in distilled water. Flakes (5.1 cm × 5.1 cm × 1.5 cm; 2" × 2" × 0.6") were sliced from the radial wood surface using a disk flaker. Flakes were dried at 105°C for 24 hours to determine dry weights and were equilibrated at ambient conditions to achieve 6-7% moisture content (MC).

4.1.2.2 Methods

4.1.2.2.1. Doubly labeled PMDI (^{15}N, ^{13}C) synthesis

Synthesis of doubly labeled PMDI resin was conducted as described previously [1, 2] with the following modifications. The acid catalyzed condensation of formaldehyde with ^{15}N-aniline was conducted with aniline to formaldehyde molar ratio of 4:1 and an aniline to HCl molar ratio of 1:1.5.

The synthesis of ^{13}C-phosgene was conducted by reacting chlorine (3.58g, 50.4 mmol) with ^{13}C-carbon monoxide (1.22L, 50.4g) in 1,2-dichlorobenzene (ODCB) [2].

ODCB (75 mL) was transferred into a sealed, dry 100 ml graduated cylinder using a canula. Chlorine gas was bubbled into the ODCB until the desired amount (3.58g) was obtained. The Cl_2/ODCB solution was transferred to a 200 ml flask fitted with two stopcock valves. One stopcock opening was sealed with a rubber septum, while the other was connected to the reactor vessel through chemical resistant tubing. The reactor was a 5-necked 1L glass reactor vessel (1 L Ace Glass medium-pressure glass reactor), which was initially evacuated to a pressure of 0.5 mm Hg and then cycled with dry nitrogen and vacuum twice before filling it with ^{13}C-carbon monoxide. The Cl_2/ODCB solution was then forced into the reactor using compressed nitrogen. The reactor was sealed off and the reaction was allowed to proceed at 55°C for 36-48 hrs under vigorous agitation. The reactor was then cooled to room temperature and excess chlorine was removed by the addition of 0.5 ml of 1-phenyl-1-cyclohexene. Phosgene was purified by transferring it to a cold trap (immersed in liquid nitrogen) by intermittent application of vacuum on the cold trap. After the phosgene purification/transfer was complete, ODCB (100 ml) was added to the cold trap through a canula. The phosgene/ODCB solution was then allowed to warm to room temperature. The phosgene yield (57%) was determined by iodometric titration [6].

The phosgenation was conducted in a separate 5-necked 1L glass reactor vessel (1 L Ace Glass medium-pressure glass reactor). ^{15}N-polyamine was vacuum-dried (60°C, 0.6 mm Hg) for two hrs in a 50 ml double-neck flask. ODCB (25ml) was transferred into the flask through a canula and the solution was allowed to cool to room temperature. A dark brown polyamine/ODCB solution was obtained. Phosgene/ODCB solution was transferred into the evacuated (0.5 mm Hg) 5-neck glass reaction kettle submerged in an

ice water bath. The polyamine/ODCB solution was then transferred into the reactor through a canula, while maintaining vigorous agitation with magnetic stirring. The reactor was sealed off and slowly heated to 180°C followed by reaction at that temperature for 20 minutes. During reaction, the gas pressure inside the reactor was released twice at 10 and 20 minutes, after the reaction temperature (180°C) was attained. After phosgenation, the reaction mixture was filtered under a nitrogen blanket into a 250 ml round-bottomed flask using a Buchner glass filter. The reaction mixture was vacuum distilled at 0.3 mm Hg and 60°C to remove ODCB. The doubly labeled resin was heat treated to remove chlorine-containing impurities and to break down MDI dimers. The flask containing the resin was immersed into a 200°C oil bath for 5 minutes under mild nitrogen flow. After the heat treatment, the flask was quench cooled by spraying acetone onto the flask followed by submerging the flask into a cold water bath. The doubly labeled PMDI resin was stored under anhydrous N_2 in a dessicator in the presence of anhydrous sodium sulfate. Two batches of doubly labeled PMDI resin were synthesized over a period of two years, hereafter referred to as PMDI-I and PMDI-II.

4.1.2.2.2. PMDI characterization

Resin isocyanate contents were determined following a 1 in 10 scale version of ASTM D 5155-91 test method C. The resin (0.078 g) was reacted with dibutylamine/toluene solution (2M, 2 ml) in the presence of 1,3,5-trichlorobenzene (2.5 ml) and dry methanol (25 ml). The solution was then titrated to pH=4 using standard HCl solution (0.1N). The isocyanate content for the ^{15}N-^{13}C-PMDI resin was 30.3% for PMDI-I and 30.5% for PMDI-II.

PMDI molecular weight was determined with size exclusion chromatography (SEC) at 40°C using a differential refractometer and a differential viscometer with tetrahydrofuran mobile phase. The resin (0.05 g) was converted to its corresponding urea derivative by reaction with excess diethylamine (1 ml) in dry chloroform for 30 minutes. The residual diethylamine and chloroform was removed by rotational evaporation. The resultant molecular weight was corrected for urea derivatization. The molecular weight of the ^{15}N-^{13}C-PMDI resin was M_n=353, M_w=378 for PMDI-I and M_n=378, M_w=550 for PMDI-II.

The resin monomer ratio was determined by Gas Chromatography (Hewlett Packard HP6890) using a capillary column (Hewlett Packard HP-5) using dry chloroform as solvent. The isomer ratio obtained from GC analysis was 4,4': 2,4': 2,2' = 95:5:0 for PMDI-I. The isomer ratio was not measured for PMDI-II, but our experience has shown that the isomer ratio exhibits a minor variation from that shown for PMDI-I.

The resins were also analyzed using ^{15}N and ^{13}C solution state NMR. ^{15}N solution NMR was performed on a Varian 500 MHz NMR spectrometer with ^{15}N-glycine as an external standard. ^{13}C solution NMR was performed on a Varian 400 MHz NMR spectrometer operating at 100.577 MHz and using TMS as reference. The resin was dissolved in $CDCl_3$ for performing the solution NMR. The different solution NMR spectra are shown in the appendix (figures A.6.1.1 – A.6.1.4).

4.1.2.2.3. Preparation of PMDI/wood Composite samples

Doubly labeled PMDI resin (15% based on wood weight) was applied on two wood flakes. The resin was sandwiched between the flakes and pressed at selected temperatures (100°, 120°, 180° and 220°C) under 3.45 MPa (500 psi) pressure for 3

minutes. PMDI-I was used to prepare the following samples: two samples at 100°, 120° and 220°C and one sample at 180°C for each wood species. PMDI-II resin was used to prepare three samples cured at 100° and 120°C for each wood species. The composite samples were stored in a dessicator over calcium sulfate before NMR acquisition.

4.1.2.2.4. Preparation of acetylated wood/PMDI composite samples

Dry YP wood flakes (5.1 cm × 5.1 cm × 1.5 cm; 2" × 2" × 0.6") were vacuum (~0.1 mm Hg) impregnated with acetic anhydride (AA) for 1 hour, and then heated at 110°C for 9 hours. AA-treated samples were slowly cooled to room temperature and soxhlet extracted with acetone for 24 hours. Samples were dried under vacuum (~0.1 mm Hg) at 40°C for 24 hours. The weight gain in wood samples after acetylation was ~15% (based on dry untreated wood). Acetylated YP flakes were then equilibrated at ambient conditions to achieve ~8% MC. Doubly labeled PMDI-II (15% based on wood weight) was applied on two acetylated flakes. The resin was sandwiched between the flakes by pressing at 120°C under 3.45 MPa (500 psi) for 3 minutes. The composite samples were stored in a dessicator over indicating calcium sulfate before NMR acquisition.

4.1.2.2.5. Solid State NMR Measurements

^{15}N Cross-Polarization/Magic Angle Spinning (CP/MAS) NMR was performed on a Bruker MSL-300 MHz spectrometer operating at 30.43 MHz using a variable contact time pulse at room temperature. The delay between scans was 6 seconds. All spectra were referenced to ^{15}N-glycine at 31 ppm. Small discs were cut out of the wood composites using a paper hole puncher and filled into a zirconium oxide rotor. The rotor was spun at 4.0 kHz during the NMR acquisition. The following table (4.1.1) shows the different samples analyzed.

Table 4.1.1. Compilation of the number of separately bonded composite samples and the corresponding number of NMR acquisitions per sample as a function of wood species and cure temperature.

Wood Species	PMDI	Cure Temperature (°C)	Number of samples	Number of acquisition/sample
Pine and Poplar	I	100	2	2
	II		3	1
	I	120	2	2
	II		3	1
	I	180	1	2
	I	220	2	2
Acetylated Poplar	II	120	2	1

A variable contact time ^{15}N CP/MAS experiment was conducted at room temperature for each sample with the contact time ranging from 0.1 to 12 milliseconds (samples prepared with PMDI-I) or 0.1 to 6 milliseconds (samples prepared with PMDI-II). Twelve hundred scans were performed at each contact time for samples prepared with PMDI-I, while 3000 scans were performed for those prepared with PMDI-II.

4.1.2.2.6. Spectral Analysis (Decomposition)

The ^{15}N solids NMR spectra were decomposed using NUTS® software. An adjustable algorithm was employed using a 75% Gaussian & 25% Lorentzian fitting procedure; this combination was selected because it provided the best simulation of the original spectrum. The spectra were decomposed (over the range from about 90 – 120 ppm) into three components: 111 ppm biuret imide, 104 ppm urea peak and ~99.5 ppm urethane peak. During the decomposition process, the biuret imide and urea peak chemical shifts were fixed while the urethane peak was allowed to vary between 102 – 99.5 ppm. Details of this process are discussed later.

4.1.2.2.7. Mode-I Fracture Testing: Specimen preparation and fracture testing

Approximately flatsawn boards of poplar and pine (30.5 cm × 2.54 cm × 5.04 cm; 12' × 1' × 2") were cut into 30.5 cm/1' sections (billets). Each billet was cut into 15 mm (0.59") thick laminae with a 3-5° grain angle following the procedure of Gagliano & Frazier [7]. The laminae were conditioned to 10% equilibrium moisture content (EMC) in an environmental chamber. Just prior to bonding, the laminae were planed to a 10 mm thickness. The bonding surfaces of two laminae were coated with commercial PMDI resin with an adhesive coverage of ranging from 80-120 g/m^2. The coated laminae were then sandwiched together and pressed at 175°C and 0.55 MPa for 20 minutes. These were reconditioned to 10% EMC and cut into dual cantilever beam, DCB, specimens (200 mm × 20 mm × 10 mm). Each laminate yielded 5 to 6 specimens. DCB specimens were tested according to the procedure of Gagliano & Frazier [7]**.** Each DCB sample was pulled open in Mode-I cleavage in a cyclic fashion; each sample yielded 10 – 20 cycles which provides the corresponding number of crack initiation and arrest energies for each specimen. The data was analyzed using a compliance correction method [7, 8]. All of the measured initiation and arrest energies were simply averaged across all pine samples and all poplar samples, respectively. 8 DCB samples were tested for each wood species.

4.1.3. Results and Discussion

Figure 4.1.2 shows the dry bond fracture toughness of poplar and pine DCB specimens bonded with PMDI resin.

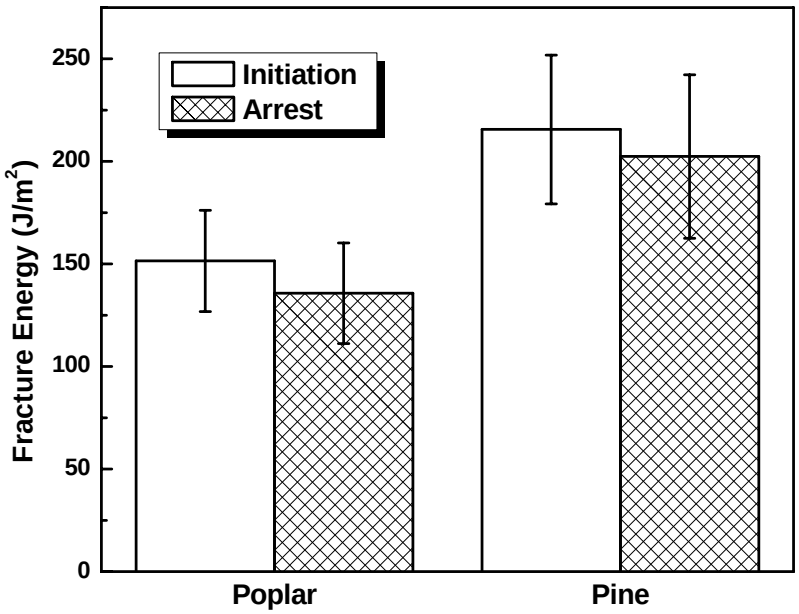

Figure 4.1.2. Effect of wood species on the mode I fracture energy of wood bonded with PMDI resin. Average of 102 (poplar) and 65 (pine) crack initiation/arrest cycles. Error bars represent ±1 standard deviation.

It is apparent that PMDI provides a better dry bond performance with pine than with poplar. Because of the compliance correction employed in the fracture data analysis, these results are independent of bulk wood density and modulus variations. Consequently, this species dependent performance must arise from differences intrinsic to the wood chemistry and anatomy. In other words, this species dependence is likely a result of: differences in cure chemistry, differences in interphase morphology, differences in heat and mass transfer (during cure) which are a complex manifestation of wood anatomical differences, or a combination of these effects. In an effort to understand this species dependence, solid-state nuclear magnetic resonance, NMR, was employed to evaluate the cure chemistry and rotating frame, proton spin-lattice relaxation time of PMDI bonds to SYP and YP.

While a double-labeled PMDI resin was prepared for this study, the following discussion focuses entirely upon the nitrogen spectra. The full utility of the double-label

will be the subject of a subsequent publication. Figure 4.1.3 shows an example nitrogen spectrum of a composite wood sample bonded with labeled PMDI resin.

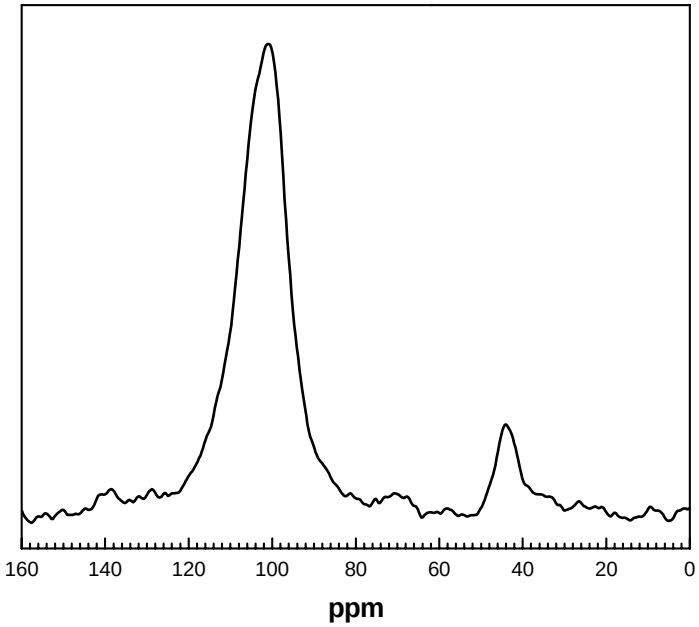

Figure 4.1.3. ^{15}N solid-state NMR spectrum of a wood composite sample bonded with doubly labeled PMDI resin. (Pine wood, cured at 120°C for 3 min, 1 millisecond contact time)

Previous studies have demonstrated the following nitrogen assignments in the solids NMR spectrum: 138 ppm, unprotonated biuret imide; 111 ppm, protonated biuret amide; 104 ppm protonated urea; 97 – 100 ppm, protonated urethane, and; 44 ppm, unprotonated isocyanate. Figure 4.1.3 reveals that the signals from different protonated nitrogen atoms (urethanes, ureas and biurets) are substantially overlapping. Spectral decomposition was employed to obtain qualitative estimates of the relative amounts of biuret, urea, and urethane linkages in the signal region from about 90 – 120 ppm. As demonstrated in Figure 4.1.4, the spectra were decomposed into three components: 111 ppm biuret imide, 104 ppm urea peak and ~99.5 ppm urethane peak. During the decomposition process, the biuret imide and urea chemical shift peaks were fixed while the urethane peak was allowed to vary between 102 – 99.5 ppm. Please note that the nitrogen signals in this

region are almost certainly more complex than suggested by the spectral decomposition strategy employed here. For example, it is very likely that this spectral region contains signals from allophonates, and possibly also from amides (which arise from the NCO reaction with hemicellulose carboxylic acids). Finally, the signal dispersion for biurets, ureas and urethanes is also unknown. Consequently, the spectral decomposition presented here provides a crude understanding of the relative signal areas which have been labeled for convenience as: biuret, urea and urethane.

A qualitative relative concentration of biurets, ureas and urethanes was obtained by correcting the decomposed signals for differential cross-polarization (T_{NH}) and rotating frame proton relaxation ($T^{H}_{1\rho}$) (figure 4.1.4).

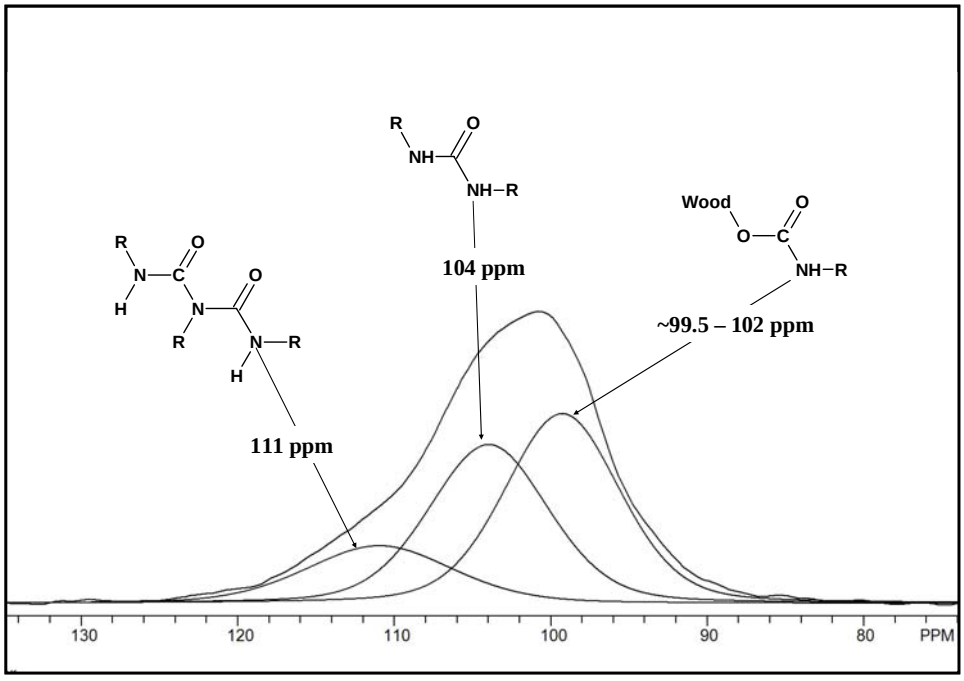

Figure 4.1.4. Example ^{15}N spectrum and the associated spectra decomposition of a wood-doubly labeled PMDI composite showing urea, urethane and biuret amide peaks.

In other words, the decomposed peak areas were fitted to the following equation[9]:

$$I(\tau) = I^* \frac{T^H_{1\rho}}{T^H_{1\rho} - T_{NH}} \left(e^{-\frac{\tau}{T^H_{1\rho}}} - e^{-\frac{\tau}{T_{NH}}} \right) \qquad (4.1.1)$$

where, I(τ) is the nitrogen magnetization (area) at a given contact time, τ,

$T^H_{1\rho}$ is the proton spin-lattice relaxation time in the rotating frame,

T_{NH} is the ^1H-^{15}N cross-polarization time,

I* is the nitrogen magnetization (area) when the cross-polarization is instantaneous and the rotating frame relaxation is infinitely long; it is also known as the corrected area and represents the relative percent composition of each chemical species present in the large central resonance shown in Figures 4.1.3 & 4.1.4 (from ~85 to 125ppm). Since the peak area was obtained by decomposing the central nitrogen resonance, the "*concentration*" in this study represents the relative concentration of the different chemical moieties with respect to the decomposed peak only, not their true concentration in the bondline.

4.1.3.1. Effect on Cure Chemistry

Figure 4.1.5 shows the variation of the relative urethane, urea and biuret concentrations in the wood-PMDI bondline as a function of wood species and cure temperature.

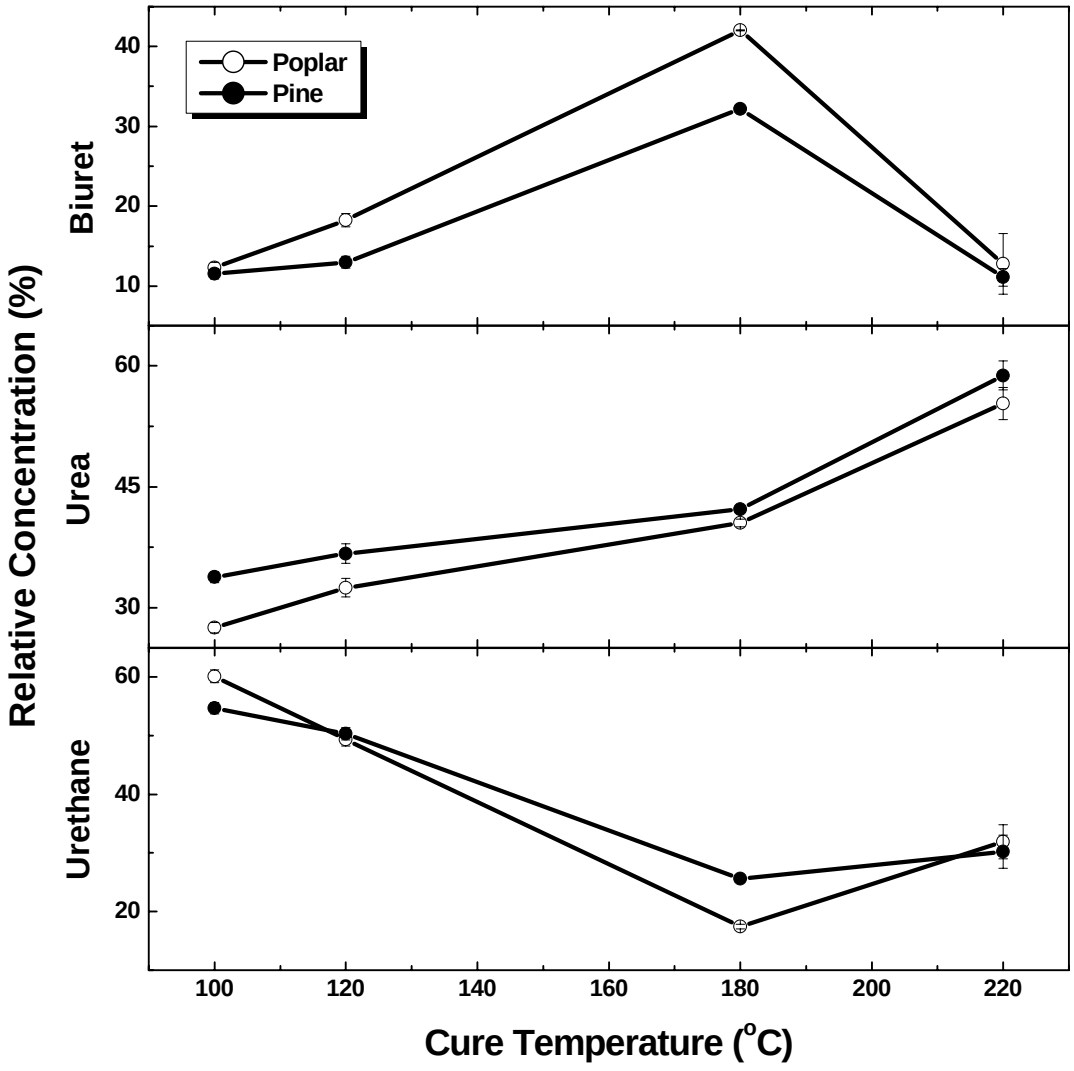

Figure 4.1.5. Effect of cure temperature and wood species on the relative concentration of biuret, urea and urethane in the wood-PMDI bondline. Data points at 100 and 120°C are an average of 7 NMR acquisitions using PMDI-I and also PMDI-II; points at 180 and 220°C represent an average of 2 and 4 NMR acquisitions, respectively, both using PMDI-I. Error bars represents standard deviation.

The first notable point taken from figure 4.1.5 is that the wood species appear to have a minor effect, or no effect, on the cure chemistry. There are instances in which the two woods cause a statistically significant difference; this is particularly true at the lower cure temperatures where each datum is an average of 7 observations. However, given the qualitative nature of this analysis, it seems appropriate to err on the conservative side by

stating that the different woods cause little or no overall difference in cure chemistry. Furthermore, not shown in Figure 4.1.5 is the fact that the results from PMDI-I (which was prepared by Malmberg) and PMDI-II (prepared by Das) are quite similar. As in previous studies [1, 5], the cure temperature has a significant influence on the cure chemistry (direct comparison with those previous works is impossible because of the different methods employed). As the cure temperature increases from 100°C to 180°C, the biuret and urea concentrations increase; at 220°C the urea increases further while the biuret exhibits a sharp reduction. The urethane concentration shows a steady decrease in concentration from 100°C to 180°C; at 220°C there is little or no additional change. Figure 4.1.5 indicates that biuret and urethane linkages undergo thermal decomposition, which correlates with an increase in urea concentration. Again, it must be emphasized that the concentrations indicated in Figure 4.1.5 represent relative areas within the signal region (85 – 125 ppm) according to a simplified spectral decomposition. For example, if urethanes were actually present at 30 -60% of the central resonance, then the detection of urethane would not have been as difficult as the literature suggests [1, 5, 10-12]. We believe that the relative urethane concentration is overestimated by the simplicity of the decomposition. Furthermore, the urethane must be overestimated because we permitted the urethane chemical shift peak to vary over a 2.5 ppm region during the decomposition, while the biuret and urea chemical shifts were fixed- this process was adopted because it provided the best simulation of the parent spectrum. We submit that the true concentrations are a reflection of Figure 4.1.5, but the actual concentrations cannot be obtained from this method. This point will become more apparent, as another deficiency of the spectral decomposition is revealed below.

Since urethane detection is of such great interest, poplar samples were acetylated and subsequently cured with the labeled resin to determine the effect on urethane formation. The acetylation reaction caused a weight gain of 15% (maximum weight gain that can be obtained upon acetylation is ~22% [13]), which means that many wood hydroxyl groups are still available for urethane formation. Figure 4.1.6 demonstrates that acetylation reduces but does not eliminate urethane signal intensity in the 97 – 100 ppm region; the 100 ppm reference line reveals the subtle difference caused by acetylation.

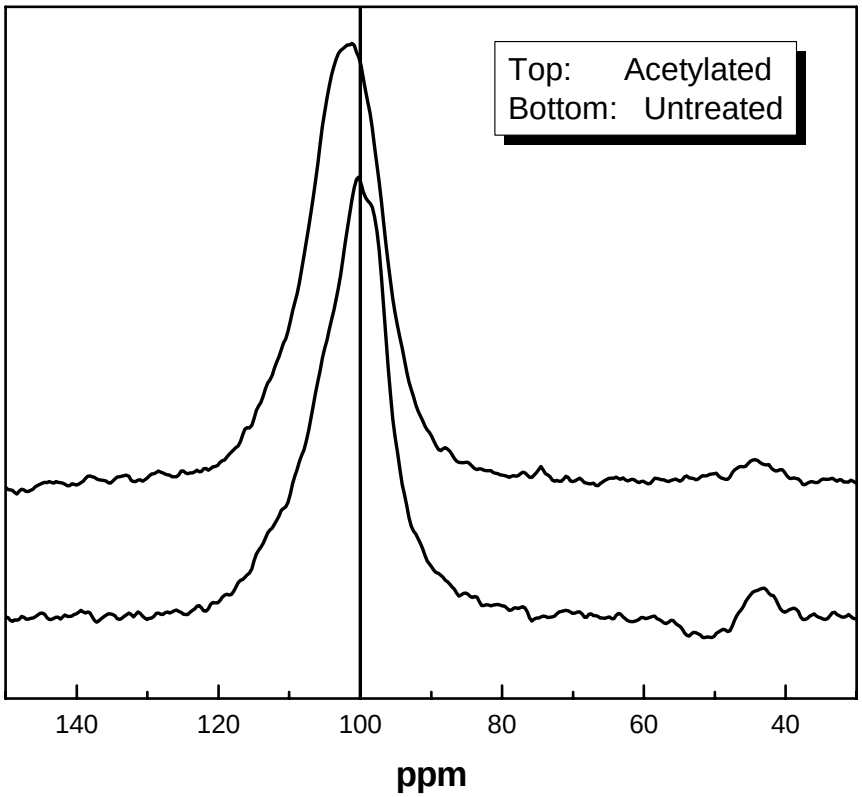

Figure 4.1.6. Effect of acetylation on the ^{15}N-spectra of doubly labeled PMDI/wood composites samples (0.3 millisecond contact time).

This speaks to the general deficiency of the spectral decomposition process employed here- even when little or no urethane is expected to appear, the acetylated sample still shows significant signal in the urethane region. Apparently, the urethane region (97-100 ppm) contains signals from non-urethane linkages and this provides

further insight into the urethane overestimation discussed previously. The relative concentrations from the spectral decomposition are shown in Figure 4.1.7. As expected, acetylation caused a drastic reduction of the signal in the urethane region.

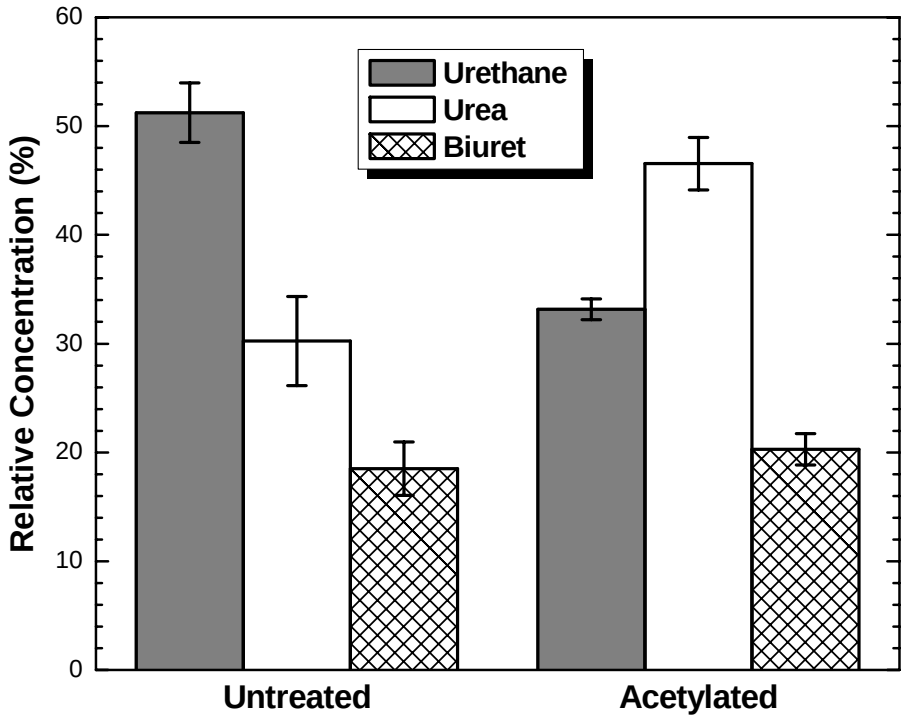

Figure 4.1.7. Effect of acetylation on the relative concentration of various chemical species. Number of replications: 2 for acetylated sample and 7 for untreated samples. Composites cured at 120°C for 3 min at 3.5 × 10^4 kPa pressure.

4.1.3.2. Effect on Bond Morphology

All chemically distinct species have been observed to have similar rotating frame proton relaxation ($T^H_{1\rho}$) in homogeneous systems [14]. This is attributed to spin diffusion, which involves the transfer of magnetization among the abundant protons of the different chemical species. This magnetization transfer occurs over nano-scale domains and is known to be ineffective across phase boundaries. Due to ineffective spin diffusion, chemical species in heterogeneous systems exhibit different $T^H_{1\rho}$ values. In this study, the morphology (homogeneous or heterogeneous) of the wood-PMDI bondlines was

investigated by monitoring the $T^{H}_{1\rho}$ values of urethane, urea and biuret species. The relaxation constants for each chemical species (i.e. urethane, urea and biuret) were determined by fitting the decomposed peak areas into equation 4.1.1.

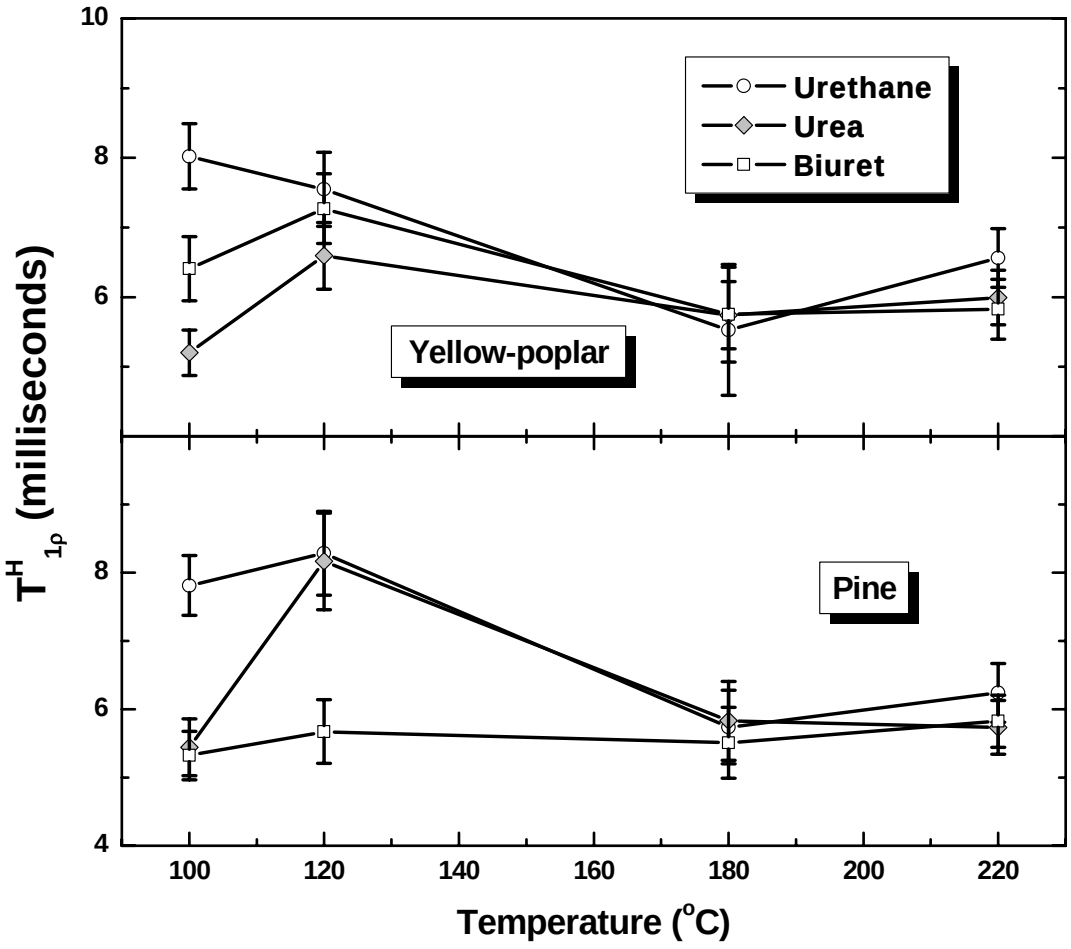

Figure 4.1.8. Variation of proton rotating frame relaxation ($T^{H}_{1\rho}$) of urea, urethane and biuret linkages with cure temperature and wood species. Error bars represents standard deviation

Figure 4.1.8 shows the variation of $T^{H}_{1\rho}$ of the different chemical species with cure temperature and wood species. For both woods, increasing cure temperatures caused the convergence of all $T^{H}_{1\rho}$ values to a common value. This shows that increasing cure temperatures improve the effectiveness of spin diffusion. In other words, at lower cure temperatures the wood/PMDI bond-lines display heterogeneous characteristics, which

disappear at higher cure temperatures. This may be due to increases in crosslink density, which is also reflected in the corresponding increase in the concentration of urea-type structures.

At lower cure temperatures (<120°C), there seems to be a species effect on the morphology of the wood-PMDI bondline. In yellow-poplar, the $T^{H}_{1\rho}$ values of all the chemical species were statistically different from each other; while in pine there seems to be some closer association between the urethane and biuret domains. This species effect was found to disappear at higher cure temperatures.

The results of this study indicate species effects that are most significant at low cure temperatures. The low temperature cure chemistry effect is minor but statistically significant; the low temperature morphological effect is clear. Again, it is difficult to attribute these low temperature effects to a species dependence of PMDI performance. Nevertheless, these findings suggest that low temperature cure effects should be the emphasis of future studies. We can devise a possible scenario (based on these findings) to explain the species dependence of PMDI performance.

4.1.3.3. Implications of this study to the OSB manufacturing process

In OSB manufacture, the adhesive is sprayed on the flakes, which are then arranged into a mat and pressed to form the final board. During the pressing operation, the platen temperatures are ~200°C, in order to obtain a core temperature of ~100-120°C. Thus, there is a significant temperature gradient in the mat. The findings of this study indicate that the species effect (using southern pine and yellow-poplar) may be significant in the panel core, and insignificant near the faces. While the low temperature cure chemistry displayed only minor differences in this study, it is possible that these minor differences

could influence core properties. Regarding morphology, it is clear that nano-scale differences occur at low cure temperatures. Such morphological differences could be the root of the species dependence of PMDI performance in OSB core material. Again, this is a scenario consistent with the present findings. More work, which better simulates mat conditions, is required to test this low cure-temperature hypothesis.

4.1.4. Conclusions

The following conclusions can be drawn from this study:

- A spectral decomposition process was employed to provide some insight into the relative concentrations of urea, biuret and urethane.
- This spectral decomposition appears to overestimate the amount of urethane formation because PMDI cure with acetylated wood suggests that the urethane signal region contains a significant quantity of non-urethane species.
- With increase in cure temperature, the urethane concentration decreased and the urea concentration increased; the biuret concentration increased at moderate temperatures and then declined at the highest cure temperature.
- With increase in cure temperature, the morphology of wood-PMDI bondline shifted from a heterogeneous to a relatively homogeneous system.
- Wood acetylation led to a drastic decrease in urethane concentration and a concomitant increase in urea concentration.
- There was a small but statistically significant species effect on both the cure chemistry and morphology of wood-PMDI bondline, which disappeared at higher cure temperatures.

References

1. Ni, J.; Frazier, C. E. *Journal of Adhesion* **1998,** 66, 89-116.
2. Zhou, X.; Frazier, C. E. *International Journal of Adhesion and Adhesives* **2001,** 21, 259-264.
3. Johns, W. E.; Maloney, T. M.; Saunders, J. B.; Huffaker, E. M.; Lentz, M. T. In 16th W.S.U. Particleboard Symposium, 1982; 1982; p 71.
4. Ball, G. W. In 15th W.S.U. Particleboard Symposium, 1981; 1981; p 265.
5. Bao, S.; Daunch, W. A.; Sun, Y.; Rinaldi, P. L.; Marcinko, J. J.; Phanopoulos, C. *Journal of Adhesion* **1999,** 71, 377-394.
6. Rush, C. A.; Danner, C. E. *Analytical Chemistry* **1948,** 20, (7), 644-646.
7. Gagliano, J. M.; Frazier, C. E. *Wood and Fiber Science* **2001,** 33, (3), 377-385.
8. Blackman, B.; Dear, J. P.; Kinloch, A. J.; Osiyemi, S. *J. Mater. Sci. Lett.* **1991,** 10, 253-256.
9. Mehring, M., *High-Resolution NMR Spectroscopy of Solid Polymers*. Springer-Verlag: Berlin, 1983.
10. Wendler, S. L.; Frazier, C. E. *Journal of Adhesion* **1995,** 50, 135-153.
11. Wendler, S. L.; Frazier, C. E. *International Journal of Adhesion and Adhesives* **1996,** 16, 179-186.
12. Wendler, S. L.; Frazier, C. E. *Journal of Applied Polymer Science* **1996,** 61, 775-782.
13. Rowell, R. M., In *Handbook of Wood Chemistry and Wood Composites*, Rowell, R. M., Ed. CRC Press: Boca Raton, 2005; pp 77-98.
14. Schaefer, J.; Stejskel, E. O.; Buchdahl, R. *Macromolecules* **1977,** 10, (2), 384-404.

4.2. DSC Analysis of Wood-PMDI Cure Kinetics

In this study the cure kinetics of the wood-PMDI system was analyzed for both pine and poplar woods, using the multiple-heating rate devised by Ozawa[1].

4.2.1. Experimental

4.2.1.1. Materials

PMDI resin was obtained from Huntsman Polyurethane (Rubinate® 1840). The resin was transferred into glass bottles and stored under nitrogen.

Two wood species were selected for analysis: yellow-poplar, YP (*Liriodendren tulipifera*) & southern yellow pine, SYP *(Pinus spp*.). Flakes (50.8 mm × 50.8 mm × 15.2 mm; 2" × 2" × 0.6") were sliced from the radial wood surface using a disk flaker. Flakes were dried at 105°C for 24 hours to determine dry weights and were equilibrated at ambient conditions to achieve ~14% moisture content (MC).

4.2.1.2. Methods

4.2.1.2.1. Sample preparation

Small discs were punched from the YP flakes. The discs were immersed in resin for 1 min. The resin impregnated discs were placed on a Kimwipe® tissue paper under pressure (14.2 kg) for 10 min, to remove excess resin. The sample was then enclosed in a hermetic pan and tested. The resin loading obtained by this procedure was 29.6 (± 6.5) % (based on dry wood).

Small wood discs were punched from SYP flakes. Resin was applied on a Teflon film whereby the resin formed small beads. A small bead of resin was applied on the wood disc. Excess resin was removed from the impregnated disc by placing it on a tissue

paper under pressure (14.2 kg). The resin impregnated samples were then enclosed in a hermetic pan and tested. The resin loading obtained by this method was 23.1 (± 8.9) % (based on dry wood).

4.2.1.2.2. DSC analysis

All DSC experiments were conducted on a Q100 DSC from TA Instruments®. The cure exotherm peak for the wood-PMDI system was determined at five different heating rates: 2°C/min, 4°C/min, 6°C/min, 8°C/min and 10°C/min (5 replications at each heating rate) in the temperature range of -90° to 180°C.

4.2.2. Results and discussion

The cure kinetics of PMDI with two different wood species (southern pine and yellow-poplar) was tested with DSC. The kinetic parameters (E_{act}, Z and k) were determined following the multiple heating rate technique (ASTM E 698-79). Figure 4.2.1 shows the variation of the cure exotherm peaks (T_p) with heating rate (β) for both wood species.

Results show that at all heating rates pine T_ps were significantly lower than the corresponding yellow-poplar T_ps. The data was used to construct Ozawa plots i.e. $-\ln\left(\frac{\beta}{T_p^2}\right)$ vs. $\frac{1}{T_p}$ (figure 4.2.2).

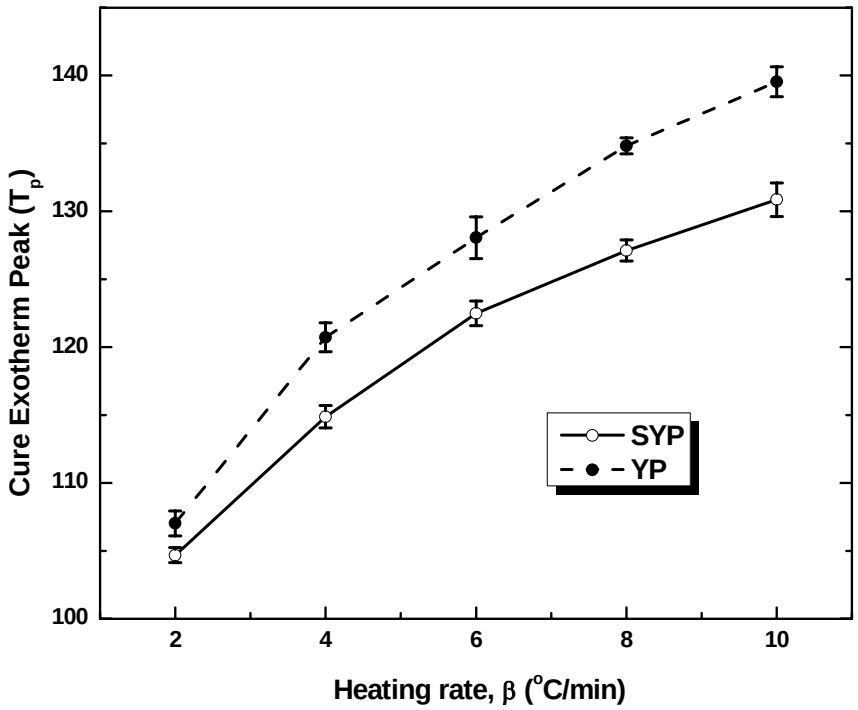

Figure 4.2.1. Effect of wood species on the cure exotherm peak temperature for wood/PMDI systems at different heating rates. Error bars represent standard deviation.

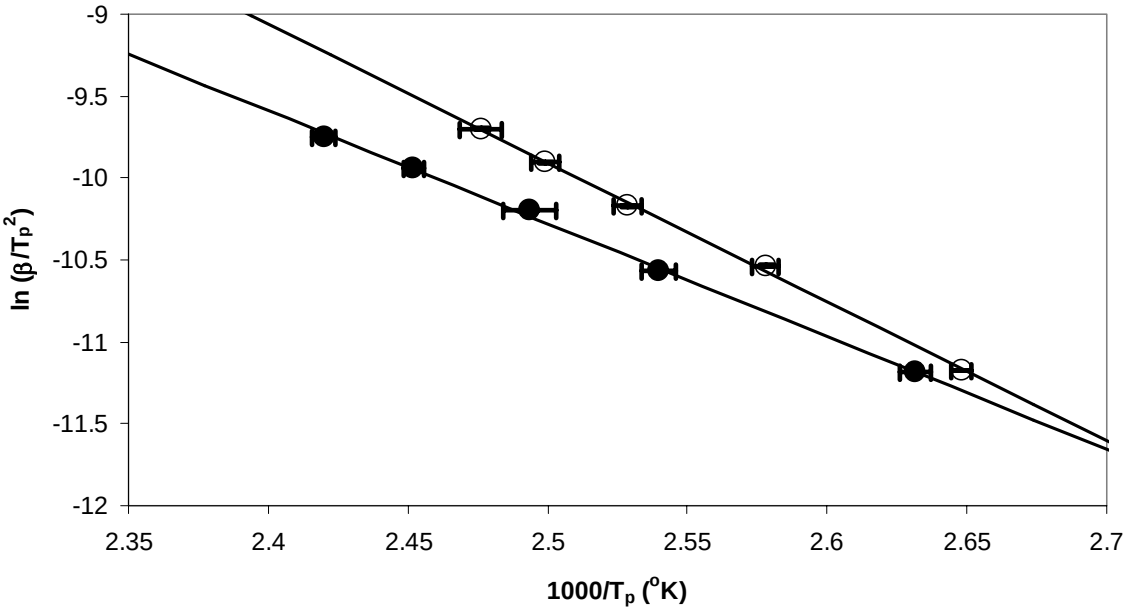

Figure 4.2.2. Ozawa plot for the cure of PMDI resin with SYP and YP wood flakes. X and Y error bars represent standard deviation.

The kinetic parameters were calculated from the slope (E_{act}) and intercept (Z) of the above plot, which are shown in Table 4.2.1. From the kinetic parameters, the reaction rate (k) was calculated by equation 4.2.1

$$k = Ze^{-\frac{E_{act}}{RT}} \qquad (4.2.1)$$

Table 4.2.1. The kinetic parameters for the wood/PMDI cure reaction.

Kinetic Parameters	Pine	Poplar
E_{act} (kJ/mol)	70.07 ± 1.34	56.91 ± 1.08
$Z \times 10^6$ (sec^{-1})	591.64 ± 254.98	6.36 ± 2.2
k at 100°C (sec^{-1})	0.091	0.068

The results obtained in our studies were similar to those obtained for the wood-PMDI system in the past (table 4.2.2).

Table 4.2.2. Kinetic parameters for Wood-PMDI system as obtained in past studies.

Experimental conditions	E_{act} (kJ/mol)	$Z \times 10^6$ (sec^{-1})
Aspen flakes with PMDI (7%) in water-saturated environment [2]	62.1	4.28
Aspen wood flour (12% MC) with PMDI (50:50, based on wet wood) [3]	68.1	-

Two different reactions may occur in the wood-PMDI system; the resin may react with the wood hydroxyl group to form urethanes or may react with the moisture to form polyurea-type structures. The latter reaction is preferred because of the low mobility of the wood hydroxyl groups [3]. Thus, in this study we were probing the cure kinetics of water with PMDI in the presence of the wood. DSC analysis has shown that PMDI reacts with water in the temperature range of 87°-117°C and the E_{act} for this reaction was ~430-440 kJ/mol[4]. Significant reduction of E_{act} for this reaction was observed in the presence

of wood. Thus, the reaction of PMDI resin with water is catalytically activated in the presence of lignocellulosic materials.

Results from this study show that all the kinetic parameters are significantly different between the wood species analyzed. The activation energy of the cure of PMDI-wood system was significantly higher in pine relative to yellow-poplar. This signifies that the energy barrier for the cure reaction was much higher in pine than yellow-poplar. But due to the higher Z-value (which signifies the number of collisions taking place during reaction), the reaction rate in pine is much higher than yellow-poplar; which signifies that the cure of PMDI is faster in pine. This signifies that the resin-wood interaction or the catalytic activation of the water-PMDI reaction was larger in pine, making the above mentioned reaction more facile.

References

(1) ASTM-E-698. Philadelphia, PA, 1988; Vol. 14.02.
(2) Harper, D. P.; Walcott, M. P.; Rials, T. G. *International Journal of Adhesion and Adhesives* **2001**, *21*, 137-144.
(3) He, G.; Yan, N. *International Journal of Adhesion and Adhesives* **2005**, *25*, 450-455.
(4) Pizzi, A.; Owens, N. A. *Holzforchung* **1995**, *49*, 269-272.

4.3. Dynamic & Static Mechanical Analysis of Wood-PMDI Interactions

The results obtained in this study have been presented in three different papers:

- "**Fundamental aspects of the dynamic mechanical analysis of wood**": This paper discusses the effect of different experimental parameters (such as thermal history, wood species and grain orientations) on the linear viscoelastic limit and DMA of wood. Most of the work presented in this paper was conducted jointly by N. Sun and the author.

- "**Probing the species-dependent interactions between wood and polymeric isocyanate resins by dynamic mechanical analysis**": This paper discusses how DMA was utilized to probe the wood-PMDI interactions in both dry and plasticized conditions. Results from experiments conducted on both single cantilever bending and submersion tension modes are presented in this paper.

- "**Characterization of the polymeric isocyanate-wood interactions by creep in dry and ethylene-glycol plasticized conditions**": The wood-PMDI interactions were conducted with static creep test in both dry and plasticized conditions.

Results that were not discussed in the above papers are presented in the appendix (6.3, 6.4 and 6.5)

Fundamental Aspects of the Dynamic Mechanical Analysis of Wood

Nanjian Sun, Sudipto Das and Charles E. Frazier*

Wood Science and Forest Products, Virginia Tech, Blacksburg, VA 24061-0323

4.3.1.1. Introduction:

Dynamic mechanical analysis (DMA) is a powerful tool for investigating the structure/morphology and property relationships of materials. In the last two decades, many studies have been conducted on the DMA of wood for purposes of studying the structural arrangement of wood polymers through their relaxation behavior.

The main softening transitions for wood polymers in the dry state occur at high temperatures, where significant wood decomposition takes place. For example, the in situ glass transition of dry cellulose, hemicellulose and lignin occur at 200°-250°C, 150°-220°C and ~205°C, respectively [1]. Furthermore, secondary relaxations in dry wood have been observed in the temperature range of -150° to 200°C; these very weak transitions are attributed to small scale motions of wood polar groups and/or adsorbed water [2-4].

Salmén [1,5-13] has conducted extensive studies on the softening behavior of in situ lignin under water-saturated conditions, demonstrating that the lignin transition is affected by wood species [5,6], chemical composition [8], grain orientation [11] and chemical modification of wood [13]. Salmén has also studied the softening behavior of hemicellulose by humidity scans at constant frequency and temperatures [9,12].

Much of the DMA of wood has focused on the thermal transitions of wood polymers, the knowledge of which is important in applications such as thermomechnical pulping, or to determine the interactions and organization of different wood polymers in

the cell wall. Much less work has been published about various fundamental experimental parameters, such as wood grain orientation, thermal history etc. on the DMA of wood.

One of the most important experimental parameters which affects DMA is the systematic measurement of the linear viscoelastic region (LVR) of wood samples. In a DMA experiment, the sample must be deformed at an amplitude/strain, which is within LVR of the material. Within the LVR, the polymer packing is not altered and the material response is independent of the applied strain. Thus, the response within the LVR is directly related to the intrinsic sample properties and morphology. DMA experiments are generally performed at the highest strain/amplitude within the LVR in order to obtain the highest signal/noise ratio. In other words, it is desirable to identify the optimal acquisition parameters in order to enhance the analysis and to ensure that such parameters do not themselves cause an erroneous response. We are not aware of any studies on the effect of various wood and experimental parameters (grain orientation, wood species, temperature, etc.) on the LVR of wood.

The mechanical properties of wood are also known to depend on the sample moisture content below the fiber saturation point (FSP). Thus, wood DMA is most reliable if the sample moisture content does not change during the course of the experiment. Contemporary DMA equipment generally lacks any means of precisely controlling the relative humidity in the sample chamber. Consequently, the simplest and perhaps most reliable wood DMA should be conducted under completely dry conditions or when the sample is immersed in solvent (submersion mode). In this study, the effect of various experimental parameters on the DMA of completely dry wood will be discussed.

One motivation for this work is simply that dry wood DMA is the easiest way to probe wood transitions. Of course, dry samples will only reveal weak secondary relaxations; nevertheless, it does offer fundamental insight into the nature of wood, as will be demonstrated.

4.3.1.2. Experimental:

4.3.1.2.1. Materials

Two different wood species were tested: yellow-poplar, YP (*Liriodendren tulipifera*) & southern yellow pine, SYP *(Pinus* spp.). These woods were obtained as standard lumber from two different local sources. Samples were machined from the sapwood of both woods using two different grain orientations (hereafter referred to as "longitudinal" and "radial" samples). Longitudinal sample dimensions were 40 mm (longitudinal) × 10 mm (tangential) × 4 mm (radial) [1.6" x 0.4" x 0.16]; radial sample dimensions were 40 mm (radial) × 10 mm (tangential) × 4 mm (longitudinal). All samples were dried (at room temperature) over phosphorous pentoxide (P_2O_5), until no weight loss was observed (not less than about 2 days).

4.3.1.2.2. Methods

All DMA tests were performed on a TA instruments® DMA 2980 using a dry air purge of the sample chamber; most samples were analyzed in single-cantilever bending, and a few experiments were conducted in 3-point bending. The samples remained dry and exhibited mass losses of less than 0.5% (measured before and after sample analysis). All experiments were replicated 3 or 5 times to confirm the presented results.

4.3.1.2.2.1. Determination of the linear viscoelastic region

Samples were secured in a single cantilever bending clamp with a clamping torque of ~115 cm.N (10 lb-in). The linear viscoelastic region (LVR) of DMA samples was determined using a strain sweep test; where the sample was sinusoidally deformed with increasing amplitude/strain (0.0029-0.143% strain, 1-50 μm amplitude) at a constant frequency (1 Hz). The LVR boundary was arbitrarily defined as the strain that caused a 5% or less reduction in the initial storage modulus, E'. All samples were thermally treated at 150°C for 10 minutes prior to the strain sweep experiments. Samples were first heated at 10°C/min to 150°C and annealed there for 10min to erase all the previous thermal history. The sample was then cooled at 10°C/min down to the setting temperature and was held isothermal for 20min before the constant 1Hz strain sweep test.

4.3.1.2.2.2. Dynamic testing

Samples were secured in a single cantilever bending clamp with a clamping torque of ~115 cm.N (10 lb-in). All dynamic scans (from -150° to 150°C) were performed at a heating rate of 5°C/min & 1Hz frequency. The samples were equilibrated at the lowest temperature (-150°C) for 20 minutes before scanning.

4.3.1.3. Results and Discussion

The influence of sample clamping was initially investigated by comparison of results with 3-point bending and with single-cantilever bending. Using 3-point bending, the sample storage modulus varied significantly, from as low as 2000MPa to 17000MPa for longitudinal poplar samples; whereas, the storage modulus varied much less when using single-cantilever bending (from 3000 to 6000Mpa). The stiffness variation

observed with 3-point bending was believed to arise from sample indentation. Consequently, we find that cantilever bending is preferred over 3-point bending.

Figure 4.3.1.1 shows the LVR limit of pine and poplar samples at different temperatures, in both the radial & longitudinal directions.

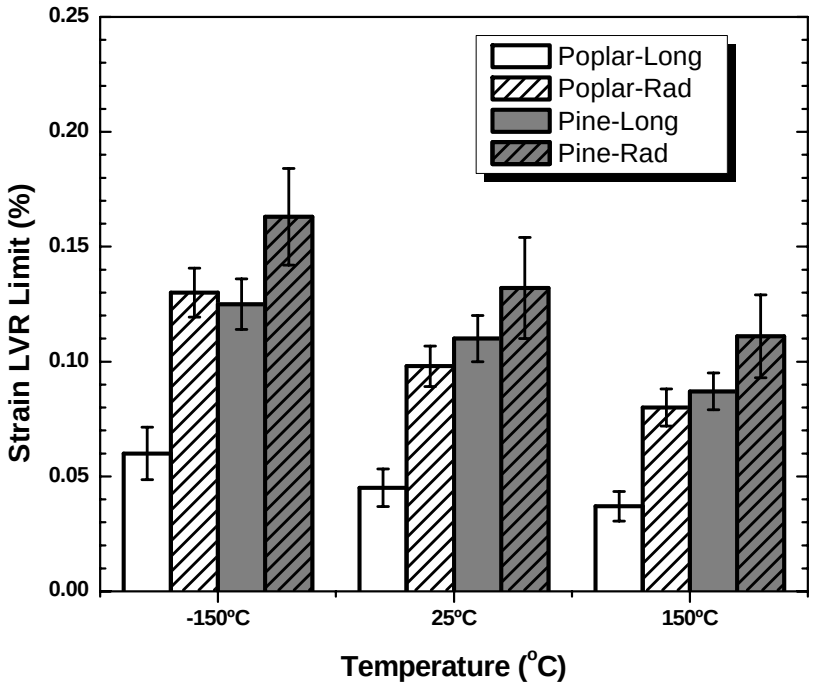

Figure 4.3.1.1. Effect of temperature, wood species & grain orientation on the mean LVR limit of poplar and pine wood samples. Each sample was first annealed at 150°C for 10min, then cooled at 10°C/min to the experimental temperature, where they were equilibrated for 20 min, before the 1Hz strain sweep test. Error bars represent ± 1 standard deviation which is based upon three observations from separate samples.

Under similar conditions, the LVR limit of radial samples was significantly larger than for the corresponding longitudinal samples. The influence of grain orientation on the LVR limit reflects the supramolecular ordering of the different wood polymers. In the longitudinal samples, the applied strain is mostly sustained by the semicrystalline cellulose fibrils (if we simply consider the S2 layer). On the other hand, the strain imposed on the radial samples is mostly focused on the amorphous matrix polymers.

When the LVR is exceeded, the amorphous polymers experience a significant disruption in conformation and packing. Since the longitudinal samples exhibit a lower LVR limit, the longitudinal grain orientation apparently promotes sampling of amorphous polymers which (on average) are relatively restricted in motion, such as we might expect near the fibril surfaces.

Figure 4.3.1.1 also shows that the LVR decreased slightly as the temperature was increased. Furthermore, pine samples exhibited a significantly higher LVR limit than the corresponding poplar samples. This observation might tempt us to conclude that the LVR limit is species dependent; perhaps softwoods have a higher LVR than hardwoods. However, this is pure speculation in light of the small sampling presented here. Nonetheless, this raises an interesting question- could a systematic analysis of the LVR limit provide a means for material comparison, much as the temperature and breadth of the lignin glass transition does? Perhaps so, but apparently great care would be required. In a separate (and slightly different) set of experiments using samples from a different source, the results found were in disagreement with those shown in Figure 4.3.1.1. Representing a separate source of samples, Figure 4.3.1.2 again demonstrates that radial samples provide a greater LVR limit than longitudinal ones. However in this case, the effects of temperature are different, where increasing temperature causes an increase in the LVR. Furthermore, the samples represented in Figure 4.3.1.2 exhibit LVR limits which are significantly lower than those in Figure 4.3.1.1. The source of this discrepancy is unknown; but this demonstrates that regular LVR measurements should be standard wood DMA protocol. Perhaps the discrepancies (in Figures 4.3.1.1 & 4.3.1.2) are related to natural wood variation, or possibly to differences in hygrothermal history.

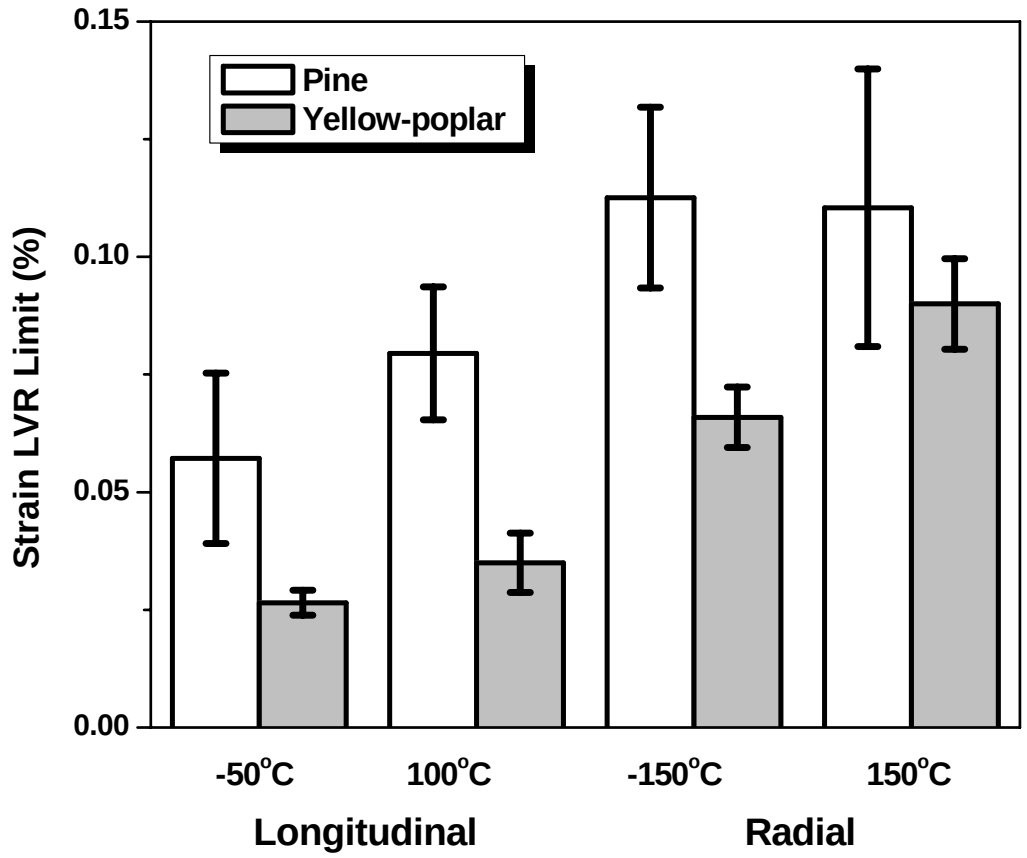

Figure 4.3.1.2. Effect of temperature, wood species & grain orientation on the LVR limit of samples prepared from wood obtained from a different source. Samples were first heated at 10°C/min to 150°C and annealed there for 10min. The sample was then cooled at 10°C/min down to the setting temperature and was held isothermal for 20min before the constant 1Hz strain sweep test. (5 replications each)

In this work, thermal history was found to be extremely important. Figure 4.3.1.3 shows two sequential dynamic scans of a single dry longitudinal pine sample. Notice that all relaxations are secondary in nature; the tan δ intensities are all below 0.02. However, the onset of a major softening appears at 150°C. The 1st scan is significantly different from the 2nd scan; the storage modulus generally decreased from the 1st to the 2nd scan, and while the 1st scan showed four tan δ relaxations (at -120°, -50°C, 30°C and 100°C), only two relaxations (at -105° and 25°C) were observed in the 2nd scan. These observations were highly replicable and similar effects were seen in poplar samples also.

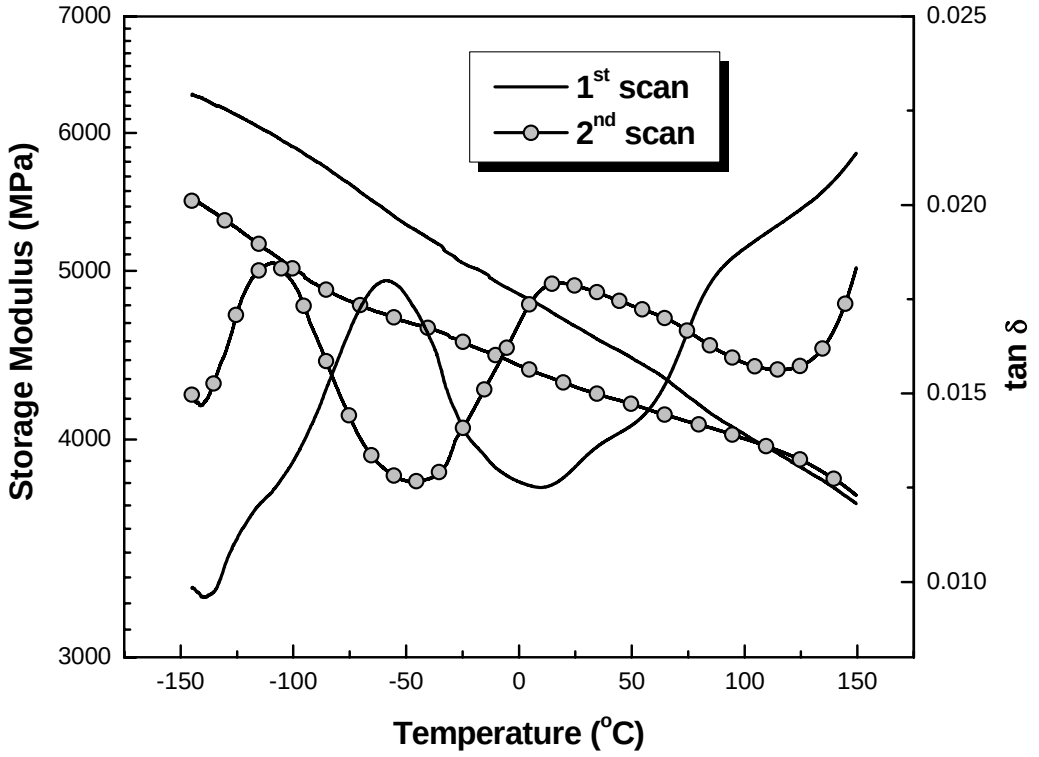

Figure 4.3.1.3. Two sequential dynamic scans of dry longitudinal pine from -150° to 150°C. Sample initially cooled at 10°C/min to -150°C (10 μm amplitude, 0.03% strain, 1Hz frequency, 5°C/min heating rate, 10°C/min cooling rate)

The differences in 1st and 2nd dynamic scans are not caused by changes in the wood moisture content. These experiments were initiated with completely dry samples, and mass changes over the course of the analyses were insignificant (< 0.5%).

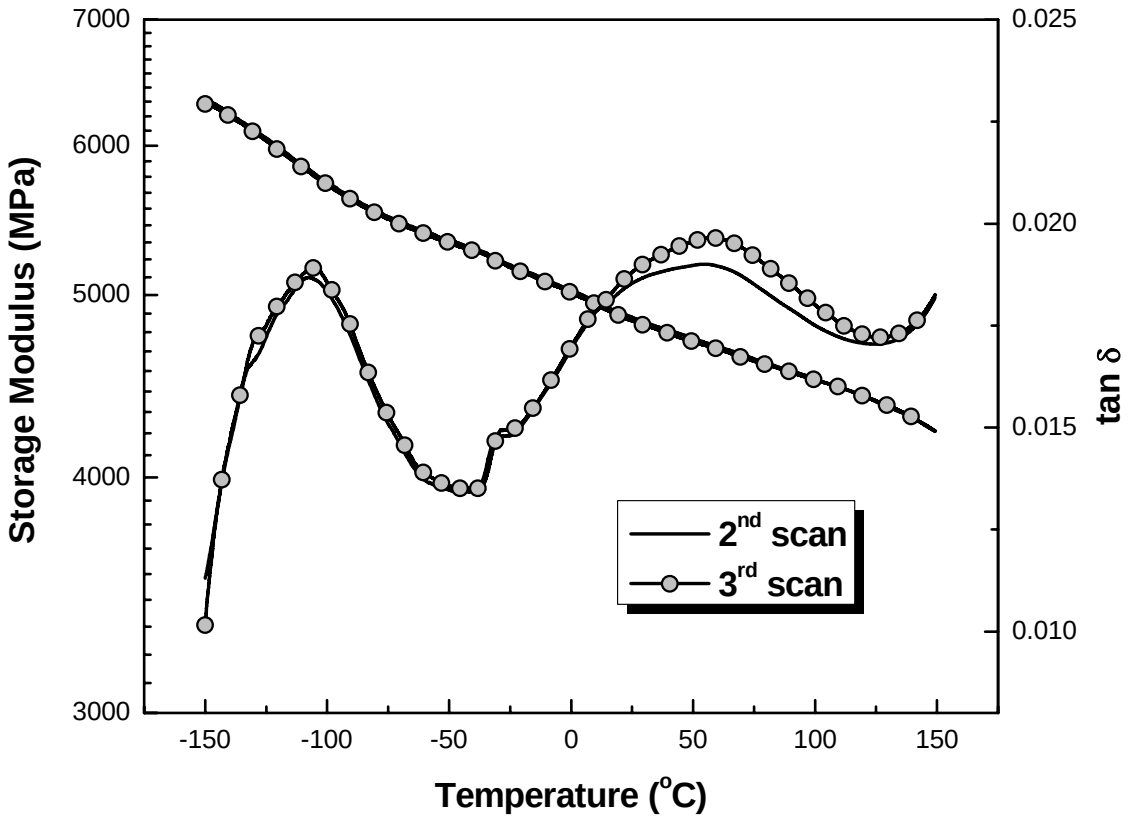

Figure 4.3.1.4. Second and third sequential dynamic scans of longitudinal pine from -150° to 150°C Sample initially cooled at 10°C/min to -150°C (10 μm amplitude, 0.03% strain, 1Hz frequency, 5°C/min heating rate, 10°C/min cooling rate)

Figure 4.3.1.4 shows the 2nd and 3rd sequential scans for a separate longitudinal pine sample. This demonstrates that the first scan alters the sample response, and results in a reproducible response in the 2nd and 3rd thermal scans.

In order to determine if the thermal treatment imposed during the 1st scan caused a permanent or reversible change, poplar samples were subjected to the 1st scan and the second scan was conducted after various sample storage times (storage over P_2O_5 at room temperature). Note that this experiment was conducted over a narrower temperature range (-100°C - 150°C). Careful inspection of the tan δ data in Figure 4.3.1.5 reveals that the scans appear organized as a collection of similar pairs. For example, 2nd scans after 0 and

6 hours storage appear quite similar; they both appear as typical 2nd scans acquired immediately after the 1st scan. Likewise, tests after 10 and 18 hours sample storage are similar, but the longer storage time has resulted in a partial reversion back towards the 1st scan behavior; this is particularly evident in the high temperature region. Finally, the 2nd scan after 48 hours storage appears essentially identical to the 1st scan. Note the scans shown in figure 4.3.1.5 were performed on the same sample.

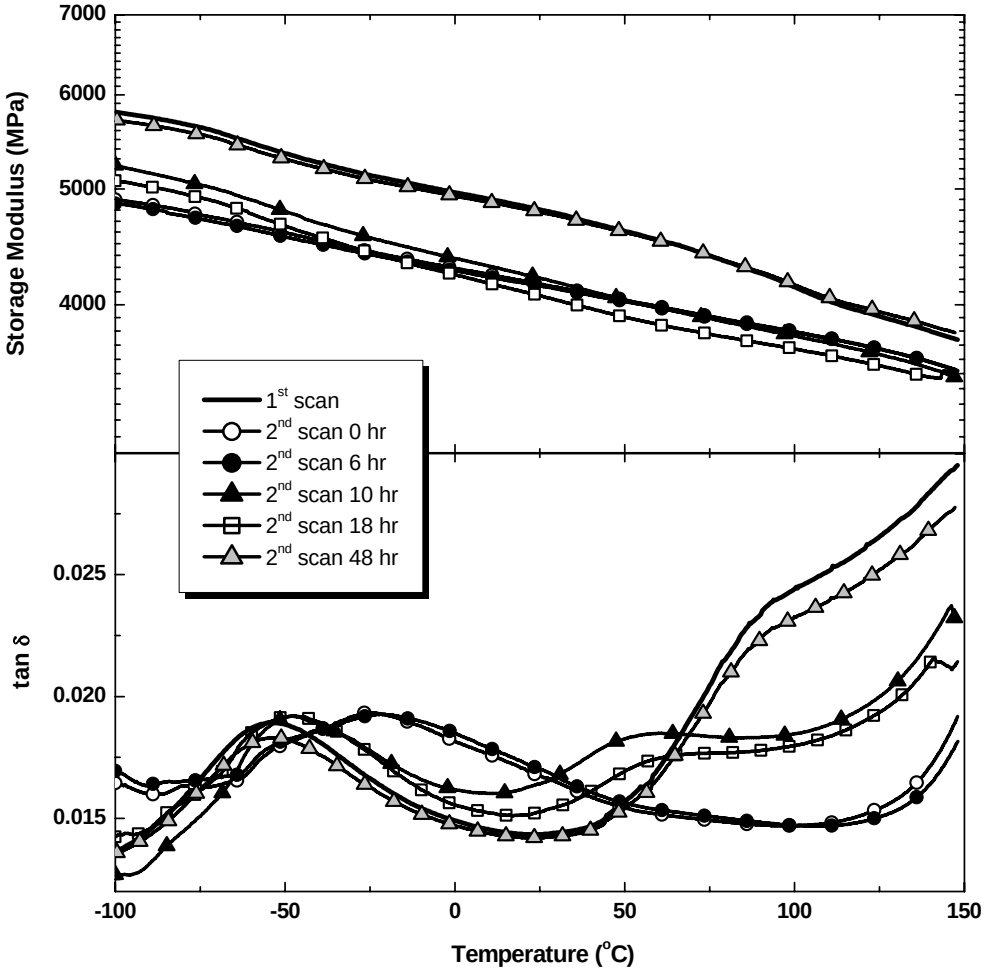

Figure 4.3.1.5. Influence of sample storage time (in hours) after the first thermal scan for longitudinal poplar samples. All scans were performed on the same sample. A typical 1st scan is shown along with 2nd scans following the storage times indicated. Sample equilibrated at lowest temperature for 20 min before scan (5°C/min heating rate, 10°C/min cooling rate, 1 Hz frequency, 0.03% strain)

Figure 4.3.1.5 indicates that the effects caused by scanning dry poplar up to 150°C are entirely reversible. We believe that this will also be true for pine samples, but this experiment was not conducted. Figure 4.3.1.5 suggests that the thermal treatment from the initial scan disrupts wood polymer packing and/or associations, and that the polymers relax back to their original state after 48 hours at room temperature. And while this experiment was conducted with dry wood, this thermal disruption and relaxation might still involve the site exchange of tightly bound water. In any event, it is clear that wood thermal history is an important issue to address, as for all polymeric materials [14,15].

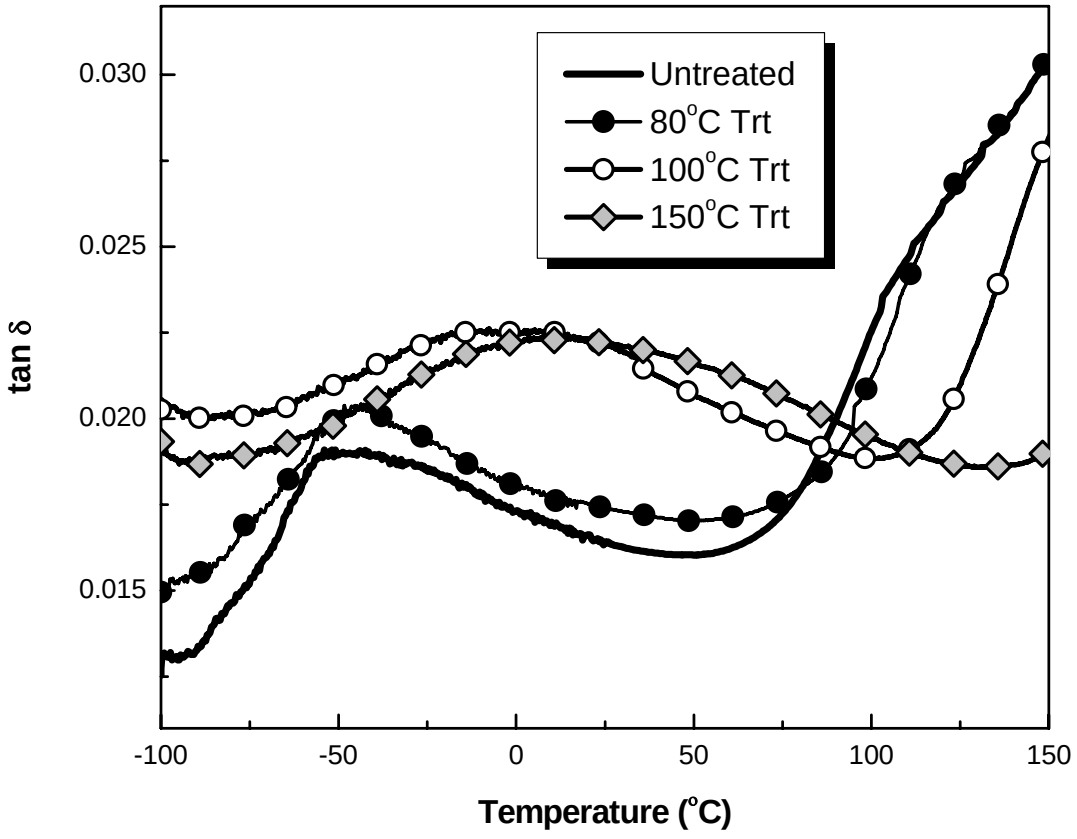

Figure 4.3.1.6. Variation of the thermal scans (tan δ) of longitudinal YP sample after annealing for 30 minutes at different temperatures (80°, 100°, 150°C) (5°C/min heating rate, 1 Hz frequency, 0.03% strain)

Since scanning to 150°C causes a reversible disruption of wood polymers, one wonders what minimum temperature is required to initiate this effect. In order to address this question, a series of samples was isothermally treated for 30 minutes at 80°, 100° or 150°C and then cooled and scanned to 150°C (figure 4.3.1.6). The isothermal treatment at 80°C did not cause a change in the wood response; the scan following the 80°C treatment is very similar to a typical 1st scan. In contrast, a 30 minute annealing at 100°C does disrupt the wood structure, providing a scan which is similar, but not identical, to a 30 minute treatment at 150°C.

4.3.1.4. Conclusions:

This work demonstrates that the DMA of dry wood requires attention to several details:

- The limit of the linear viscoelastic region is significantly affected by the sample grain orientation, wood species and sample source.
- As with all polymeric materials, the dynamic mechanical response of dry wood is dependent upon the sample thermal history.
- The thermal treatment of dry wood at temperatures from approximately 100 - 150°C causes a reversible disruption in wood polymer packing.
- Dry wood relaxes back to its original state in 48 hours

References

(1) Back, E. L.; Salmen, L. *TAPPI* **1982**, *65*, 107-110.
(2) Obataya, E.; Norimoto, M.; Tomita, B. *Journal of Applied Polymer Science* **2001**, *81*, 3338-3347.
(3) Sugiyama, M.; Obataya, E.; Norimoto, M. *Journal of Materials Science* **1998**, *33*, 3505-3510.
(4) Backman, A. C.; Lindberg, K. A. H. *Journal of Materials Science* **2001**, *36*, 3777-3783.
(5) Olsson, A.-M.; Salmen, L. In *Cellulosics: Chemical, Biomedical and Material Aspects*; Kennedy, J. F.; Phillips, G. O.; Williams, P. A., Eds.; Ellis Horwood: New York pp 257-262.
(6) Olsson, A.-M.; Salmen, L. In *Viscoelasticity of Biomaterials*, ACS Symposium Series 489 ed.; Glasser, W. G.; Hatakeyama, H., Eds.; American Chemical Society: Washington D.C., 1992; pp 133-143.
(7) Olsson, A.-M.; Salmen, L. In *International Conference of COST Action E8*: Copenhagen, Denmark, 1997; pp 269-279.
(8) Olsson, A.-M.; Salmen, L. *Nordic Pulp and Paper Research Journal* **1997**, *12*, 140-144.
(9) Olsson, A.-M.; Salmen, L. In *Hemicellulose: Science and Technology*; Gatenholm, P.; Tenkanen, M., Eds.; American Chemical Society: Washington D.C., 2004; pp 184-196.
(10) Salmen, N. L.; Back, E. L. *TAPPI* **1977**, *60*, 137-140.
(11) Salmen, L. *Journal of Materials Science* **1984**, *19*, 3090-3096.
(12) Salmen, L.; Olsson, A.-M. *Journal of Pulp and Paper Science* **1998**, *24*, 99-103.
(13) Bjorkman, A.; Salmen, L. *Cellulose Chemistry and Technology* **2000**, *37*, 7-20.
(14) Hutchinson, J. *Progress in Polymer Science* **1995**, *20*, 703-765.
(15) Struik, L. *Physical Aging in Amorphous Polymers and Other Materials*; Elservier: Amsterdam, 1978.

Probing the Species-dependent Interactions between Wood and Polymeric Isocyanate Resins by Dynamic Mechanical Analysis

Sudipto Das, C.E. Frazier
Department of Wood Science and Forest Products
Virginia Polytechnic Institute and State University
230 Cheatham Hall, Blacksburg, VA 24061-0323

4.3.2.1. Introduction

Polymeric isocyanate (PMDI) resins are commonly used for the manufacture of particulate wood-based composites such as oriented strandboard (OSB). In 2001, PMDI accounted for ~20% of the total resin solids used in the North American OSB industry [1]. This is because of the various advantages offered by PMDI resins which include faster cure, no formaldehyde emission, and superior mechanical properties. The growing importance of this resin to the wood products industry has stimulated research intended to improve our understanding of PMDI/wood interactions. This study uses mechanical spectroscopy, or dynamic mechanical analysis (DMA), to probe the PMDI/wood interphase and how it varies between two woods, yellow-poplar and southern yellow pine. These woods are commonly used in the southeastern United States for the manufacture of OSB.

Many studies have been conducted on the DMA of wood. Salmen *et al.* [2-9] for example have extensively studied water-saturated wood using DMA, demonstrating that the major transition observed in the temperature range of 20° to 140°C is due to the softening of in situ lignin [3,9]. The lignin softening or glass transition (T_g) was observed to depend on the wood species [3,4], where hardwood lignins soften at lower temperatures due to lower crosslinking (or more syringyl units) [6]. The lignin T_g was also found to vary

according to the grain orientation of the DMA sample; the tan δ peak for the in situ lignin transition occurred at a slightly higher temperature in the axial direction than in the transverse direction. [9,10]. It has also been demonstrated [9,11] that the lignin T_g may be described by the William-Landel-Ferry (WLF) equation [12]. More recently, Laborie *et al.* [13] successfully demonstrated how the lignin T_g in ethylene glycol (EG) plasticized wood may be analyzed by the cooperativity analysis [14-16], a method which reveals the nature of segmental interactions.

Only a few DMA studies have been conducted in the recent past specifically dealing with PMDI/wood interactions [17-19]. Uncured liquid PMDI resins have been shown to plasticize wood; subsequent cure caused a corresponding increase in the wood stiffness [17]. Another study investigated wood interactions with PMDI and also with urea-formaldehyde (UF); where in contrast to UF, PMDI was shown to alter wood relaxations [18,19]. This led the authors to conclude that PMDI resin changed the molecular packing of wood polymers due to deep resin penetration and intimate molecular associations.

The present study extends the prior DMA of PMDI/wood interactions through the use of simple dynamic thermal scans and also of time/temperature superposition of pine and poplar woods.

4.3.2.2. Experimental

4.3.2.2.1. Materials

Commercial PMDI resin (Huntsman Rubinate 1840) was obtained from Hunstman Polyurethanes and was used as received. Acetic anhydride (97%), HPLC grade acetone (99.9%) and ethylene glycol were purchased from Aldrich chemical company and used as received.

Two wood species were selected for analysis: yellow-poplar, YP (*Liriodendren tulipifera*) & southern yellow pine, SYP *(Pinus spp*.). Wood samples were analyzed using two different grain orientations (subsequently referred to as "longitudinal" & "radial"). Longitudinal samples had dimensions of 40 mm (longitudinal) x 10 mm (tangential) x 4 mm / (radial) [1.6" x 0.4" x 0.16"] ; radial samples were 40 mm (radial) x 10 mm (tangential) x 4 mm (longitudinal) [1.6" x 0.4" x 0.16"]. A separate collection of radial samples (27 mm / 1.06" radial x 2 mm 0.079" tangential x 1.5 mm / 0.06" longitudinal) were also prepared for analysis in a tension-mode solvent-submersion clamp. All samples were initially dried (105°C for 24 hr) and then equilibrated to 6-7% moisture content (MC), before further treatment.

4.3.2.2.2. **Methods**

4.3.2.2.2.1. Wood Acetylation

Samples were impregnated with acetic anhydride (AA) under vacuum (~0.1 mm Hg). The wood samples were then heated in AA at 110°C for 9 hours (h), whereafter they were acetone extracted for 24 h. These acetylated samples were dried under vacuum (~0.1 mm Hg) at 40°C for 24 h. Samples were then equilibrated to 8-9% MC before further treatments. The increase in sample weight after acetylation was ~18% for poplar and ~16% for pine (based on dry wood).

4.3.2.2.2.2. Resin impregnation

Moisture-equilibrated samples (untreated and acetylated) were impregnated with liquid PMDI resin using an open-cell method, using either neat PMDI or PMDI dissolved in anhydrous acetone. The samples were first impregnated with resin (neat resin or resin-acetone solution) using various pressures and treatment times, followed by the

application of vacuum (30 min, ~0.1 mm Hg). These resinated samples were then cured at 120°C for 2 h. Two types of control samples were prepared in order to achieve the same thermal history as for the resinated wood samples. With respect to samples that were resinated and cured with neat PMDI, controls were prepared by initially equilibrating to a 6-7% MC, followed by heating at 120°C for 2 h. For samples which were resinated using acetone/PMDI solutions, controls were impregnated with pure anhydrous acetone (using the open-cell process described above), and then subsequently heated at 120°C for 2 h. All control and resin-treated samples were stored under dry conditions (over phosphorous pentoxide in a dessicator) before further analysis.

4.3.2.2.2.3. Ethylene-glycol plasticization

Samples (control, acetylated and resin impregnated) were impregnated with EG under vacuum (~0.1 mm Hg) for 30 min. Impregnated samples were then treated in EG at 100°C (110°C for small radial samples) for 1 h. after the treatment, the heat source was removed and the samples were allowed to cool slowly to room temperature (RT). The cooling rate was monitored and found to be 1.5°C/min from 110°-40°C and 0.5°C/min from 40°C to RT. The samples were stored in EG before further analysis.

4.3.2.2.2.4. Dynamic tests

All DMA tests were conducted on a TA Instruments® 2980 DMA. Two different clamps were used for analysis: single cantilever bending and submersion tension.

4.3.2.2.2.4.1. Single-cantilever bending mode

Dry and EG-plasticized samples with different grain orientations (longitudinal and radial) were analyzed in single cantilever bending mode along or across the long axis of the sample. The linear viscoelastic limit (LVR) was determined by conducting a strain-sweep

experiment, where the sample was sinusoidally deformed with increasing strain/amplitude at 1 Hz frequency. The LVR limit was arbitrarily defined as the strain which resulted in a 5% reduction in the initial storage modulus, E'; the initial modulus was that measured at 0.006% strain or 2 μm amplitude. The strain (%) LVR limit for longitudinal poplar, radial poplar, longitudinal pine and radial pine was 0.045%, 0.11%, 0.098% and 0.132% respectively at 25°C. All dry samples were thermally treated in the DMA before analysis. The thermal treatment consisted of rapidly heating (25°C/min) the sample to 150°C, where it was equilibrated for 10 min and then cooled at 10°C/min to -150°C. Dynamic thermal scans were conducted as follows: 0.057% strain [20 μm amplitude] for radial samples; 0.029-0.043% strain [10-15 μm amplitude] for longitudinal samples; heating rate: 5°C/min (dry samples) and 2°C/min (EG-plasticized samples); frequency: 1 Hz.

4.3.2.2.2.4.2. Submersion Tension mode

The smaller radial samples were analyzed in tension parallel to the radial direction using the TA Instruments submersion tension clamp. The DMA thermal control was inactivated and the DMA sample chamber was left in the open configuration. This allowed for the use of a separate thermal control system which consisted of a small tape heater bonded directly to the submersion clamp, and which was controlled by a digital thermal controller. The accuracy of the thermal controller was ±0.5°C. During the experiment, the sample was submerged completely in EG. The LVR limit was determined by a static force-ramp experiment, where the sample was deformed at a constant rate (1N/min). The LVR limit was calculated as the strain at which the stress vs. strain plot became non-linear. LVR limit was determined at 40°, 80° and 120°C for every

wood sample type. The analysis was conducted using isothermal frequency-sweep segments performed over the temperature range of 40° to 120°C. The frequency was varied from 0.5 to 10 Hz. A 10- minute thermal equilibration was employed prior to every isothermal frequency-sweep segment. The tensile strain was progressively raised with increasing experimental temperature, but was in all cases within the LVR.

4.3.2.3. Results and Discussion

4.3.2.3.1. Dynamic analysis in single cantilever bending mode

4.3.2.3.1.1. Effect of wood grain orientation:

Wood is an anisotropic material having unique and independent mechanical properties in three mutually perpendicular axes namely, longitudinal (axial direction), radial and tangential (collectively known as transverse direction). The longitudinal axis is parallel to the fiber direction; the radial axis is normal to the fibers as the radius of a circle (tree stem), while the tangential axis is perpendicular to the grain but tangent to the growth rings. Only a few studies [10,20] have analyzed the dynamic mechanical properties of wood in different grain directions. Salmen [10] measured the viscoelastic properties of ***water-saturated wood*** in the axial and transverse directions. Results showed that the in situ lignin softening occurred at slightly higher temperatures in the axial samples than the corresponding transverse samples. But the author attributed these observations to the anatomical differences of the samples, which reflected the diverse influences of the reinforcing components in two directions. Another study [20] analyzed the dynamic responses of ***dry wood*** in the radial and tangential directions and found that the intensity of secondary relaxations were larger and at higher temperatures in the tangential samples, relative to the corresponding radial samples. In this study, the dynamic mechanical

responses of wood in two different grain orientations (longitudinal and radial directions) were analyzed, to determine which sample orientation is better suited for the evaluation of the PMDI/wood interactions.

Figure 4.3.2.1 shows the variation of the LVR limits of dry wood samples with grain orientation at different temperatures.

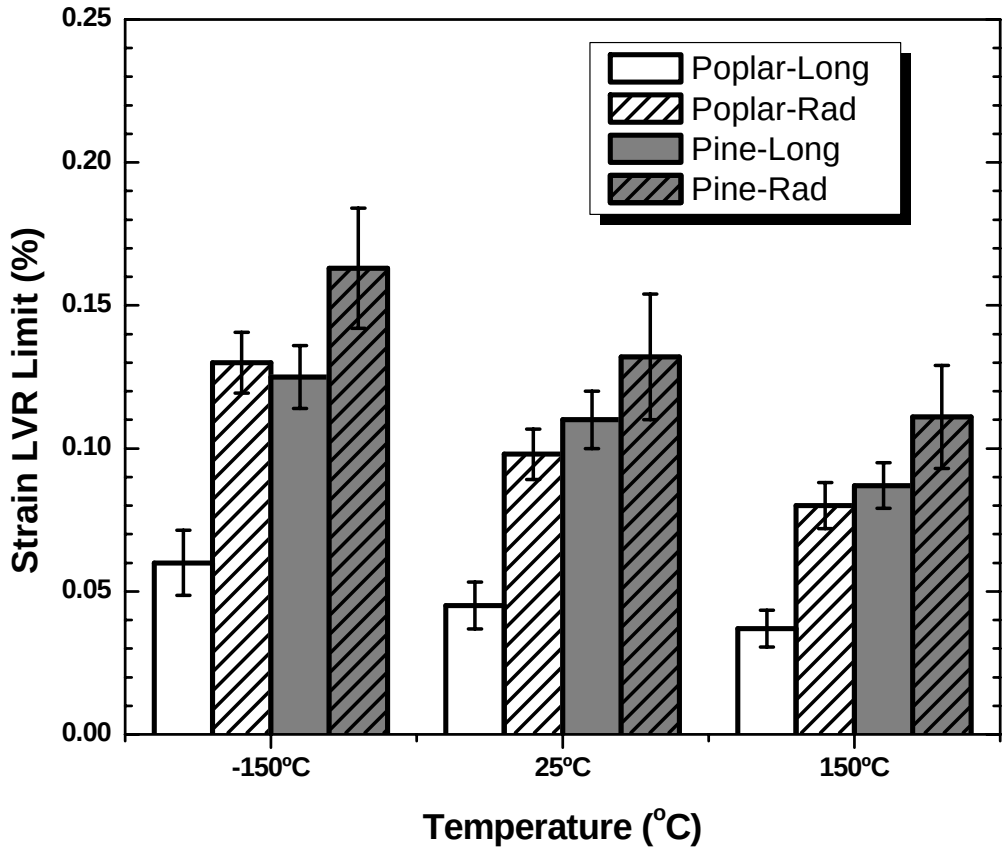

Figure 4.3.2.1. Effect of temperature, wood species & grain orientation on the LVR limit of dry wood samples. Each means is based upon three of observations; error bars represent ±1 standard deviation.

The LVR limit of radial samples was found to be larger than the corresponding longitudinal samples, under all conditions. Thus, use of radial samples over longitudinal samples was preferred because it allowed the use of higher strain/amplitude during DMA tests, which in turn gave a higher signal/noise ratio.

Figure 4.3.2.2 shows the dynamic scans of EG-plasticized radial and longitudinal pine samples. Both samples showed a major relaxation, which is due to the softening of in situ lignin [13,21].

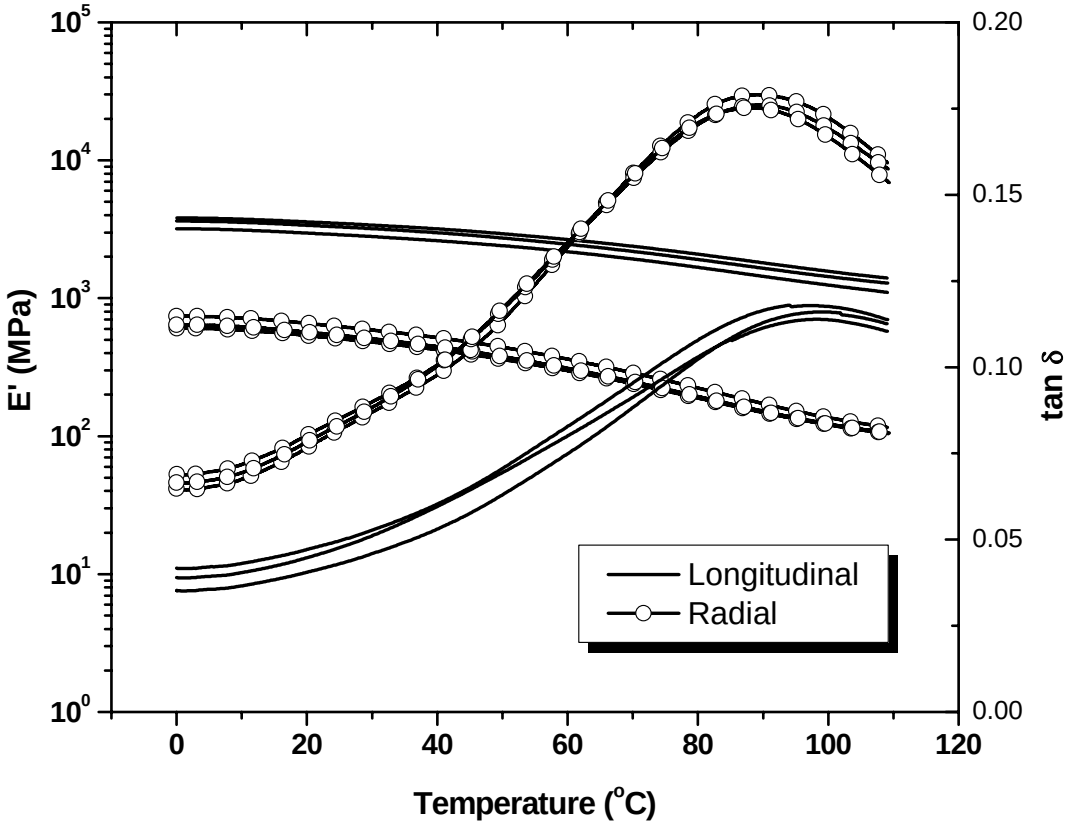

Figure 4.3.2.2. Effect of grain orientation on the dynamic scans of EG-plasticized pine samples (0.06% strain, 1 Hz, 2°C/min heating rate, 3 replications each).

But the lignin transition of radial samples was found to be more energetic and at a slightly lower temperature than the corresponding longitudinal samples. Similar results were also observed for the corresponding poplar samples.

In this study, the effect of resin on the wood morphology was studied by observing changes in the lignin relaxation. The radial wood samples were preferred over the longitudinal samples, because in addition to having a higher LVR limit (which provided a higher signal/noise ratio), the radial samples exhibit a more energetic and

slightly lower temperature lignin transition. While the temperature difference is minor, the radial samples will help to minimize plasticizer loss and thermal degradation.

4.3.2.3.1.2. Impregnation method: Neat resin vs. resin solution

Wood samples were resin-treated with two methods: 1) using neat PMDI, or 2) using acetone/PMDI solutions. Regarding the use of neat PMDI, the resin content of the radial samples was varied by controlling pressure (P), pressure time (PT) and vacuum time (VT). Table 4.3.2.1 shows the final resin contents (after cure at 120°C for 2 h) of pine and poplar radial samples under different impregnation conditions.

Table 4.3.2.1. Effect of different impregnation parameters on the mean final resin content of radial samples; standard deviations are also shown.

Wood Species	P (kPa)	PT (min)	VT (min)	Mean resin content (%)	# Replicates
Pine	427.5	30	30	16.2 ± 2.7	48
	34.5	10	30	12.1 ± 1.2	20
Yellow-poplar	427.5	30	30	23.2 ± 3.2	26
	34.5	10	30	37.6 ± 13.6	20
	34.5	10	10	10.1 ± 0.9	17
	275.8	15	30	23.1 ± 8.9	20

Under similar impregnation conditions, the final resin content in poplar samples was higher than that in pine. The variation in the final resin content was rather high when using neat PMDI; it was also difficult to obtain resin contents below 10%.

Impregnations using the resin/acetone solutions were controlled by varying the solution concentration, while fixing the other impregnation parameters as follows: pressure=10 psi (68.95 kPa), pressure time=15 min and vacuum time= 15 min. Figure 4.3.2.3 shows the variation of the final resin content (after cure) with resin-acetone solution concentration.

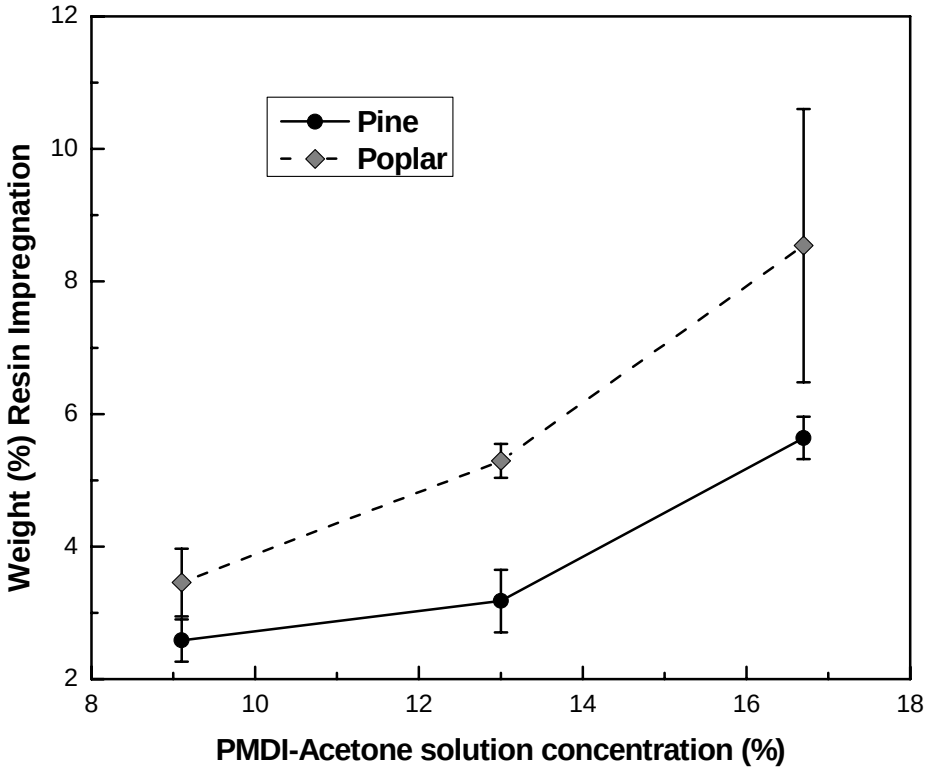

Figure 4.3.2.3. Variation of the cured resin content of radial samples with resin solution concentration. Each mean is based upon 10 observations; error bars represent ±1 standard deviation.

Under similar impregnation conditions (for both neat resin and resin solution), the resin impregnation in YP samples was higher than SYP samples. The control over the final cured resin content was better using resin solution as compared to neat PMDI. For certain analyses, the resin solution impregnated samples are preferred to those impregnated by neat PMDI. And while the solution impregnated samples do not accurately reflect industrial conditions, it is believed that they do reflect fundamental aspects of the wood/resin interactions. However, one must be concerned about how poplar and pine samples may differ in acetone swelling. For example, if pine swells ***substantially different*** from poplar, then it might be possible for the solution impregnation to selectively swell (and resinate) different components of the wood cell

wall. Table 4.3.2.2 shows the maximum tangential swelling for different wood species in acetone.

Table 4.3.2.2. Maximum tangential swelling of different woods in acetone

Wood	Swelling conditions	Tangential swelling (%)
Sitka spruce [22]	23°C, 100 days	5.7 ± 0.2
Douglas-fir [22]	23°C, 100 days	4.6 ± 0.2
Southern Pine [23]	25°C, 24 h	5.6
Sugar maple [22]	23°C, 100 days	7.1 ± 0.2
Quaking aspen [22]	23°C, 100 days	7.5 ± 0.2

The swelling conditions were similar in all cases except for the southern pine sample. The results show that there was a slight difference between the swellings of different wood species in acetone (swelling was slightly larger in hardwoods), but the differences were not considered large enough to result in selective swelling of poplar over the corresponding pine samples.

4.3.2.3.1.3. Dynamic thermal scans of dry and EG plasticized wood

Figure 4.3.2.4 shows the thermal scans of dry, control wood samples, illustrating the differences between pine and poplar samples.

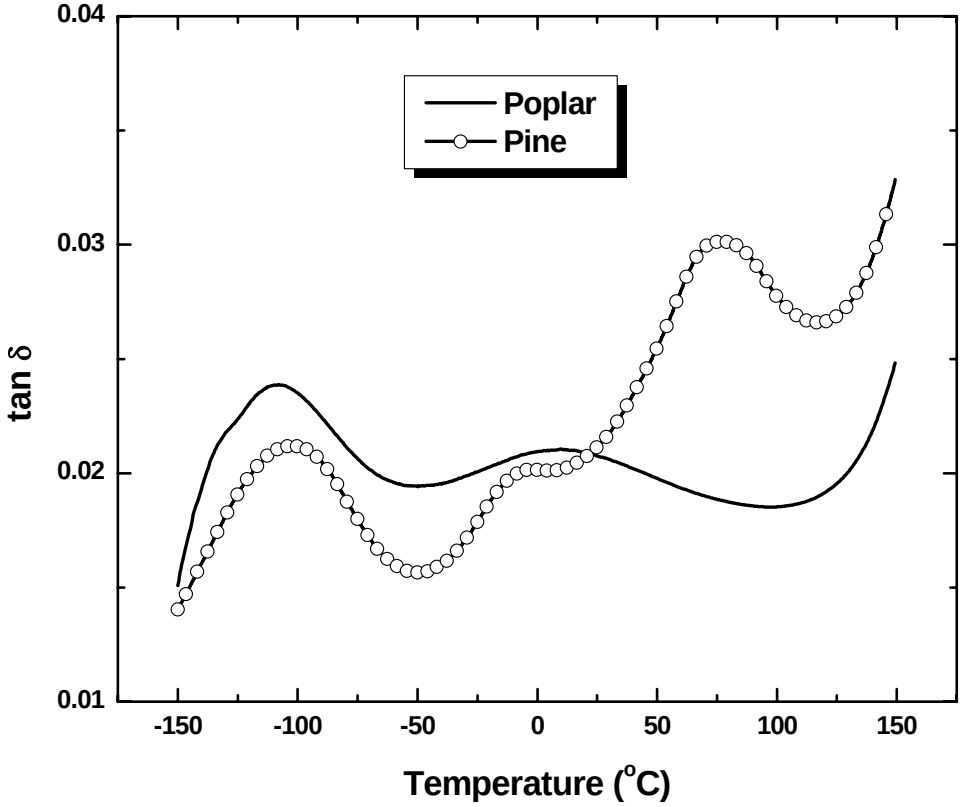

Figure 4.3.2.4. Variation of the dynamic thermal scans of dry radial wood samples with species. Dynamic scans succeeded a thermal treatment at 150°C for 10 min followed by cooling at 10°C/min to -150°C (5°C/min heating rate, 0.057% strain, 20mm amplitude, 1 Hz frequency).

Both showed a relaxation peak at ~-105°C, which may be attributed to the site exchange of moisture [11] or to the motion of wood methylol groups [24]. At higher temperatures, pine exhibited two relaxations (-10° and 75°C), while only one broad relaxation centered at ~30°C was observed for poplar samples- the precise nature of these transitions is unknown and not discussed in the literature. All of these transitions appear to be secondary in nature because of their very low tan δ intensity. However, both woods show the onset of a significant relaxation at ~ 120°C, which probably reflects initiation of the

glass transition of any one or perhaps all of the structural wood polymers. The main softening of dry wood polymers lies beyond 150°C; the in situ T_g's of cellulose, hemicellulose and lignin in dry wood are reported to occur at 200°-250°C, 170°-220°C and ~205°C respectively [5,25].

Figure 4.3.2.5 shows the dynamic scans of control and resin impregnated pine samples at different resin impregnation levels.

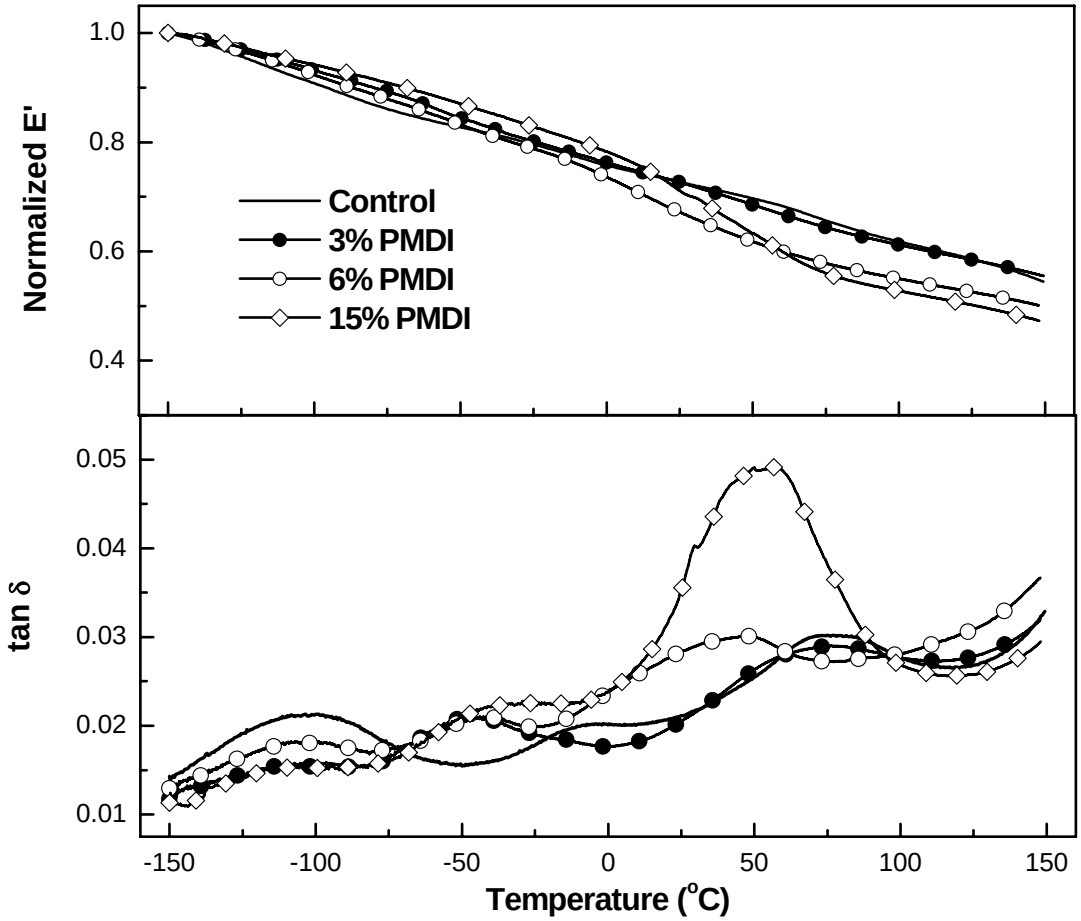

Figure 4.3.2.5. Effect of resin loading on the dynamic scans of dry radial Pine samples (0.06% strain, 1Hz frequency, 5°C/min heating rate). These dynamic scans succeeded thermal treatments at 150°C for 10 min. Method of resin impregnation: solution for 3 and 6% PMDI and neat resin for 15% PMDI

The intensity of the low temperature tan δ relaxation (-105°C in the control) decreased upon resin impregnation. This may be attributed to immobilization of the wood methyol groups due to reaction with the resin, or to a disruption of the site-exchange of adsorbed moisture. Regarding the minor tan δ relaxation at -10°C in the control sample, Figure 4.3.2.5 demonstrates that all resin-loading levels appear to depress this transition to a temperature of approximately -50°C, with little or no effect on tan δ intensity. In contrast, the highest temperature tan δ relaxation (75°C in the control) exhibits a highly variable effect of PMDI treatment: 3% PMDI appears to cause little or no effect; 6% PMDI caused a slight temperature depression, and little change in tan δ intensity; and 15% PMDI caused a slight temperature depression (which is less than that for 6% PMDI) but it also causes a substantial increase in the tan δ intensity. Regarding the storage modulus, it is interesting to note that 6 and 15% PMDI appear to cause a noticeable softening near 50°, a softening which is not seen in the control and 3% PMDI samples.

Similar trends were also observed with resin impregnation for poplar samples (figure 4.3.2.6). The low temperature tan δ relaxation (~105°C) in poplar, was slightly depressed in the presence of the resin. The high temperature (~30°C) relaxation was observed to shift to higher temperatures (~50°C) with resin impregnation (3.5% PMDI); with further resin impregnation, the intensity of the relaxation was found to increase.

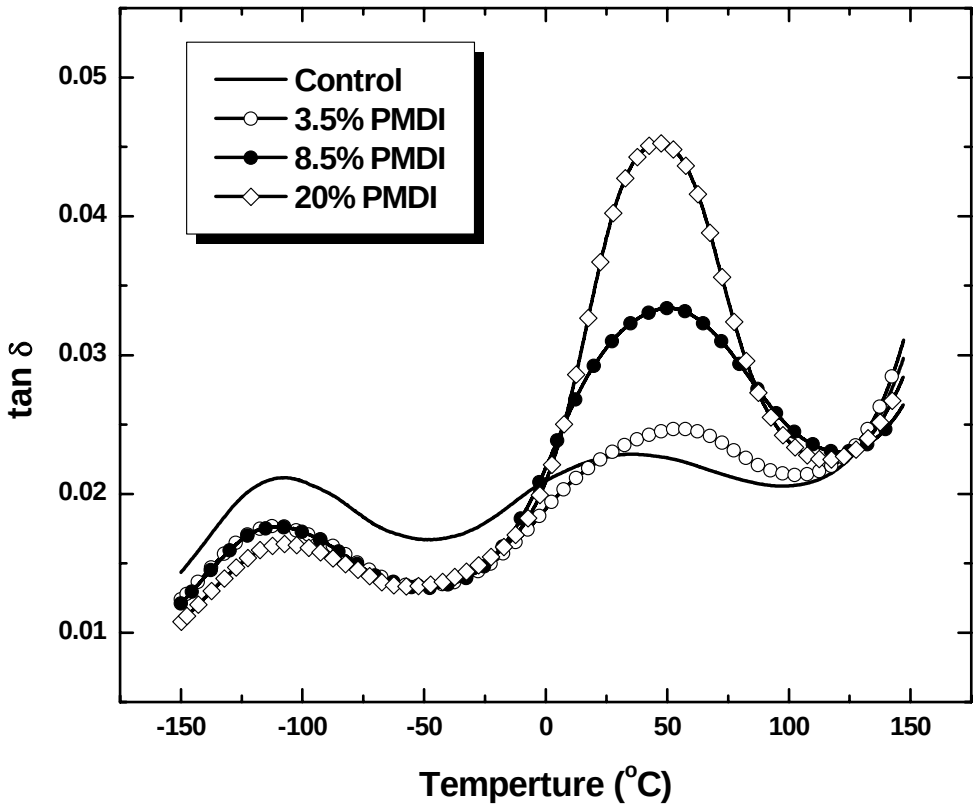

Figure 4.3.2.6. Effect of resin loading on the dynamic scans of radial poplar samples (0.06% strain, 1Hz frequency, 5°C/min heating rate). These dynamic scans succeeded thermal treatments at 150°C for 10 min. Method of resin impregnation: solution for 3.5 and 8.5% PMDI and neat resin for 20% PMDI.

The dry DMA scan effects presented in Figure 4.3.2.5 and 4.3.2.6 were very reproducible, which showed that while resin impregnation had minor effects on the dry thermal scans of poplar, a relatively larger change was observed for the corresponding pine samples. Consequently, the dry DMA scans reveal interesting PMDI/wood interactions. However these interactions are difficult to interpret because the precise nature of these secondary relaxations is unknown. And while the effects seen in Figures 4.3.2.5 and 4.3.2.6 are interesting, they provide no insight on the species effect of PMDI/wood interactions. Perhaps the actual lignin, cellulose and/or hemicellulose glass

transitions would reveal more about PMDI/wood interactions; but they cannot be observed in dry wood without the attending thermal decomposition.

This is indeed why previous investigators have studied and manipulated the effects of wood plasticizers which depress wood polymer glass transitions into an experimentally accessible temperature range [2-9,21,26,27]. Ethylene glycol (EG) is an efficient wood plasticizer, which is known to decrease the lignin T_g to ~80°C [13,21]. Figure 4.3.2.7 shows the dynamic scans of EG-plasticized radial pine and poplar wood samples before (control) and after resin impregnation (neat resin impregnation).

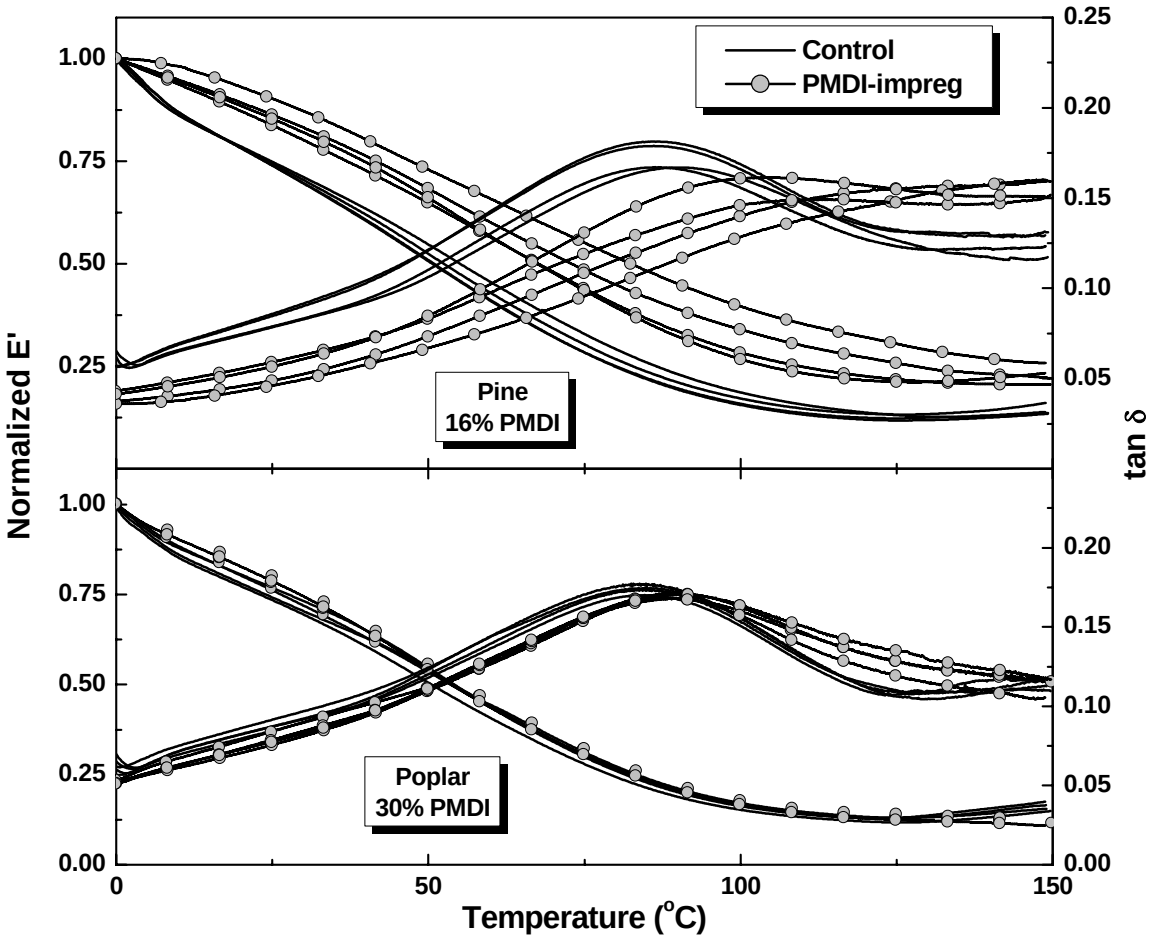

Figure 4.3.2.7. Dynamic scans of EG-plasticized control and PMDI-impregnated (neat resin impregnation) poplar and pine samples (0.06% strain, 1 Hz frequency, 2°C/min heating rate) [4 replications each]

Previous studies [4] have shown that hardwood lignins soften at a lower temperature than softwoods. But in this study with EG plasticization, the lignin softening temperatures were found to be similar for both pine and poplar (~86°C).

Figure 4.3.2.7 demonstrates that PMDI treatment had only minor effects on the YP lignin glass transition: the tan δ maximum is slightly increased (from 85°C to ~90°C); the transition breadth is also slightly increased; and the storage modulus appears unaffected. In contrast, PMDI treatment had a more dramatic effect on the SYP samples: the tan δ maximum increased to approximately 100°C; the transition breadth increased significantly; and the storage modulus (normalized at the 0°C response level) also increased. The great benefit of EG plasticization is apparent here- Figure 4.3.2.7 demonstrates that the PMDI/lignin interaction is significantly greater in SYP than in YP, even though the resin loading was higher in YP (~23.4% vs. 17% in SYP).

But examination of the plasticizer contents of the resin impregnated samples after the dynamic scans sheds a shadow of doubt on the conclusions drawn from the above figure. Table 4.3.2.3 shows the resin content and plasticizer content of wood samples before and after thermal analysis.

Table 4.3.2.3. Sample parameters of plasticized wood samples before and after dynamic scans (3 replications each).

Sample	Resin content (%)	Plasticizer before test (%)	Plasticizer after test (%)
Pine control	-	115.04 ± 4.6	38.5 ± 1.7
Pine-PMDI	16 ± 1.8	16.5 ± 0.8	7.5 ± 0.5
Poplar control	-	143.8 ± 9.3	50.4 ± 5.1
Poplar-PMDI	31.2 ± 6.2	79.8 ± 8.2	36.6 ± 4.6

Resin treatment inhibited plasticizer uptake; the EG content (before test) of impregnated pine samples were found to be significantly smaller than the corresponding poplar samples. Significant plasticizer loss was also observed in the course of the dynamic scans. The problem was found to be most severe for the resin impregnated samples; specifically for the resin impregnated pine samples. In order to investigate the basis of these huge differences in plasticizer uptake for resinated pine and poplar samples, the cell structures of resin impregnated wood samples were analyzed with fluorescence microscopy. Figure 4.3.2.8 shows the fluorescence micrographs of resin-impregnated (neat resin) pine and poplar samples. The resin contents of the wood samples were 16% for pine and 31% for poplar.

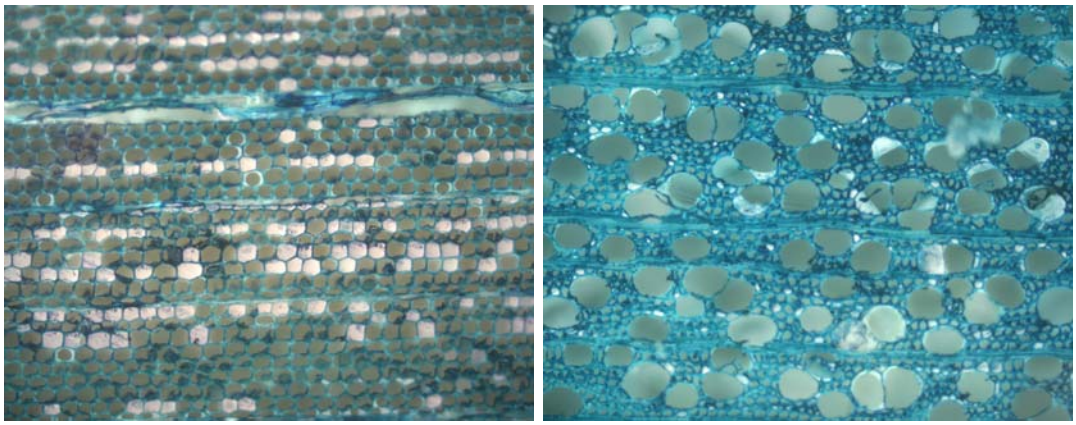

Figure 4.3.2.8. Fluorescence micrographs of resin impregnated pine (left) and poplar (right) samples. View represents the microtomed (4 mm) sections from the radial surface of samples. Microtomed sections were stained with 0.5% aqueous Toluidine Blue solution.

An open-cell method was used for PMDI impregnation because it is known to result in deep impregnation with low net retention of the resin [28], where the wood cell structure would remain open for unobstructed flow/conduction of plasticizer. But, the micrograph shows that numerous pine cell lumens were clogged with the cured resin. On the other hand, the cell structure of poplar sample was observed to be relatively open; most of the

vessels were unclogged, only the small diameter tracheids were blocked up with the resin. The resin was also found to finely coat the inside of the poplar vessels. Thus, the differences in the plasticizer uptake for resin impregnated samples can be attributed to the anatomical differences of the different wood species.

Thus, the plasticizer uptake was significantly smaller in pine due to its clogged cell structure; the plasticizer content of the resin impregnated pine samples was below its fiber saturation point (FSP) at the start of the dynamic scans (~16% plasticizer before test) due to insufficient plasticizer penetration. The dynamic scans of resin impregnated pine samples may have been severely affected by the variation of the plasticizer content (due to EG evaporation) in the course of the experiment (> 3 hr), since wood mechanical properties are known to vary with its solvent content below the FSP. Consequently, the effect of resin impregnation could not be analyzed by comparison of the control and neat resin impregnated pine samples (Figure 4.3.2.7). On the other hand, due to the relatively open cell structure, the poplar samples were above their FSP throughout the dynamic scan; hence, the effect of resin impregnation on the in situ lignin relaxation could be analyzed by Figure 4.3.2.7. PMDI treatment had only minor effects on the lignin glass transition: the tan δ maximum is slightly increased (from 85°C to ~90°C); the transition breadth is also slightly increased; and the storage modulus appears unaffected.

Similar experiments were performed on resin-solution impregnated wood samples, where the differences between the plasticizer content between the resin-impregnated samples were not as large as those observed in neat resin impregnated samples (table 4.3.2.4). Significant plasticizer loss was also observed with the resin-solution impregnated samples, but the plasticizer content at the end of the dynamic scans

was significantly larger in these samples relative to the neat resin impregnated samples (table 4.3.2.3).

Table 4.3.2.4. Sample parameters of plasticized resin-solution impregnated wood samples before and after dynamic scans (5 replications each).

Sample	Resin Content (%)	Plasticizer before test (%)	Plasticizer after test (%)
Pine control	-	143.4 ± 13.4	52.5 ± 11.4
Pine-PMDI	5.72 ± 0.6	105.2 ± 6.4	59.3 ± 2.2
Poplar control	-	143.2 ± 8.2	50.5 ± 5.6
Poplar-PMDI	8.1 ± 1.6	121.9 ± 9.4	65.6 ± 7.1

This suggests that the resin is distributed more uniformly in resin-solution impregnated samples. The differences in plasticizer content between the resin-solution impregnated pine and poplar samples were also significantly less relative to the corresponding neat-resin impregnated samples. Figure 4.3.2.9 shows the effect of resin impregnation on the in situ lignin transition of pine and poplar samples.

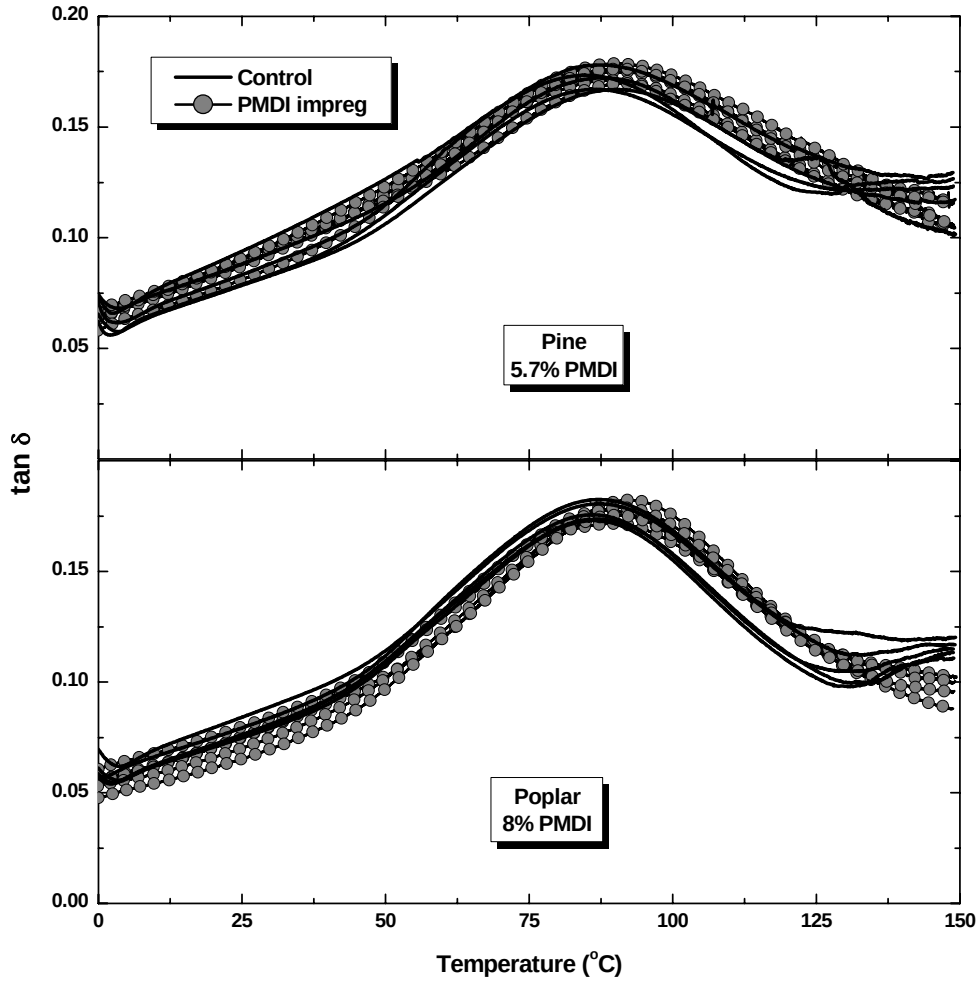

Figure 4.3.2.9. Effect of resin impregnation on the in situ lignin transition of pine and poplar wood (0.06% strain, 1 Hz frequency, 2°C/min heating rate) [5 replications each]

In the presence of the resin, the in situ lignin transition for both woods was broadened and slightly shifted (~5°C) to higher temperature; but the effect was found to be relatively greater in poplar samples, which might be due to slightly higher resin content in the latter (~8% vs. 5.7% in pine).

In an effort to reveal more about the PMDI/lignin interactions seen in Figure 4.3.2.9, both woods were subjected to acetylation and then similarly analyzed for the effects of PMDI treatment. During acetylation, wood samples were treated with acetic

anhydride which results in partial replacement of wood hydroxyl (-OH) groups by acetyl (-$OCOCH_3$) groups. The weight of the wood samples was found to increase upon acetylation (16% increase for poplar and 18% increase for pine). Figure 4.3.2.10 shows the effect of acetylation on the dynamic scans of dry poplar samples.

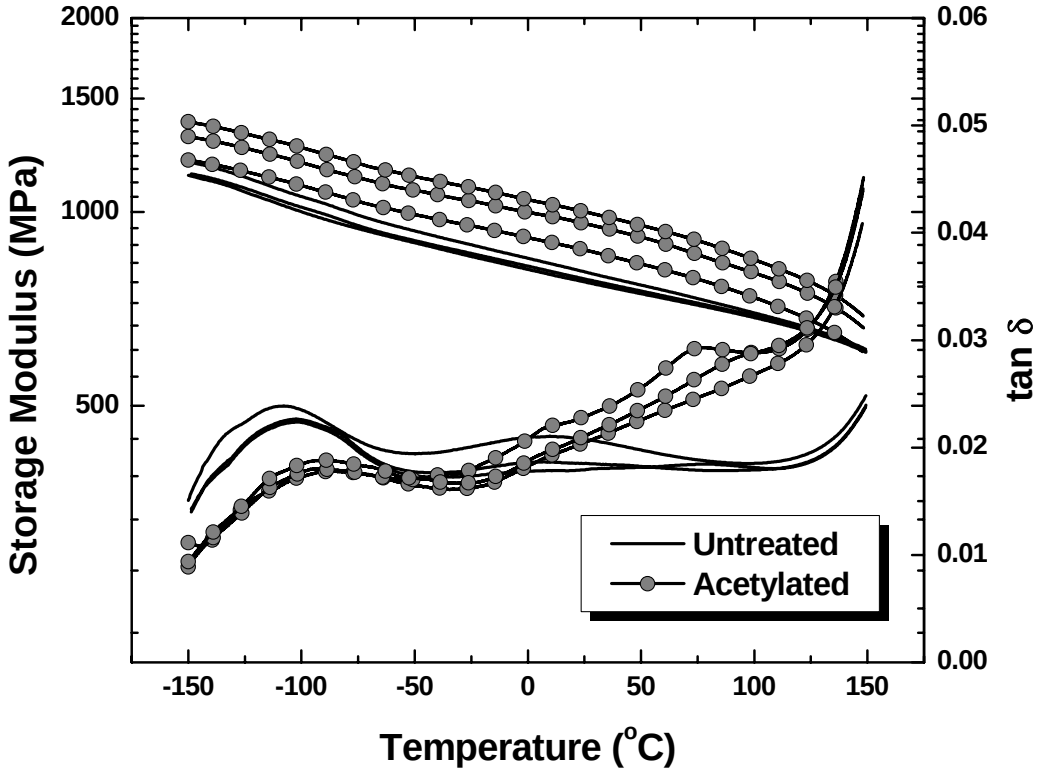

Figure 4.3.2.10. Dynamic thermal scans of dry control and acetylated poplar samples (0.06% strain, 1 Hz frequency, 5°C/min heating rate); These thermal scans were preceded by a thermal treatment at 150°C for 10 min [3 replications each].

The intensity of the low temperature relaxation (~-105°C) was found to decrease and shift to higher temperatures upon acetylation. This may either be due to the replacement of the hydroxyl groups by acetyl groups or may be due to the decrease in moisture content of wood (acetylation increases the hydrophobicity of wood). The intensity of the relaxation at ~30°C was also found to increase significantly. A very significant increase in tan δ was observed at higher temperatures (~120°C) signifying the inception of a major

wood relaxation. Thus, acetylation decreased the temperature at which the major wood relaxation occurred in dry wood samples, which may be attributed to the increase in free volume of the wood samples due to the replacement of the hydroxyl groups with acetyl groups. Thus, acetyl groups act as an "*internal plasticizer*" for wood.

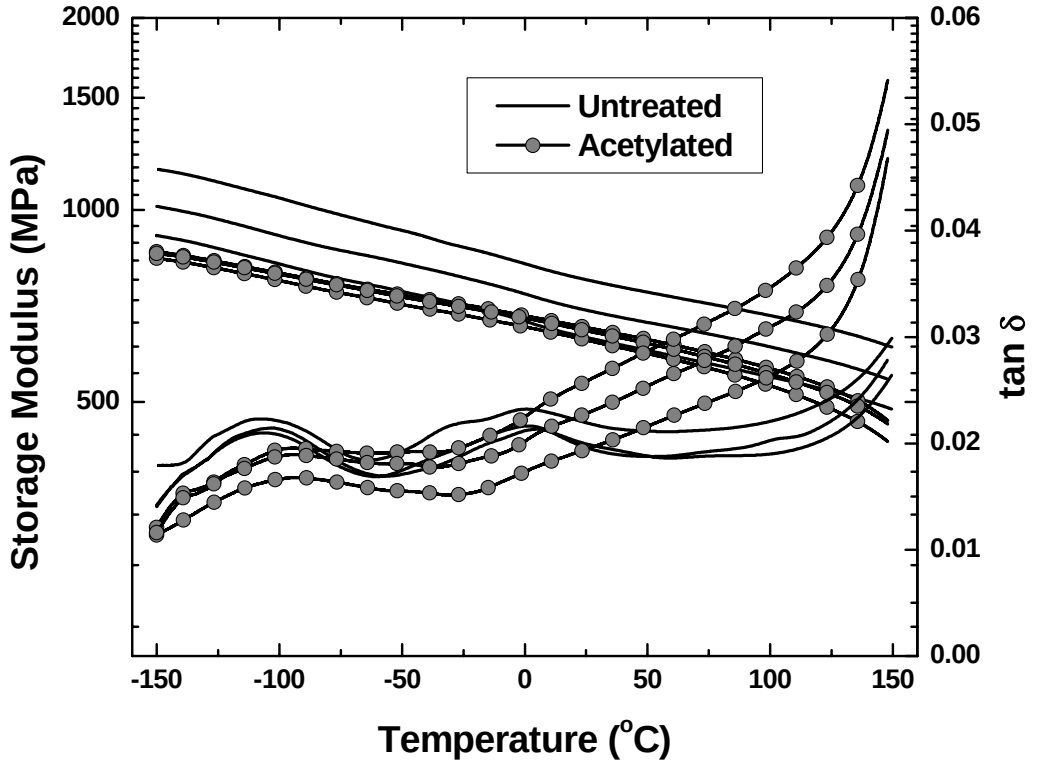

Figure 4.3.2.11. Dynamic thermal scans of dry control and acetylated pine samples (0.06% strain, 1 Hz frequency, 5°C/min heating rate); These thermal scans were preceded by a thermal treatment at 150°C for 10 min [3 replications each].

Similar trends were also observed for pine samples (Figure 4.3.2.11), except the change in the intensity of the low temperature relaxation (~-105°C) was smaller and the increase in the tan δ at higher temperatures (~120°C) was significantly larger in pine relative to the poplar samples.

Replacement of reactive hydroxyl groups by the inert, hydrophobic acetyl groups should in principle decrease the ability of the wood to interact with the PMDI resin, if the

resin-wood interactions were occurring through the hydroxyl groups of the wood polymers. Thus, dynamic thermal scans were performed on ethylene glycol plasticized acetylated wood samples which had been resin treated. The following table describes the resin contents and the plasticizer contents of samples before and after the dynamic scans.

Table 4.3.2.5. Sample parameters of plasticized resin-solution impregnated acetylated wood samples before and after dynamic scans (4 replications each).

Sample	Resin Content (%)	Plasticizer before test (%)	Plasticizer after test (%)
Acetylated Pine	-	172.2 ± 5.1	81.6 ± 2.8
Acetylated Poplar	-	145.3 ± 2.9	64.1 ± 0.6
Acetylated Pine-PMDI	25.9 ± 3.1	36.3 ± 1.9	22.2 ± 1.9
Acetylated Poplar-PMDI	40.1 ± 4.8	61.3 ± 4.3	40.6 ± 2.8

The plasticizer content of acetylated samples was found to decrease with resin impregnation. The plasticizer content was also found to decrease in the course of the dynamic scans, but the effect was not as severe as observed for unacetylated resin impregnated samples (table 4.3.2.3); the plasticizer content of both the acetylated resin impregnated samples at the end of the experiments was high enough to be above the FSP.

Figure 4.3.2.12 shows the dynamic scans of EG-plasticized acetylated radial wood samples before (control) and after resin impregnation. The samples were impregnated with neat resin, giving a final resin content of 26% and 40%, for acetylated pine and poplar samples, respectively. After acetylation, the lignin transition was found to shift to higher temperatures (from 85°C to 125°C). This is because, acetylation increased the hydrophobicity of wood (by replacement of hydrophilic –OH groups by hydrophobic $–OCOCH_3$ groups), which in turn reduces the plasticization efficiency of EG.

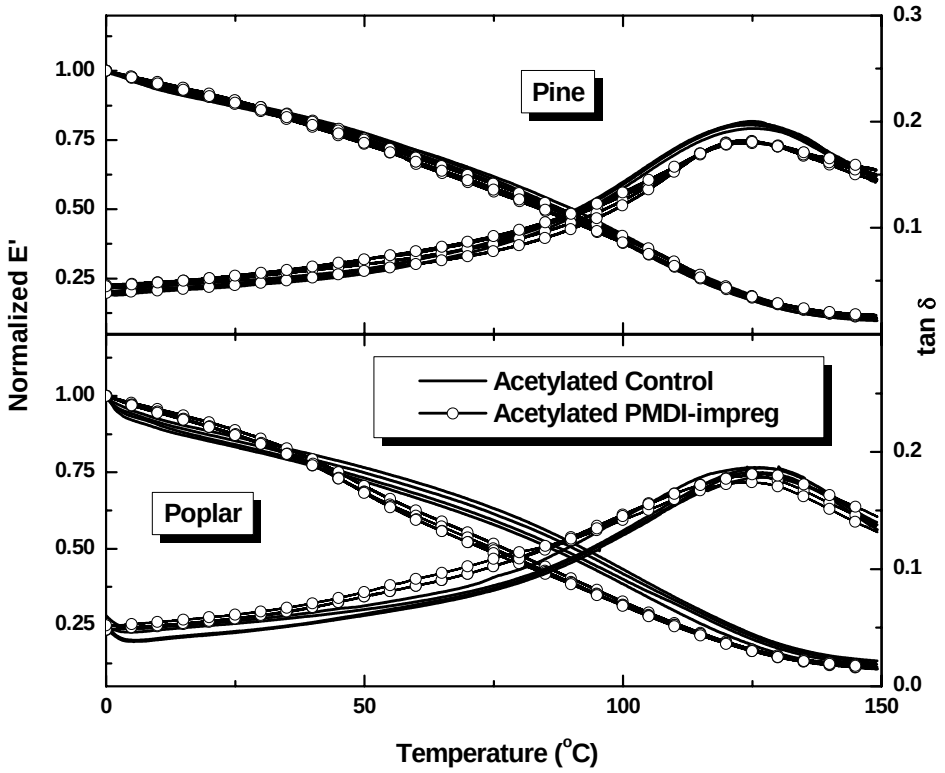

Figure 4.3.2.12. Effect of resin impregnation on EG-plasticized acetylated radial pine and poplar samples ((0.06% strain, 1 Hz frequency, 2°C/min heating rate) [4 replications each]

The lignin transitions for both acetylated wood species were found to be affected slightly by resin impregnation. The changes in the lignin transition that were observed in untreated samples (i.e. broadening and shifting of lignin transition to higher temperatures) were found to decrease significantly in acetylated samples. Thus, the changes in lignin transition in un-acetylated and resin impregnated samples may be attributed to the interactions between lignin hydroxyl groups and resin; this interaction may be primary (through covalent bond formation) or secondary (through hydrogen bonding) in nature. Since acetylation prevented the PMDI/lignin interaction that was observed in unacetylated wood, it is tempting to conclude that the normal PMDI/lignin interaction involves urethane formation. Perhaps this is true to some extent, but it is also clear that acetylation will significantly alter wood free volume and inter-segmental

interactions. So the effects of acetylation on the PMDI/lignin interaction may be consistent with various hypotheses of PMDI action, but no definitive conclusions can be reached. Suffice it to say that acetylation dramatically alters wood and its ability to interact with PMDI.

Again, the benefits of using EG plasticized wood have been demonstrated. Consequently, this approach was expanded by conducting a time/temperature superposition analysis of samples which are fully immersed in liquid EG.

4.3.2.3.1.2. Dynamic analysis in submersion tension mode

A more quantitative analysis of lignin/PMDI interactions was conducted in submersion tension mode with small radial wood samples which were immersed in EG. Samples were impregnated with PMDI/acetone solutions (19% PMDI concentration for pine and 16.4% for poplar) under similar conditions as before and cured to obtain ~8% resin impregnation (based on dry wood). All samples were plasticized by EG at 110°C for 1 h. Initially, dynamic thermal scans of the plasticized small radial samples were performed in ***single cantilever bending mode.*** Table 4.3.2.6 shows different sample parameters before and after the dynamic scans.

Table 4.3.2.6. Sample Parameters of plasticized small radial samples before and after dynamic scans.

Sample	Plasticizer before test (%)	Plasticizer after test (%)
Control Pine	134.2 ± 1.1	94.3 ± 0.7
Control Poplar	135.5 ± 0.8	92.6 ± 1.6
Pine-PMDI	98.2 ± 1.4	56.4 ± 1.3
Poplar-PMDI	110 ± 0.5	51.2 ± 1.8

Though all samples lost plasticizer during the thermal scans, the plasticizer content at the end of the experiments was high enough to be above the FPS. The effect of the resin on these samples was found to be quite similar to those observed for the larger samples (figure 4.3.2.8). Results showed that the effect of resin impregnation on the pine samples was relatively more significant than the corresponding poplar samples.

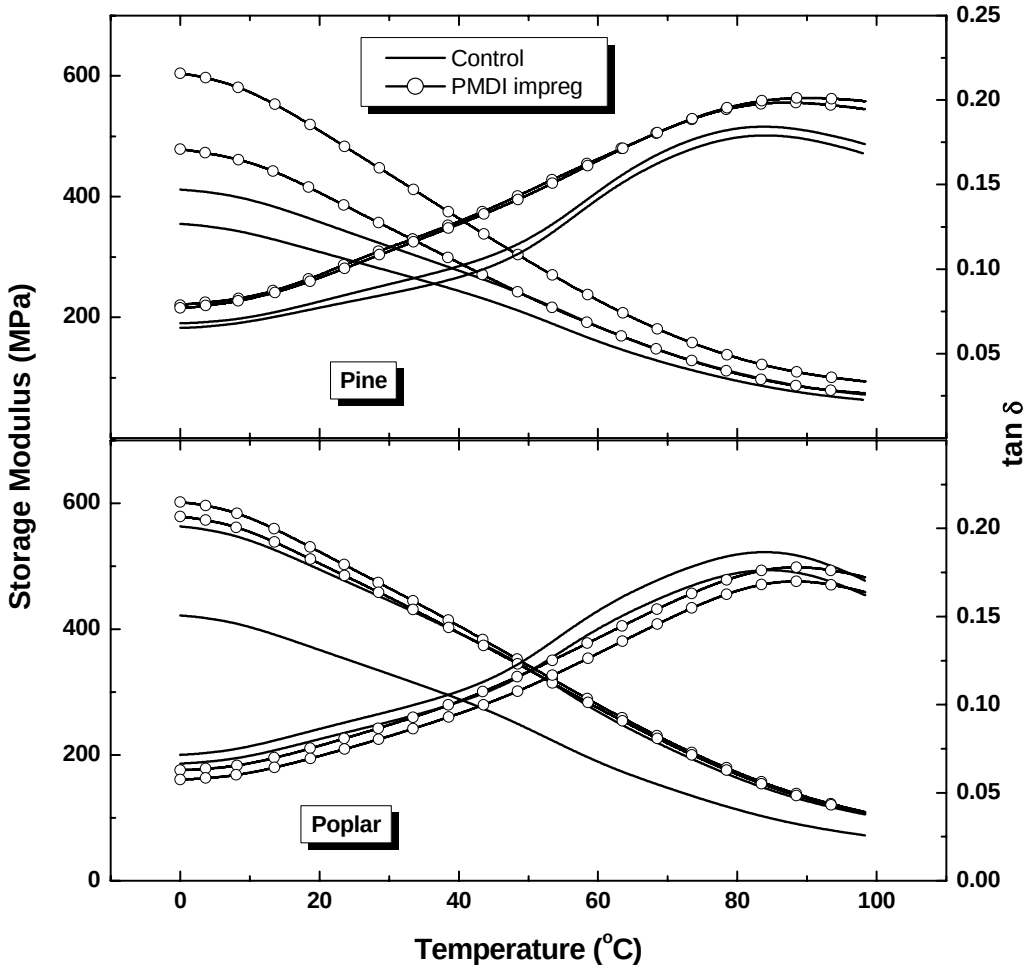

Figure 4.3.2.13. Dynamic thermal scans of ethylene glycol plasticized small radial control and resin solution impregnated (~8%) samples performed on a single cantilever clamp in bending mode (2°C/min heating rate, 1 Hz frequency, 0.043% strain) [2 replications each]

The in situ lignin relaxations of resin impregnated pine samples were significantly broader and at a slightly higher temperature than the control samples. Similar results were also observed in the poplar samples, but the changes were relatively smaller than those

observed in pine. Thus, the resin was found to interact more with the pine samples. Thus, the dynamic thermal scans provided us with a qualitative idea about the species dependent resin effect; in order to get a quantitative idea about the resin effects, further studies were conducted in the submersion tension mode.

Isothermal frequency sweeps were performed over the temperature range of 40° to 120°C. At every temperature, the sample was deformed at a strain/amplitude which was within its linear viscoelastic region (determined separately by force ramp experiments). The LVR region was found to increase with temperature, consequently, the deformation strain was increased with temperature (from about 0.05% at 40°C to 0.1% at 120°C) in order to achieve a high signal-to-noise ratio. The isotherms were shifted horizontally using a reference temperature of 80°C, to construct the mastercurve for each sample. Figure 4.3.2.14 shows the E', E" and tan δ mastercurves of control pine and poplar samples. The creep isotherm shifts were conducted and optimized using the storage modulus data (no vertical shifting was employed); the resulting shift factors were then also applied to the loss modulus and tan δ data. As shown, the shift of the storage modulus master curves was very good, but much less perfect for the loss modulus and tan δ data. This is perhaps also true for others who have created DMA master curves for plasticized wood; because the literature reveals that only storage modulus master curves have been published previously [3,4,9,13]. In the loss modulus data, it was found that the lowest frequency data point was always in slight disagreement with the rest of the data. The effect of this erroneous datum was then amplified in the tan δ master curves. It is believed, although not thoroughly verified, that this erroneous point was caused by an

instrumental error- it was found that the lowest frequency datum was always problematic, regardless of what the actual frequency was.

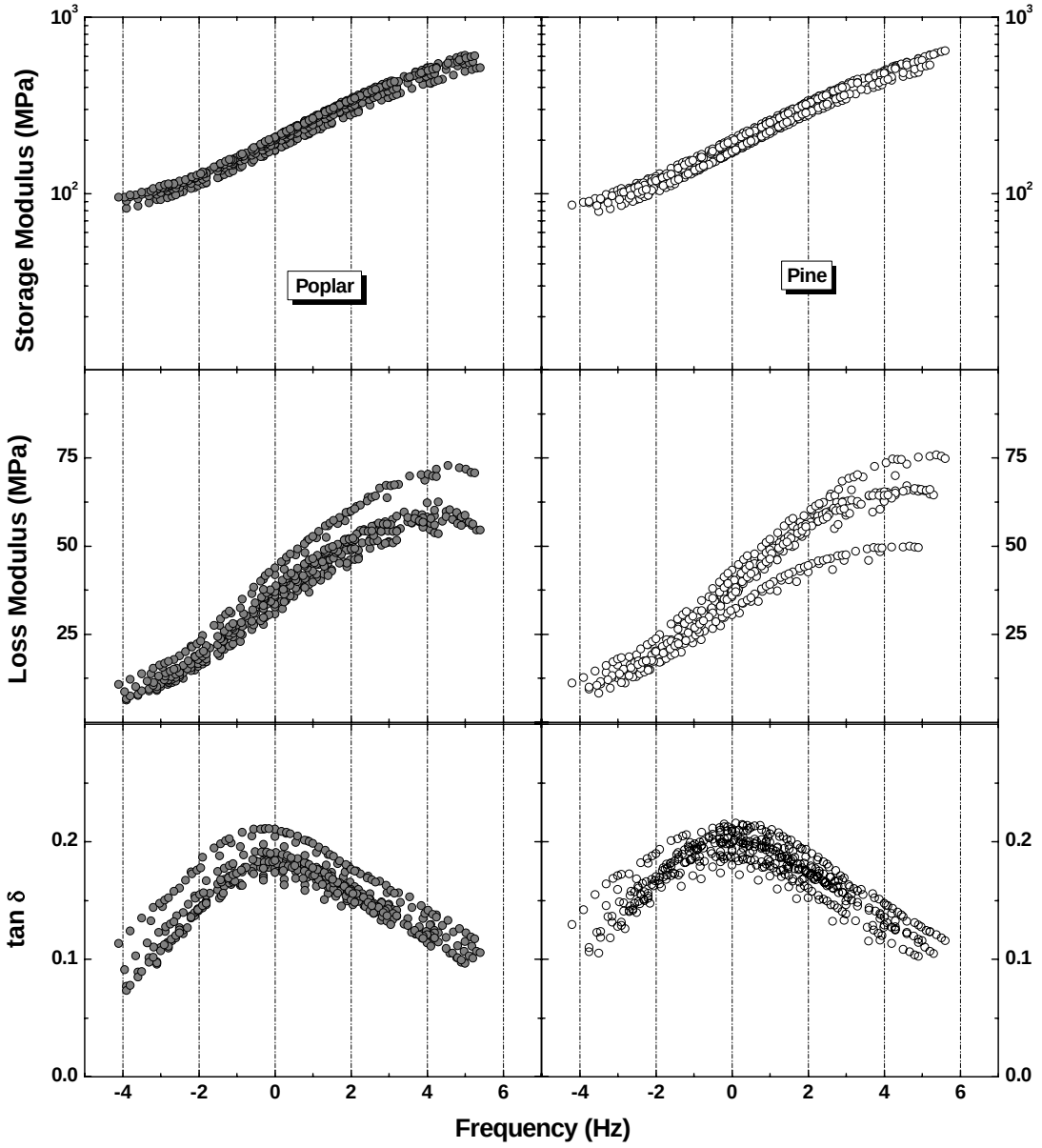

Figure 4.3.2.14. Storage modulus, loss modulus and tan δ mastercurves of control pine and poplar samples immersed in liquid EG. Reference temperature = 80°C (5 replications each).

Results show that the mastercurves of plasticized pine were slightly different from the corresponding poplar samples. The storage modulus mastercurves were found to be similar for both woods tested. The pine loss modulus perhaps exhibits maxima at higher

frequencies when compared to pine. The poplar tan δ curves exhibit maxima which are clearly at lower frequencies than for pine. The temperature of 80°C was selected as the reference for both woods mostly as a matter of convenience, because the dynamic thermal scans suggested that there was no T_g difference between the woods. However, this is clearly not the case. The lower frequency tan δ maximum seen for poplar indicates that the poplar T_g is actually higher than that for pine; this is in direct contradiction to the literature [4] which generally indicates that softwoods have higher Tg's than hardwoods because of differences in the monolignol ratios.

Figures 4.3.2.15 and 4.3.2.16 show the effect of resin impregnation on the mastercurves of pine and poplar samples, respectively.

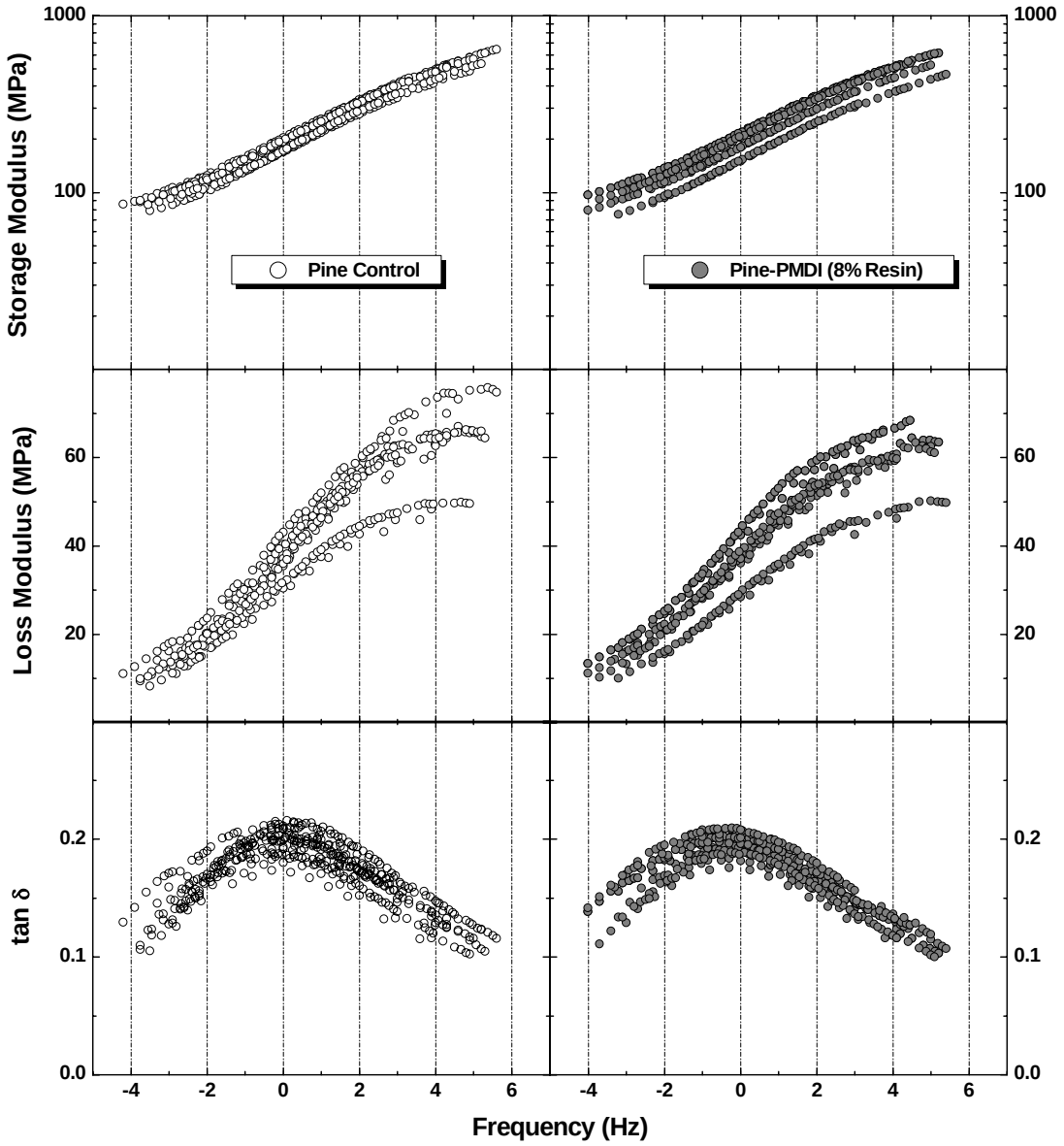

Figure 4.3.2.15. Comparison of pine-control and pine-PMDI submersion-tension mastercurves for storage modulus, loss modulus and tan δ (5 replications each).

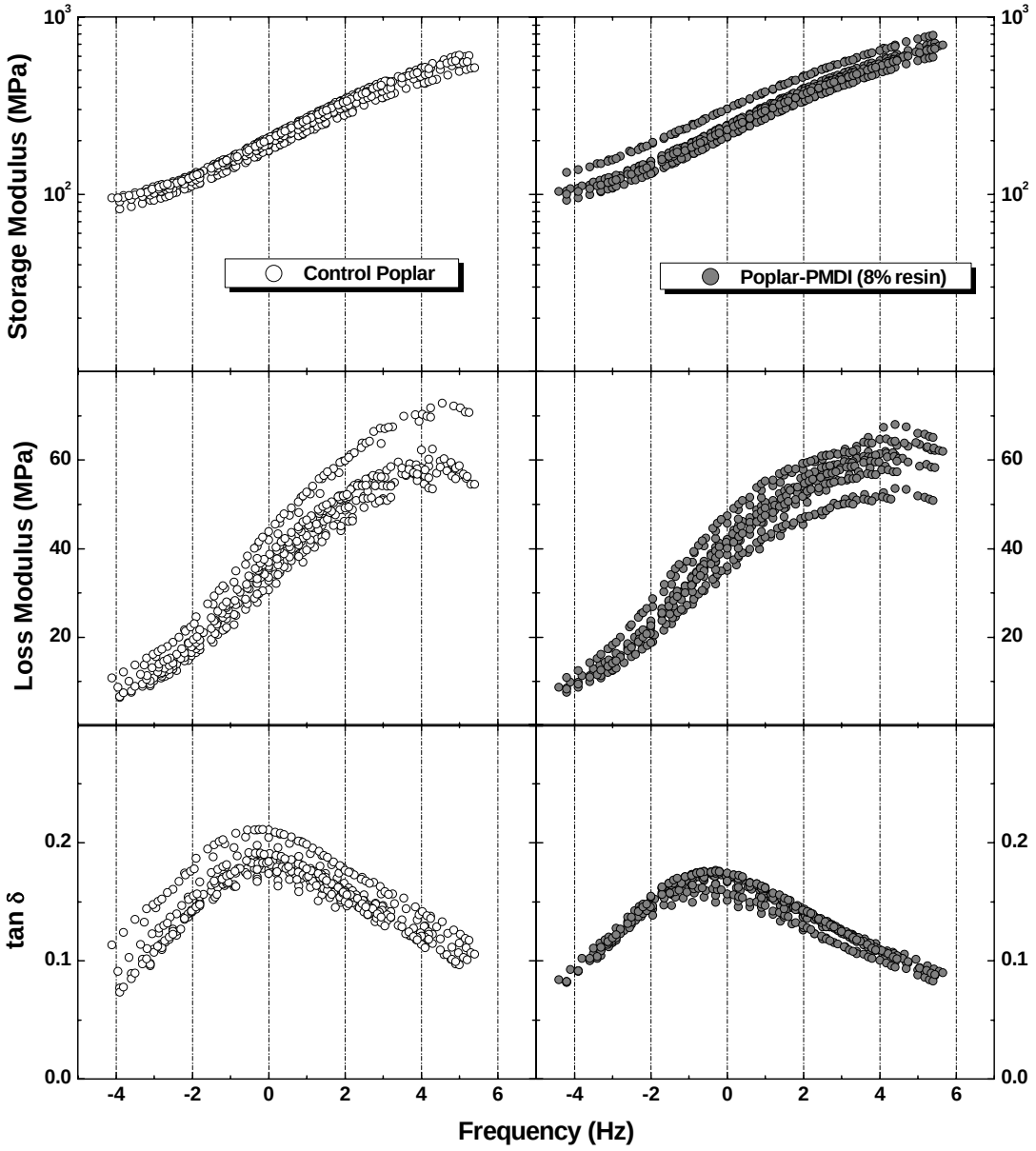

Figure 4.3.2.16. Comparison of poplar-control and poplar-PMDI submersion-tension mastercurves for storage modulus, loss modulus and tan δ (5 replications each).

The mastercurves provided more insight on the effects of resin impregnation on the lignin relaxations than the dynamic scans (figure 4.3.2.13). Both dynamic scans and the mastercurves showed that the lignin T_g increased with resin impregnation. But the mastercurves also showed that the intensity of the poplar tan δ decreased upon resin impregnation. Both pine and poplar tan δ was found to shift to lower frequencies upon

resin impregnation; but the change was relatively larger in pine. The intensity of the pine loss modulus mastercurves showed a slight decrease. Resin impregnation also resulted in a significant broadening (~1 decade) of the poplar tan δ mastercurves.

It is sometimes difficult to detect the effect of resin on the wood samples, by analyzing the mastercurves. The shift-factor plots give a better representation of the effects of the resin. Figure 4.3.2.17 shows the effect of resin impregnation on the shift-factor plots of pine and poplar wood samples. Though the analysis was performed within the in situ lignin softening temperature range, very little curvature was observed in the shift-factor plots of both wood samples.

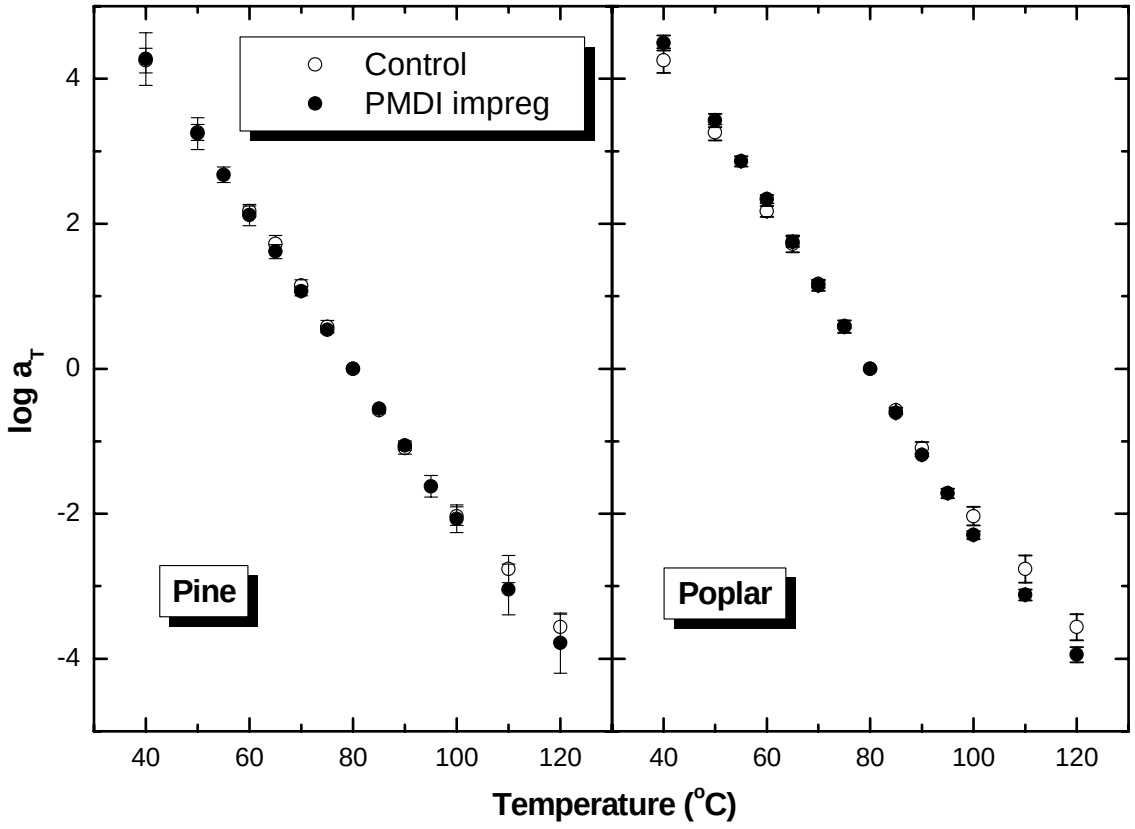

Figure 4.3.2.17. Effect of resin impregnation on the shift-factor plots of SYP and YP samples analyzed in submersion-tension TTS (5 replications each).

The shift factor plots showed that the temperature dependence of the lignin transition changes only slightly in the presence of the resin; deviation from the control shift-factor plot was observed at higher temperatures and the effect was relatively larger in poplar samples. The data from 40°C to 75°C were fitted to the Arrhenius equation, while the data from 75° to 120°C were fitted to the WLF equation, in order to determine the effect of resin impregnation on the activation energy (E_{act}) of the in situ lignin transition and WLF parameters (C_1, C_2) (Figure 4.3.2.18). The fit of the shift-factor plots to the WLF and Arrhenius equations was found to be very good and are shown in the appendix (appendix 6.10)

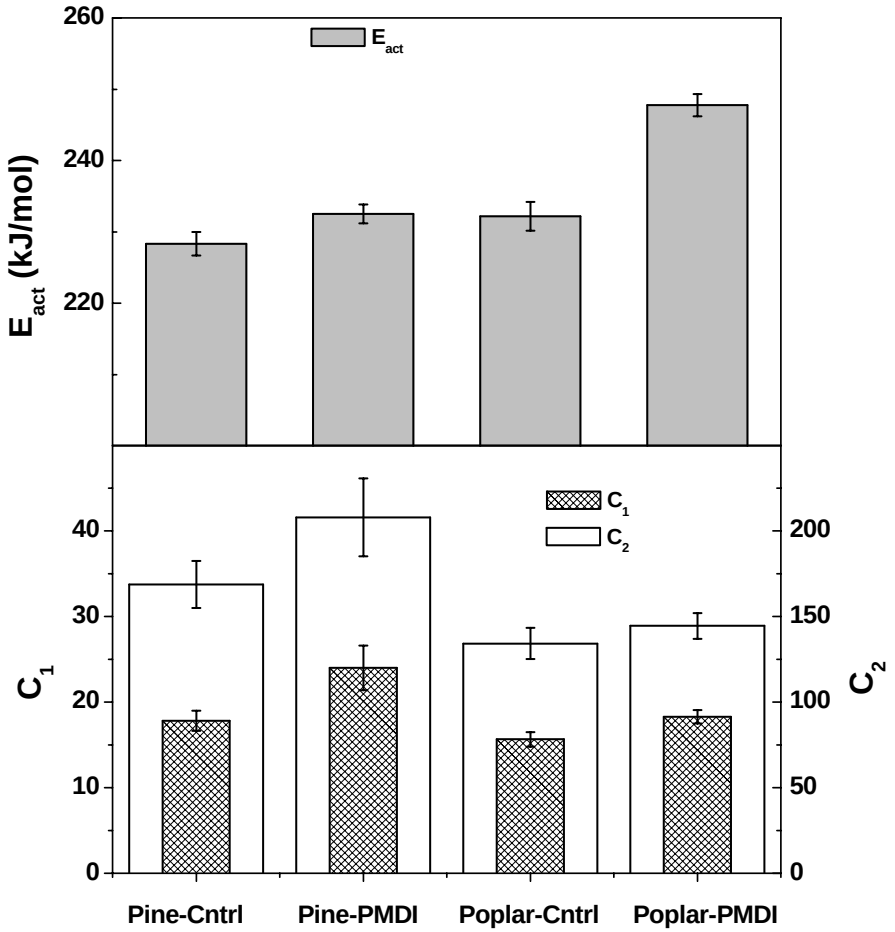

Figure 4.3.2.18. Effect of resin impregnation on the E_{act} and WLF parameters of SYP and YP.

Unlike previously reported studies [4], which showed that the E_{act} of hardwood lignins are higher than softwood lignins, our results showed that the E_{act} of the lignin transition for plasticized control samples were found to be similar (~230 kJ/mol) between the wood species tested. Lignin E_{act} was found to increase in the presence of resin for both wood species, but the change was relatively greater in poplar.

The WLF parameter, C_1 is known to be inversely proportional to the fractional free volume, f_g [29]. C_1 was found to increase for both wood species upon resin impregnation, which may be attributed to the decrease in f_g. The change in C_1 was higher in pine, which suggests that there was a relatively greater decrease in the pine f_g compared to that of poplar. C_2 was also found to increase with resin impregnation and the change was found to be greater in pine than poplar.

4.3.2.4. Conclusions

The species-dependent interactions between wood and isocyanate resins were successfully probed by DMA in both dry and plasticized conditions. The following conclusions were drawn from this study:

- Radial samples were found to be better suited for probing the wood-resin interactions relative to longitudinal samples. This was because the former had a relatively larger LVR limit and the in situ lignin relaxations were more intense and at a lower temperature than the corresponding longitudinal samples.
- Resin impregnation was conducted with either neat resin or with resin-acetone solution. The latter was preferred because it provided better control over the final resin content.

- DMA scans of dry wood samples provided ample proof of wood-resin interactions. But it did not provide any indication of the species-dependent nature of this interaction since the precise nature of the relaxations observed in these samples are unknown.
- DMA scans of ethylene glycol plasticized wood samples showed that resin interacted with the in situ lignin relaxation of both wood species tested; the relaxation was found to shift slightly to higher temperatures and broaden. The wood-PMDI interactions were found to decrease upon acetylation, which might suggest that the interaction was occurring through the lignin hydroxyl groups.
- The wood-PMDI interactions were studied quantitatively by the application of TTS principle, in the submersion tension mode. Mastercurves (E', E" and tan δ) were constructed by horizontal shifting of the frequency isotherms over the in situ lignin glass transition. The mastercurves provided a better insight on the effects of resin impregnation on the in situ lignin relaxation compared to the dynamic scans. The relaxation was found to shift to lower frequency in the presence of the resin; but the change was relatively larger in pine. The poplar tan δ mastercurves also show significant broadening (larger than pine) under similar conditions. But, the resin impregnation was found to have only slight effects on the activation energy and WLF parameters for the in situ wood lignin relaxation.

References

(1) Sellers, T. *Forest Products Journal* **2001**, *51*, 12-22.
(2) Salmen, L.; Olsson, A.-M. *Journal of Pulp and Paper Science* **1998**, *24*, 99-103.
(3) Olsson, A.-M.; Salmen, L. In *Cellulosics: Chemical, Biomedical and Material Aspects*; Kennedy, J. F.; Phillips, G. O.; Williams, P. A., Eds.; Ellis Horwood: New York pp 257-262.
(4) Olsson, A.-M.; Salmen, L. In *Viscoelasticity of Biomaterials*, ACS Symposium Series 489 ed.; Glasser, W. G.; Hatakeyama, H., Eds.; American Chemical Society: Washington D.C., 1992; pp 133-143.
(5) Olsson, A.-M.; Salmen, L. In *International Conference of COST Action E8*: Copenhagen, Denmark, 1997; pp 269-279.
(6) Olsson, A.-M.; Salmen, L. *Nordic Pulp and Paper Research Journal* **1997**, *12*, 140-144.
(7) Olsson, A.-M.; Salmen, L. In *Hemicellulose: Science and Technology*; Gatenholm, P.; Tenkanen, M., Eds.; American Chemical Society: Washington D.C., 2004; pp 184-196.
(8) Salmen, N. L.; Back, E. L. *TAPPI* **1977**, *60*, 137-140.
(9) Salmen, L. *Journal of Materials Science* **1984**, *19*, 3090-3096.
(10) Salmen, L. In *Proceeding of the 2nd Conference of European Rheologists*; Giesekus, H.; Hibberd, M. F., Eds.; Springer-Verlag: Prague, 1980; pp 234-235.
(11) Kelley, S. S.; Rials, T. G.; Glasser, W. G. *Journal of Materials Science* **1987**, *22*, 617-624.
(12) William, M. L.; Landel, R. F.; Ferry, J. D. *Journal of American Chemical Society* **1955**, *77*, 3701-3707.
(13) Laborie, M.-P. G.; Salmen, L.; Frazier, C. E. *Holzforschung* **2004**, *58*, 129-133.
(14) Ngai, K. L. *Journal of Physical Chemistry B* **1999**, *103*, 5895-5902.
(15) Ngai, K. L.; Plazeck, D. J. *Rubber Chemistry and Technology Rubb. Rev.* **1995**, *68*, 376-434.
(16) Ngai, K. L.; Rendell, R. W. *Journal of Non-Crystalline Solids* **1991**, *131-133*, 942-948.
(17) Marcinko, J. J.; Newman, W. H.; Phanopoulos, C.; Sander, M. A. In *International Particleboard/Composite Materials Symposium*; Maloney, T. M.; Leonhardy, L. H.; Lentz, M. T.; Wells, S., Eds.: Pullman, Washington, 1995; pp 175-183.
(18) Marcinko, J. J.; Devathala, S.; Rinaldi, P. L.; Bao, S. *Forest Products Journal* **1998**, *48*, 81-84.
(19) Marcinko, J. J.; Rinaldi, P. L.; Bao, S. *Forest Products Journal* **1999**, *49*, 75-78.
(20) Backman, A. C.; Lindberg, K. A. H. *Journal of Materials Science* **2001**, *36*, 3777-3783.
(21) Sadoh, T. *Wood Science and Technology* **1981**, *15*, 57-66.
(22) Mantanis, G. I.; Young, R. A.; Rowell, R. M. *Holzforschung* **1994**, *48*, 239-248.
(23) Rowell, R. M. In *Handbook of Wood Chemistry and Wood Composites*; Rowell, R. M., Ed.; CRC Press: Boca Raton, 2005; pp 77-98.
(24) Sugiyama, M.; Obataya, E.; Norimoto, M. *Journal of Materials Science* **1998**, *33*, 3505-3510.

(25) Back, E. L.; Salmen, L. *TAPPI* **1982**, *65*, 107-110.
(26) Salmen, N. L. *Pulp Paper Can. Trans Techn. Sec.* **1979**, *5*, TR-45.
(27) Salmen, N. L.; Back, E. L. *TAPPI* **1984**, *60*, 137.
(28) Laboratory, F. P. *Wood Handbook: Wood as an Engineering Material*; USDA: Madison, WI, 1999.
(29) Menard, K. P. *Dynamic Mechanical Analysis: A Practical Introduction*; CRC Press: Boca Raton, Florida, 1999.

Characterization of the Polymeric Isocyanate-Wood interactions by Creep in Dry and Ethylene-glycol Plasticized conditions

Sudipto Das, C.E. Frazier
Virginia Polytechnic Institute and State University
230 Cheatham Hall, Blacksburg, VA 24061-0323

4.3.3.1. Introduction

Extensive research has been conducted on the creep response of wood. Creep experiments involve the instantaneous application of a constant stress followed by monitoring of the resultant deformation over time. Many studies have analyzed the effects of different experimental parameters such as temperature, moisture, wood species, grain direction, stress level, etc. on the creep behavior of wood. A few studies [1-4] have utilized the time-temperature superposition principle (TTSP) to predict the long-term response of wood. This was done by performing short-term isothermal creep experiments at different temperatures, followed by shifting the creep isotherms with respect to a reference temperature to generate a mastercurve. The mastercurve describes the long-term response of the material at the reference temperature. Findley and Peterson [1] have used 2000 h (~$10^{6.9}$ sec) creep data to successfully predict the creep response of canvas, paper and asbestos laminates, over a time period of 92000 h (~$10^{8.5}$ sec). Gressel [2] used short-term creep data (2000 h, $10^{6.9}$ sec) of spruce, pine and beech wood, to predict the response over a time-period of 80000 h (~$10^{8.5}$ sec). Bond [3] developed long-term creep models for different woods (Douglas-fir, southern pine, yellow-poplar) in both tension and compression modes using TTSP. Short-term creep experiments were conducted on

wood samples in the temperature range of 20° to 80°C, which were then used to construct mastercurves by both horizontal and vertical shifting to a reference temperature (T_{ref}) of 20°C. The shift-factor plot was linear and thus showed Arrhenius behavior. The shift-factor plot was fitted to the Arrhenius equation (equation 4.3.3.1) to calculate the activation energy (E_{act}).

$$\log a_T = \frac{E_{act}}{2.303R}\left(\frac{1}{T} - \frac{1}{T_{ref}}\right) \qquad (4.3.3.1)$$

The activation energies of all woods tested were ~ 17 – 35 kcal/mol. The validity of the long-term creep models generated by TTSP was also successfully tested with a long-term (~10^7 sec, 105 days) creep test on yellow-poplar and pine samples in both tension and compression modes. Samarasinghe *et al.* [4] also used TTSP to develop long-term compression creep models for southern pine. Short-term creep (17 hr, ~$10^{4.8}$ sec) experiments were performed in the temperature range of 21° to 65°C at an equilibrium moisture content of 9%. The short-term data were shifted to construct a mastercurve (T_{ref} = 21°C), which was able to predict responses up to 6.4 years (~$10^{8.3}$ sec). The shift-factor plot was also found to be Arrhenius in nature with average activation energy of ~28 kcal/mol. None of the studies has attempted to fit the experimental shift-factor data to the Williams-Landel-Ferry equation.

Several empirical models have been proposed in the literature to model the creep behavior of wood under constant stress conditions. Empirical analogues were obtained by fitting experimental creep data to a mathematical function. Several studies [2-6] have found that the creep mastercurves could be fitted to the empirical power law model (equation 4.3.3.2).

$$J_t = J_0\left(1 + at^b\right) \qquad (4.3.3.2)$$

where, J_t is the creep compliance at time t,

J_0 is the initial creep compliance

a and *b* are estimated parameters.

Both Bond [3] and Samarasinghe [4] used nonlinear regression analysis to fit their creep mastercurves to the power model, and obtained similar values for the estimated parameters (*a* and *b*). The model was then used to predict long-term behavior of wood. Thus, all past studies have used the TTS principle in conjunction with creep as a predictive tool; but no one has used this method to analyze wood-resin interactions.

In this study, the interaction between polymeric isocyanate (PMDI) resin and wood will be studied by static creep tests in both dry and plasticized wood conditions. The interactions will be investigated by analyzing the changes of the wood relaxations in the presence of PMDI resin. There are two main advantages in using this static method to analyze wood/resin interactions. Firstly, previous studies have shown that the main wood polymer relaxations occur above ~180°C, where significant degradation occurs [7,8]. The temperature of the main wood relaxations can be lowered by solvent plasticization and/or by using low frequency perturbations[8,9]. Plasticization typically requires sample immersion and is therefore experimentally challenging. This difficulty might be alleviated by employing creep experiments with plasticized wood without using complete sample immersion. In other words, creep analysis will allow the use of lower temperatures, low enough such that complete sample immersion may be unnecessary. Secondly, the creep compliance curves can be used to precisely model the wood relaxations. Recently Laborie *et al.* [10] used an indirect method to determine the

cooperativity of the lignin glass transition (T_g) in ethylene glycol plasticized wood. The resultant shift-factor plots were fitted to the empirical version of the coupling model [11] to obtain the coupling parameter, *n*, which reflects inter-segmental interactions (or the breadth of the relaxation distribution). In contrast to Laborie's work, the present study directly fits the Kohlrausch-Williams-Watts (KWW) equation (equation 4.3.3.3) [12] to the creep response of wood.

$$\phi(t) = \exp\left[-\left(\frac{t}{\tau}\right)^{1-n}\right] \qquad (4.3.3.3)$$

This provides a more accurate description of wood relaxations, as will be discussed below during the analysis of PMDI/wood interactions.

4.3.3.2. Experimental

4.3.3.2.1. Materials

PMDI resin was obtained from Huntsman Polyurethanes (Rubinate 1840) and used as received.

Two wood species were selected for analysis: yellow-poplar (*Liriodendren tulipifera*) and southern yellow pine *(Pinus spp*.). Sample dimensions were 40 mm (radial) × 10 mm (tangential) × 4 mm (longitudinal axis) [1.58" × 0.4" × 0.16"]. All samples were initially dried and then equilibrated to 6-7% moisture content (MC) before further treatments.

4.3.3.2.2. Methods

4.3.3.2.2.1. Resin impregnation

Moisture-equilibrated samples were impregnated with PMDI resin using an *open-cell* method. The samples were first impregnated with a resin-acetone solution under pressure (~69 kPa; 10 psi) in a pressure reactor for 15 minutes (The resin-acetone solution concentration was varied to obtain different resin loadings). The excess resin solution was removed from the samples by application of vacuum (~ 0.1 mm Hg) for 15 minutes. Samples were then cured at 120°C for 2 h. The cured samples were stored over phosphorous pentoxide, P_2O_5, in a dessicator.

In order to evaluate the effect of PMDI treatment on wood relaxations, ***control*** samples with similar thermal history as the resin-impregnated samples were prepared. These samples were initially equilibrated to 6-7% MC, and they were pressure (115 cm.N; 10 psi) impregnated with anhydrous acetone, followed by vacuum treatment (~ 0.1 mm Hg) for 15 minutes. They were then thermally treated at 120°C for 2h and stored over P_2O_5 until further analysis.

4.3.3.2.2.2. Ethylene-glycol plasticization

Samples were impregnated with ethylene glycol (EG) under vacuum (~ 0.1 mm Hg) for 30 minutes at room temperature. EG impregnated samples were stored in EG at room temperature until tested.

4.3.3.2.2.3. Dynamic tests

All dynamic thermal scans were performed on a TA Instruments 2980 DMA in single cantilever bending mode. Thermal scans were performed at 5°C/min with a strain of 0.05% at 1 Hz frequency. All dry samples were thermally treated in the DMA before

analysis. It consisted of rapid (25°C/min) heating of the sample to 150°C, followed by a 10 minute equilibration at 150°C; then it was slow cooled (5°C/min) to the initial temperature, before performing the subsequent thermal scans.

EG impregnated samples were clamped to the DMA [~115 cm·N (10 lb-in) torque] and then slowly cooled (5°C/min) to -150°C. Thermal scans were performed with the following experimental parameters: 20 μm amplitude, 0.057% strain, 2°C/min heating rate and 1 Hz frequency.

4.3.3.2.2.4. Creep experiments

All experiments were conducted in a Q800 TA Instruments® DMA in single cantilever bending mode.

4.3.3.2.2.4.1. Sequential isothermal creep experiments with dry samples

The samples were clamped in the DMA with a torque of ~115 cm·N (10 lb-in). All samples were subjected to a thermal treatment prior to the experiment in the DMA. Samples were rapidly (25°C/min) heated to 120°C and held at that temperature for 30 min. They were then slow cooled (2°C/min heating rate) to 50°C. Three hour isothermal creep experiments were sequentially conducted at 50°, 90° and 120°C on each sample; samples were equilibrated at each temperature for 30 min before conducting the creep experiments. Six replications were conducted for each system.

A constant static load of 0.8 MPa was applied during the creep tests, which was within the linear viscoelastic region (LVR) of the wood samples. The LVR limit was determined by conducting a dynamic, strain-sweep experiment, where the sample was sinusoidally deformed with increasing strain/amplitude at 1 Hz frequency. The LVR limit was arbitrarily defined as the strain which resulted in a 5% reduction in the initial storage

modulus, E'; the initial modulus was that measured at 0.006% strain or 2 μm amplitude. The LVR limit was found to decrease slightly with temperature. The LVR limit was found to be at ~0.1% strain and 1.1 MPa stress at 150°C.

4.3.3.2.2.4.2. Isothermal creep experiments with EG plasticized samples

EG plasticized samples were clamped into the DMA with a clamping torque of ~ 115 cm·N (10 lb-in). All samples were thermally treated in the DMA before analysis; the thermal treatment consisted of rapid (25°C/min) heating of the sample to 90°C, where it was equilibrated for 30 min. The samples were then quench-cooled (20°C/min) to 50°C. The samples were equilibrated at 50°C for 30 min, and then subjected to a 3 h creep experiment. 5 replications were conducted for each sample system. A constant static load of 0.8 MPa was applied during the creep test, which was within the LVR limit. The LVR limit at 25°C was determined by conducting a dynamic, strain-sweep experiment as described previously (2.2.4.1). The LVR limit was found to be at ~0.143% strain and 1.4 MPa stress at 25°C.

4.3.3.2.2.4.3. Creep-Mode Time-temperature superposition

EG plasticized samples were clamped in the instrument with a clamping torque of ~115 cm·N (10 lb-in). All samples were thermally treated at 95°C for 30 min as described previously (2.2.4.2). Afterwards, the samples were either slow-cooled (5°C/min) or quench-cooled (20°C/min) to the lowest temperature. Isothermal creep (1000 sec) experiments were performed in the temperature range of 5° to 95°C. The samples were equilibrated at each temperature for 10 min before each creep segment. A constant static load of 0.8 MPa was applied during the creep test. 5 replications were conducted for each sample system.

4.3.3.3. Results and Discussions

4.3.3.3.1. Effect of resin impregnation on the dynamic thermal response of dry samples

Figure 4.3.3.1 shows the effect of resin (solution) impregnation and cure on the 1 Hz dynamic thermal response of dry poplar and pine samples; note that these are completely dry samples. Let us first consider the general thermal response of the unresinated (control) samples. Both woods exhibit 2 or 3 weak relaxations in the temperature range of -150° to 150°C, which must be generally described as secondary transitions because they are all less than about 0.03 tan δ units.

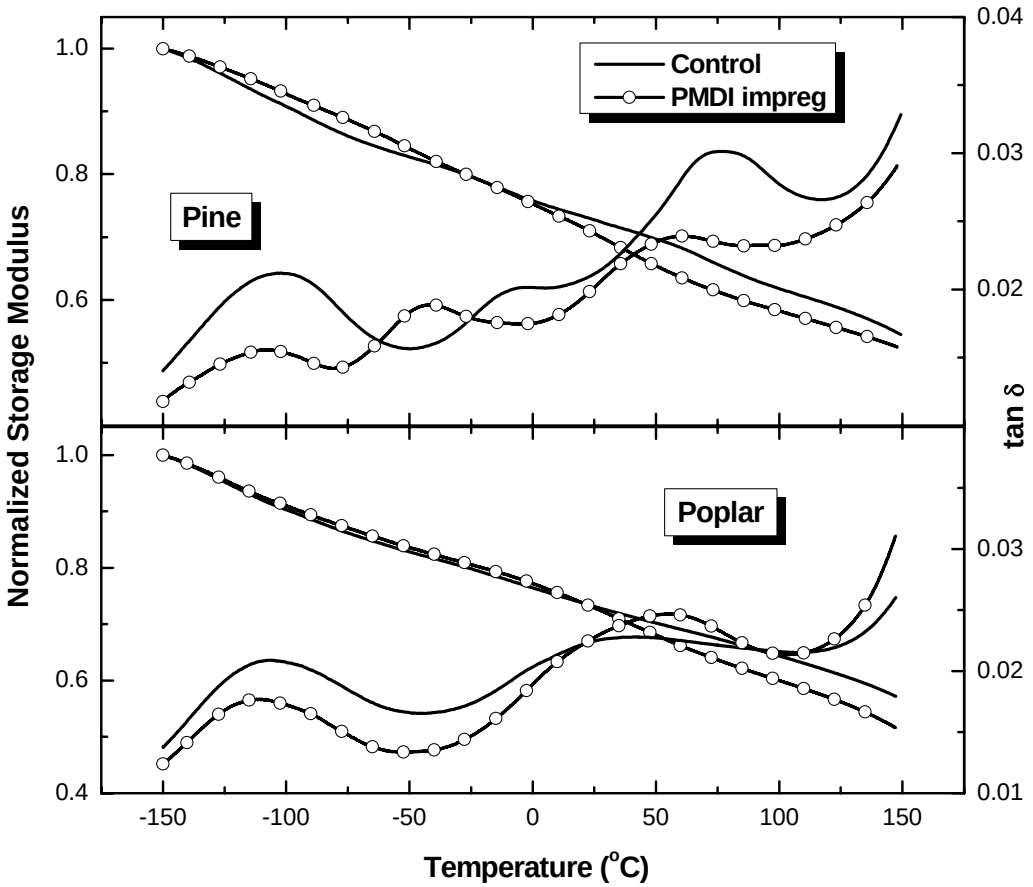

Figure 4.3.3.1. Effect of resin solution impregnation and cure (3% cured resin based on dry wood) on the dynamic thermal scans of dry southern pine and yellow-poplar samples. Note that these scans preceded a 10 minute thermal treatment at 150°C.

Both woods exhibit a relaxation near ~-105°C, which has been attributed to the site exchange of moisture [13] or to the motion of wood methyol groups [14]. Although not demonstrated here, this dry control sample thermal response is highly reproducible. At higher temperatures, pine exhibited two relaxations (-10° and 75°C), while only one broad relaxation centered at ~30°C was observed for poplar samples. Both woods also exhibited the initiation of a more energetic relaxation at ~ 120°C; this is probably the onset of major lignin softening, or perhaps a combination of lignin and hemicellulose softening.

Results illustrate that resin impregnation and cure significantly altered the thermal response of dry pine samples. The intensity of the lowest temperature relaxation (-105°C) was reduced, and the other two peaks (-10° and 75°C) appear to have shifted to lower temperatures (and perhaps slightly broadened) relative to the control sample. In contrast, poplar samples showed only minor changes from resin impregnation and cure; the intensity of the lowest temperature transition decreased slightly, while the high temperature peak was slightly shifted to higher temperatures. The effects shown in Figure 1 were reproducible, as demonstrated in Figure 4.3.3.2.

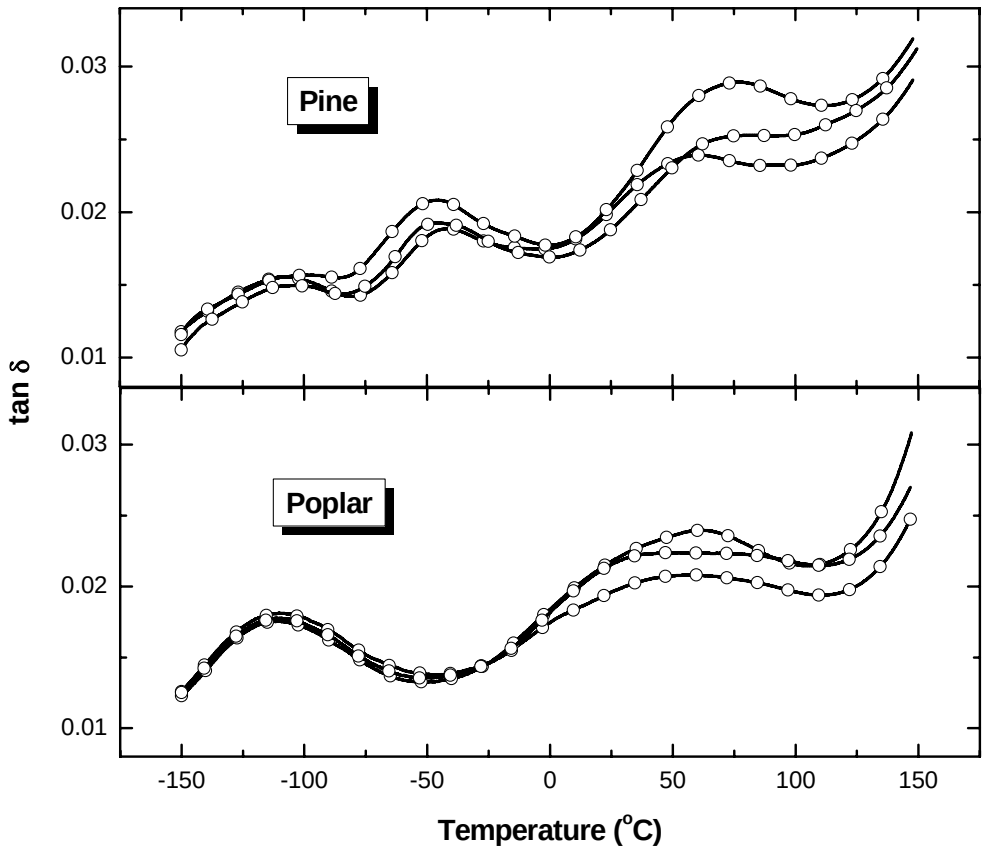

Figure 4.3.3.2. Dynamic scans of resin solution impregnated (3% cured resin on dry wood) wood samples (3 replications each). Note that these are completely dry samples and that these scans succeed a 10 minute thermal treatment at 150°C.

It is apparent that resination and cure affected the dynamic thermal response of both woods. However, the effects are slightly different for the two woods and perhaps more significant for pine than for poplar. This information will serve as a point of reference as we consider the creep response of similarly treated samples, below.

4.3.3.3.2. Isothermal creep with dry samples

The creep compliance of dry wood samples was sequentially determined at 50°, 90° and 120°C for each sample. Figure 4.3.3.3 demonstrates the sequential creep compliance of poplar and pine control samples; these are completely dry samples.

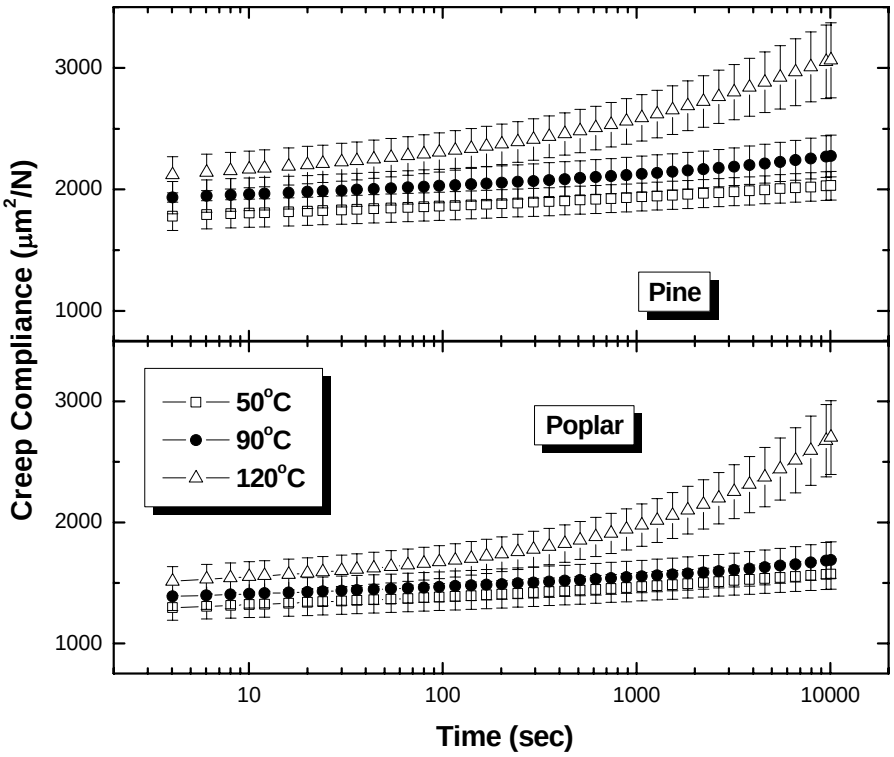

Figure 4.3.3.3. Creep response of dry control pine and poplar samples subjected to sequential creep analysis at three temperatures. Prior to creep testing, all samples were heated at 120°C for 30 min and slow cooled (2°C/min) to 50°C; all samples were subjected to a 30 minute thermal equilibration at each experimental temperature. Each datum is the mean of 6 isochronous data points from 6 creep experiments at each temperature; error bars represent ± 1 standard deviation.

The control pine samples were more compliant than the corresponding poplar samples under all conditions. Both woods showed an increase in compliance with temperature, as expected. The temperature increase from 50° to 90°C led to a slight increase in the compliance for both woods; but the relative increase was more for pine than poplar samples. A large increase in compliance was observed as the temperature was increased to 120°C for both wood species. Overall, the temperature dependence of the sequential creep compliance is consistent with the thermal responses shown in Figure 4.3.3.1. The samples creep very little at 50°C and 90°C; whereas the creep compliance increases

dramatically at 120°C which corresponds to the onset of major softening in the dynamic thermal scans.

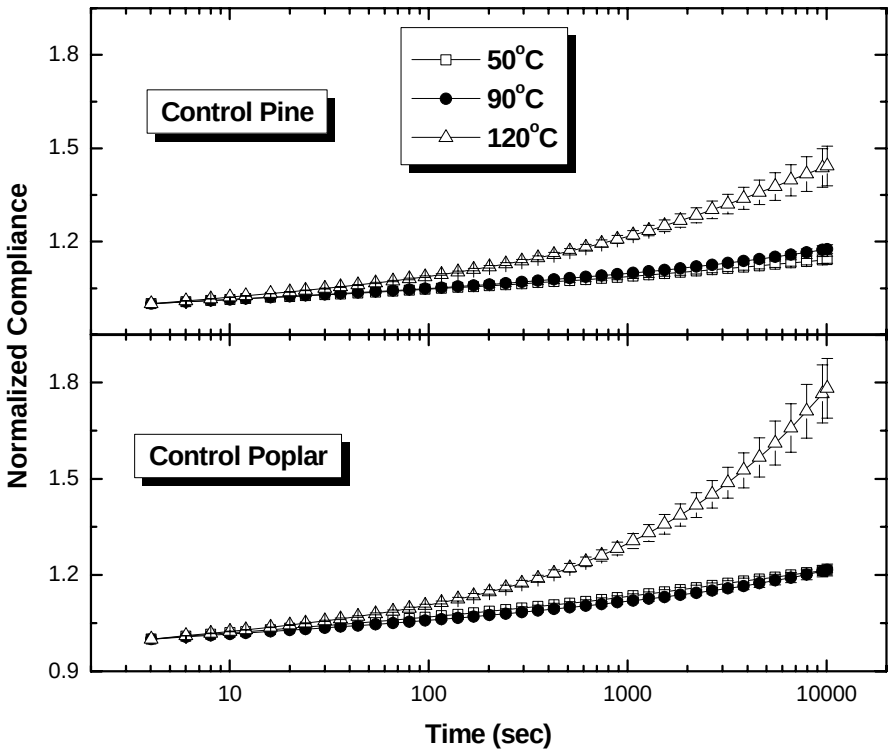

Figure 4.3.3.4. Normalized creep response of control wood samples at different temperatures. Each datum is the mean of 6 isochronous data points from 6 creep experiments at each temperature; error bars represent ± 1 standard deviation.

Figure 4.3.3.4 shows the normalized creep response of the control wood samples (normalized by the 4 sec compliance) at different temperatures, which in turn represents the relative rate of change of compliance from their initial value. The relative changes in compliance for both wood samples were similar at 50° and 90°C. However, the relative increase in compliance at 120°C showed a significant species dependence; while poplar was stiffer than pine, the former showed a much greater creep rate at 120°C.

As previously mentioned, the creep responses are explained by examining the dynamic scans of the corresponding control samples. Only low energy secondary

transitions were observed for both woods in the temperature range of 50°-90°C. Consequently, the control sample creep rates are minor at 50° and 90°C. The slight increase in compliance that was observed (from 50°C to 90°C) exclusively for pine samples. The large creep compliance increase at 120°C is attributed to the inception of large-scale segmental motions, as observed in the dynamic scans of the corresponding samples (figure 4.3.3.1). The 120°C creep rate differences (between poplar and pine) may correlate to the differences in monolignol composition (the lignin syringyl to guiacyl ratio). Hardwood lignins (of water-saturated wood) soften at lower temperatures than corresponding softwood lignins [15-17]. This is attributed to the lower crosslink density of hardwood lignins which results from the greater quantity of syringyl units. Thus, the greater creep rate in poplar might simply reflect the lower lignin crosslink density (lower lignin T_g) as compared to pine. Admittedly, this is a simplistic explanation which does not consider the influence of wood polysaccharides. Since these samples are completely dry, we must expect that the poplar/pine creep differences also reflect variations in the quantity, order and packing of amorphous polysaccharides. In this regard, hemicelluloses are likely a controlling factor since amorphous cellulose is itself extremely rigid [18].

The effects of resin solution impregnation and cure were studied using this sequential creep analysis. The resin impregnation was conducted using an *open-cell* method with resin-acetone solutions (10% concentration for poplar and 13% for pine) that resulted in a cured resin content of 3% (based upon dry wood). Figures 4.3.3.5, 4.3.3.6 and 4.3.3.7 demonstrate the effects of resin solution impregnation and cure on the 50°, 90° and 120°C sequential creep responses, respectively.

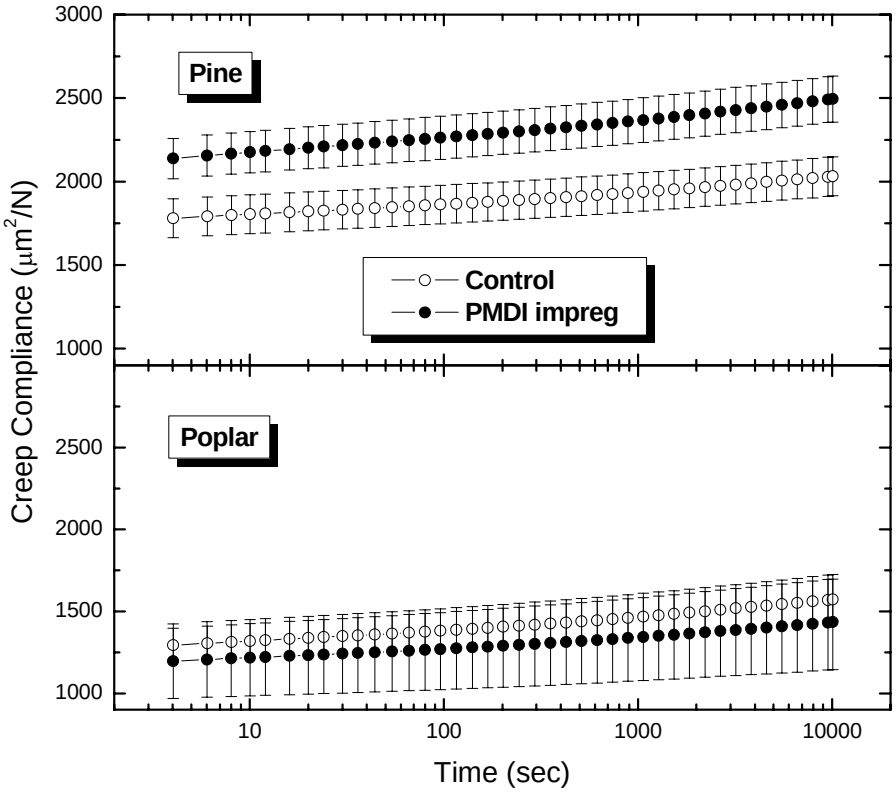

Figure 4.3.3.5. Effect of resin solution impregnation and cure on the 50°C creep compliance of pine and poplar samples. Prior to creep testing, all samples were heated at 120°C for 30 min and slow cooled (2°C/min) to 50°C; all samples were subjected to a 30 minute thermal equilibration at each experimental temperature. Each datum is the mean of 6 isochronous data points from 6 creep experiments at each temperature; error bars represent ± 1 standard deviation.

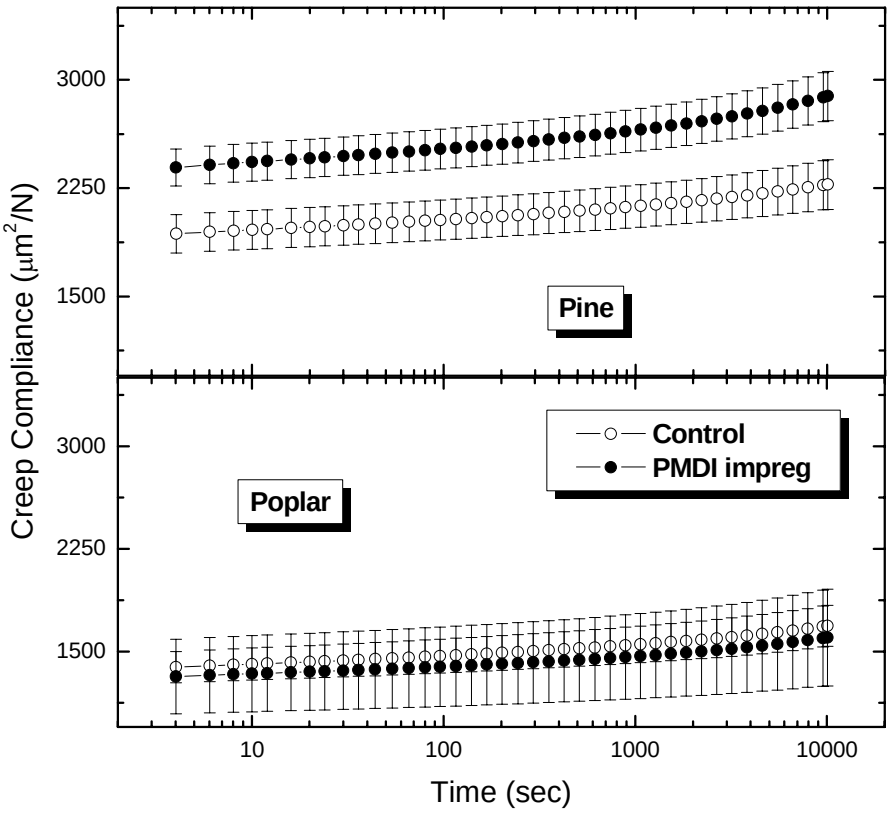

Figure 4.3.3.6. Effect of resin solution impregnation and cure on the 90°C creep compliance of pine and poplar samples. Prior to creep testing, all samples were heated at 120°C for 30 min and slow cooled (2°C/min) to 50°C; all samples were subjected to a 30 minute thermal equilibration at each experimental temperature. Each datum is the mean of 6 isochronous data points from 6 creep experiments at each temperature; error bars represent ± 1 standard deviation.

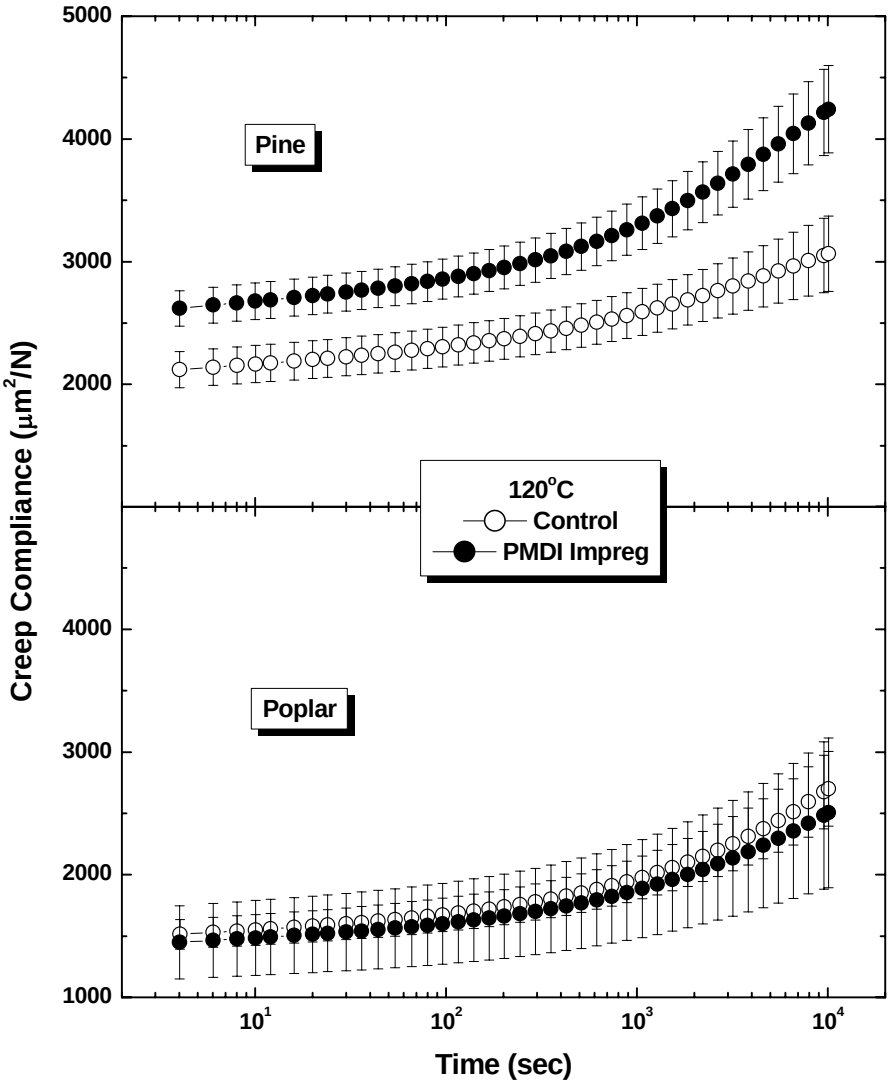

Figure 4.3.3.7. Effect of resin solution impregnation and cure on the 120°C creep compliance of pine and poplar samples. Prior to creep testing, all samples were heated at 120°C for 30 min and slow cooled (2°C/min) to 50°C; all samples were subjected to a 30 minute thermal equilibration at each experimental temperature. Each datum is the mean of 6 isochronous data points from 6 creep experiments at each temperature; error bars represent ± 1 standard deviation.

A species dependent resin effect was observed in Figures 4.3.3.5, 4.3.3.6 and 4.3.3.7. While, resin impregnation and cure caused an increase in pine compliance, poplar showed a slight decrease in compliance; the latter effect was found to be statistically insignificant. A stiffening of the wood was expected in the presence of the resin, but instead we observed a compliance decrease (in pine).

The effects of resin solution impregnation and cure on the relative creep rates (normalized creep compliances) are seen in Figures 4.3.3.8, 4.3.3.9 and 4.3.3.10.

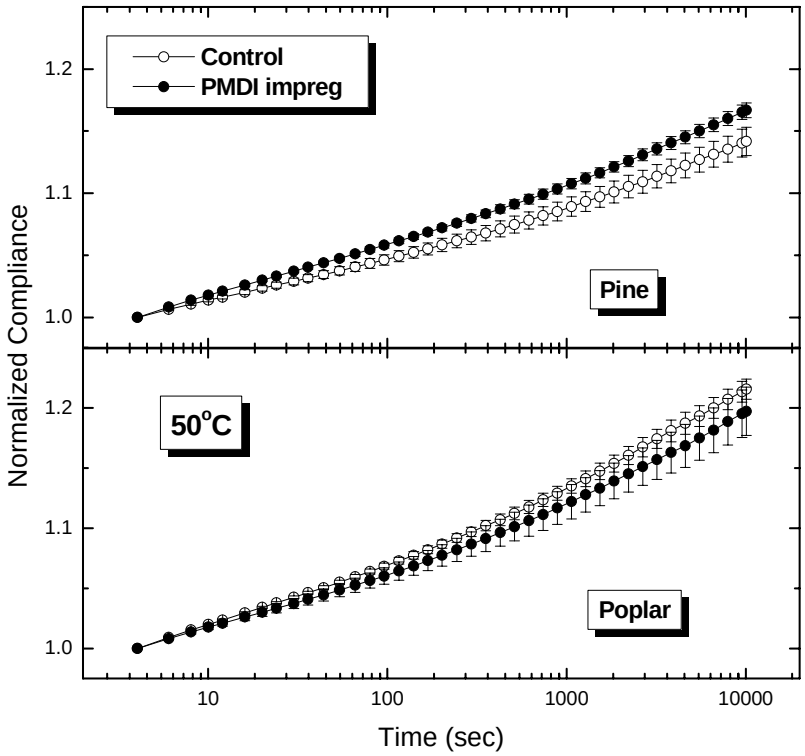

Figure 4.3.3.8. Effect of resin impregnation on the relative change of compliance for wood samples at 50°C. Each datum is the mean of 6 isochronous data points from 6 creep experiments; error bars represent ± 1 standard deviation.

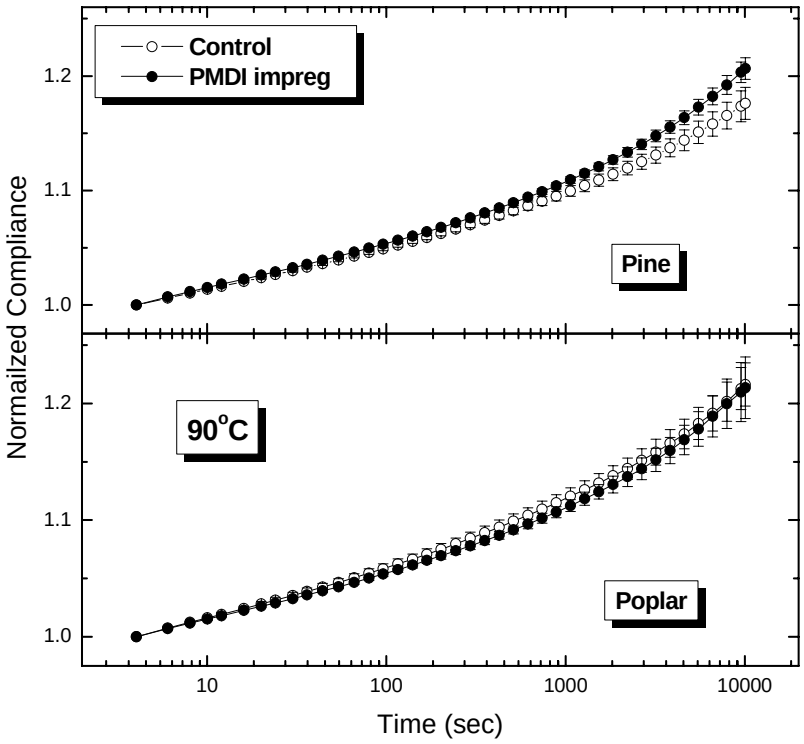

Figure 4.3.3.9. Effect of resin impregnation on the relative change of compliance for wood samples at 90°C. Each datum is the mean of 6 isochronous data points from 6 creep experiments; error bars represent ± 1 standard deviation.

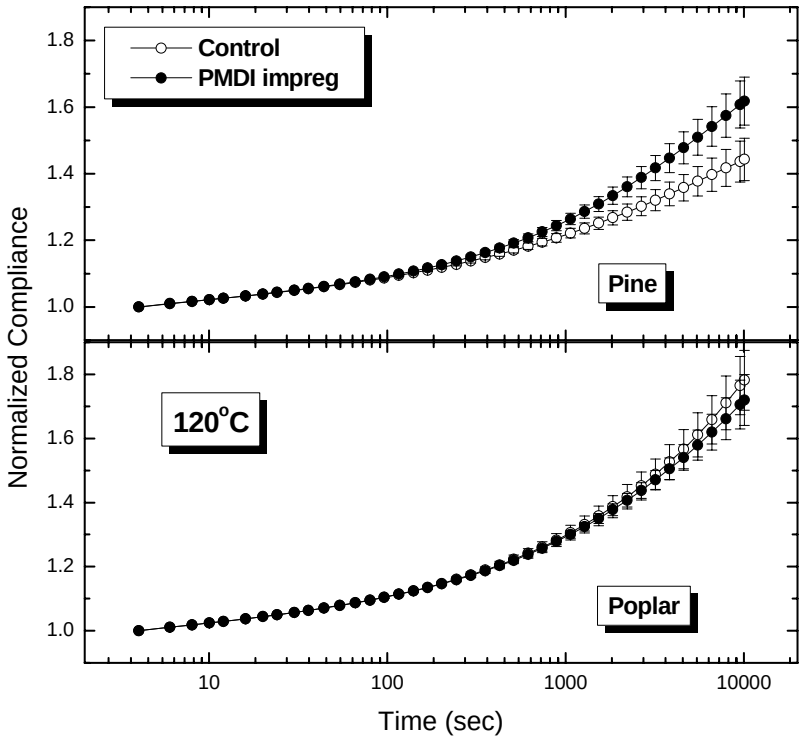

Figure 4.3.3.10. Effect of resin impregnation on the relative change of compliance for wood samples at 120°C. Each datum is the mean of 6 isochronous data points from 6 creep experiments; error bars represent ± 1 standard deviation.

Figures 4.3.3.8, 4.3.3.9 and 4.3.3.10 demonstrate that resin solution impregnation and cure alters the creep rate of pine samples, while the poplar samples show little or no effect from the resin treatment.

The normalized creep compliance curves actually reflect more than just the relative creep rates. The overall shapes of these normalized curves (and the changes caused by resin treatment) indicate important details about the mechanism of segmental relaxation. For example, the creep response of these wood samples is accurately described by the Kolrausch-Williams-Watts (KWW) [19] form of the generalized creep equation, as follows:

$$D(t) = D_u + (D_r - D_u) \times \left[1 - \exp\left\{ -\left(\frac{t}{\tau} \right)^{1-n} \right\} \right] \qquad (4.3.3.4)$$

where, $D(t)$ is the time dependent compliance,

D_u is the unrelaxed compliance,

D_r is the relaxed compliance (compliance at long creep times),

τ is the relaxation time constant, and,

n is the coupling parameter, which reflects the breadth of the creep relaxation distribution. The KWW equation is an empirical relationship which is very effective for describing relaxations in synthetic polymers. Furthermore, Ngai has independently developed a model for polymer segmental relaxations which (for glassy polymers) is identical to the KWW relationship [20-24]. Consequently, Ngai provides a molecular interpretation of the fitting parameters τ and n. The simplicity of the model (hereafter referred to as the coupling model) is perhaps its primary appeal. It indicates that polymer relaxations follow a simple exponential with a characteristic relaxation time (τ). However, this exponential is "stretched" by a factor (1-n) where n is the coupling parameter which reflects the coupled motions of polymer segments. This coupling represents the extent of intermolecular cooperativity among non-bonded segments. The coupling or cooperativity parameter has values from 0 to 1, where higher values indicate that the motion of any one segment increasingly requires the coordinated motion of nearby segments.

In this study, the influence of PMDI resin treatment on wood polymer coupling is quantified by fitting the KWW equation to the creep compliance. The creep compliance curves (shown in figures 4.3.3.5, 4.3.3.6 and 4.3.3.7) were fitted to the KWW equation (equation 4.3.3.4) in order to determine the coupling and relaxation parameters. Table 4.3.3.1 shows the fitting results for the control pine samples at 50°, 90° and 120°C.

Table 4.3.3.1. Relaxation parameters for control pine samples obtained by fitting to the KWW equation.

Temperature (°C)	R^2	τ	*n*
50°C	0.9997	$9.37\times10^{10} \pm 2.17\times10^{10}$	0.904 ± 0.003
	0.9998	$1.34\times10^{10} \pm 2.4\times10^{10}$	0.903 ± 0.003
	0.9996	$1.32\times10^{11} \pm 3.53\times10^{10}$	0.915 ± 0.003
	0.9998	$2.07\times10^{11} \pm 1.7\times10^{10}$	0.943 ± 0.002
	0.9998	$2.37\times10^{10} \pm 4.47\times10^{9}$	0.906 ± 0.002
	0.9998	$2.09\times10^{10} \pm 3.55\times10^{9}$	0.914 ± 0.002
90°C	0.9993	$2.03\times10^{8} \pm 3.67\times10^{7}$	0.847 ± 0.004
	0.9993	$34.83\times10^{8} \pm 9.25\times10^{8}$	0.886 ± 0.004
	0.9992	$7.78\times10^{7} \pm 1.32\times10^{8}$	0.833 ± 0.005
	0.9996	$1.54\times10^{9} \pm 2.63\times10^{8}$	0.888 ± 0.003
	0.9987	$3.45\times10^{7} \pm 6.45\times10^{6}$	0.816 ± 0.006
	0.9987	$3.45\times10^{7} \pm 6.45\times10^{6}$	0.816 ± 0.006
120°C	0.9995	$1.72\times10^{5} \pm 4.31\times10^{4}$	0.748 ± 0.004
	0.9984	$2.97\times10^{6} \pm 2.19\times10^{5}$	0.866 ± 0.007
	0.9984	$4.91\times10^{5} \pm 6.25\times10^{3}$	0.794 ± 0.001
	0.9987	$3.47\times10^{5} \pm 1.57\times10^{4}$	0.805 ± 0.006
	0.9998	$1.74\times10^{5} \pm 3.04\times10^{3}$	0.749 ± 0.003
	0.9998	$1.74\times10^{5} \pm 3.04\times10^{3}$	0.749 ± 0.003

Table 4.3.3.1 demonstrates that the KWW equation accurately represents wood creep relaxations. This is a nontrivial result for two reasons. Firstly, this demonstrates that wood polymer relaxations occur with a mechanism that is similar to that seen in synthetic polymers. Secondly, the quality of the fit enables us to quantify wood relaxations in a systematic fashion. Consequently, it is now possible to determine how various chemical treatments (in this case PMDI treatment) influence wood relaxations. Of course the short-term creep data in Figures 4.3.3.5, 4.3.3.6 and 4.3.3.7 covers only 4 decades of time. Consequently, one must question how accurately the fitting results reflect the true nature of wood relaxations for this data. Nevertheless, this fitting procedure does allow for a

sensitive measure of the creep response. Later we will see how time/temperature equivalence allows us to extend the creep data over a much broader time frame, which will improve the power of the fitting procedure.

Figure 4.3.3.11 shows the variation of the KWW parameters as a function of temperature for control pine and poplar samples.

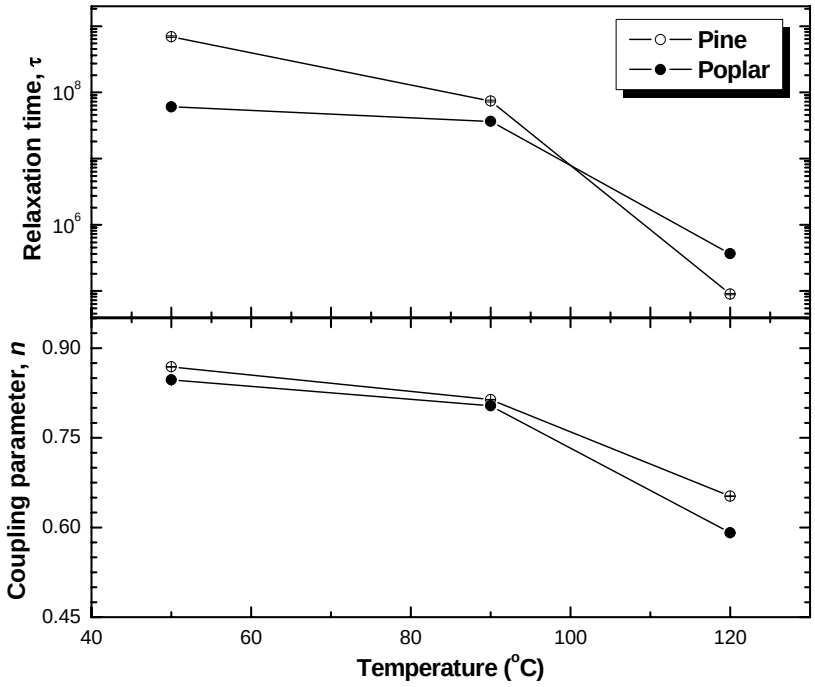

Figure 4.3.3.11. Variation of coupling parameter and relaxation times of control southern pine and yellow-poplar samples with temperature. Each datum is the mean from 6 creep experiments; error bars represent ± 1 standard deviation.

The coupling parameter of the control pine was lower than the corresponding poplar samples at all experimental temperatures. However, the differences are numerically minor and perhaps only truly significant at the highest temperature. The species differences in relaxation time appear to be more significant, where pine has longer relaxation times at 50° and 90°C; but the times cross over at 120°C. This wood species effect on the fitting results must reflect fundamental differences (and similarities) in the packing and supramolecular ordering of hardwoods versus softwoods.

The coupling parameter was found to decrease with increasing temperature. The decrease in the coupling parameter was relatively minor as the temperature increased from 50° to 90°C; but a significant decrease was observed at 120°C. The relaxation times for both woods also showed similar trends i.e. a slight decrease from 50° to 90°C, followed by a drastic decrease from 90° to 120°C. The large differences in relaxation time and coupling parameters between the lower temperatures (50° and 90°C) and 120°C indicate that different wood cell wall motional regimes are being probed at the various experimental temperatures.

Figure 4.3.3.12 shows the effect of resin impregnation on the coupling parameters of pine and poplar at the different experimental temperatures. It is seen that in certain cases, the very low resin treatment (3%) affected wood coupling parameters. Resin treatment did not have a significant effect on the 50°C coupling parameter for either wood. Both woods exhibit a small decrease in the 90°C coupling; the effect being slightly greater in pine. The 120°C data show a clear wood species effect in that the poplar coupling is unaffected; while PMDI treatment causes a significant decrease in the 120°C pine coupling.

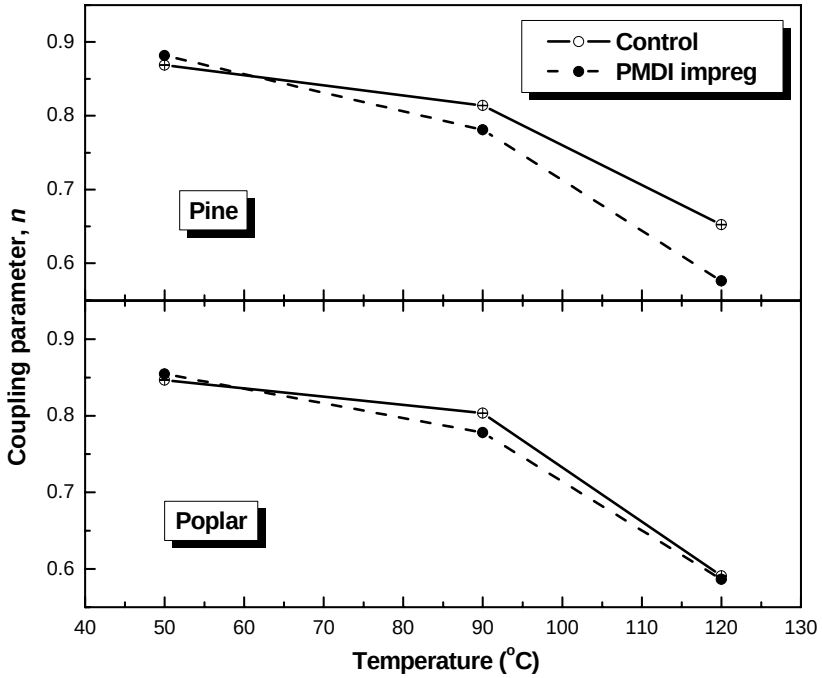

Figure 4.3.3.12. Effect of resin impregnation on the coupling parameters of YP and SYP at different temperatures. Each datum is the mean from 6 creep experiments; error bars represent ± 1 standard deviation.

At 120°C, the creep relaxation is likely due to the onset of large-scale lignin (or lignin-hemicellulose) motions (Recall that the dynamic thermal scans show the inception of a major transition at 120°C, Figure 4.3.3.1). Considering the reactivity of PMDI, we might expect the resin treatment to **increase** the relaxation coupling. Instead when the resin treatment did have an effect, we see that coupling was actually **reduced**, which suggests that the resin altered the polymer packing of the pine in a fashion that reduced inter-segmental interactions. Note that resin impregnation and cure led to an increase in compliance for the pine samples (Figure 4.3.3.7), which might be related to the reductions in pine coupling parameters.

Figure 4.3.3.13 shows the effect of resin impregnation and cure (~3% resin) on the relaxation times of pine and poplar samples at different temperatures. The relaxation times for both control and resin-impregnated wood samples were found to decrease with

temperature. The effect of resin impregnation on the relaxation times of the different wood species was found to be most significant at 50°C.

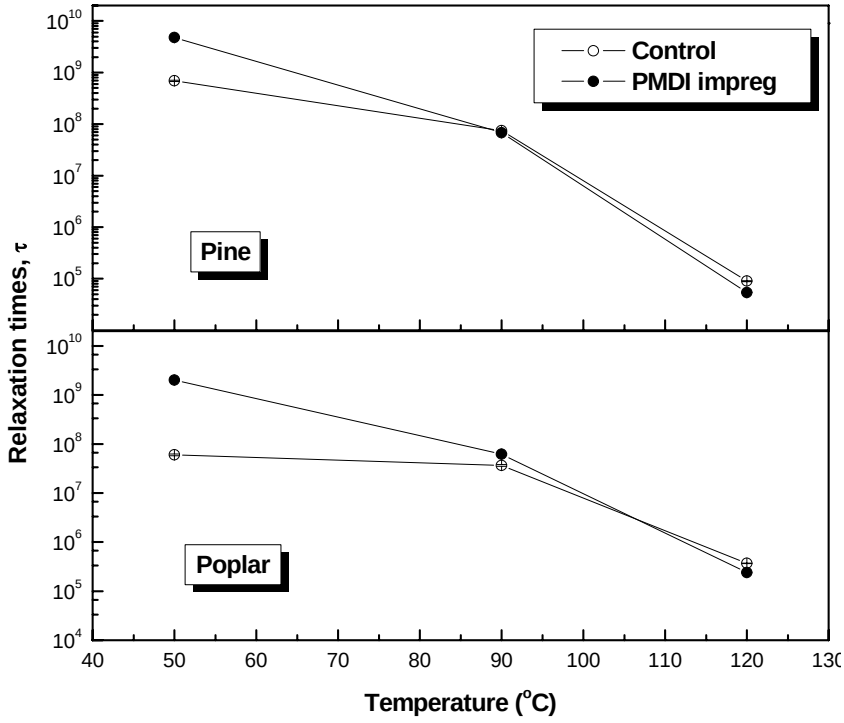

Figure 4.3.3.13. Effect of resin impregnation and cure on the relaxation times of pine and poplar wood samples at different temperatures. Each datum is the mean from 6 creep experiments; error bars represent ± 1 standard deviation.

The 50°C relaxation times of both wood species significantly increased in the presence of resin; but the increase was greater for the poplar samples. Thus, resin treatment altered the packing of the wood polymers in such a way that the relaxation times increased, without altering the cooperativity of the PMDI-wood system at this temperature (*n* did not change at 50°C with resin impregnation). We expected to see an increase in coupling parameter along with the increase in relaxation times, but there was only 3% resin in the wood which was distributed evenly due to the solvent impregnation process. Significant changes in all KWW parameters may have been observed at higher resin impregnations.

Thus, dry creep analysis is a novel method of probing the supramolecular structures of wood. Significant differences in the relaxation mechanisms were observed between wood species by this method. This method was successful in analyzing the effect of resin impregnation on the molecular packing of wood at very low resin impregnation levels. The wood relaxations can be effectively modeled by the KWW equation. Significant resin effects were observed on the wood relaxations times at both low and high temperatures. At low temperatures, the resin altered the wood relaxations without altering the cooperativity of the wood-PMDI system. But at higher temperatures, the resin decreased the inter-segmental interactions of the lignin and/or lignin-hemicellulose polymers, without affecting their relaxation times. Generally speaking, it seems as if resin treatment affected the relaxations of pine wood more than the poplar.

4.3.3.3.3. Effect of resin impregnation on the dynamic scans of EG-plasticized wood

Figure 4.3.3.14 shows the dynamic thermal scans of ethylene glycol plasticized control and resin impregnated wood samples. Both woods show a major transition which is due to the softening of in situ lignin. Previous studies have shown that hardwood lignins soften at a lower temperature than the corresponding softwood lignins [15,16]. But no differences in the softening temperatures of EG softened pine and poplar lignins were observed in the dynamic thermal scans obtained in this study; the softening of pine was found to be slightly broader than the poplar samples. The lignin softening was found to change in the presence of the resin for both woods.

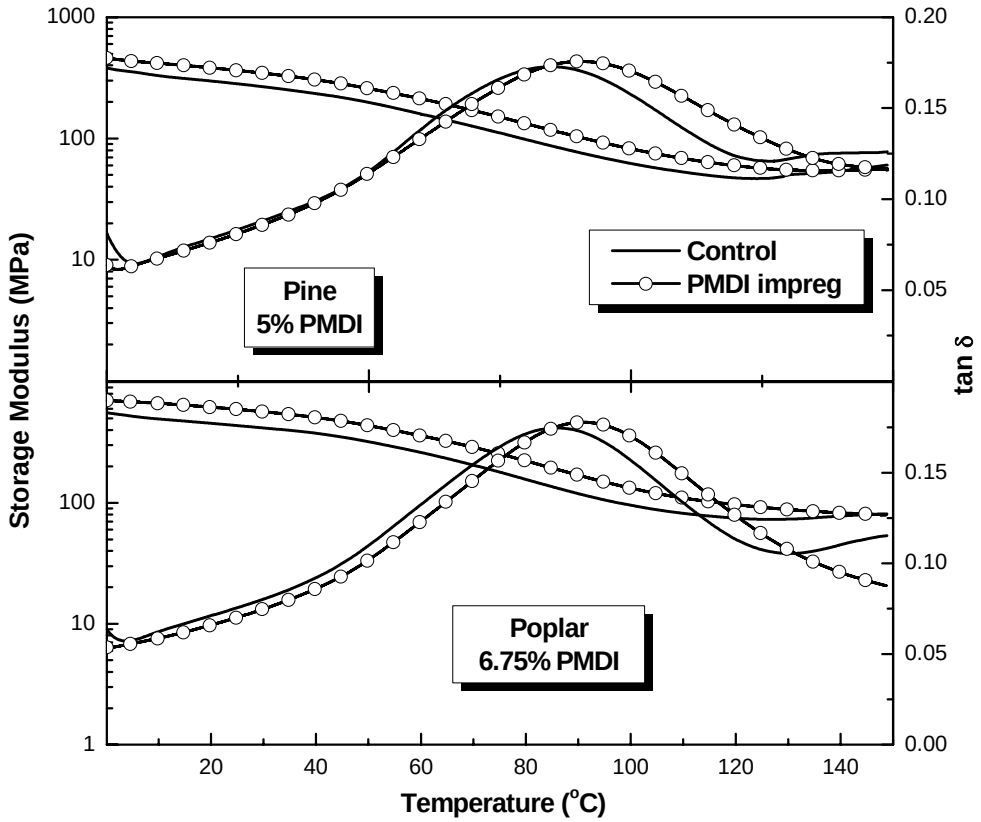

Figure 4.3.3.14. Effect of resin impregnation and cure on the dynamic scans of ethylene glycol plasticized wood. (2°C/min heating rate, 0.057% strain (20 μm amplitude), 1 Hz frequency).

The lignin softening shifted to slightly higher temperatures and became broader; however, the change in lignin relaxation was more pronounced in pine than poplar (it was relatively broader in pine in spite of its smaller resin content relative to the poplar samples).

The dynamic thermal scans give us a qualitative idea of the species-dependent interaction of the resin with lignin. In order to analyze the resin effect quantitatively, long-term (3 h) isothermal creep experiments were performed on EG-plasticized wood samples.

4.3.3.3.4. Isothermal creep on EG-plasticized wood

Three hour creep experiments were performed at 50°C on both control and resin impregnated wood samples, all of which were plasticized by ethylene glycol. The wood relaxations that are being probed by this test were entirely different from those observed in the dry samples. The low creep temperature was selected to minimize plasticizer loss during the experiment. Table 4.3.3.2 shows that all samples lost plasticizer in the course of the experiment; but the plasticizer content at the end of the experiment was above the fiber saturation point of the wood samples.

Table 4.3.3.2. Sample parameters for 3 hr isothermal creep experiments

Sample*	PMDI content (%)	Plasticizer content before test (%)	Plasticizer content after test (%)
Pine control	-	124.86 ± 9.4	94.14 ± 9.15
Poplar Control	-	147.26 ± 6.51	104.57 ± 3.25
Pine PMDI	5.29 ± 0.26	124.61 ± 5.29	87.09 ± 6.8
Poplar PMDI	5.5 ± 0.19	106.07 ± 3.44	84.01 ± 8.56

* Five replications each

Samples were impregnated with a resin acetone solution (13% for poplar and 20% for pine) to obtain similar resin impregnations. Figures 4.3.3.15 and 4.3.3.16 show the creep compliance curves of EG-plasticized wood samples.

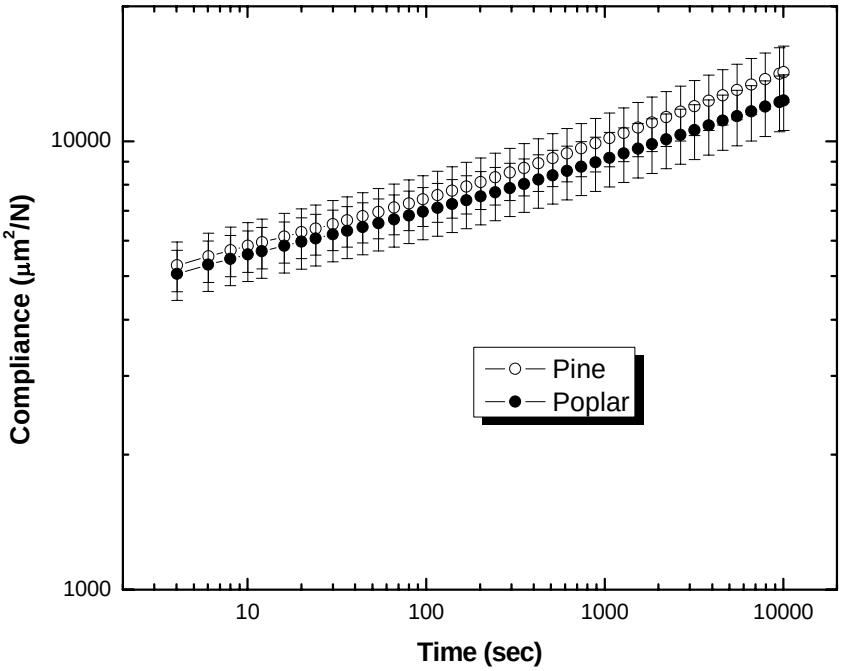

Figure 4.3.3.15. Three hour isothermal creep curves of EG-plasticized control poplar and pine samples. Each datum is the mean of 5 isochronous data points from 5 creep experiments; error bars represent ± 1 standard deviation.

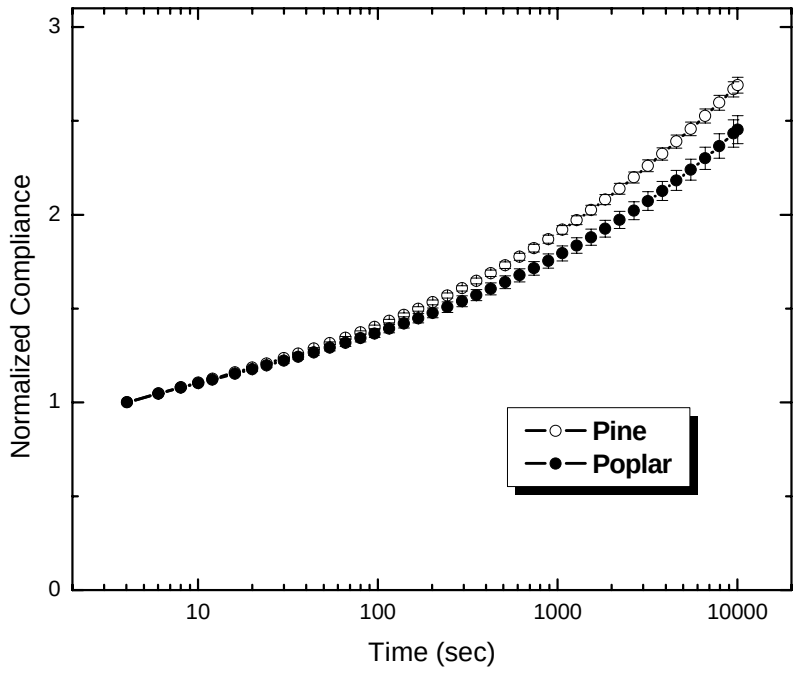

Figure 4.3.3.16. Normalized three hour isothermal creep curves for ethylene glycol plasticized wood samples. Each datum is the mean of 5 isochronous data points from 5 creep experiments; error bars represent ± 1 standard deviation.

There is little difference between the creep compliance curves of pine and poplar (figure 4.3.3.15), but the shapes of the creep curves are different (figure 4.3.3.16). The effect of resin impregnation on the creep compliance of plasticized wood samples is shown in figures 4.3.3.17 and 4.3.3.18.

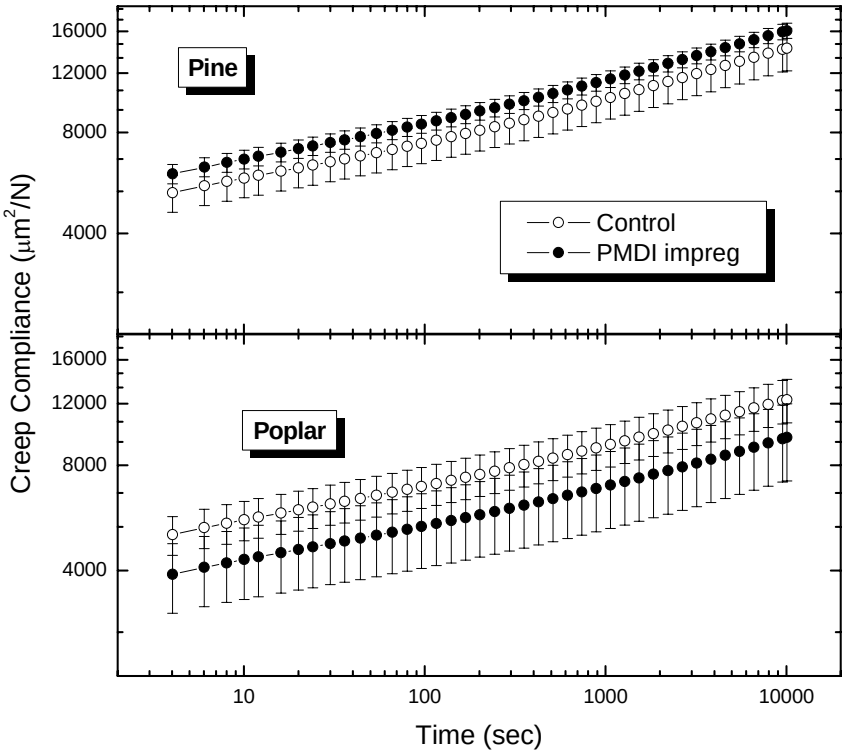

Figure 4.3.3.17. Effect of resin impregnation and cure on the three hour isothermal creep compliance of ethylene glycol plasticized wood samples. Each datum is the mean of 5 isochronous data points from 5 creep experiments; error bars represent ± 1 standard deviation.

The effect of resin impregnation on the plasticized woods was found to be consistent with those observed in the dry wood samples (figures 4.3.3.5, 4.3.3.6 and 4.3.3.7); while pine showed an increase in compliance, poplar became relatively stiffer in the presence of the resin. But unlike the dry samples, the resin effect was relatively larger in poplar. But these effects were not statistically significant.

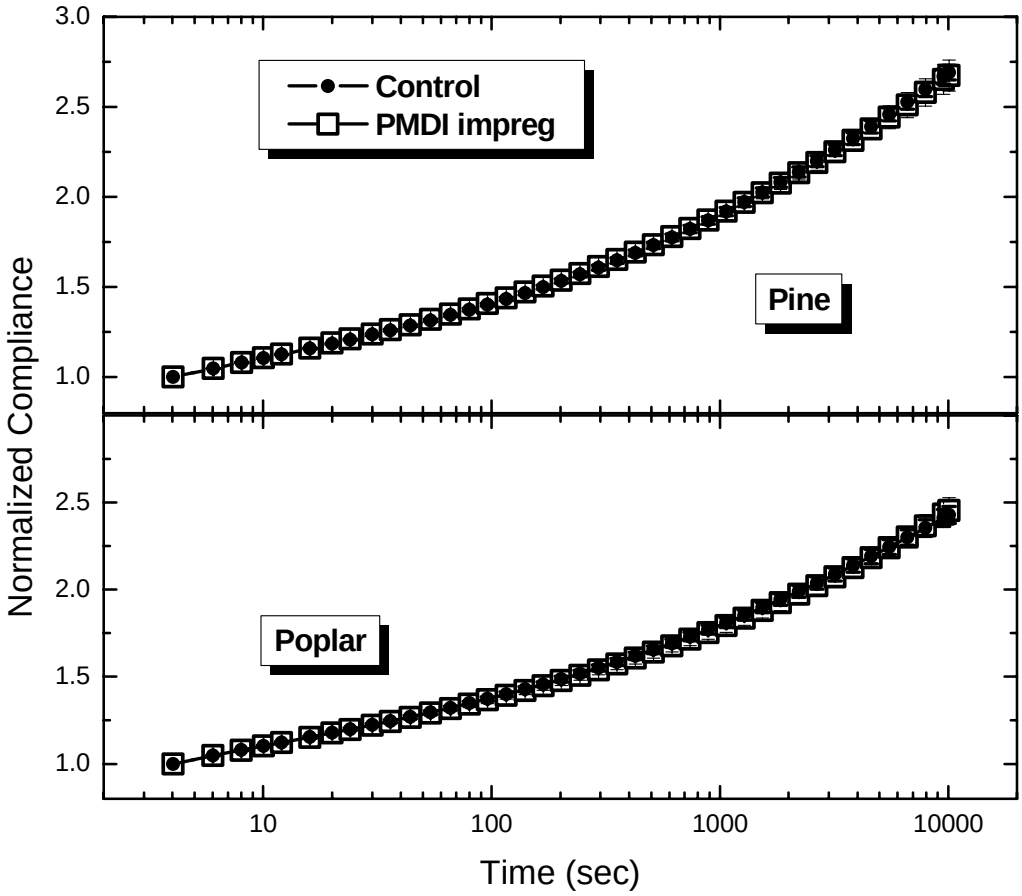

Figure 4.3.3.18. Effect of PMDI resin treatment on the normalized three hour isothermal creep compliance of ethylene glycol plasticized wood samples. Each datum is the mean of 5 isochronous data points from 5 creep experiments; error bars represent ± 1 standard deviation.

Furthermore, Figure 4.3.3.18 shows that resin treatment had no effect on the shape of the creep curves for both wood species.

Table 4.3.3.3 shows the KWW fitting parameters for the different plasticized wood samples.

Table 4.3.3.3. KWW fitting parameters for ethylene glycol plasticized wood samples

Sample	R^2	$\tau \times 10^{-5}$(sec)	*n*
Pine control	0.9996	7.66 ± 0.19	0.763 ± 0.001
	0.9997	6.35 ± 0.14	0.754 ± 0.001
	0.9998	6.19 ± 0.12	0.761 ± 0.001
	0.9997	6.39 ± 0.13	0.769 ± 0.001
	0.9997	6.39 ± 0.13	0.769 ± 0.001
Poplar Control	0.9997	6.0 ± 0.13	0.781 ± 0.001
	0.9996	6.8 ± .17	0.782 ± 0.001
	0.9997	5.64 ± 0.13	0.783 ± 0.001
	0.9997	6.36 ± 0.14	0.781 ± 0.001
	0.9997	6.24 ± .014	0.782 ± 0.001
	0.9997	6.0 ± 0.13	0.782 ± 0.001
Pine-PMDI	0.9998	4.8 ± 0.08	0.764 ± 0.001
	0.9998	5.28 ± 0.09	0.772 ± 0.001
	0.9997	7.37 ± 0.18	0.757 ± 0.001
	0.9998	4.98 ± 0.09	0.766 ± 0.001
Poplar-PMDI	0.9992	10.12 ± 0.4	0.779 ± 0.001
	0.9996	51.84 ± 1.7	0.791 ± 0.001
	0.9996	51.05 ± 1.64	0.795 ± 0.001
	0.9991	1545 ± 102.1	0.769 ± 0.001
	0.9995	38.02 ± 1.37	0.793 ± 0.001

The coupling parameters for the ethylene glycol plasticized control samples (~0.78) were found to be significantly smaller than the corresponding dry samples (~0.86) at the same temperatures (50°C). The inter-segmental interactions decreased in these systems due to the presence of the plasticizer. The relaxation times (~10^5 sec) of the plasticized samples also decreased relative to the dry samples (~10^8 sec) for the same reason.

The variations of the KWW parameters for the different wood samples are shown in Figure 4.3.3.19.

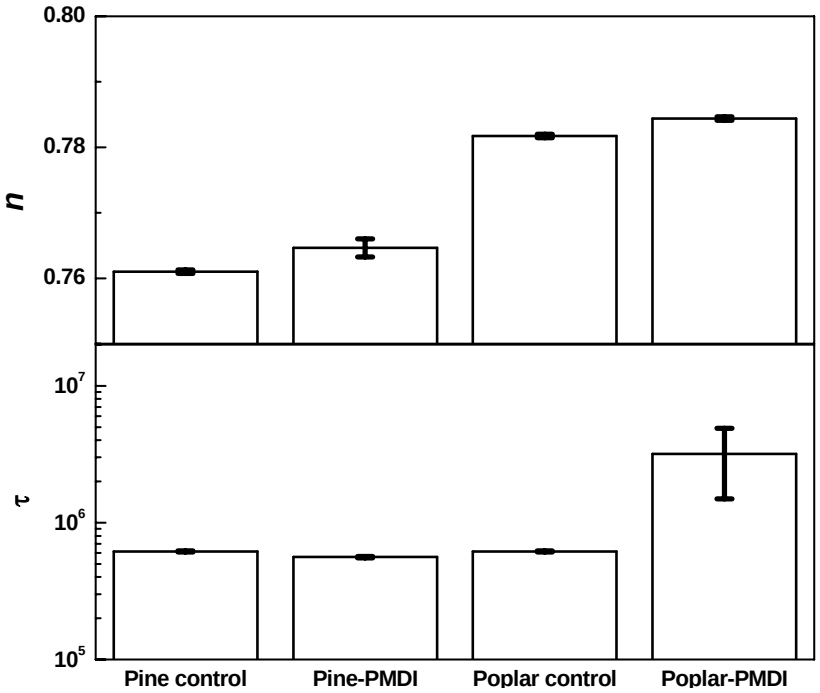

Figure 4.3.3.19. Effect of resin impregnation on the KWW parameters of EG-plasticized pine and poplar samples subjected to 3 hour creep (5 replications each). Error bars represent ± 1 standard deviation.

The coupling parameter for pine was slightly smaller than for the poplar samples. The resin had no effect on the coupling parameters for both woods. The pine relaxation times were unaffected by the resin, but the relaxation for poplar showed a very slight increase. Overall, resin treatment had little or no effect on the three hour isothermal creep response of both EG plasticized woods. This is somewhat surprising given the fact that the sequential creep response of dry samples was significantly altered. This discrepancy might be explained by the fact that the respective experiments probe entirely different aspects of wood polymer relaxations.

4.3.3.3.5. Time-temperature superposition on EG-plasticized wood

The effect of resin impregnation and cure on the in situ lignin relaxation of EG-plasticized wood was also analyzed by the time-temperature superposition principle. Isothermal short-time (1000 sec) creep experiments were conducted over the lignin transition (15° to 95°C) on ethylene glycol plasticized samples; the isotherms were then shifted at a reference temperature of 80°C to construct a mastercurve (Figure 4.3.3.20). The creep mastercurve shows a minor inflection, which is attributed to the softening of lignin. Notice also that this mastercurve spans approximately 11 decades of time, as opposed to only 3 decades for the previous creep experiments.

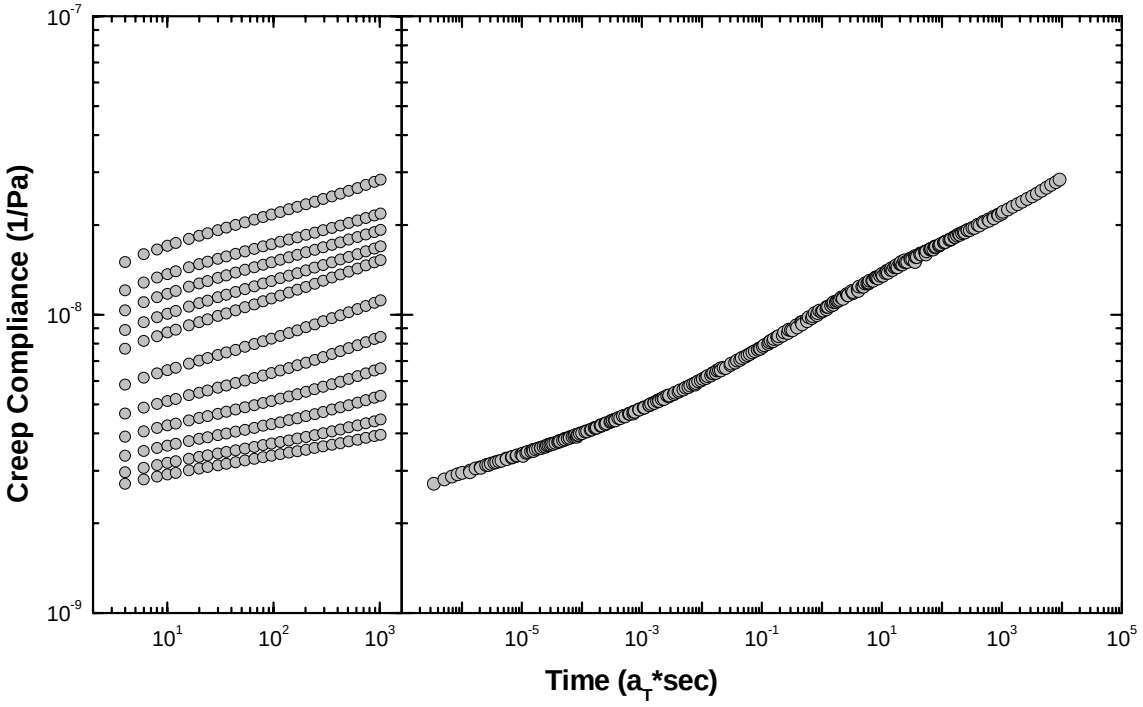

Figure 4.3.3.20. Mastercurve construction from creep data (T_{ref} = 80°C). Poplar control wood sample, thermally treated at 90°C for 30 min., quench-cooled to 5°C, followed by isothermal creep segments (1000 sec) in the temperature range of 5° - 90°C.

The following table shows the different sample parameters used in these experiments.

Table 4.3.3.4. Summary of sample resin content (on dry wood) and also ethylene glycol contents before and after the TTS creep segments.

Sample*	Resin content (%)	EG content before test (%)	EG content after test (%)
Pine control	-	130.6 ± 10.6	52.9 ± 8.2
Poplar control	-	144.2 ± 7.9	47.0 ± 2.9
Pine-PMDI	5.5 ± 0.2	94.3 ± 6.8	54.7 ± 3.9
Poplar-PMDI	5.3 ± 0.3	104.6 ± 16.5	49.8 ± 4.7

*Five replications each

Significant plasticizer loss was observed during the course of the experiments; however the samples were thought to be above the fiber saturation point (FSP) over the entire period (8.2 h) of the experiment. But results showed that smooth mastercurves were not obtained for samples with final plasticizer contents of from ~35-40% (based on dry wood). This led us to estimate the FSP of wood in ethylene glycol to be ~35-40%, though the FSP was not determined experimentally. So while plasticizer loss did not fall below the fiber saturation point over the experimental temperature range, EG loss was more significant at higher temperatures (95°C). In other words, higher temperature creep segments were unobtainable with this method, due to higher plasticizer loss at temperature greater than 90°C. Figure 4.3.3.21 shows the mastercurves for plasticized control pine and poplar samples. Both woods showed similar creep compliance mastercurves, however, the poplar mastercurves were found to cover a slightly broader time span than the corresponding pine samples.

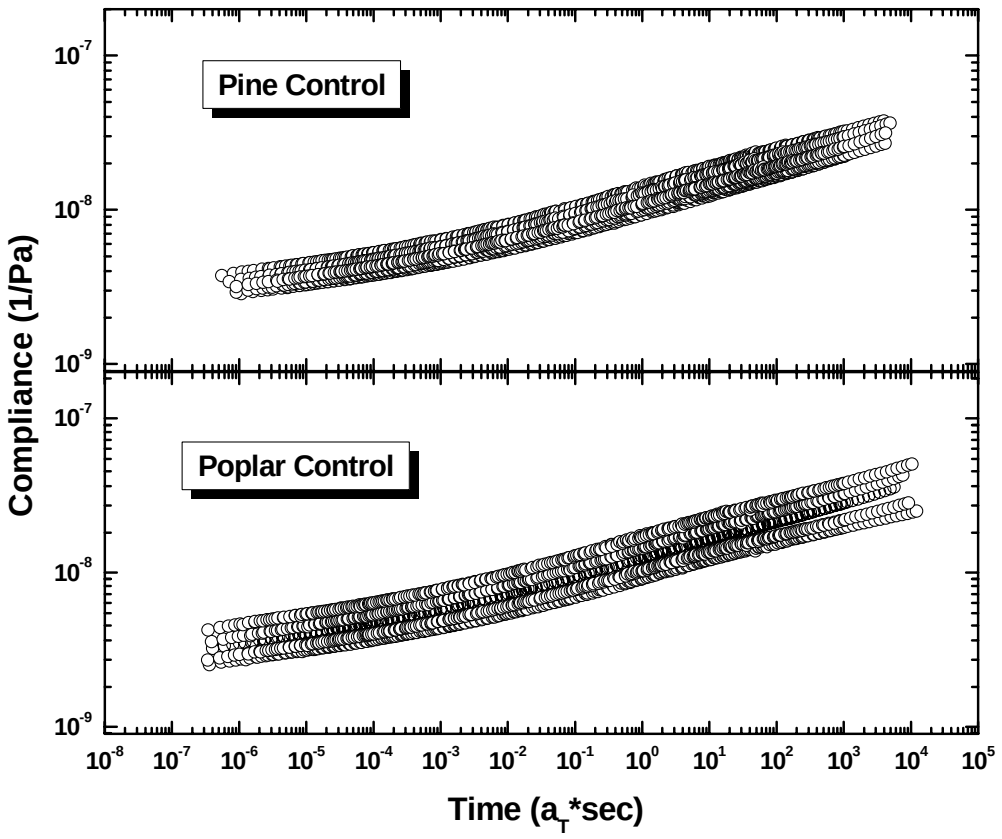

Figure 4.3.3.21. Creep mastercurves of plasticized control wood samples (5 replications each).

All wood samples were thermally treated at 95°C for 30 min in the DMA prior to isothermal creep experiments. The samples were then either slow-cooled (5°C/min) or quench-cooled (20°C/min) from 95°C to 15°C, followed by the isothermal short-term creep segments. Figure 4.3.3.22 compares the shift-factor plots from plasticized poplar and pine samples under two different cooling conditions, slow cooling and quench cooling (from the initial 95°C, 30 min thermal treatment).

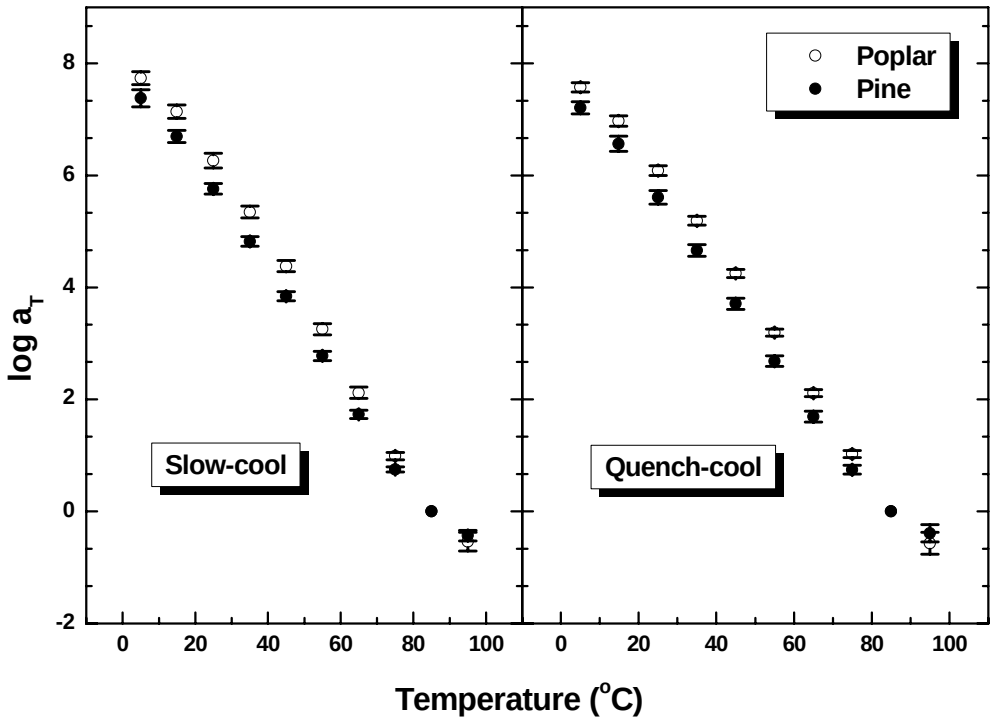

Figure 4.3.3.22. Effect of wood species on the shift-factor plots of ethylene glycol plasticized pine and poplar samples under different cooling conditions (5 replications each).

The shift factor plots in Figure 4.3.3.22 demonstrate that pine and poplar exhibit a minor but significant difference in the temperature dependence of the EG modified relaxation. Also, note that the shift factor plots exhibit only a minor degree of curvature in the high temperature region which certainly spans the lignin glass transition (Figure 4.3.3.14). The temperature dependence of the T_g relaxation for synthetic polymers typically shows highly nonlinear behavior. The slight curvature observed in this study may be due to the fact that we are probing only a small fraction of the sample, lignin which constitutes ~28% of wood. This slight curvature may also reflect the complexity of the lignin structure and ordering. In terms of Angell's concept of fragility [25,26], EG plasticized in situ lignin resembles a "strong" glass, where the temperature dependence of the

relaxation is more linear in nature. This implies that the lignin relaxation is restricted to relatively few different configuration states.

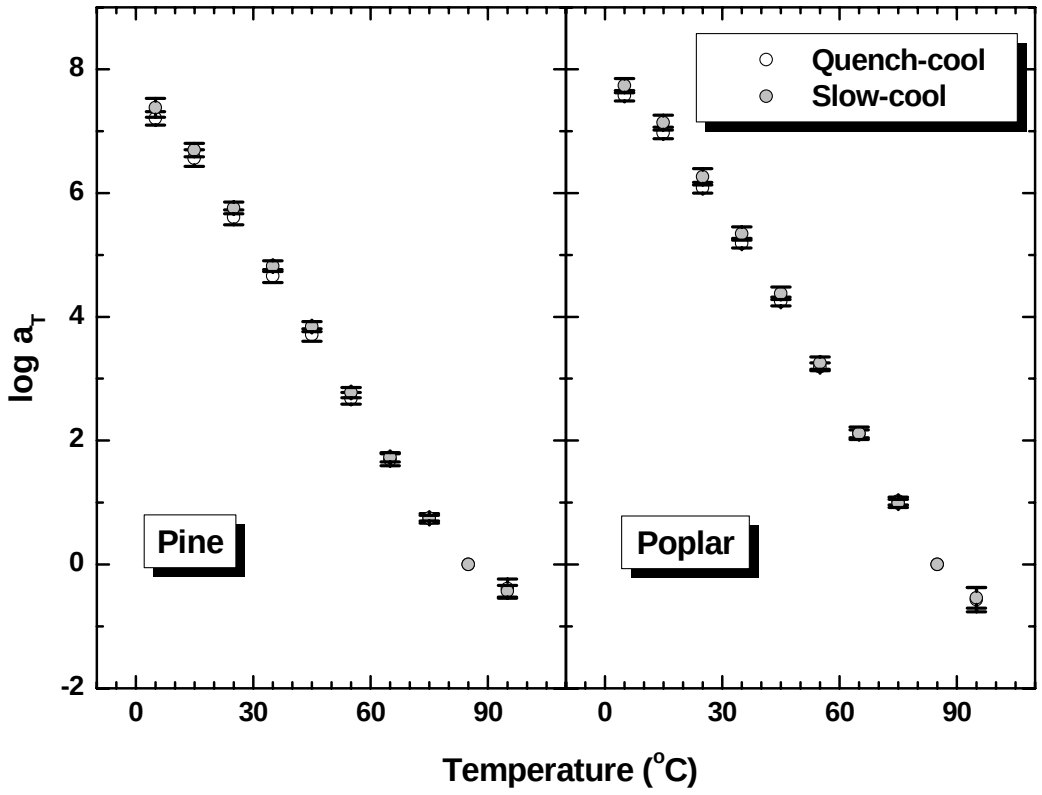

Figure 4.3.3.23. Effect of cooling rate on the shift-factor plot of ethylene glycol plasticized wood samples. Samples thermally treated at 90°C for 30 min followed by quench/slow (5°C/min) cooled to 15°C. 1000 sec creep experiments were performed in the temperature range of 15°-90°C. T_{ref} = 80°C. (5 replications each).

The results show that the shift factor plots of poplar are independent of the cooling rate. Previous studies (chapter 4.3.1) have shown that the thermal history significantly affects the dynamic mechanical properties of dry wood samples. But in the plasticized state, the free volume of wood samples is significantly increased due to the presence of the ethylene glycol. In other words, the plasticizer dominates free volume effects, and temperature effects are excluded.

Similar studies were also performed on resin impregnated wood samples, which were **quench-cooled** from the thermal treatment step to the initial creep segment. Figure 4.3.3.24 shows the effect of resin on the creep compliance curves of ethylene glycol plasticized wood samples.

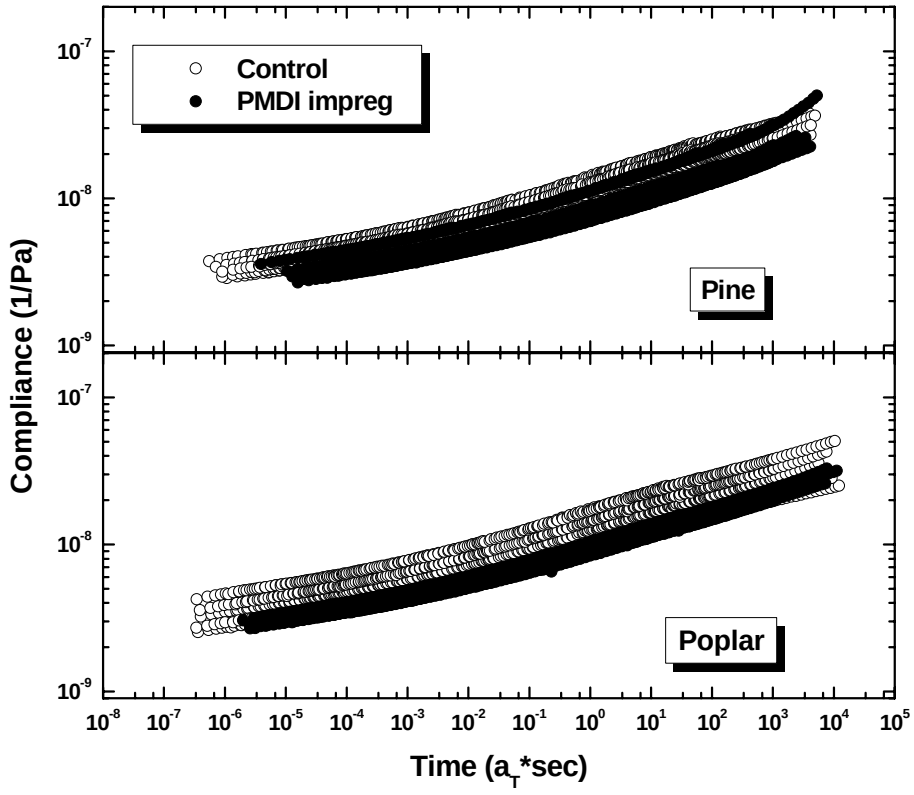

Figure 4.3.3.24. Effect of resin impregnation and cure on the creep compliance mastercurves of plasticized wood samples. Samples thermally treated at 90°C for 30 min followed by quench cooling to 15°C. 1000 sec creep experiments were performed in the temperature range of 15°-90°C. T_{ref} = 80°C. (5 replications each).

Figure 4.3.3.24 demonstrates that resin treatment had a slight stiffening effect on both woods. The mastercurves of the resin impregnated samples were also found to cover a narrower time span than the corresponding control samples. The effect of the resin treatment on the shift factor plots is shown in figure 4.3.3.25.

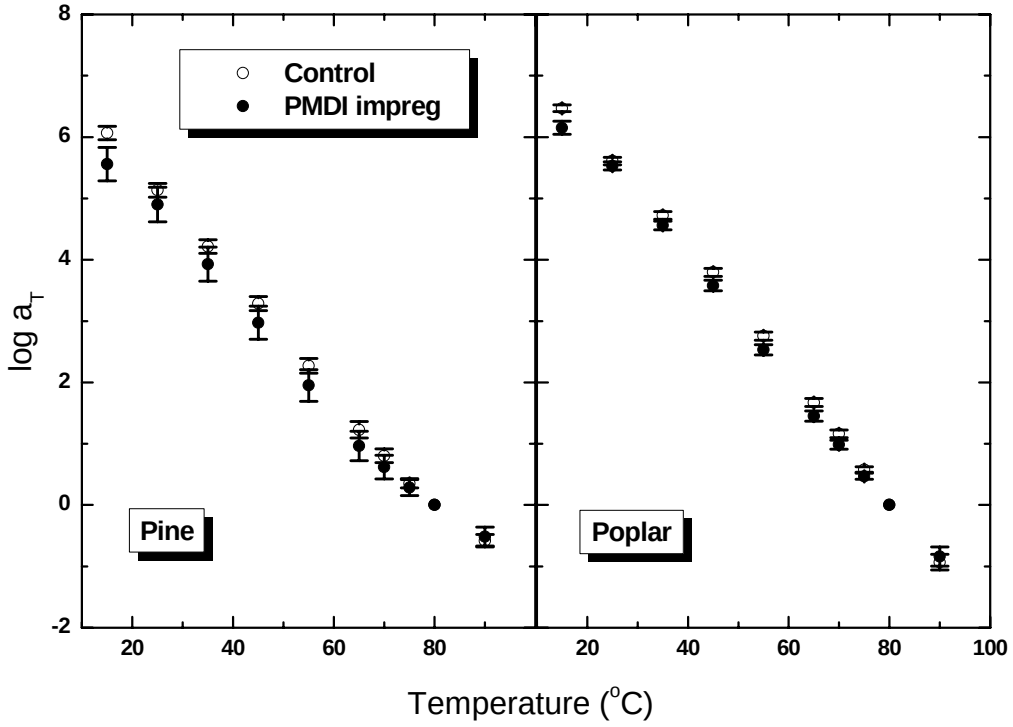

Figure 4.3.3.25. Effect of resin impregnation on the shift factor plots of ethylene glycol plasticized wood samples. Samples thermally treated at 90°C for 30 min followed by quench cooling to 15°C. 1000 sec creep experiments were performed in the temperature range of 15°-90°C. T_{ref} = 80°C. (5 replications each).

The resin was found to have a small effect on the shift factor plots of the plasticized wood samples; the effect was relatively greater at lower temperatures. The shift factors were used to calculate the activation energy (E_{act}) for the lignin relaxation and the WLF constants (C_1 and C_2). The shift factors in the temperature range of 15° to 65°C were fitted to the Arrhenius equation (equation 1) to calculate the lignin E_{act}, while those in the temperatures range of 65° to 95°C were fitted to the WLF equation. Figure 4.3.3.26 shows the effect of resin impregnation on the E_{act} and WLF constants of the in-situ lignin transition.

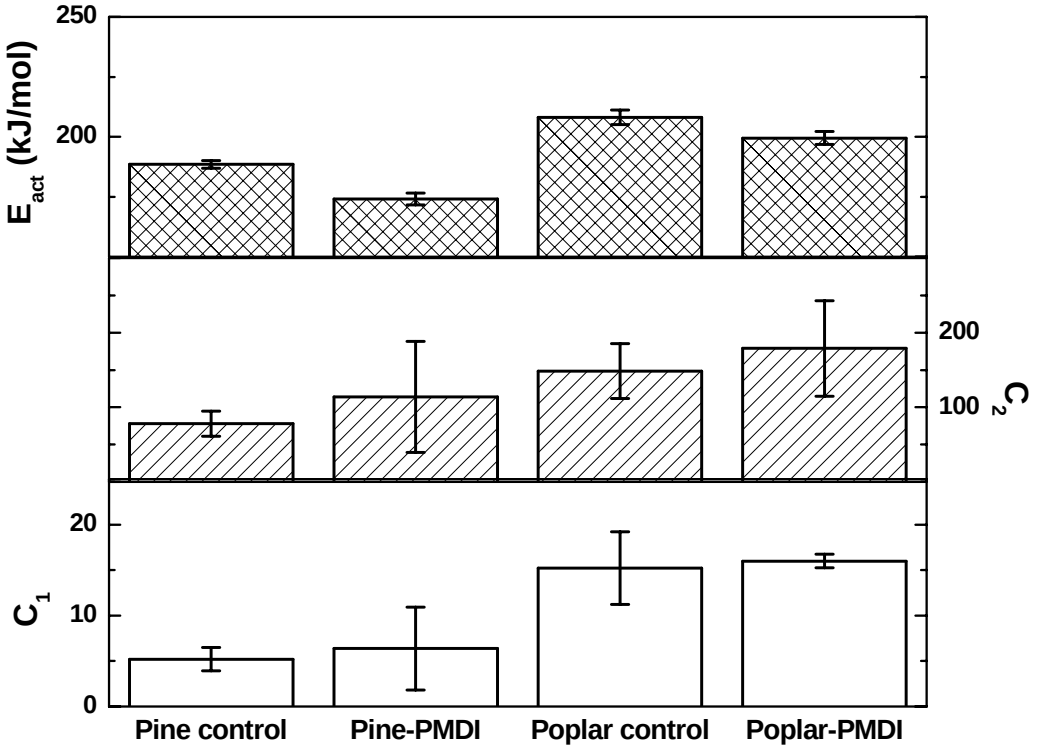

Figure 4.3.3.26. Effect of resin impregnation on the activation energy and WLF constant of the in situ lignin relaxation in radial EG-plasticized wood samples (5 replications each).

Previous studies [15-17] have shown that hardwood lignins soften at lower temperatures and have significantly lower E_{act} than the corresponding softwood lignins. But this analysis shows that the E_{act} of in-situ lignin of control pine (~188 kJ/mol) was slightly lower (but statistically significant) than the corresponding poplar (~208 kJ/mol) samples. Resin impregnation was found to decrease the lignin E_{act} for both wood species; but the change was greater in pine samples. However, keep in mind that these activation energies were calculated over the highly linear low temperature region of the shift factor plot, and this does not necessarily reflect the true activation energy of the glass transition.

The WLF constants for the control samples were significantly different between the wood species tested; C_1 and C_2 of poplar were significantly larger than pine. The

constants were found to increase with resin impregnation, but the changes were not statistically significant.

The creep mastercurves of the different wood systems were also fitted to the KWW equation (equation 4.3.3.4), in order to analyze the effect of resin treatment on the coupling of the lignin relaxation. The following table shows that the KWW equation can be successfully used to describe the relaxation of ethylene glycol plasticized wood using time/temperature superposition.

Table 4.3.3.5. KWW fitting parameters for ethylene glycol plasticized wood mastercurves.

System	R^2	τ (sec)	*n*
Pine control	0.9998	117960	0.830
	0.9998	4311.5	0.820
	0.9998	4886.8	0.820
	0.99988	5709.6	0.825
	0.9998	42910	0.829
Pine-PMDI	0.99978	134000	0.819
	0.9995	194950	0.813
	0.9998	85615	0.821
	0.9973	274010	0.811
	0.9972	255990	0.803
Poplar control	0.9997	41920	0.837
	0.9996	5923.7	0.830
	0.9997	1636.1	0.826
	0.9995	2855	0.828
	0.9997	3223	0.833
Poplar-PMDI	0.9995	721660	0.839
	0.9997	975460	0.841
	0.9993	80979	0.828
	0.9998	91313	0.833
	0.9994	112840	0.824

Figure 4.3.3.27 shows the effect of resin impregnation on the coupling parameter and relaxation times of pine and poplar samples.

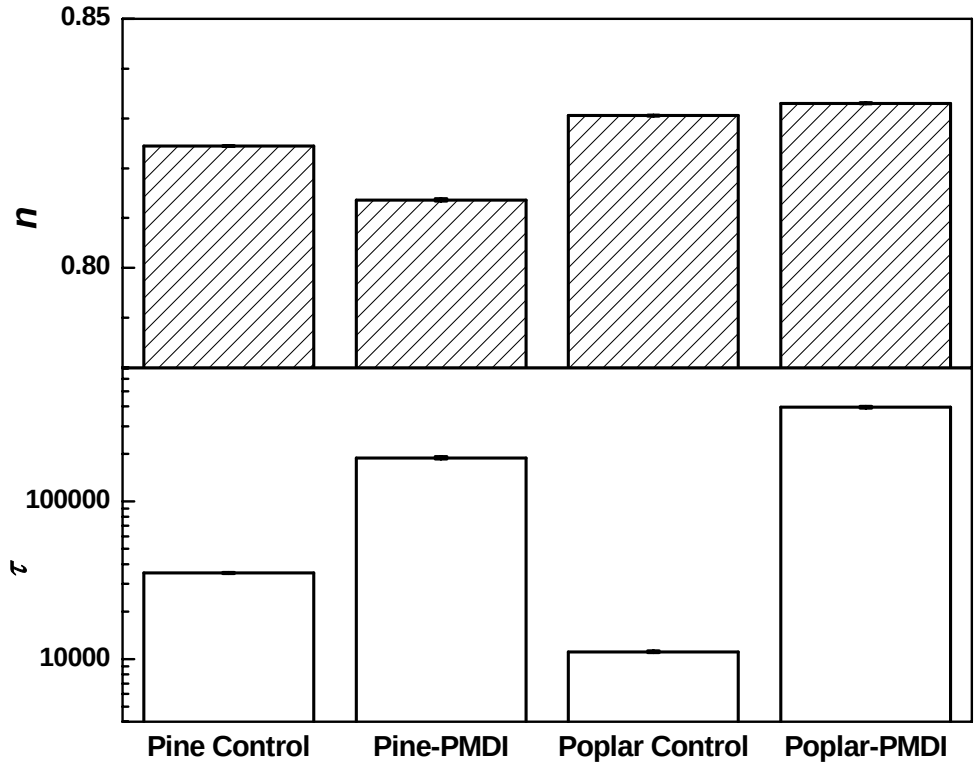

Figure 4.3.3.27. Comparison of the KWW coupling parameter and relaxation times of the EG plasticized transition in control and resin treated wood samples, using time/temperature superposition (5 replications each). Error bars represent ±1 standard deviation.

The coupling parameter and relaxation times for both woods were found to be similar. Resin impregnation had very slight effects on the coupling parameters of the mastercurves, but it increased the relaxation times for both woods significantly; the increase in relaxation times was relatively greater in poplar samples. The overall effect of the resin impregnation on the KWW relaxation parameters seems to be significant in pine, even though the numerical differences are small.

4.3.3.4. Comparison of Coupling Parameters obtained from different Creep experiments

Different creep experiments were performed in this study to probe the wood relaxations and wood/resin interactions under dry and ethylene glycol plasticized conditions; the relaxations probed in these experiments were significantly different from each other. The following table compares the coupling parameters obtained for control wood samples through different creep experiments.

Table 4.3.3.6. Comparison of control wood coupling parameters

Experiment type - Sample condition	Temperature (°C)	Coupling Parameter	
		Pine	Poplar
3 h creep - Dry	50	0.90 – 0.94	0.83 – 0.87
	90	0.82 – 0.89	0.78 – 0.83
	120	0.75 – 0.87	0.52 – 0.69
3 h creep - EG-plasticized	50	0.75 – 0.77	0.78
1000 sec creep-TTSP - EG-Plasticized	80 (T_{ref})	0.82 – 0.83	0.82 – 0.84

The dry creep experiments were performed at 50°, 90° and 120°C. The coupling parameters were similar at 50° and 90°C, while that at 120°C was significantly different. The differences in the coupling parameters observed at the different temperatures in dry wood samples may be attributed to the fact that different wood cell wall motional regimes are being probed at the various experimental temperatures.

The following table shows the coupling parameters of some common synthetic polymers.

Table 4.3.3.7. Coupling Parameters for some common synthetic polymers [11]

Polymer	Coupling Parameter
Polyisobutylene	0.45
Poly(methyl acrylate)	0.57
Polypropylene	0.65
Poly(vinyl chloride), PVC	0.76

The coupling parameter reflects the structural features (such as polarity, symmetry) of the polymer backbone. In general, polymers with regular and flexible repeat units exhibit low coupling constants, while those having a rigid backbone with polar and bulky pendent groups show a higher coupling constant [24]. The coupling parameters for dry wood were significantly higher than most common synthetic polymers (except PVC). The high degree of coupling observed in wood relative to the low cooperativity values of **neat, homogeneous** synthetic resins, may be attributed to the highly **complex, composite** structure of wood, where the cellulose microfibril bundles are embedded in a matrix of amorphous hemicelluloses and lignin.

The coupling parameters for dry wood samples were also found to be significantly different between the wood species tested; *n* for pine was significantly higher than the corresponding poplar samples, under similar conditions. These differences may be attributed to the variation of the supramolecular packing of polymers in the wood cell-wall.

The coupling parameters obtained from the 3h isothermal creep experiments on plasticized wood samples were lower (~0.7) relative to those obtained for dry samples at 90°C (~0.8). This decrease in coupling parameter may be attributed to the presence of the plasticizers; plasticizers increase the free volume, which in turn decrease the inter-chain interactions.

The in situ lignin relaxation was analyzed by performing isothermal creep experiments over the lignin T_g temperature range. Laborie *et al.* [10] also analyzed the in-situ lignin relaxations in ethylene glycol plasticized wood systems. In their study the wood plasticization was conducted at 120°C for 1 hr in ethylene glycol, which caused

some solvolysis (ethylene glycol bath became brown after treatment). But in this study the plasticization was conducted under much milder conditions (90°C for 1 hr), which left the wood structure relatively intact. Thus, our coupling parameters were much larger than those reported by Laborie *et al.* (0.19 ± 0.04 for poplar).

4.3.3.5. Conclusions

It is believed that this is the first demonstration of the applicability of the KWW relationship to the wood creep response, and that the Ngai cooperativity model can be used to interpret the effects of wood chemical treatments. The relaxation parameters were found to be dependent on the wood species which points to the differences in the supramolecular ordering of polymers in the cell wall between wood species.

The effect of resin impregnation on the in situ lignin relaxations were analyzed with ethylene glycol plasticized wood samples by two different creep experiments: long term isothermal creep and TTS principle. The long term creep results showed that the KWW parameters were essentially unaffected by the resin impregnation, while slight changes were observed with the mastercurves. These results suggest that the in situ lignin relaxation was only slightly changed in the presences of the resin.

A species-dependent resin effect was observed on the relaxations of wood polymers in the dry state; resin impregnation was found to increase the compliance of pine, while poplar became relatively stiffer under similar conditions. The effect of the resin was also found to be relatively larger in pine, where the inter-segmental cooperativity was found to decrease in the presence of the resin at higher temperatures. The changes in the coupling parameter at higher temperature suggest significant interaction of the resin with the amorphous polysaccharide components of wood.

References

(1) Findley, W. N.; Peterson, D. B. *Proceedings ASTM* **1958**, *58*, 841-861.
(2) Gressel, P. *Holz Roh-werks* **1984**, *42*, 293-301.
(3) Bond, B. H. In *Department of Wood Science and Forest Products*; Virginia Tech: Blacksburg, VA, 1993.
(4) Samarasinghe, S.; Loferski, J. R.; Holzer, S. M. *Wood and Fiber Science* **1994**, *26*, 122-130.
(5) Holzer, S. M.; Loferski, J. R.; Dillard, D. A. *Wood and Fiber Science* **1989**, *21*, 376-392.
(6) Gamalath, S. S. In *Department of Wood Science and Forest Products*; Virginia Tech: Blacksburg, VA, 1991.
(7) Olsson, A.-M.; Salmen, L. *Nordic Pulp and Paper Research Journal* **1997**, *12*, 140-144.
(8) Salmen, L.; Olsson, A.-M. *Journal of Pulp and Paper Science* **1998**, *24*, 99-103.
(9) Salmen, L. *Journal of Materials Science* **1984**, *19*, 3090-3096.
(10) Laborie, M.-P. G.; Salmen, L.; Frazier, C. E. *Holzforschung* **2004**, *58*, 129-133.
(11) Plazek, D. J.; Ngai, K. L. *Macromolecules* **1991**, *24*, 1222-1224.
(12) Strobl, G. *The Physics of Polymers*, 2nd ed.; Springer: Berlin, 1997.
(13) Kelley, S. S.; Rials, T. G.; Glasser, W. G. *Journal of Materials Science* **1987**, *22*, 617-624.
(14) Sugiyama, M.; Obataya, E.; Norimoto, M. *Journal of Materials Science* **1998**, *33*, 3505-3510.
(15) Olsson, A.-M.; Salmen, L. In *Cellulosics: Chemical, Biomedical and Material Aspects*; Kennedy, J. F.; Phillips, G. O.; Williams, P. A., Eds.; Ellis Horwood: New York pp 257-262.
(16) Olsson, A.-M.; Salmen, L. In *Viscoelasticity of Biomaterials*, ACS Symposium Series 489 ed.; Glasser, W. G.; Hatakeyama, H., Eds.; American Chemical Society: Washington D.C., 1992; pp 133-143.
(17) Bjorkman, A.; Salmen, L. *Cellulose Chemistry and Technology* **2000**, *37*, 7-20.
(18) Back, E. L.; Salmen, L. *TAPPI* **1982**, *65*, 107-110.
(19) Alves, N. M.; Ribelles, J. L. G.; Tejedor, J. A. G.; Mano, J. F. *Macromolecules* **2004**, *37*, 3735-3744.
(20) Ngai, K. L. *Journal of Physical Chemistry B* **1999**, *103*, 5895-5902.
(21) Ngai, K. L.; Plazeck, D. J. *Rubber Chemistry and Technology Rubb. Rev.* **1995**, *68*, 376-434.
(22) Ngai, K. L.; Rendell, R. W. *Journal of Non-Crystalline Solids* **1991**, *131-133*, 942-948.
(23) Ngai, K. L.; Roland, C. M. *Macromolecules* **1992**, *25*, 1844.
(24) Ngai, K. L.; Roland, C. M. *Macromolecules* **1993**, *26*, 6824-6830.
(25) Angell, C. A. *Journal of Research of the National Instutute of Standards and Technology* **2001**, *102*, 171.
(26) Angell, C. A. *Science* **1995**, *267*, 1925.

4.4. Thermogravimetric Analysis of Wood-PMDI Interactions

4.4.1. Introduction

This study was undertaken in order to analyze the utility of thermogravimetric analysis for probing the interactions between wood and PMDI resin. The interactions were probed by analyzing the effect of resin impregnation on the degradation patterns of wood; specifically how the wood thermograms are affected by the reaction products of PMDI resin and wood. PMDI resin can react with wood in several ways, but just two are considered significant; it can react with the wood hydroxyl groups to form urethane linkages, or it may react with the wood moisture to form polyurea-type structures.

Wood polysaccharides contain aliphatic hydroxyl groups, which may react with the resin to form corresponding alkyl urethanes. Wood also contains phenolic hydroxyl groups as components of the lignin structure and as low molecular weight phenolic extractives. These may react with the resin to form the corresponding aromatic urethanes. The thermal degradation of polyurethanes has been extensively studied, and perhaps because these materials are relatively unstable. The onset of urethane thermal degradation is known to occur in the following order [1]:

aryl-urethane-aryl (120°C) < aryl-urethane-alkyl (200°C) < alkyl-urethane-alkyl

Grassie and Zulfiqar [2] studied the thermal degradation of an aromatic polyurethane prepared from 1,4-butanediol and methylene bis(4-phenyl isocyanate). The degradation of this polyurethane was observed to start at ~240°C; the degradation was found to be a depolymerization-condensation process in which the two monomers were formed (isocyanate and alcohol) initially, which was followed by reaction of these monomers to form various volatile products such as tetrahydrofuran, dihydrofuran, carbon dioxide,

water, butadiene, hydrogen cyanide and carbon monoxide, along with residual carbodiimide and urea structures.

In this study, the thermal degradation of a model polyurea was studied and compared with the degradation patterns of wood cured with PMDI, in order to gain insight into wood-PMDI interactions.

4.4.2. Experimental

4.4.2.1. Materials

PMDI resin was obtained from Huntsman Polyurethane® (Rubinate 1840) and used as received.

Two different wood species were tested: yellow-poplar (*Liriodendren tulipifera*) & southern yellow pine *(Pinus spp*.). Flakes (5.1 cm × 5.1cm × 1.5cm; 2" × 2" × 0.6")) were sliced from the radial wood surface using a disk flaker. Flakes were dried at 105°C for 24 hours to determine dry weights and were equilibrated at ambient conditions to achieve 6-7% moisture content (MC).

4.4.2.2. Methods

4.4.2.2.1. Polyurea synthesis

PMDI resin was reacted with excess water (1:3) under vigorous stirring conditions. Polyurea was obtained in the form of white beads, which were dried in air at room temperature and thermally treated at 120°C for 2 h in air, before analysis.

4.4.2.2.2. Wood Acetylation

Wood flakes were vacuum impregnated with acetic anhydride (AA) (0.1 mm Hg for 30 minutes) in a glass reactor. The impregnated flakes were treated with AA at 110°C for 9 hours in the same reactor. The samples were then extracted with acetone in a

sohxlet to remove the reaction by-products (acetic acid) and unreacted AA. The samples were dried under vacuum (0.1 mm Hg for 24 hours). The weight gain from acetylation was ~18-19%. Samples were equilibrated to ~10% moisture content by storing them over a saturated solution of Potassium carbonate ($K_2CO_3.6H_2O$) [~40% relative humidity], until a constant weight was achieved

4.4.2.2.3. Resin impregnation

All samples were impregnated with acetone-PMDI solution (20% and 50%). Wood flakes were impregnated with the solution under pressure (10 psi for 15 minutes) in a pressure reactor. The excess resin was removed by vacuum (0.1 mm Hg for 15 minutes). The resin impregnated samples were then cured in an oven (120°C for 2h). The cured samples were stored under dry conditions (over phosphorous pentoxide, P_2O_5, in a dessicator) until tested.

Control samples were prepared which had the same treatment history as the resin impregnated samples. Wood flakes were pressure treated with acetone (10 psi for 15 minutes) in a pressure reactor, followed by vacuum treatment (0.1 mm Hg for 15 minutes). The samples were heat treated (120°C for 2 hours) and stored under dry conditions (over P_2O_5 in a dessicator) before analysis.

4.4.2.2.4. TGA experiment

All experiments were performed in a TA Instruments® Q500 TGA in the high resolution mode. Small wood disks were punched out of the wood flakes with a paper hole puncher. The sample weights ranged between 5-8 mg. Sample weight change was monitored in the temperature range of 25°-1000°C with a heating rate of 50°C/min in the

high resolution mode (resolution value =1; sensitivity value =4). All samples were analyzed in either air or nitrogen environments.

4.4.3. Results and Discussion

4.4.3.1. Thermal degradation of a model polyurea

PMDI resin was reacted with excess water to form the model polyurea, which may be significantly different from the polyurea structures formed by the reaction of the resin with wood moisture. Moisture exists in wood as water in the cell walls (bound water) and in the liquid state in the cell lumens (free water). At the fiber saturation point (FSP), the cell walls are completely saturated, and no water exists in the cell lumens i.e. all moisture exists in the bound state below the FPS.

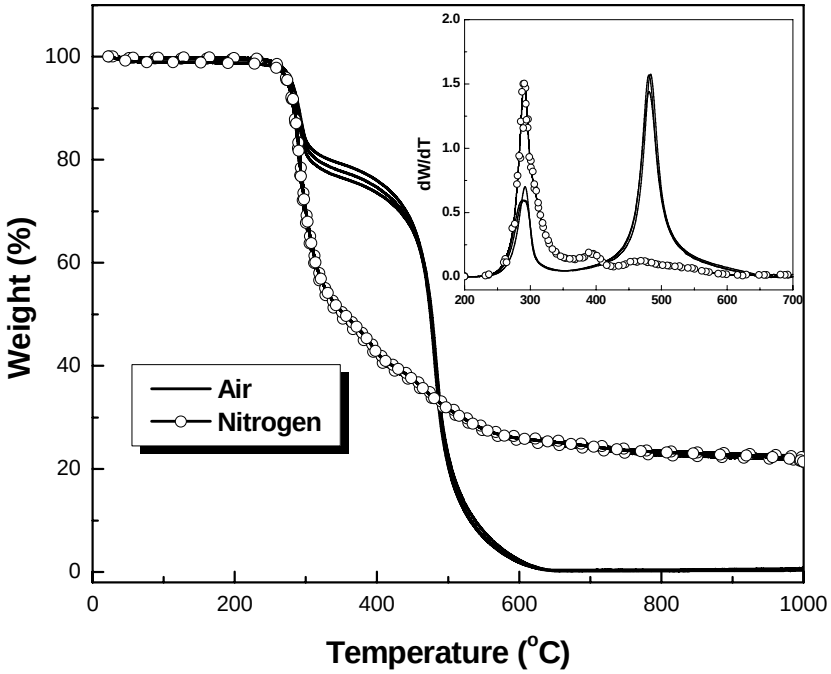

Figure 4.4.1. Weight loss and derivative weight loss (dW/dT, inset) profile of polyurea in air and nitrogen (3 replications).

The wood samples used in our study had 6-7% MC, and hence were all below the FSP. Thus, all the water available to the resin for reaction was bound water. This bound water

is relatively less accessible to the resin than the free water, used in the synthesis of the model polyurea. Thus, the model polyurea may be more crosslinked than the polyurea structures formed in the wood.

Figure 4.4.1 shows the thermal degradation pattern of polyurea in air and nitrogen. The thermal degradation of polyurea was found to be dependent on the degradation atmosphere. The initiation of major weight loss occurred at the same temperature (~220°C) for both atmospheres. Polyurea degradation is a two-step process in air. The first degradation step occurred in the temperature range of 220° - 320°C with a weight loss of 20%. Major weight loss occurred in the second stage (320° - 660°C) of the degradation process (80%).

In nitrogen atmosphere, major weight loss occurred in the temperature range of 220° - 360°C (50% weight loss). The weight losses in the temperature ranges of 360°-630°C and 630°-1000°C were 24% and 3.7% respectively. The char yield at the end of the experiment was ~22%. Thus, though the initial weight loss of polyurea (in both air and nitrogen) occurred at the same temperature, the weight loss was significantly higher in air, as expected.

4.4.3.2. Thermal degradation of control wood

Figure 4.4.2 shows the thermal degradation of control pine samples in air and nitrogen.

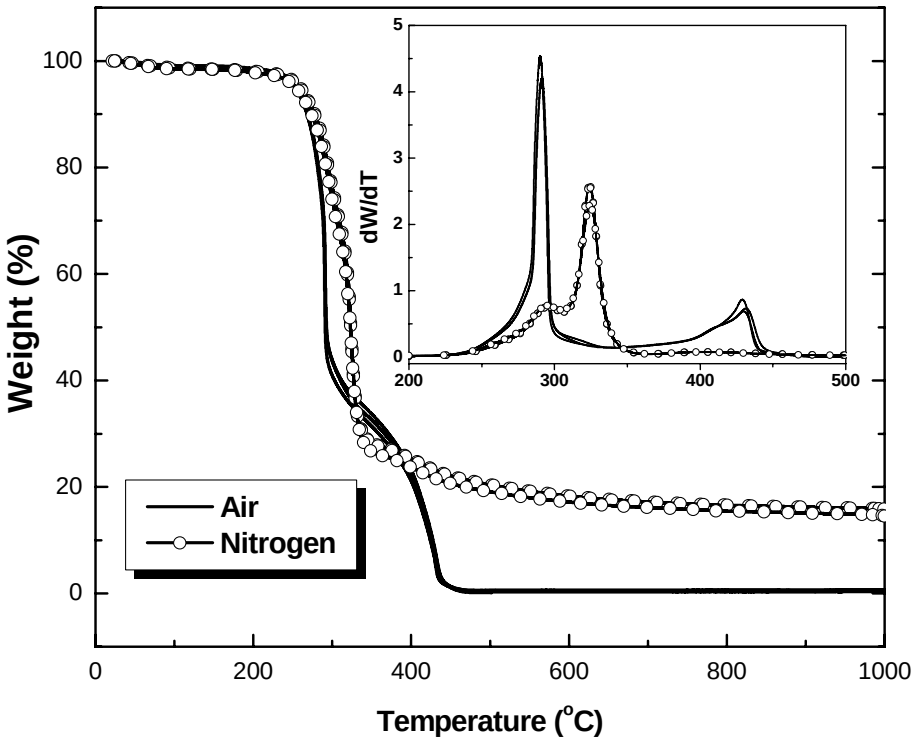

Figure 4.4.2. The weight loss and derivative weight change, dW/dT (inset) of control pine samples in air and nitrogen atmospheres (3 replications each).

In air, three different degradation zones were observed. In zone 1 (0° to 220°C) there was negligible change (2.4%) in weight. A significant weight loss (55.5%) was observed in zone 2 (220° to 306°C), which according to literature is attributed to the degradation of the holocellulose (cellulose and hemicellulose) components of wood [3]. The rest of the sample [high molecular weight (MW) lignin components] degraded completely in zone 3 (306° to 470°C).

The degradation pattern in nitrogen atmosphere also showed three different zones. The weight loss in zone 1 (0° - 220°C) was small (2.4%). The weight loss in zone 2 (220° - 365°C) was ~70.3%. Unlike, air degradation, two degradation steps were observed in zone 2. The first weight loss (25.4%) was due to degradation of the hemicellulose components (appeared as a shoulder on the main cellulose degradation peak in dW/dT).

The second weight loss (45.5%) in this zone was due to the degradation of the cellulose component. The holocellulose degradation occurred over a much broader temperature range in nitrogen (146°) relative to that observed in air (86°). The weight change in zone 3 (365° - 530°C) was ~7.8%. The weight of the sample did not show any significant change at higher temperatures (530° - 1000°C). The char yield at 1000°C was ~15.5%. Thus, separation between the different holocellulose components was achieved in nitrogen [4].

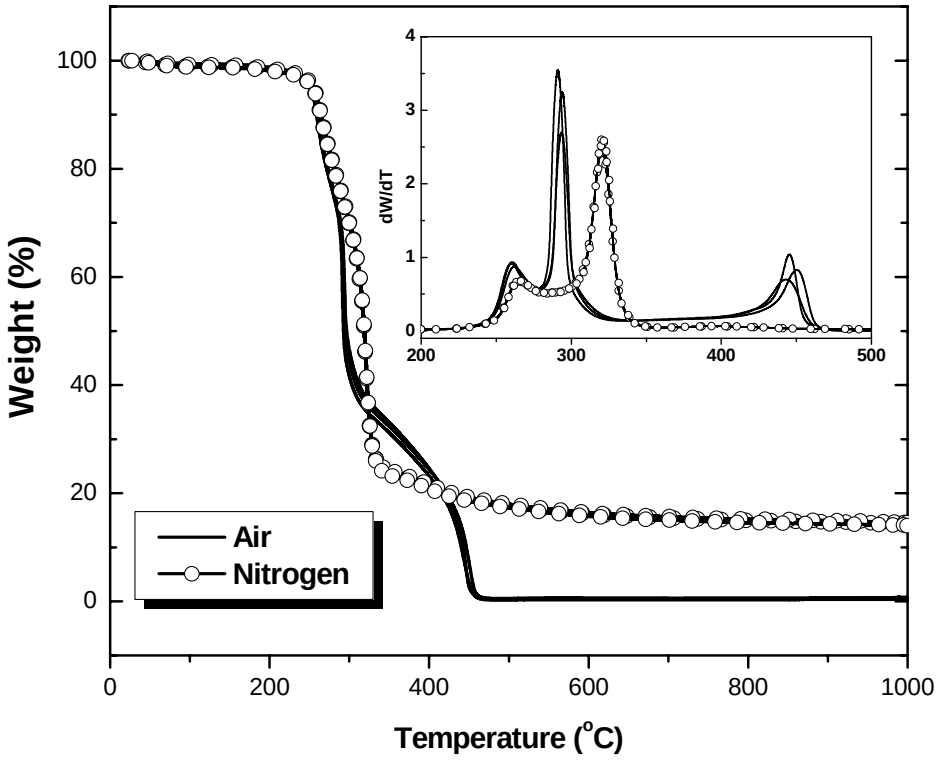

Figure 4.4.3. The weight loss and derivative weight change, dW/dT (inset) of control poplar samples in air and nitrogen atmospheres (3 replications each).

The TGA thermograms of poplar were found to be very similar to that of the pine samples with some characteristic differences (figure 4.4.3).

- Unlike pine samples, resolution of the hemicellulose and cellulose degradation was obtained in both atmospheres; but the resolution was better in nitrogen.

- The weight loss due to holocellulose degradation was found to be larger than that of pine in both atmospheres (64% vs. 55% in air & 74% vs. 68% in nitrogen).

4.4.3.3. Thermal degradation of PMDI-impregnated wood:

Samples were impregnated with PMDI-acetone solution with an open-cell method; resin impregnation under pressure followed by removal of excess resin with vacuum. The resin loading was varied by controlling the resin solution concentration (table 4.4.1).

Table 4.4.1. Effect of resin solution strength on the resin loading in wood samples

Samples*	Resin loading (%)	
	20% PMDI-acetone solution	50% PMDI-acetone solution
Pine	10.24 ± 0.9	40.48 ± 4.73
Poplar	12.51 ± 0.73	50.67 ± 2.88
Acetylated Pine	16.75 ± 2.11	-
Acetylated Poplar	12.05 ± 0.67	-

*3 replications each

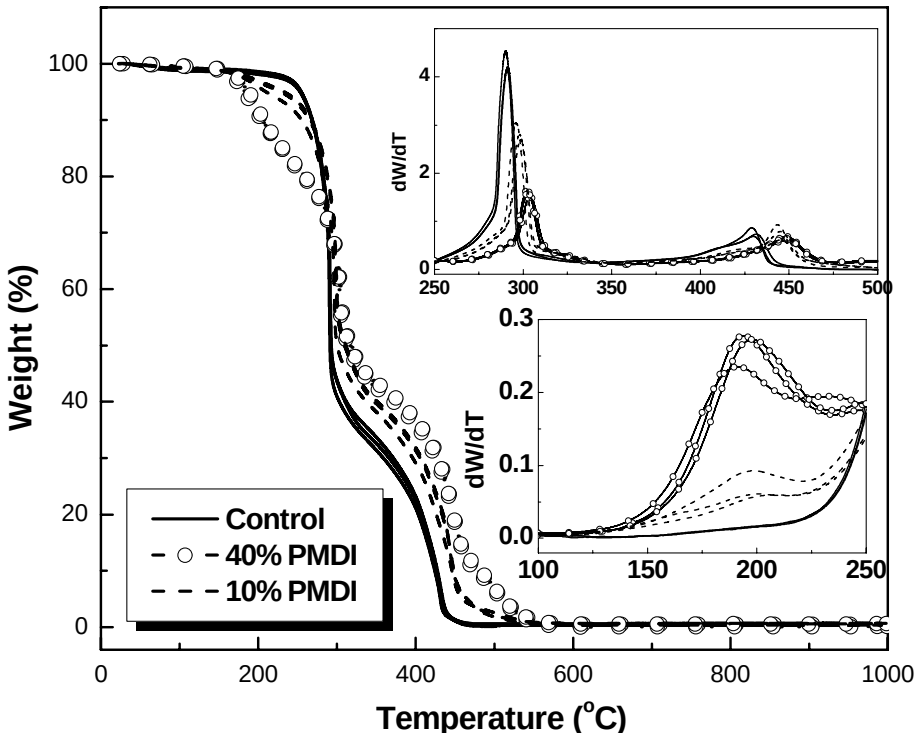

Figure 4.4.4. Comparison of the thermal degradation of control and PMDI-impregnated pine samples at two different resin loadings in air.

Figure 4.4.4 compares the thermal degradation of control pine with PMDI-impregnated pine samples in air at two different resin loadings (10 & 40% based on dry wood). Both resin impregnated samples showed an initial degradation in the temperature range of 125° - 225°C, which was absent in the control sample (dW/dT inset); sample weight loss in this temperature range was found to increase with increasing resin loading (5.9% for 10% resin and 18.1% for 40% resin).

The holocellulose degradation peak (in dW/dT) shifted to higher temperatures with resin loading; this shift was found to increase with resin loading. The lignin degradation peak also shifted to higher temperatures on resin loading (10% resin). But it did not change on further resin impregnation (40% resin).

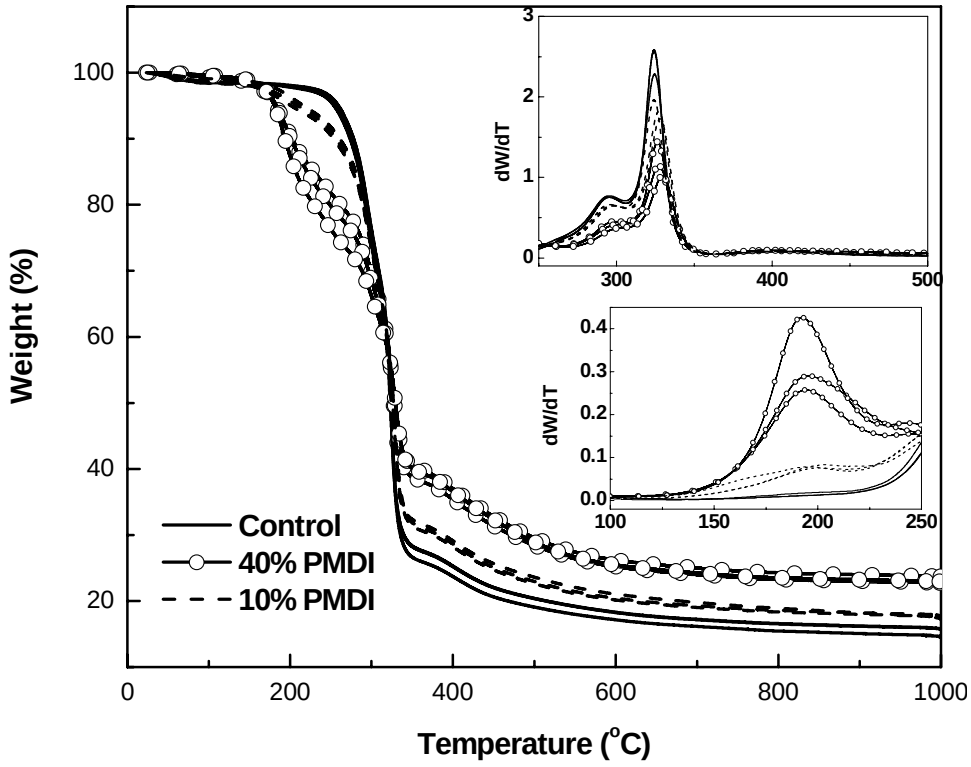

Figure 4.4.5. Comparison of the thermal degradation of control and PMDI-impregnated pine samples at two different resin loading in nitrogen.

Similar results were also obtained in nitrogen (figure 4.4.5). The low temperature weight loss (125° - 225°C) was also observed in nitrogen, which increased with resin

content (7.2% and 17.2% weight loss at 10% and 40% resin loading respectively). The thermal degradation of resin-impregnated pine samples in nitrogen showed the following characteristic differences.

- The position of both the hemicellulose and the cellulose degradation did not change in the presence of the resin.
- Significant char was obtained at the end of the experiment, which increased with the resin content (18% & 23.5% at 10% and 40% resin loading)

The TGA thermogram of resin impregnated poplar samples were very similar to the corresponding PINE samples (Appendix figures A.6.6.1 and A.6.6.2), with some characteristic differences. The initial degradation in the temperature range of 125°-250°C was also observed in YP resin impregnated samples in all atmospheres, which was found to increase with sample resin content (table 4.4.2).

Table 4.4.2. Effect of resin impregnation on the initial weight loss (%) of resin impregnated pine and poplar samples

Wood Species	Resin content (%)	Degradation Atmosphere	Weight loss (%)
Pine	10	Air	5.9
		Nitrogen	7.2
	40	Air	18.1
		Nitrogen	17.2
Poplar	12.5	Air	3.8
		Nitrogen	3.7
	50.7	Air	15.1
		Nitrogen	16

The table shows that even though resin content was higher in poplar samples, the weight loss observed in the temperature range of 125° - 250°C was higher in pine under similar conditions.

In nitrogen, the hemicellulose and cellulose degradations did not change significantly upon resin impregnation. The char yield at the end of the experiment was 21.6% for 12.5% resin content and 26.8% for 50.75% resin content, which was larger than that obtained for the corresponding pine samples.

The TGA thermogram of YP resin impregnated YP samples in air was significantly different from that of the corresponding pine samples. The holocellulose degradation for control YP samples had 2 peaks (hemicellulose and cellulose) similar to that of corresponding pine samples. But the impregnated YP samples showed a higher temperature peak (~320°C), that was absent in control samples. The lignin degradation also shifted to higher temperatures on resin impregnation.

Thus, the thermal degradation behavior of both wood species was affected by resin impregnation. A low temperature degradation was observed for both species on resin impregnation, which increased with resin loading and was unaffected by the degradation atmosphere. The weight loss due to this degradation was also found to be species dependent; it was larger in PINE than YP, under similar conditions (table 4.4.2). Polyurea, which is one of the main products in wood/PMDI cure, did not show any weight loss in this temperature range. Thus, the weight loss might be due to some species formed by the interaction between wood and resin (not polyurea).

4.4.3.4. Thermal degradation of acetylated control & resin-impregnated samples:

In order to investigate the nature of the wood-resin interactions, similar TGA studies were carried out with acetylated wood samples. Wood contains abundant hydroxyl groups which might potentially interact with the resin. Acetylation replaces the hydroxyl groups with acetyl groups that are inert to PMDI.

Wood was acetylated by treatment with acetic anhydride. Acetylation resulted in ~18% increase in wood weight (based on dry wood mass). Figures 4.4.6 and 4.4.7 illustrate the effect of acetylation on the thermal degradation of poplar samples in air and nitrogen.

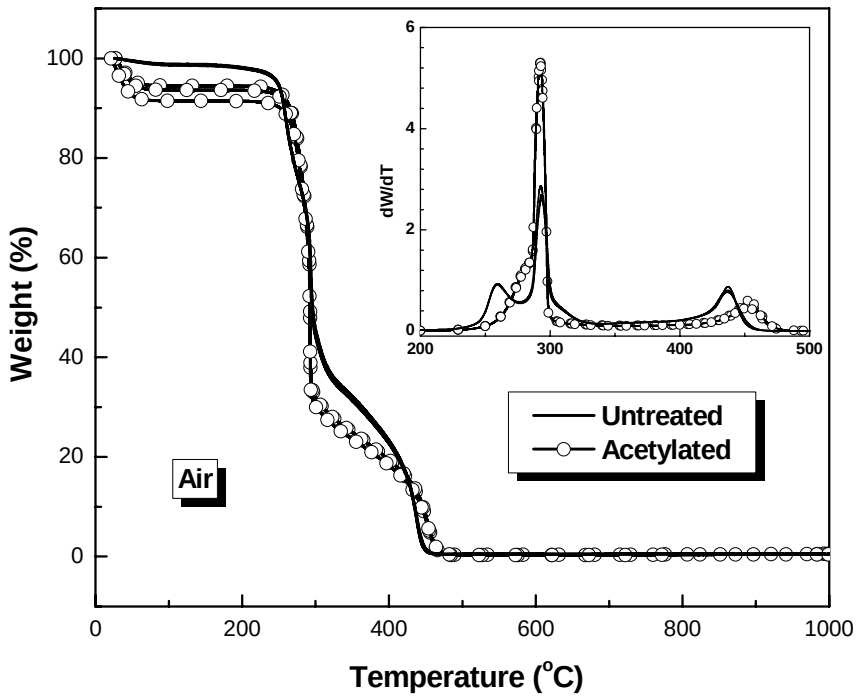

Figure 4.4.6. Effect of acetylation on the thermal degradation of poplar samples in air (3 replications each).

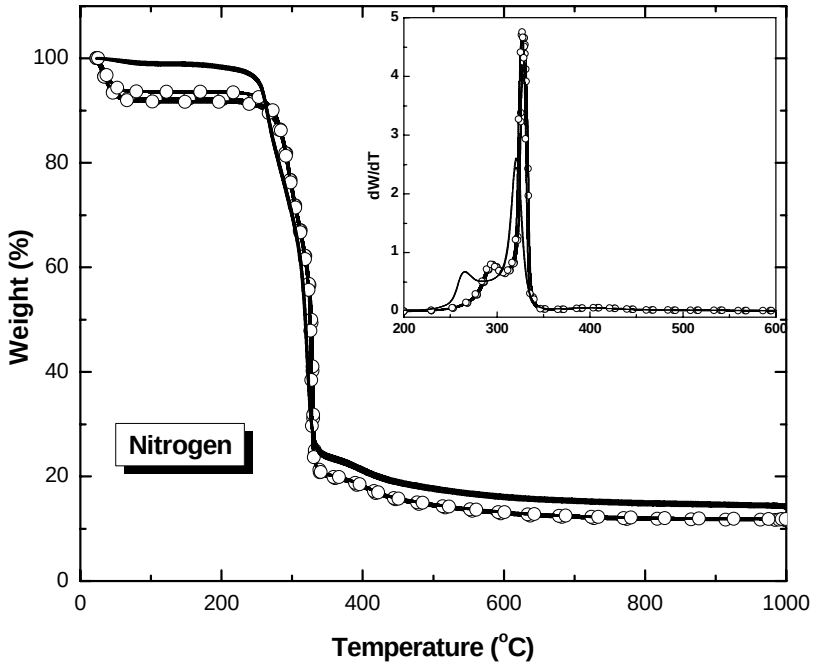

Figure 4.4.7. Effect of acetylation on the thermal degradation of poplar samples in nitrogen.

A low temperature weight loss (<100°C) was observed in acetylated samples in both air and nitrogen atmospheres, which was due to loss of moisture (acetylated samples were equilibrated to ~8% moisture content before analysis). The following characteristics differences were observed in the thermal degradation of poplar samples upon acetylation in both air and nitrogen atmospheres.

- The rate of holocellulose (cellulose and hemicellulose) degradation increased significantly (higher dW/dT peak).
- The resolution of the hemicellulose and cellulose degradations was found to decrease.

Acetylation was also found to shift the degradation of the lignin to higher temperatures (in air). The final char yield, obtained in nitrogen atmosphere, also decreased on acetylation (12.4% from 14.5% in untreated samples). Similar trends were also observed in the corresponding pine samples (Appendix figure A.6.6.3).

Acetylated samples were impregnated with resin-acetone solution (20%), resulting in a final resin content of 16.7% and 12% for pine and poplar (based on dry acetylated wood), respectively. Figure 4.4.8 shows the effect of resin on the thermograms of acetylated pine samples in air and nitrogen.

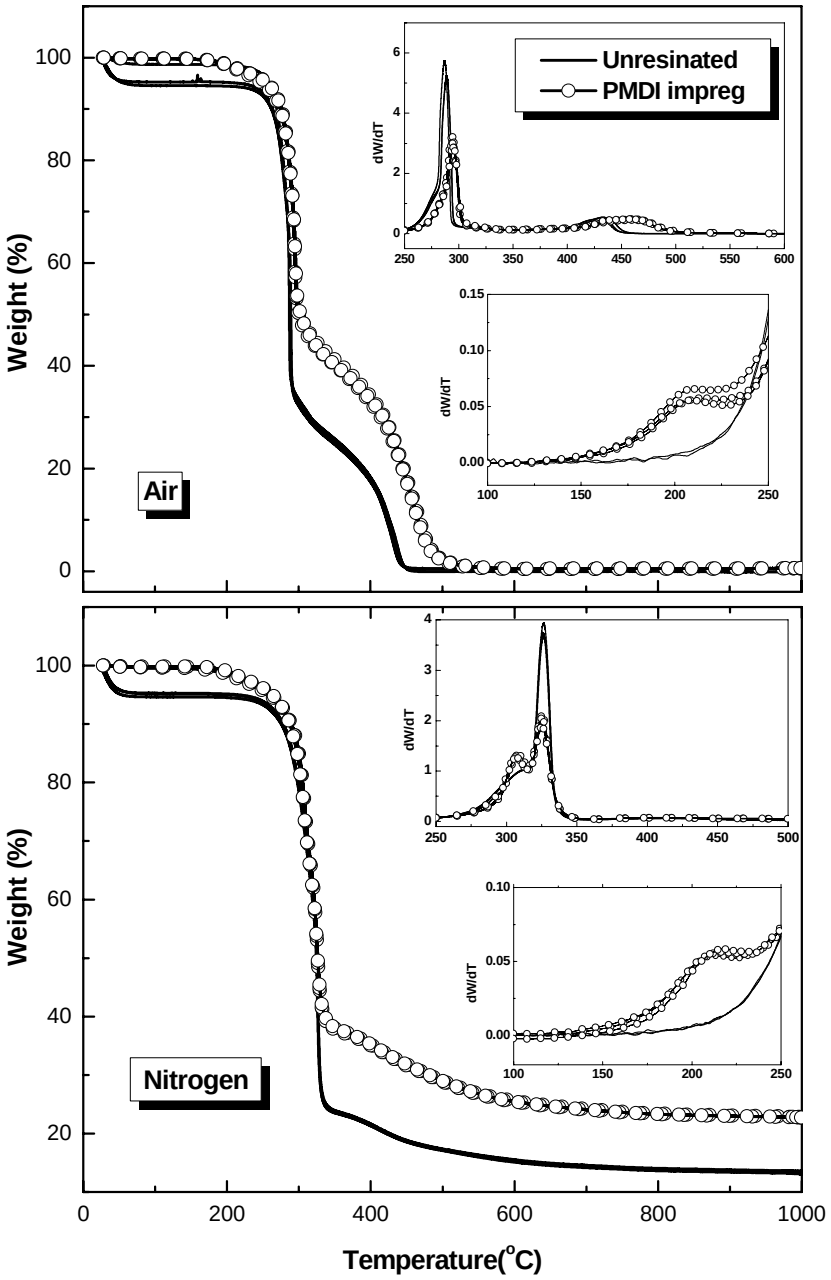

Figure 4.4.8. TGA thermograms of unresinated-acetylated and resin impregnated acetylated pine samples in air and nitrogen.

Acetylated samples showed a weight loss in the temperature range of 125° - 250°C. The unacetylated samples also showed similar low temperature (125° - 250°C) degradation in the presence of PMDI resin; it was found to increase with the resin content and was unaffected by the degradation atmosphere. But the weight change in this region was found to be much less (3%) in the acetylated resin impregnated samples relative to the corresponding unacetylated samples (5.9%), even though the resin loading was higher in the acetylated samples (10% compared to 16.75%).

The absence of the low temperature degradation in control samples suggest that it is due to some species formed by the reaction of the resin with wood. PMDI resin may react with wood in two ways; it may react with the wood moisture to from polyurea-type structures or react with the wood hydroxyl groups to form urethane linkages. Analysis of a model polyurea showed that its degradation starts at a much higher temperature (~220°C). Thus, the low temperature degradation may be due to urethane-type structures; wood may react with resin to form aromatic urethane linkages (with phenolic hydroxyl groups) which are known to degrade in this temperature range (~120°C) [1]. But the low temperature degradation was also observed in the acetylated samples, where the hydroxyl groups are substituted by inert acetyl groups. This suggested that not all the hydroxyl groups in wood are substituted upon acetylation. In order to study the chemical species present in wood flakes before and after acetylation, the samples were analyzed by infra-red (IR) spectroscopy.

The IR spectra of unmodified wood flake samples show a broad peak centered at 3340 cm^{-1}, which is attributed to the hydrogen-bonded wood hydroxyl groups (figure 4.4.9).

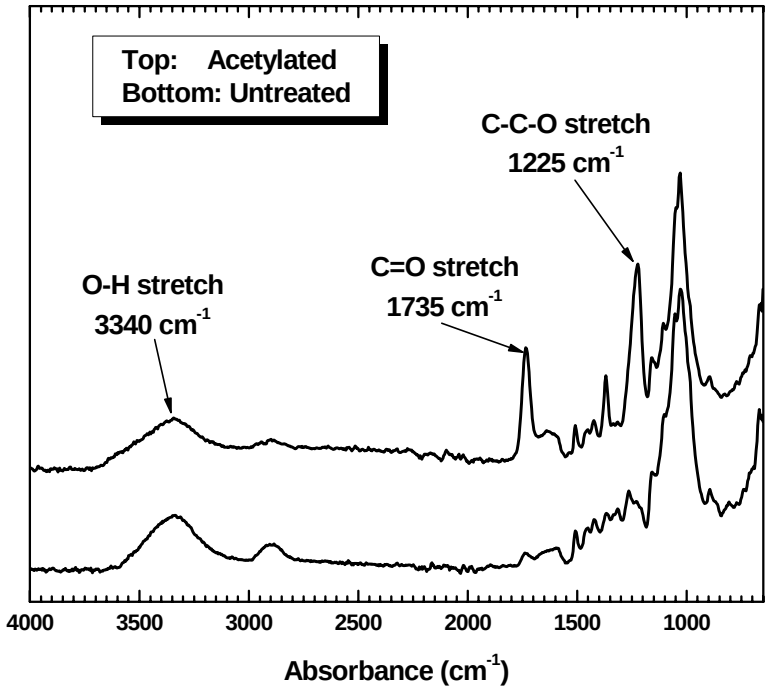

Figure 4.4.9. Comparison of the IR spectra of untreated (control) and acetylated pine wood flake.

A similar hydroxyl absorbance was also observed in acetylated samples, though it was relatively broader and of lesser intensity. Thus, significant hydroxyl groups were present in wood samples, even after acetylation. This led us to believe that the weight loss observed in the temperature range of 125° - 250°C, was probably due to degradation of urethanes, formed by the reaction of the resin with the wood hydroxyl groups. In acetylated samples, the amount of hydroxyl groups are drastically reduced, which led to the formation of smaller amounts of urethane linkages and consequently, a relatively smaller weight loss was observed in this temperature range for acetylated samples. Similar results were also observed for resin impregnated acetylated yellow-poplar samples (Figure A.6.6.4 and A.6.6.5). The weight loss in the low temperature range for these samples were 2.3% (compared to 3.8% in unacetylated samples with same resin loading).

The thermogram of impregnated samples in air also showed an increase in the thermal stability of the wood components compared to unresinated samples. The holocellulose degradation shifted slightly to higher temperatures. The lignin degradation broadened and shifted to higher temperatures (from 430° to 460°C). In nitrogen atmosphere, the separation of the hemicellulose and cellulose degradations became more pronounced after resin impregnation.

For YP samples, the holocellulose degradation showed the characteristic 3 peaks similar to that observed in the corresponding unacetylated samples. The weight loss in the lignin degradation region was significantly higher in the impregnated samples (18.85% to 37.8% after resin impregnation).

The char yield also increased significantly after resin impregnation (from 13% to 23% for PINE and from 12% to 23% for YP, after resin impregnation).

4.4.4. Conclusions:

The following conclusions could be drawn from the TGA analysis of wood impregnated with PMDI resin.

- Separation of holocellulose & lignin degradations could be achieved in air for both wood species analyzed.
- Separation of holocellulose degradations was observed in YP in both atmospheres. But the separation was more pronounced in nitrogen. Pine showed this separation in nitrogen only.
- Low temperature degradation was observed in resin-impregnated wood samples exclusively. This degradation was observed in both atmospheres and was found to increase with the resin loading. This weight loss was attributed to the degradation

of urethane linkages formed by the reaction of the resin with wood hydroxyl groups. Significant reduction in urethane degradation was also observed upon acetylation of wood.

References

(1) Wicks, Z. W. *Progress in Organic Coatings* **1975**, *3*, 73.
(2) Grassie, N.; Zulfiqar, M. *Journal of Polymer Science: Polymer Chemistry edition* **1978**, *16*, 1563-1574.
(3) Chauvette, G.; Heitz, M.; Rubio, M.; Khorami, J.; Chornet, E.; Menard, H. *Thermochemica Acta* **1985**, *84*, 1-5.
(4) Gronli, M. G.; Varhegyi, G.; Blasi, C. D. *Industrial and Engineering Chemistry Research* **2002**, *41*, 4201-4208.

5. Conclusions

In this is study the species-dependent performance of PMDI resin was probed by different characterization techniques. The following table summarizes some of the significant conclusions that were drawn from each technique.

Table C1. Summary of the major conclusions from different characterization techniques used in this study.

Characterization techniques	Major findings
Solid state NMR	• Small but significant species effect on cure chemistry at low cure temperatures. • Heterogeneous bond morphology at low cure temperatures. • Small but significant species effect on bond morphology at low cure temperatures. • Species effects disappeared at higher cure temperatures. • Homogeneous bond morphology at higher cure temperatures
DSC	• E_{act} was larger in pine. • Z was significantly larger (2 decades) in pine. • PMDI cure was found to be relatively faster in pine.
DMA: Single Cantilever bending: Dynamic scans: Dry wood	**Evidence of minor wood-PMDI interactions:** • Slight decrease in intensity of low temperature (-105°C) tan δ relaxation. • Higher temperature secondary relaxations were found to shift and show increase in intensity with the sample resin content.
DMA: Single Cantilever bending: Dynamic scans: Plasticized wood	• Slight changes in the in situ lignin relaxation in the presence of the resin in both woods; effect relatively larger in pine. • Resin-wood interaction disappeared upon acetylation.
DMA: Submersion tension: TTSP: Plasticized wood	*In the presence of resin:* • tan δ mastercurves shift to lower frequencies in both woods; the change was relatively larger in pine. • tan δ mastercurves became broader both woods; this

	change was larger in poplar. • The intensities of the poplar tan δ mastercurves were found to decrease significantly. • Slight changes in shift-factor plot; lignin relaxation broadened; effect larger in poplar. • Slight changes in E_{act}, C_1 & C_2.
Creep: Single Cantilever bending: Dry wood	*In the presence of resin:* • Pine was found to become more compliant. • Poplar became stiffer. • At 50°C: *n* did not change, τ increased; the latter was larger in poplar. • At 90°C: *n* decreased, τ unchanged; the former was larger in pine. • At 120°C: τ unchanged; *n* decreased significantly in pine.
Creep: Single Cantilever bending: Plasticized wood	<u>3 hr isothermal creep:</u> • Control pine deformed more than corresponding poplar. *In the presence of resin:* • Pine more compliant, while poplar stiffer; but changes statistically insignificant. • Changes in KWW parameters insignificant <u>TTSP:</u> • Significant species dependence of shift-factors; poplar lignin relaxation broader than pine. *In the presence of resin:* • Creep mastercurves covered shorter time period. • Slight changes in shift-factors. • Slight changes in E_{act}, C_1 & C_2; effect larger in pine. • Slight changes in KWW parameters; effect larger in pine

TGA	• Low temperature degradation in wood samples in the presence of resin. • The weight loss due to this degradation was found to increase with the sample resin content and it decreased significantly in acetylated wood. • The weight loss at this temperature range was found to be significantly larger in resin impregnated pine samples, even though the resin content of the latter were lesser than the corresponding poplar samples.

Solid state NMR studies were conducted to analyze the cure chemistry of the wood-PMDI bondline. In this study, the relative concentrations and $T^{H}_{1\rho}$ values for the different chemical species (i.e. urethane, urea and biuret) were obtained by fitting the decomposed area (from the central 101 peak in ^{15}N spectrum) into equation 4.1.1. But subsequent studies with acetylated samples showed that the spectral decomposition led to overestimation of the urethane concentration. Thus, the results obtained for both the concentration and relaxation times present a crude picture of the above mentioned parameters for the different chemical species analyzed in this study. Nevertheless, results showed a small but significant species effect on the relative concentration and bond morphology at lower cure temperatures (upto 120°C); but this effect disappeared at higher cure temperatures. This species effect observed at low cure temperatures may be a contributing factor, but the absolute value of this effect is perhaps too small to play a major role in the species-dependent performance of the PMDI resin.

DSC analysis was conducted to probe the cure kinetics of PMDI resin in the presence of wood. Results showed that the cure of PMDI resin was significantly faster in pine wood. Thus, the wood-resin interactions which catalytically activated the resin cure were larger in pine.

Thermogravimetric analysis of resin impregnated wood flakes showed the presence of a low temperature weight loss, which might be attributed to the degradation of urethane linkages. Results showed that this weight loss was significantly larger in pine, even though its resin content was lower than the corresponding poplar samples. A higher concentration of urethane linkages in the wood-PMDI bondline should result in minor changes in the bond performance but higher bond durability.

Dynamic and static mechanical analysis was found to be an important and versatile characterization tool for probing the wood-resin interactions. In this study, these tools were successfully used to analyze the effects of resin impregnation on the various in situ amorphous wood polymers. Dynamic thermal scans of dry samples showed the various secondary wood relaxations changed slightly in the presence of the resin. But since the precise origin of these secondary relaxations was not known, the species dependences could not be ascertained. This problem was alleviated by the use of ethylene-glycol plasticized wood samples, whose dynamic thermal scans revealed the softening of the in situ lignin polymers in wood. In the presence of the resin, the lignin relaxation was found to broaden and shift slightly to higher temperatures, for both woods tested; but the change was relatively larger for the poplar samples. In order to obtain a quantitative idea of the lignin-resin interactions, the relaxation was analyzed with the TTS principle in the submersion mode. Storage, loss and tan δ mastercurves were generated for each system by horizontal shifting of the isothermal frequency sweep data. The mastercurves presented better insight on the resin-lignin interactions relative to the dynamic scans. The mastercurves revealed features that were unavailable in the dynamic scans:

- The maxima of the poplar tan δ mastercurves were at a lower frequency than the corresponding pine samples.
- The poplar tan δ mastercurves were found to broaden significantly (than pine) and their intensities decreased upon resin impregnation.

Analysis of the Arrhenius and WLF parameters suggested **minor** changes in the lignin relaxation in the presence of the resin.

The use of dynamic mechanical analysis for analyzing the lignin relaxation was complicated by the evaporation of plasticizer in the course of the experiment. This problem may be solved by performing the experiment in the submersion mode, where the sample is submerged in the plasticizer throughout the experiment. But dynamic scans could not be performed in the submersion mode and TTSP analysis was cumbersome and time consuming (each TTS experiment takes ~ 6 hr). All these problems were solved by performing static (creep) experiments with plasticized wood samples. Plasticization along with the low frequency deformations led to further lowering of the lignin transition. This made it possible to conduct the experiment in lower temperature ranges which in turn reduced significant plasticizer loss during the experiment. Moreover, the creep curves could be directly fitted to the KWW equation, for a more thorough analysis of the relaxation through the coupling parameter (n) and relaxation time (τ).

The in situ lignin transition was analyzed by TTSP in the creep mode. The following table compares the Arrhenius and WLF parameters obtained for the lignin transitions through TTSP in dynamic and static modes.

Table C2. Comparison of Arrhenius and WLF parameters of lignin relaxation obtained by TTSP in dynamic and static modes.

Sample	E_{act} (kJ/mol)		C_1		C_2	
	Dynamic	Static	Dynamic	Static	Dynamic	Static
Pine Control	228.3 ± 1.6	188.5 ± 1.6	17.8 ± 1.2	5.2 ± 1.3	168.6 ± 13.7	77.9 ± 16.8
Pine PMDI	232.5 ± 1.3	174.1 ± 2.5	24.0 ± 2.6	6.38 ± 4.6	207.9 ± 22.7	114.1 ± 74.4
Poplar Control	232.5 ± 2.1	208.1 ± 3.0	15.6 ± 0.8	15.2 ± 4.0	134.2 ± 9.1	148.6 ± 36.8
Poplar PMDI	247.8 ± 1.6	199.5 ± 2.7	18.3 ± 0.8	16.0 ± 0.8	144.5 ± 7.5	178.9 ± 64.2

The activation energies obtained by the dynamic mode were found to be significantly larger than those obtained from the static mode TTSP, for both woods. The WLF parameters obtained from the different TTSP modes, were found to be similar in poplar, but were significantly different in pine. The dynamic TTSP results showed that E_{act} increased in the presence of the resin, while the opposite effect was observed from the static results; but in both cases, the change was small. Both dynamic and static results showed that the WLF parameters increased slightly upon resin impregnation. Thus, from all these results, it was concluded that the ***in situ lignin relaxation changed slightly in the presence of the resin***.

Creep experiments were also conducted on the dry wood samples at different temperatures, which gave us the opportunity to probe the secondary and amorphous polysaccharide relaxations. A thorough analysis of these relaxations was achieved by direct fitting of the creep compliance curves to the KWW equation. This is the ***first demonstration of the applicability of the KWW relationship to the wood creep response***. The KWW parameters were found to decrease with temperature; the change was relatively small at lower temperatures (up to 90°C), but a drastic decrease in both

parameters were observed at 120°C. The large differences in relaxation time and coupling parameters between the lower temperatures (50° and 90°C) and 120°C indicate that different wood cell wall motional regimes are being probed at the various experimental temperatures. The relaxation parameters (*n* and τ) for control pine samples were observed to be larger than the corresponding poplar samples at all temperatures; but the differences were significantly larger at high temperatures (120°C). This wood species effect on the KWW parameters reflect fundamental differences (and similarities) in the packing and supramolecular ordering of hardwoods versus softwoods.

Creep results showed significant changes in the relaxation parameters even at very low resin impregnation (3%). The changes were found to be minor at low temperatures (up to 90°C). But a significant species dependent resin effect was observed at 120°C; pine showed a significant decrease in *n* (from 0.65 to 0.58) without changes in τ, while no changes in *n* or τ was observed for poplar. Thus the results suggest that the resin interacted with the pine polysaccharides in a fashion that resulted in a significant decrease in the inter-segmental interactions. Analysis of ***plasticized*** samples (by dynamic scans, submersion TTSP, 3 hr isothermal creep and creep TTSP tests) showed resin had a ***minor*** effect on the wood relaxations for ***both woods***. In the plasticized state, the polysaccharide transitions are known to shift to sub-ambient temperatures and the relaxation response is exclusively due to the in situ lignin polymers. But in ***dry*** state, the effect observed was ***significant*** and was found to occur ***exclusively in pine***. Dynamic thermal scans of dry samples also showed the inception of a major transition at 120°C. This prompted us to hypothesize that the changes observed might be due to the ***in situ amorphous polysaccharide*** components in wood.

Thus, our study showed that PMDI resin interacts with both wood species and these resin-wood interactions might be occurring through the wood hydroxyl groups. But it was hard to conclude, which wood showed a relatively larger resin effect. This was because while some results suggested a larger resin effect in pine e.g.

- faster PMDI cure from DSC,
- larger amount of urethane linkages from TGA,
- larger shift in lignin T_g from both dynamic thermal scans (temperature shift) and mastercurves (frequency shift),
- relatively larger changes in WLF parameters as obtained from dynamic TTSP].

Other results suggest the reverse (i.e. resin effect was more in poplar):

- larger urethane concentrations at lower cure temperatures from SSNMR,
- larger broadening of poplar tan δ,
- significantly larger decrease in poplar tan δ mastercurve intensity,
- larger changes in shift factors and larger increase in E_{act} obtained from dynamic TTSP].

Hence, both woods showed preferential resin effects, depending upon the tool used to probe the wood-resin interaction. The resin had slight effects on the in situ lignin relaxation, but a relatively larger resin effect was observed on the amorphous polysaccharide wood components.

The major outcome of this study was the demonstration of the various, novel characterization tools for probing the supramolecular packing in wood and analyze wood-adhesive interactions.

- Thermogravimetric analysis was successfully used for the first time to analyze the wood-resin interactions. The efficacy of this tool could be improved by coupling TGA with other characterization techniques like Fourier-transfer infra-red spectroscopy or mass-spectroscopy.
- First demonstration of the applicability of the KWW relationship to the wood creep response and that the Ngai cooperativity model can be used to interpret the effects of wood chemical treatments.
- Utility of static creep experiments for studying the packing and relaxations of wood polymers.
- First successful probing of the in situ amorphous polysaccharides of wood by conventional dynamic and static mechanical analysis.
- First successful use of DMA in the submersion tension mode to generate storage, loss and tan δ mastercurves for the study of in situ lignin relaxations.

A.6.1. Synthesis and Characterization of doubly labeled PMDI Resin

A.6.1.1. Experimental

A.6.1.1.1. Materials

A.6.1.1.1.1. Polyamine Synthesis and Phosgenation

^{13}C-Carbon monoxide (99% ^{13}C) and ^{15}N-aniline (98% ^{15}N) were purchased from Cambridge Isotopes Laboratories and used as received. Paraformaldehyde, aniline, hydrochloric acid (6N), aqueous sodium hydroxide (10N) solution, anhydrous 1,2-dichlorobenzene, acetone, 1-phenyl-1-cyclohexene (95%) and gaseous chlorine were purchased from Aldrich Chemical Company and used as received. Chloroform (HPLC grade, 99.9%) was purchased from Aldrich Chemical Company and was dried over molecular sieves for 24 hrs. before use.

A.6.1.1.1.2. Phosgene Titration

Acetone (HPLC grade, 99.9%) was purchased from Aldrich Chemical Company and was dried over molecular sieves before use. Sodium Iodide (NaI, 99.5%) was purchased from Aldrich Chemical Company and stored under nitrogen when not in use. Sodium thiosulfate pentahydrate ($Na_2S_2O_3.5H_2O$, 99.5%) was purchased from Aldrich Chemical Company and used as received.

A.6.1.1.1.3. PMDI Characterization

Toluene (HPLC grade, 99.9%), anhydrous 1,3,5-trichlorobenzene (99%), tetrahydrofuran (THF, HPLC grade, 99.9%), *d*-chloroform ($CDCl_3$, 99.8%), tetramethylsilane (TMS, 99.9%), diethylamine (99.5%), and dibutylamine (99.5%) were purchased from Aldrich Chemical Company and used as received. Methanol (99.9%) was

purchased from Allied Signal and dried over molecular sieves for 24 hours before use. Commercial PMDI (Rubinate 1840) was received from Huntsman Polyurethanes and was used to compare the purity of synthesized PMDI resin.

A.6.1.1.2. Methods

A.6.1.1.2.1. Synthesis of Doubly labeled PMDI (^{15}N, ^{13}C)

The synthesis of the doubly labeled PMDI consisted of three steps [1]: synthesis of labeled polyamine (^{15}N), synthesis of labeled phosgene (^{13}C) and phosgenation of polyamine.

A.6.1.1.2.1.1. Synthesis of Labeled Polyamine (^{15}N)

The labeled polyamine was synthesized through the acid catalyzed condensation of formaldehyde and labeled aniline (^{15}N). The molar ratio of aniline to formaldehyde and aniline to HCl were 4:1 and 1:1.5 respectively. Hydrochloric acid (6N, 39.6 ml) was added to a 100 ml 3-necked flask which was placed in cold-water-bath. Labeled aniline (14.4 ml) was added to the flask slowly with a syringe. The solution was stirred vigorously. Paraformaldehyde (1.25 g) was added to the flask. The flask was removed from the cold-bath and placed in a hot oil bath (120°C). The solution was refluxed at 105°-120°C for 8 hrs. The solution was then removed from the hot bath and purified.

Before purification, the reaction mixture was neutralized by adding 10N sodium hydroxide. Then the organic layer was extracted with chloroform (3×25 ml) followed by washing with distilled water (3×25 ml) in a 250 ml separation funnel. After purification the chloroform was removed by rotational evaporation followed by vacuum distillation (0.2 mm Hg, 50°C). Residual aniline was removed by increasing the distillation

temperature to 90°C. ^{15}N-polyamine was a dark brown viscous liquid which was stored at room temperature before use.

A.6.1.1.2.1.2. Synthesis of Labeled Phosgene (^{13}C)

The labeled phosgene was synthesized using the procedure of Masaki *et al.* [2]. Unlike Masaki's procedure, no catalysts were used for the synthesis, since they didn't increase the yield significantly. 1,2-dichlorobenzene (ODCB, 75 ml) was transferred into a sealed, dry 100 ml graduated cylinder through a canula. Chlorine gas (3.54g) was bubbled into the ODCB solution until the desired amount was obtained. The Cl_2/ODCB solution was transferred to a 200 ml flask fitted with two stopcock valves. One opening was sealed with a rubber septum, while the other was connected to the reactor vessel through a chemical resistant Tygon® tubing. The reactor was a 5-necked 1L glass reactor vessel (1 L Ace Glass medium-pressure glass reactor), which was initially evacuated to a pressure of 0.5 mm Hg and then filled with ^{13}C-carbon monoxide. The Cl_2/ODCB solution was then transferred to the reactor by the application of compressed nitrogen. The reactor was sealed off and the reaction was allowed to proceed at 55°C for 36-48 hrs under vigorous agitation. The reactor was then cooled to the room temperature and excess chlorine was removed by the addition of 0.5 ml of 1-phenyl-1-cyclohexene.

Phosgene was purified by transferring it to a cold trap (immersed in liquid nitrogen) by intermittent application of vacuum on the cold trap. White particles of phosgene formed in the cold trap. ODCB (100 ml) was transferred into the cold trap through a canula. The phosgene/ODCB solution was then allowed to warm to the room temperature.

The phosgene yield was determined by iodometric titration. Phosgene/ODCB (3.5 ml) solution was transferred into a sealed Erlenmeyer flask (50 ml) through a canula. The solution was allowed to react with NaI/acetone solution (0.6N, 8ml). The liberated iodine was titrated to a colorless endpoint with an aqueous solution of $Na_2S_2O_3.5H_2O$ (0.15M). The phosgene left in the trap was used for the subsequent polyamine phosgenation.

A.6.1.1.2.1.3. Phosgenation of Polyamine

^{15}N-polyamine was vacuum-dried (60°C, 0.6 mm Hg) for two hrs in a 50 ml double-neck flask. ODCB (25ml) was transferred into the flask through a canula. A dark brown polyamine/ODCB solution was obtained.

Phosgene/ODCB solution was transferred into an evacuated 5-neck glass reaction kettle (0.5 mm Hg) submerged in an ice water bath. The polyamine/ODCB solution was then transferred into the reactor through a canula, while maintaining vigorous agitation. The reaction mixture was slowly heated to 180°C in an oil bath and maintained at that temperature for 20 minutes. It was then slowly cooled to the room temperature. The mixture was filtered into a 250 ml round-bottomed flask using a Buchner glass filter (Ace Glass) under a nitrogen blanket. ODCB was removed by performing vacuum distillation (0.3 mm Hg, 60°C). A heat treatment was then performed on the resin by immersing the flask into a 200°C oil bath for 5 minutes under nitrogen flow to break MDI dimmers and remove chlorine-containing impurities. Immediately after the heat-treatment, the flask was quench cooled by spraying acetone on the flask followed by submersion in cold water bath. The doubly labeled PMDI resin was stored in a dessicator in the presence of anhydrous sodium sulfate drying agent.

Two batches of doubly labeled PMDI resins were synthesized over a period of two years represented as PMDI-I and PMDI-II.

A.6.1.1.2.2. PMDI characterization

The resin isocyanate content was determined following a 1 in 10 scale version of ASTM D 5155-91 test method C. The resin (0.078 g) was reacted with dibutylamine/toluene solution (2M, 2 ml) in the presence of 1,3,5-trichlorobenzene (2.5 ml) and dry methanol (25 ml). The solution was then titrated to pH=4 using standard HCl solution (0.1N).

PMDI molecular weight was determined using Gel Permeation Chromatography (GPC) having a differential refractometer (Waters Model 410) and a differential viscometer (Viscotek Model 100) in THF. Waters Ultrasyragel separation column with pore diameters of 10^3, 10^2 and 10A was used. Narrow molecular weight distribution polystyrene was used to perform a universal calibration of the GPC. The resin (0.05 g) was converted to it's corresponding urea derivative by reaction with excess diethylamine (1 ml) in dry chloroform for 30 minutes. The residual diethylamine and chloroform was removed by rotational evaporation. The molecular weight of the urea derivative was determined by GPC at 40°C. The resultant molecular weight was corrected for urea derivatization.

The resin monomer ratio was determined by Gas Chromatography (Hewlett Packard HP6890) having a capillary column using dry chloroform as solvent.

The purity of the resin was determined using ^{15}N and ^{13}C solution state NMR. ^{15}N solution NMR was performed on a Varian 500 MHz NMR spectrometer with ^{15}N-glycine as an external standard. ^{13}C solution NMR was performed on a Varian 400 MHz NMR

spectrometer operating at 100.577 MHz and using TMS as reference. The resin was dissolved in $CDCl_3$ for performing the solution NMR.

A.6.1.2. Results

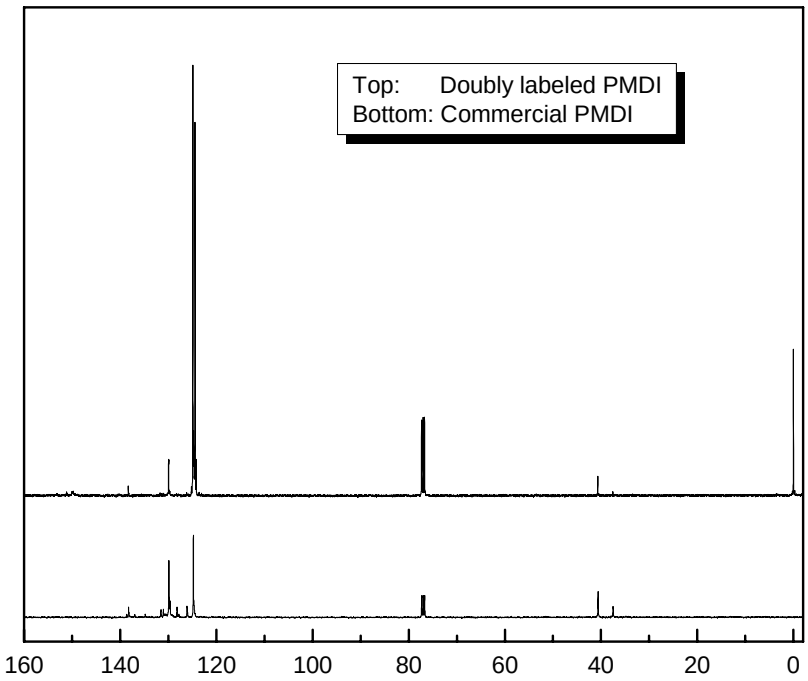

Figure A.6.1.1. Solution-state ^{13}C NMR of commercial and doubly labeled PMDI (TMS and $CDCl_3$ as internal references)

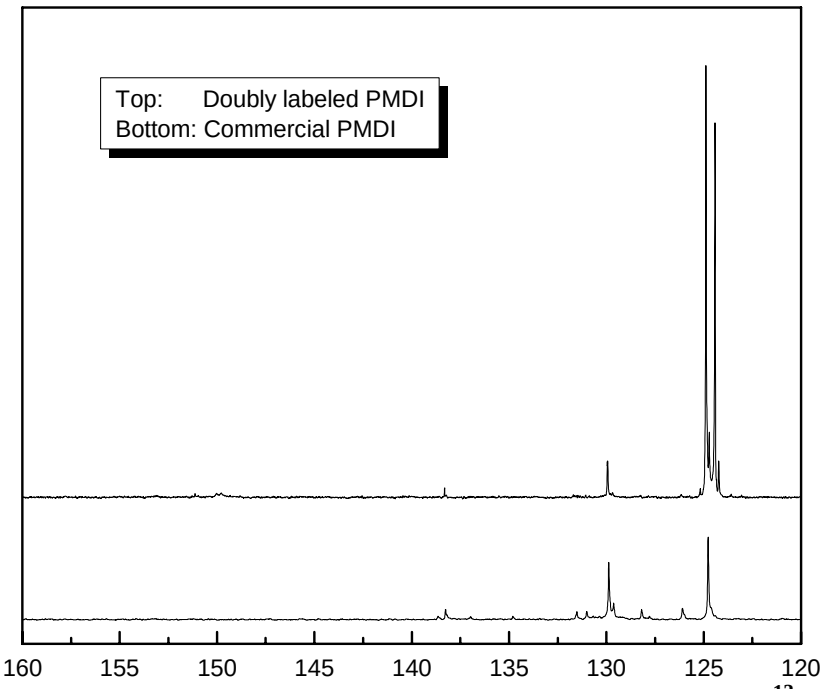

Figure A.6.1.2. Aromatic and isocyanate carbons in solution-state ^{13}C NMR (TMS and $CDCl_3$ as internal references)

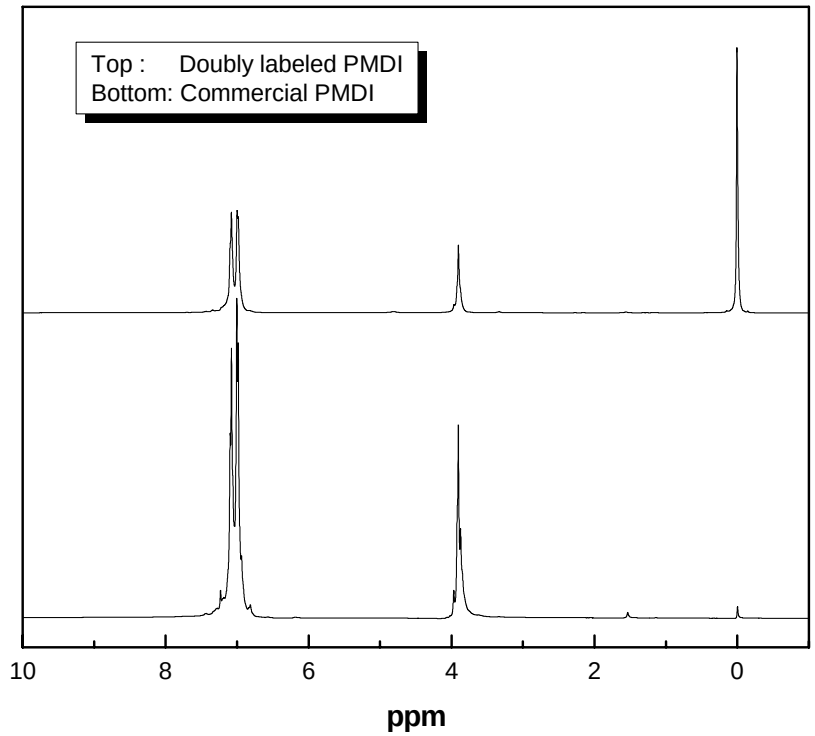

Figure A.6.1.3. Proton spectra of a commercial and doubly labeled PMDI resin (TMS as internal references)

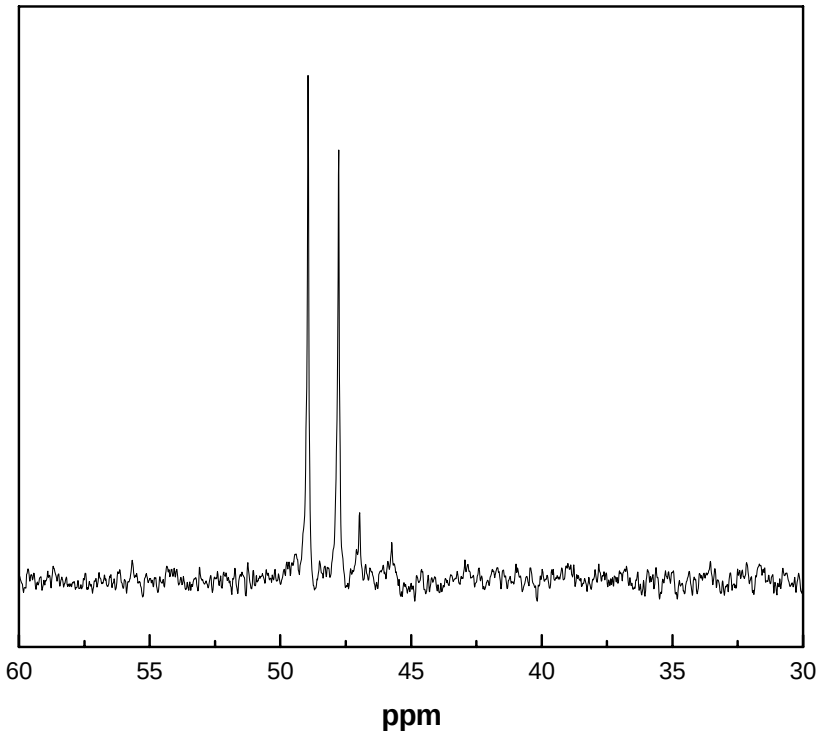

Figure A.6.1.4. Solution-state ^{15}N NMR spectrum of doubly labeled PMDI resin (referenced to ^{15}N-glycine at 31 ppm externally)

A.6.2. Effect of cure conditions on the chemistry of wood-PMDI bondlines

A.6.2.1. Experimental

A.6.2.1.1. Materials

Yellow-poplar and southern yellow pine wood flakes (5.1 cm × 5.1 cm × 1.5 cm; 2" × 2" × 0.6") were sliced from the radial wood surface using a disk flaker. Flakes were dried at 105°C for 24 hours to determine dry weights and were equilibrated at ambient conditions to achieve 6-7% moisture content (MC).

Doubly labeled PMDI resin was synthesized as described in A.5.1.

A.6.2.1.2. Methods

A.6.2.1.2.1. Preparation of Wood-PMDI composites

Doubly labeled PMDI resin (3, 10 and 15% based on wood weight) was applied on two wood flakes. The resin was sandwiched between the flakes by pressing in a press at 120°C under 3.45 MPa (500 psi) pressure for 3 or 6 minutes. Two samples were prepared at each resin content levels (with poplar only), while only one sample was prepared at the higher cure times 96 min) but for both the wood species. The composite samples were stored in a dessicator over indicating calcium sulfate before NMR acquisition.

A.6.2.1.2.2. Solid State NMR Measurements

^{15}N Cross-Polarization/Magic Angle Spinning (CP/MAS) NMR was performed on a Bruker MSL-300 MHz spectrometer operating at 30.43 MHz using a variable contact time pulse at room temperature. The delay between scans was 6 seconds. All spectra were referenced to ^{15}N-glycine at 31 ppm. Small discs were cut out of the wood

composites using a paper hole puncher and filled into a zirconium oxide rotor. The rotor was spun at 4.0 kHz during NMR experiment. Here you must also explain the number of samples and acquisitions in a clear and concise fashion.

A.6.2.1.2.3. Spectral Analysis (Decomposition)

The ^{15}N solids NMR spectra were decomposed using NUTS® software. An adjustable algorithm was employed using a 75% Gaussian & 25% Lorentzian fitting procedure; this combination was selected because it provided the best simulation of the original spectrum. The spectra were decomposed (over the range from about 90 – 120 ppm) into three components: 111 ppm biuret imide, 104 ppm urea peak and ~99.5 ppm urethane peak. During the decomposition process, the biuret imide and urea peaks were fixed while the urethane peak was allowed to vary between 102 – 99.5 ppm. Details of this process are discussed later.

A.6.2.2. Results and Discussion

A.6.2.2.1. Effect of resin content

The following figure shows the effect of resin content on the concentration of the different chemical species formed in the wood-PMDI bondline.

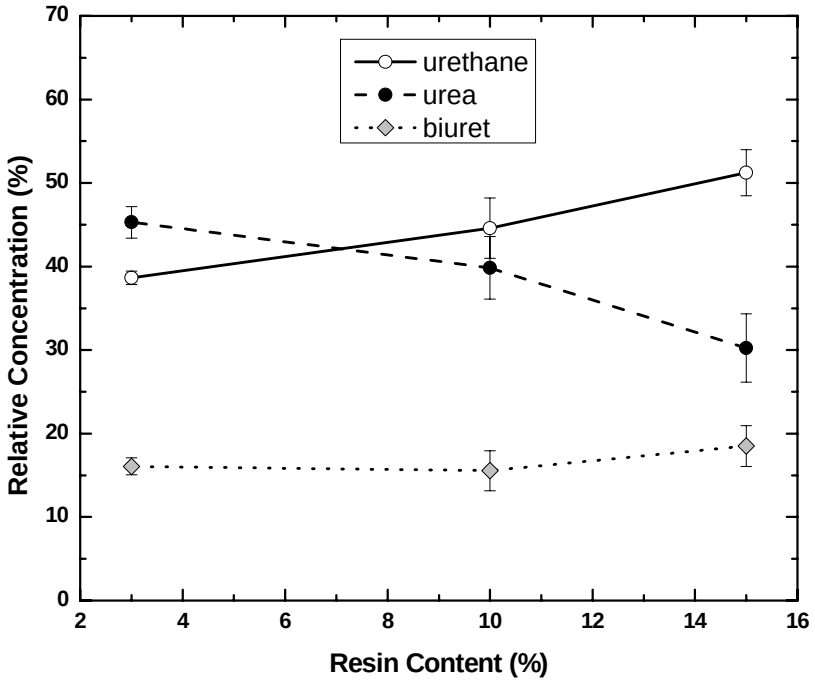

Figure A.6.2.1. Effect of wood composite resin content on the concentration of various chemicals species formed in the wood-PMDI bondline.

Results show that with the increase in resin content, the concentration of urethane increased, which was accompanied by a progressive decrease in the amount of urea in the wood-PMDI bondline. The change in the amount of biuret with increase in resin content was not significant. Figure A.5.2.2. shows the effect of resin content on the relaxation times ($T_{1\rho}$) of the different chemical species.

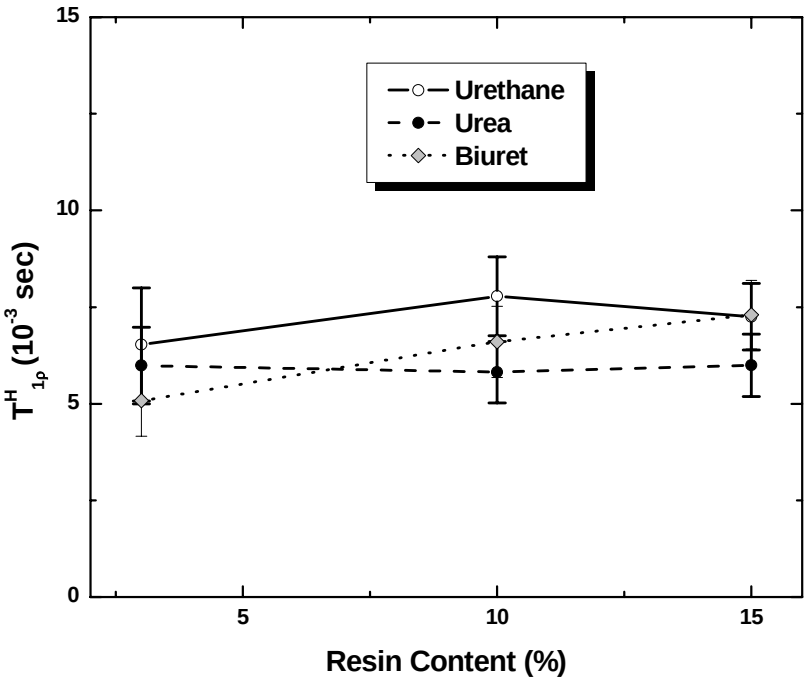

Figure A.6.2.2. Effect of resin content on the relaxations of the different chemical species in wood-PMDI composites.

Results show that the T1r values for the chemical species did not change significantly with increase in the resin contents. The morphology of the wood-PMDI bondlines was found to be homogeneous at different resin contents.

A.6.2.2.2. Effect of cure times

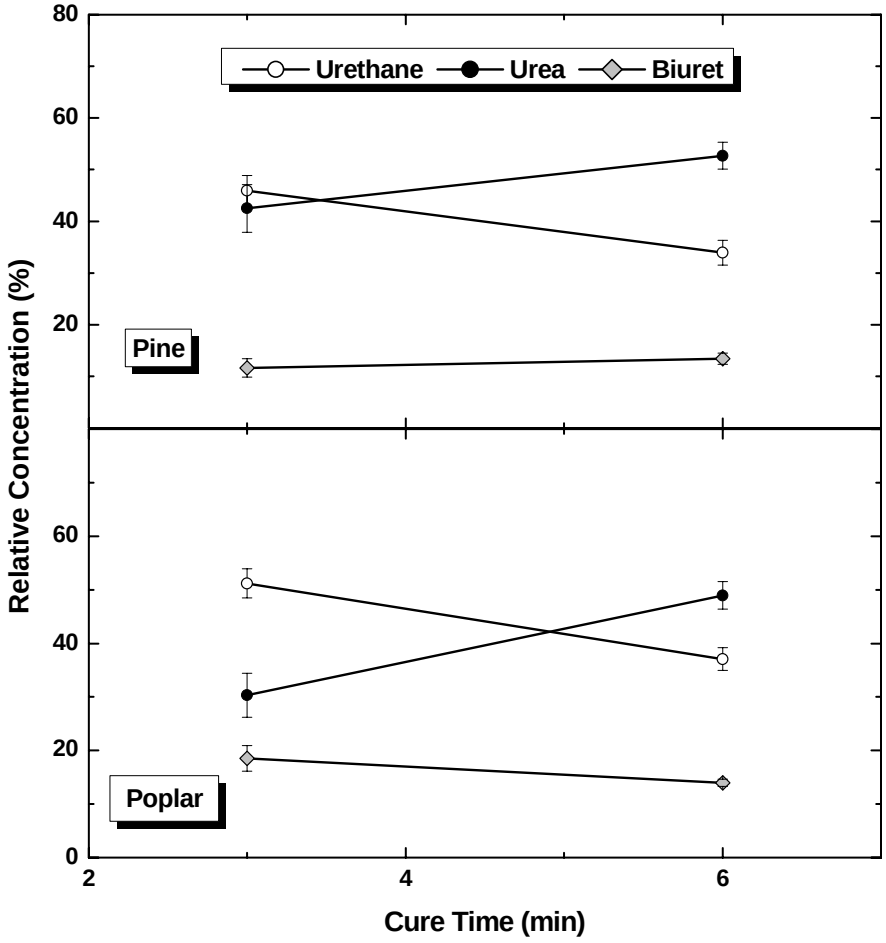

Figure A.6.2.3. Effect of cure times on the relative concentrations of urethane, urea and biuret in YP-PMDI composites.

Both woods show similar trends with the increase in cure times; urethane concentration decreased with a concomitant increase in urea concentrations, while the changes in biuret concentrations were not significant. Similar results were also observed in previous studies.

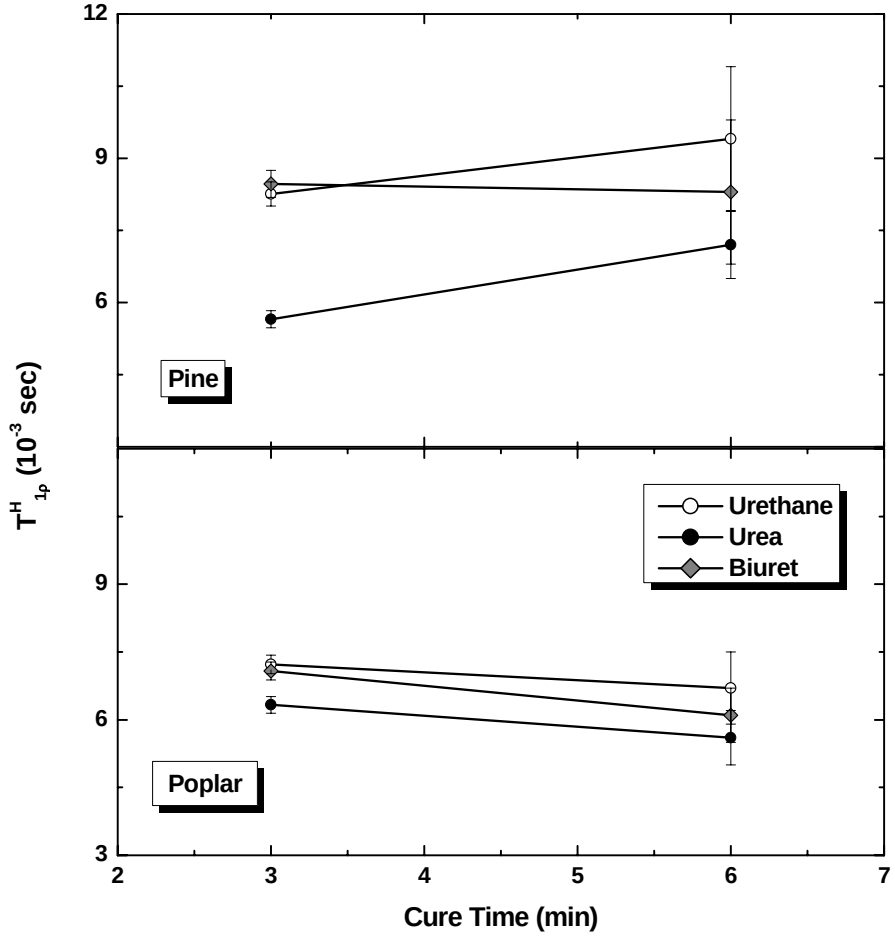

Figure A.6.2.4. Effect of cure times on the $T_{1\rho}$ values of urethane, urea and biuret.

With increase in cure times, the morphology of both wood-PMDI systems become more homogeneous.

A.6.3. DMA of Polymeric Isocyanate Resin

Dynamic thermal scans of neat PMDI resin supported on inert cellulose filter papers were performed in order to determine the glass transition (T_g) of the resin. Results from differential scanning calorimetry showed the T_g of neat PMDI resin to be at ~55°C.

A.6.3.1. Experimental

Commercial PMDI resin (Huntsman Rubinate 1840) was obtained from Hunstman Polyurethanes and was used as received.

Cellulose filter paper (40 mm / 1.6" x 10 mm / 0.4" x 0.2 mm / 0.008") was impregnated with resin (110%). Seven resin impregnated filter papers were stacked together and stored under dry conditions (over Phosphorous pentoxide), until tested.

All DMA tests were conducted on a TA Instruments® 2980 DMA in the single cantilever bending mode.

Resin impregnated filter papers were clamped into the DMA with a torque of ~ 69 cm.N (6 lb-in). samples were initially cooled slowly (5°C/min) to -150°C and equilibrated at that temperature for 10 min. the dynamic scan was performed from -150° to 25°C. the different DMA experimental parameters were: 15 mm amplitude, 0.043% strain, 5°C/min heating rate, 1 Hz frequency.

A.6.3.2. Results and Discussion

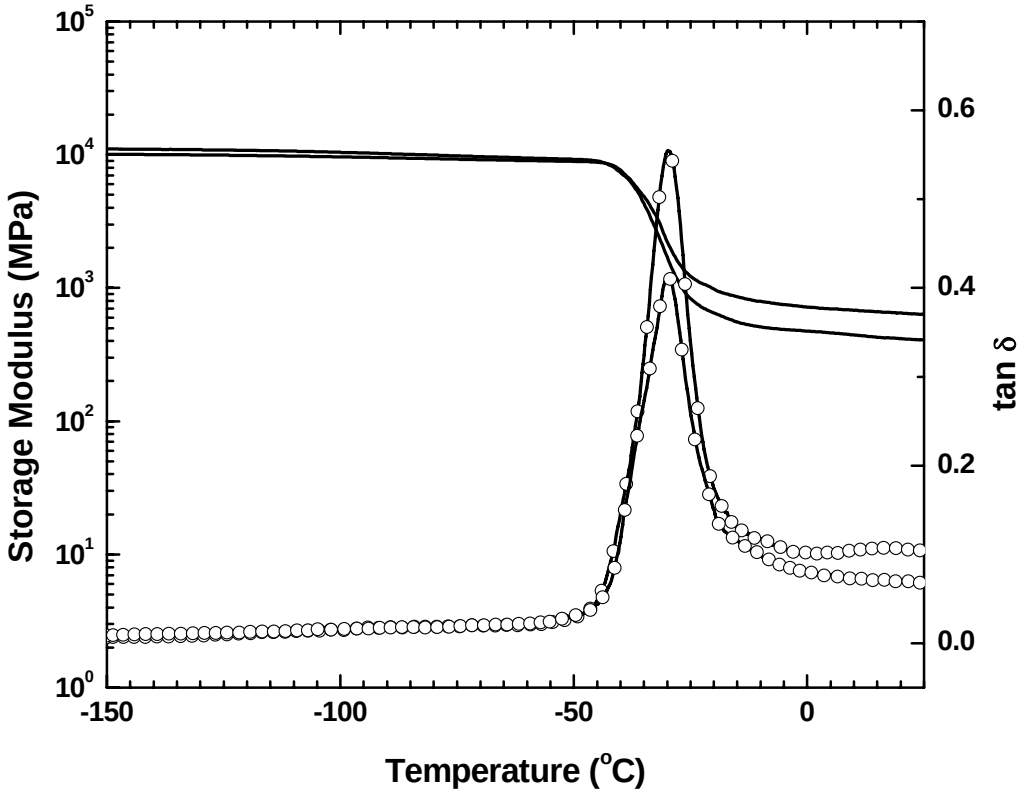

Figure A.6.3.1. Dynamic thermal scans of neat PMDI resin supported on inert cellulose filter papers (3 replications).

Results showed that the T_g of neat PMDI is at ~-30°C (from tan δ peak).

A.6.4. Dynamic thermal scans of poplar wood samples at different moisture contents.

A.6.4.1. Experimental

A.6.4.1.1. Materials

Yellow-poplar, YP (*Liriodendren tulipifera*) sample [40 mm / 1.6" (radial) x 10 mm / 0.4" (tangential) x 4 mm / 0.16" (longitudinal)] were dried at 105°C for 24h. Dried wood samples were then stored in different humidity chambers to obtain 0% (over Phosphorous pentoxide), 8% (over saturated solution of Potassium carbonate) and 15% (over saturated solution of Sodium chloride) moisture contents.

A.6.4.1.2. Methods

All tests were conducted on a TA Instruments® 2980 DMA in the single cantilever bending mode. Samples with different moisture content were clamped into the DMA with a clamping torque of ~69 cm.N (6 lb-in). The samples were initially cooled to -150°C at a heating rate of 10°C/min. The samples were equilibrated at -150°C for 10 min before performing the dynamic thermal scan to 25°C. The different experimental parameters are: 20 mm amplitude, 0.057% strain, 1 Hz frequency and 5°C/min. The sample moisture content change in the course of the experiment was minimum as shown in the following table.

Table A.6.4.1. Change in moisture content during dynamic thermal scans

Sample	MC before test (%)	MC after test (%)
Radial Yellow-poplar	8.23 ± 0.1	7.37 ± 0.65
	15.08 ± 0.38	12.94 ± 0.21

A.6.4.2. Results and Discussion

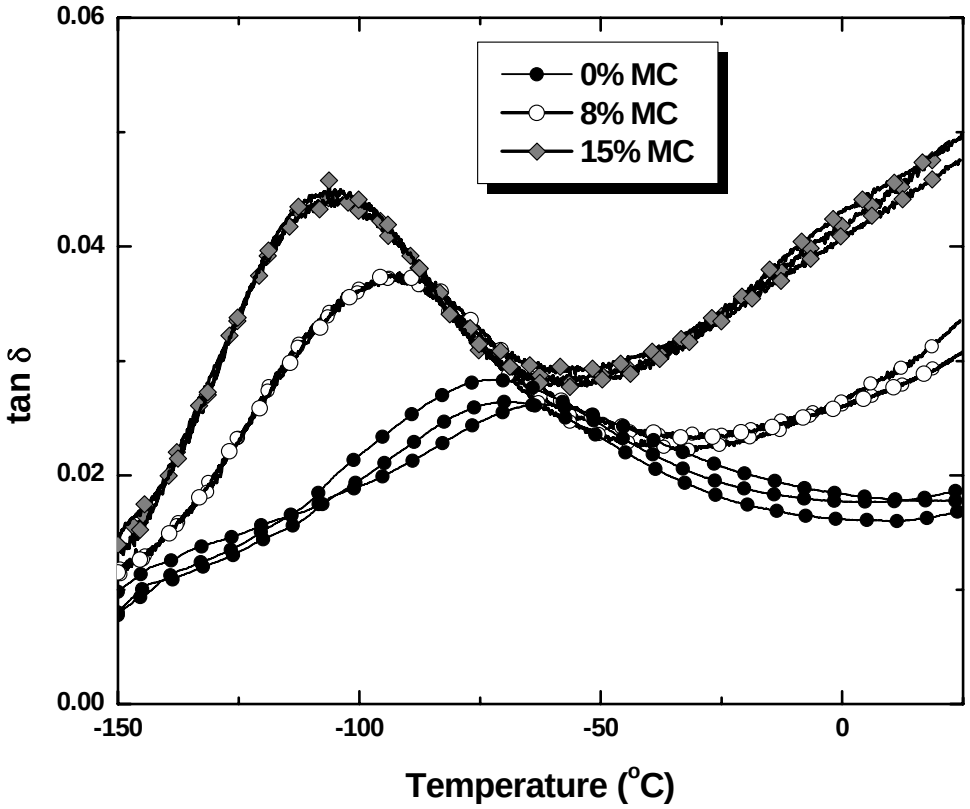

Figure A.6.4.1. Effect of moisture content on the dynamic thermal scans of poplar wood samples (3 replications each).

Control dry samples showed a relaxation centered at ~60°C. The relaxation was found to shift to lower temperatures (-95°C at 8% MC and -105°C at 15% MC), with a simultaneous increase in the intensity of the relaxation as the sample moisture content was increased. These results were similar to those reported in past studies[1, 2].

1. Sugiyama, M., E. Obataya, and M. Norimoto, Journal of Materials Science, 1998. **33**: p. 3505-3510.
2. Obataya, E., M. Norimoto, and B. Tomita, Journal of Applied Polymer Science, 2001. **81**: p. 3338-3347.

A.6.5. Effect of Resin impregnation on the Low Temperature Dynamic Scan of Wood Samples

A.6.5.1. Experimental

A.6.5.1.1. Materials

Commercial PMDI resin (Huntsman Rubinate 1840) was obtained from Hunstman Polyurethanes and was used as received.

Two wood species were selected for analysis: yellow-poplar, YP (*Liriodendren tulipifera*) & southern yellow pine, SYP *(Pinus spp*.). The wood sample dimensions were: 40 mm (radial) x 10 mm (tangential) x 4 mm (longitudinal) [1.6" x 0.4" x 0.16"]. All samples were initially dried (105°C for 24 hr) and then equilibrated to 6-7% moisture content (MC), before further treatment.

A.6.5.1.2. Methods

A.6.5.1.2.1. Resin impregnation

Moisture-equilibrated samples (untreated and acetylated) were impregnated with liquid PMDI resin using an open-cell method, using PMDI dissolved in anhydrous acetone. The samples were first impregnated with resin-solution (20%) using pressure [~69 kPa (10 psi) pressure for 15 min.], followed by the application of vacuum (~0.1 mm Hg) for 15 min. These resinated samples were then cured at 120°C for 2 h.

Control samples were prepared in order to achieve the same thermal history as for the resinated wood samples. Moisture-equilibrated samples were impregnated with pure anhydrous acetone (using the open-cell process described above), and then subsequently heated at 120°C for 2 h. All control and resin-treated samples were stored under dry conditions (under phosphorous pentoxide in a dessicator) before further analysis.

A.6.5.1.2.2. Ethylene-glycol plasticization

Samples (control and resin impregnated) were impregnated with EG under vacuum (~0.1 mm Hg) for 30 min. Impregnated samples were then treated in EG at 100°C for 1 h. Samples were then cooled slowly (0.5° - 1.5°C/min) to room temperature and stored in EG before further analysis.

A.6.5.1.2.3. Dynamic tests

All DMA tests were conducted on a TA Instruments® 2980 DMA in the single cantilever bending mode.

EG-plasticized samples were clamped to the DMA with ~115 cm.N (10 lb-in) torque, followed by slow cooling (5°C/min) to -150°C. the different experimental parameters used in the dynamic scans were: 0.057% strain (20 μm amplitude); 2°C/min heating rate; 1 Hz frequency.

A.6.5.2. Results

The resin and plasticizer content before and after the dynamic scans are shown in the following table.

Table A.6.5.1. Sample parameters of plasticized resin-solution impregnated wood samples before and after dynamic scans (5 replications each).

Sample	Resin Content (%)	Plasticizer before test (%)	Plasticizer after test (%)
Pine control	-	143.4 ± 13.4	52.5 ± 11.4
Pine-PMDI	5.72 ± 0.6	105.2 ± 6.4	59.3 ± 2.2
Poplar control	-	143.2 ± 8.2	50.5 ± 5.6
Poplar-PMDI	8.1 ± 1.6	121.9 ± 9.4	65.6 ± 7.1

The following figure shows the effect of resin impregnation on the low temperature dynamic scans of pine and poplar samples.

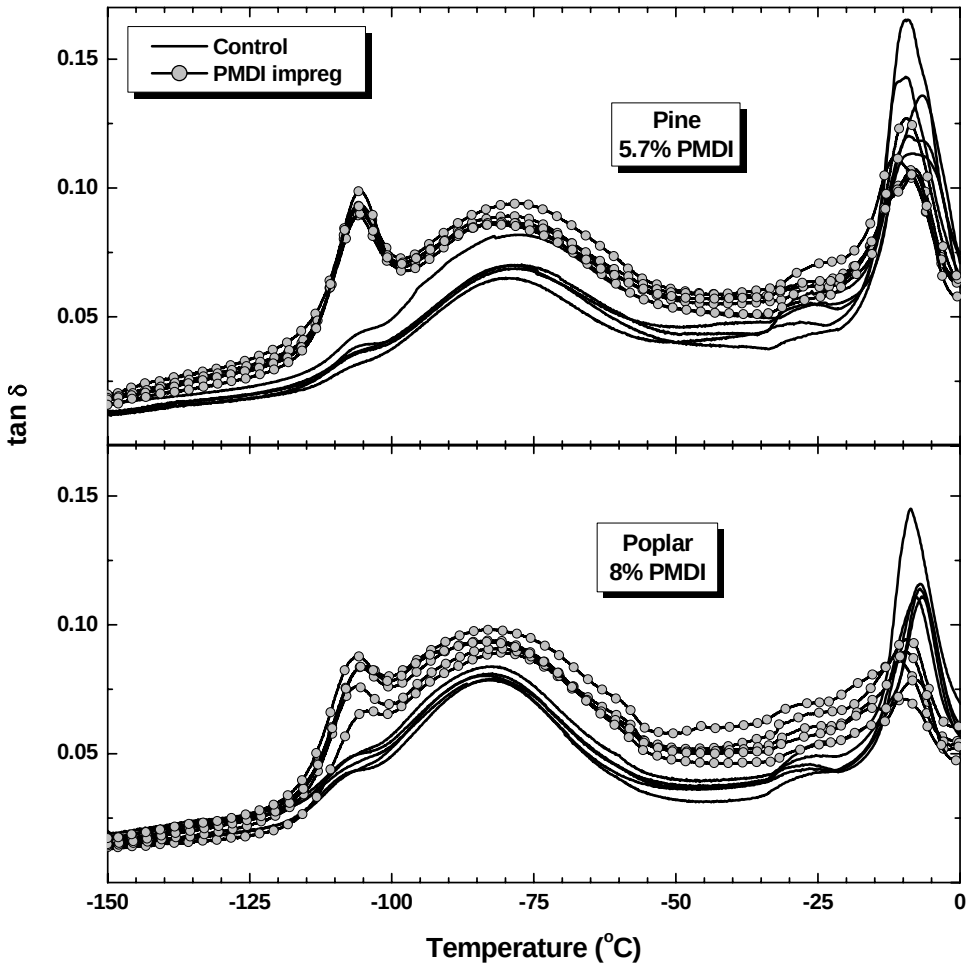

Figure A.6.5.1. Effect of resin impregnation on the low temperature dynamic scans (tan δ) of pine and poplar wood (0.06% strain, 1 Hz frequency, 2°C/min heating rate) [5 replications each]

Both control woods showed a relatively broad relaxation centered around -80°C, with a shoulder at ~ -105°C. In the presence of the resin, the central peak broadened and the intensity of the shoulder was found to increase. The effect of the resin on the relaxations was found to be relatively larger in pine, even though it had relatively less resin

impregnation. The effect of resin impregnation on the storage modulus is illustrated in the following figure.

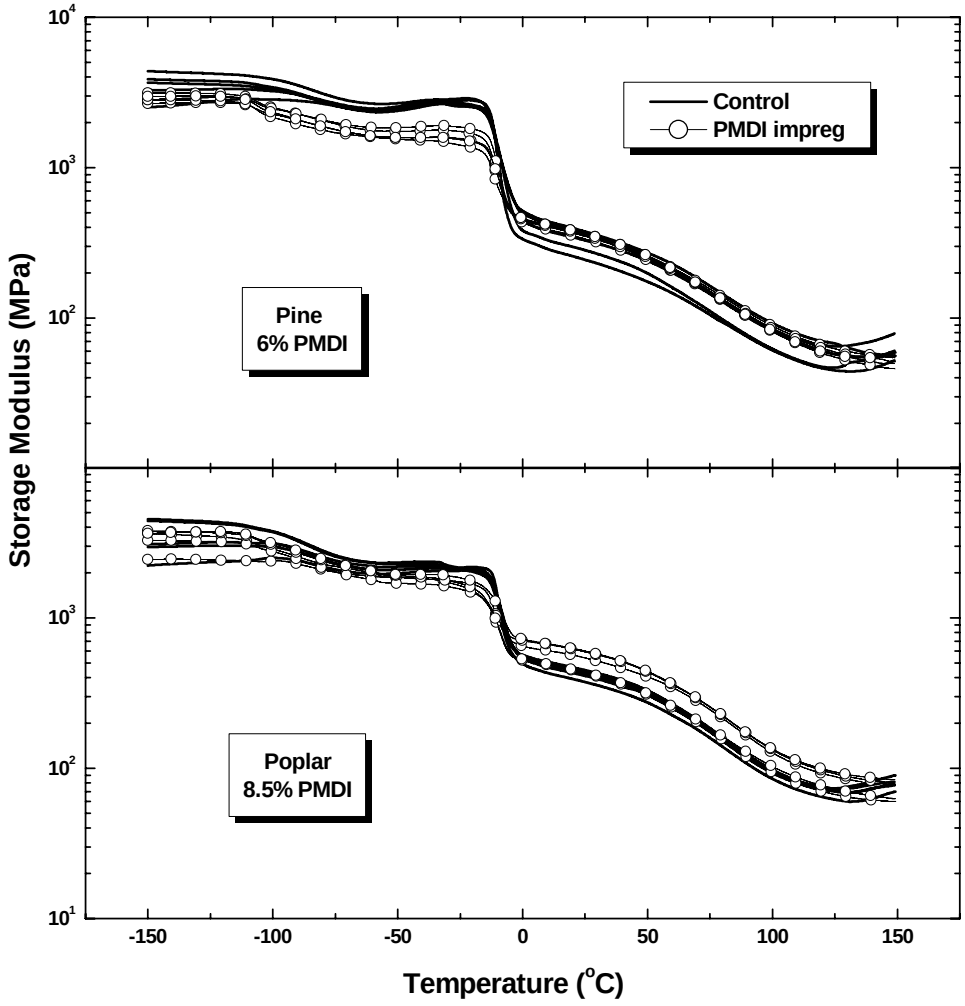

Figure A.6.5.2. Effect of resin impregnation on the low temperature dynamic scans (E') of pine and poplar wood (0.06% strain, 1 Hz frequency, 2°C/min heating rate) [5 replications each]

The storage modulus of the samples were found to decrease with resin impregnation below ~10°C. the opposite effect was observed after the plasticizer melting i.e. E' increased with resin impregnation.

A.6.6. TGA Thermograms

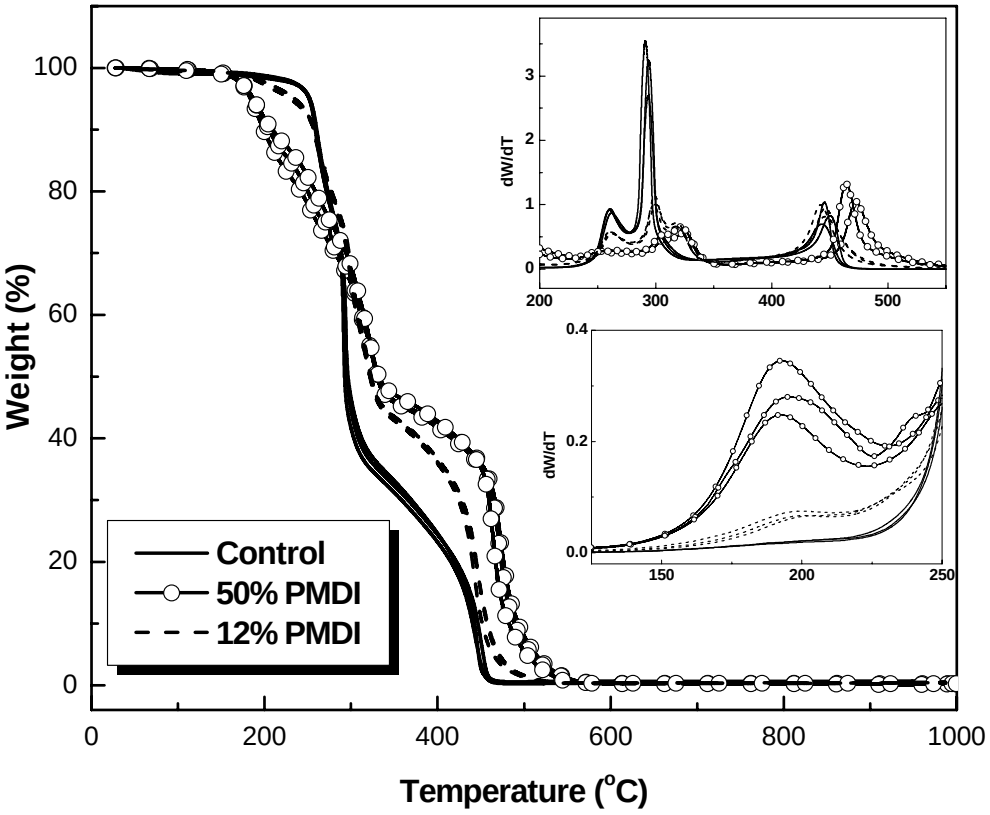

Figure A.6.6.1. Comparison of the thermal degradation of control and resin impregnated poplar samples in air (3 replications each).

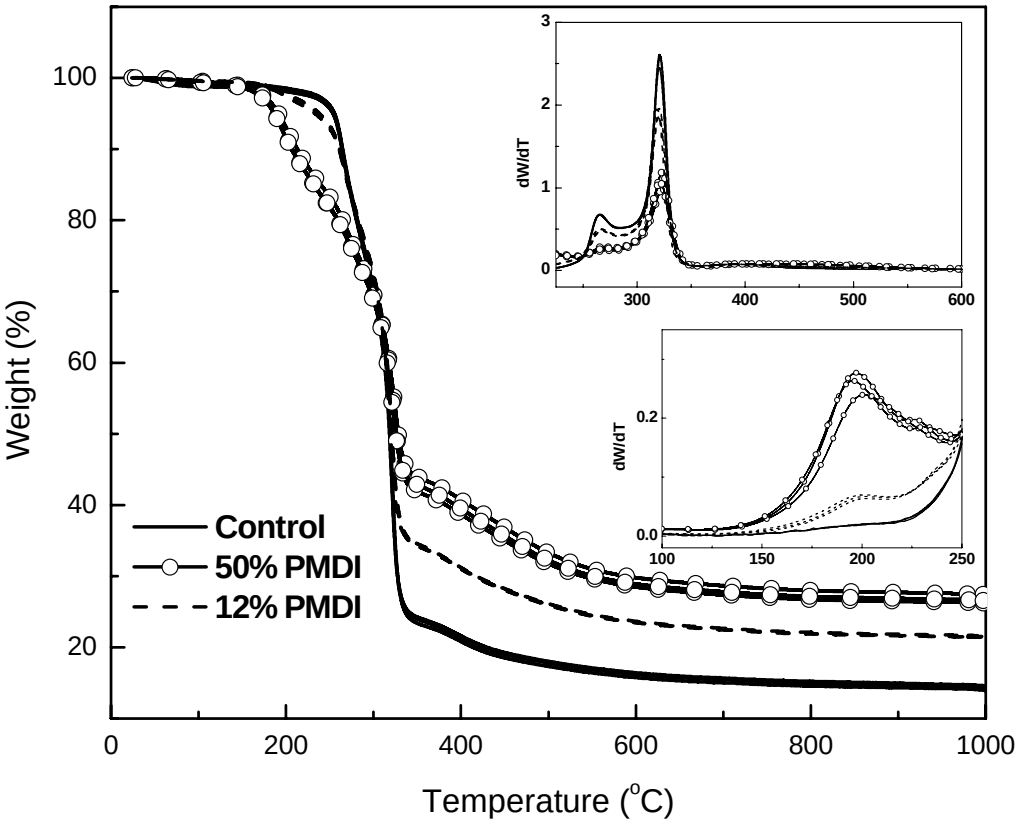

Figure A.6.6.2. Comparison of the thermal degradation of control and resin impregnated poplar samples in nitrogen (3 replications each).

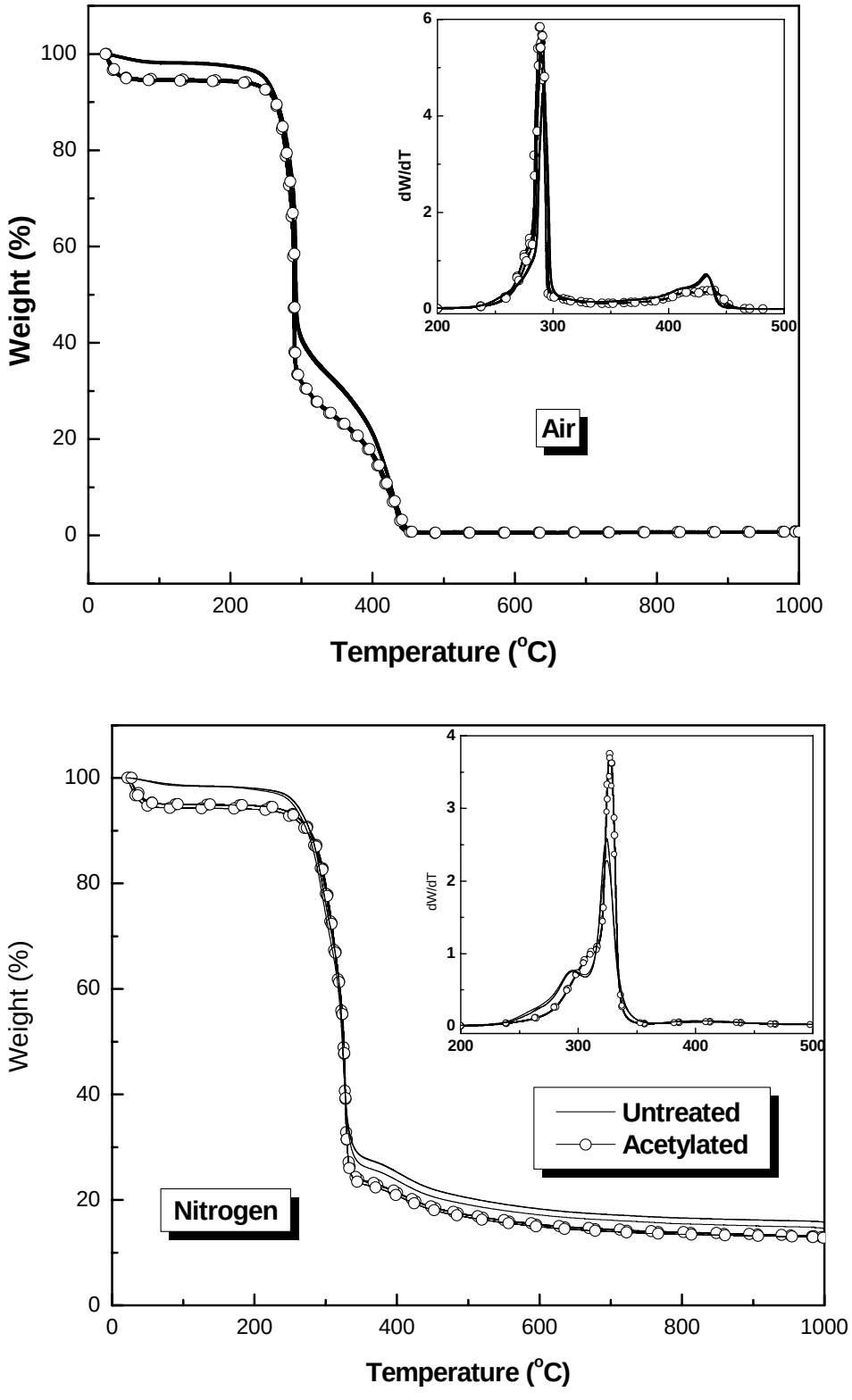

Figure A.6.6.3. Effect of acetylation on the thermal degradation of pine in air and nitrogen (3 replications each).

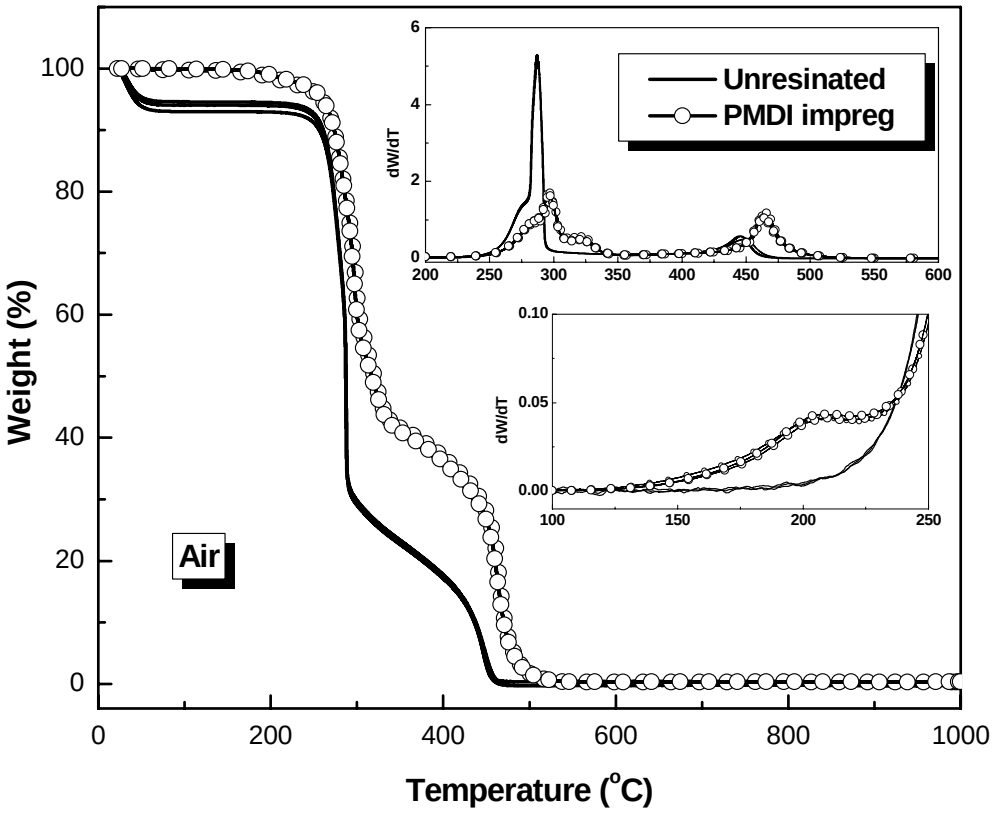

Figure A.6.6.4. Comparison of the TGA thermograms of unresinated and PMDI-impregnated acetylated poplar samples in air (3 replications each).

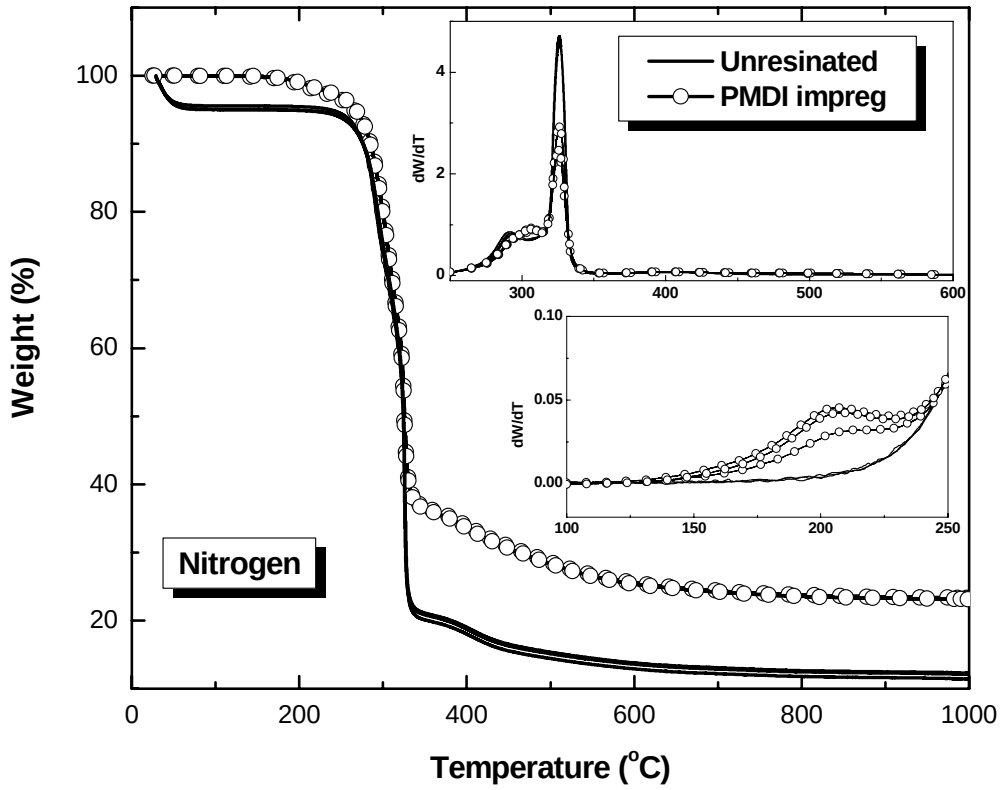

Figure A.6.6.5. Comparison of the TGA thermograms of unresinated and PMDI-impregnated acetylated poplar samples in air (3 replications each).

A.6.7. Thermogravimetric analysis of neat PMDI resin

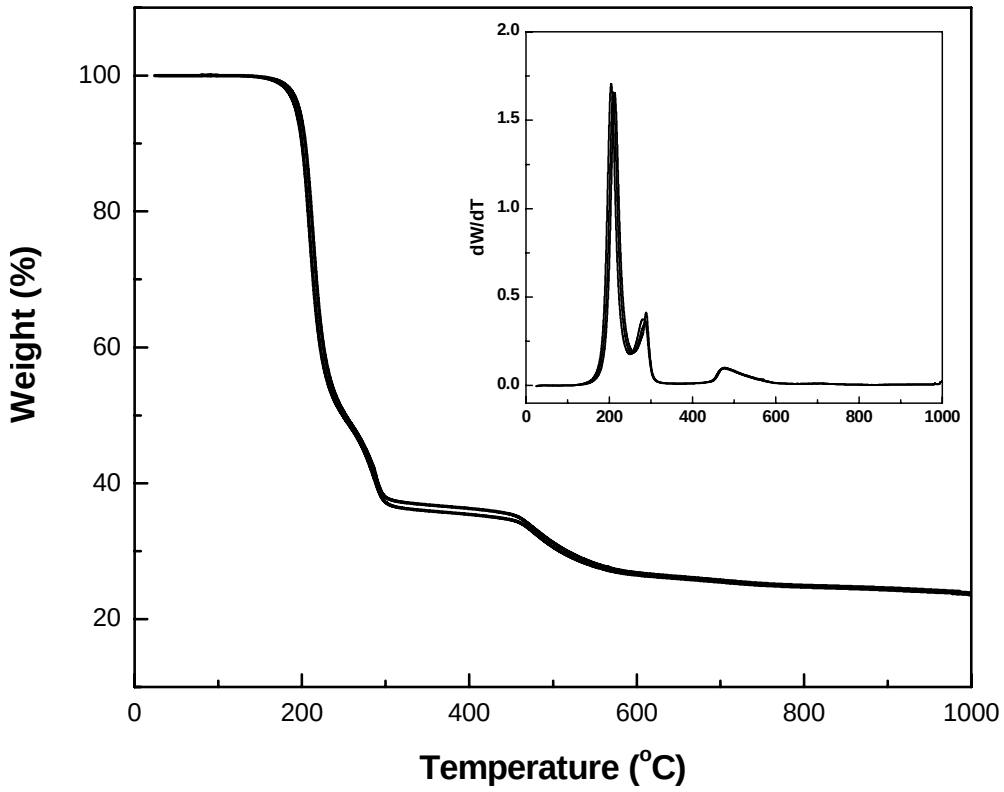

Figure A.6.7.1. Weight loss and derivative weight loss (dW/dT, inset) profile of PMDI resin in nitrogen (3 replications)

A three step degradation was observed for PMDI resin in nitrogen as reported in the literature [1]. The dW/dT curve showed three peaks at 200°, 280° and 470°C. The major degradation of the resin in nitrogen started at around 130°C. Major degradation of the resin occurred in the temperature range of 120° to 305°C (63% weight loss). Between the temperature ranges of 305° to 600°C and 600° to 1000°C, the weight loss of the resin was ~11% and 3.1% respectively. The char yield was ~23%, similar to literature (20%) [1].

Figure A.6.7.2 shows the TGA thermogram of PMDI resin in air.

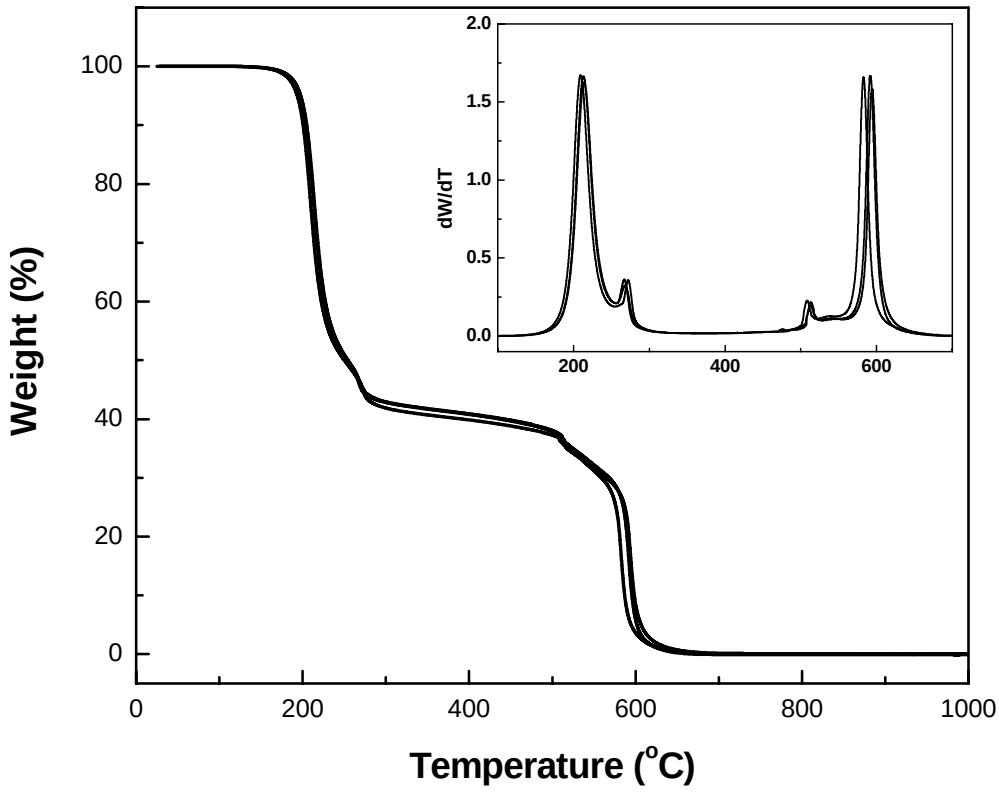

Figure A.6.7.2. Weight loss and derivative weight loss (dW/dT, inset) profile of PMDI resin in air (3 replications)

The neat resin degraded in two-steps in air. The major weight loss in the resin started around 145°C. In the first step (145° to 305°C), the sample lost 57.3% of its weight. The weight loss in the second stage (305° - 705°C) was 42.7%.

A.6.8. Characterization of Polyurea Degradation by IR-spectroscopy

In order monitor the chemical changes occurring in polyurea during degradation in air, the degraded samples were examined with infra-red (IR) spectroscopy up to 490°C. Figure A.6.8.1 shows the IR spectra of un-degraded polyurea.

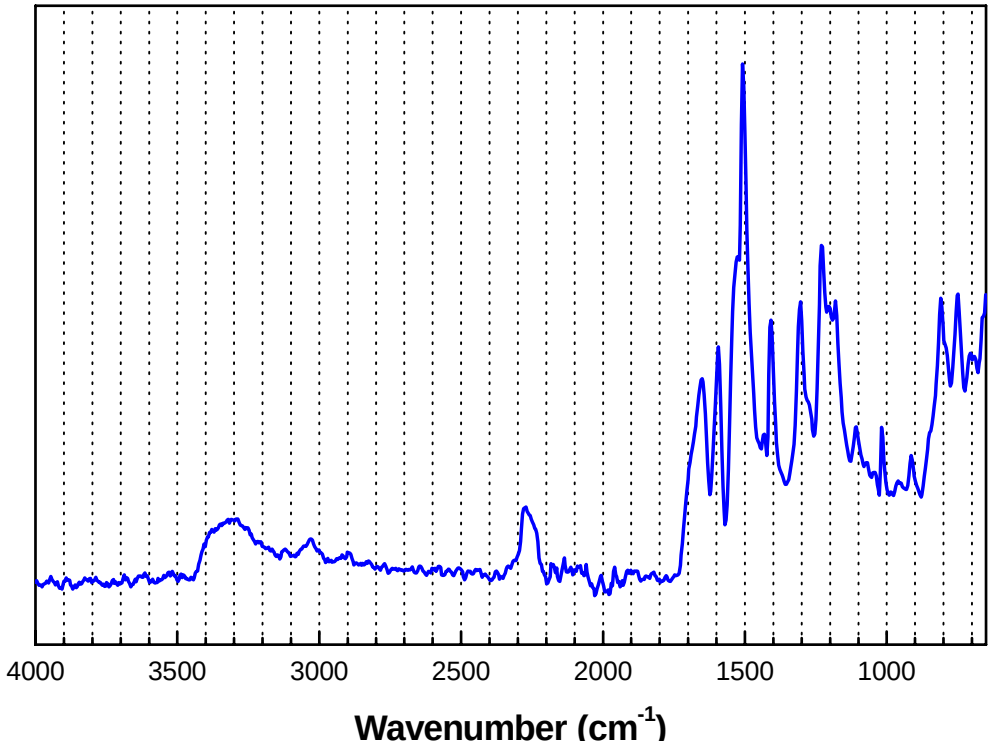

Figure A.6.8.1. IR-spectra of untreated polyurea

Table A.6.8.1 summarizes all the important peaks observed in the IR-spectra.

Table A.6.8.1. Characteristic IR peaks for polyurea [1-3]

Wavenumber (cm^{-1})	Functional groups
3310	N-H stretch
2250	NCO asymmetric stretch
1690 (shoulder)	Free Urea C=O stretch
1650	H-bonded Urea C=O stretch
1592 & 1508	Aromatic C=C stretch
1533 (shoulder)	N-H bend
1400	Benzene ring mode
1300	C-N stretch

Polyurea samples were degraded up to different temperatures and then their IR spectra were recorded. Figure A.6.8.2 shows the IR-spectra of polyurea at different temperatures.

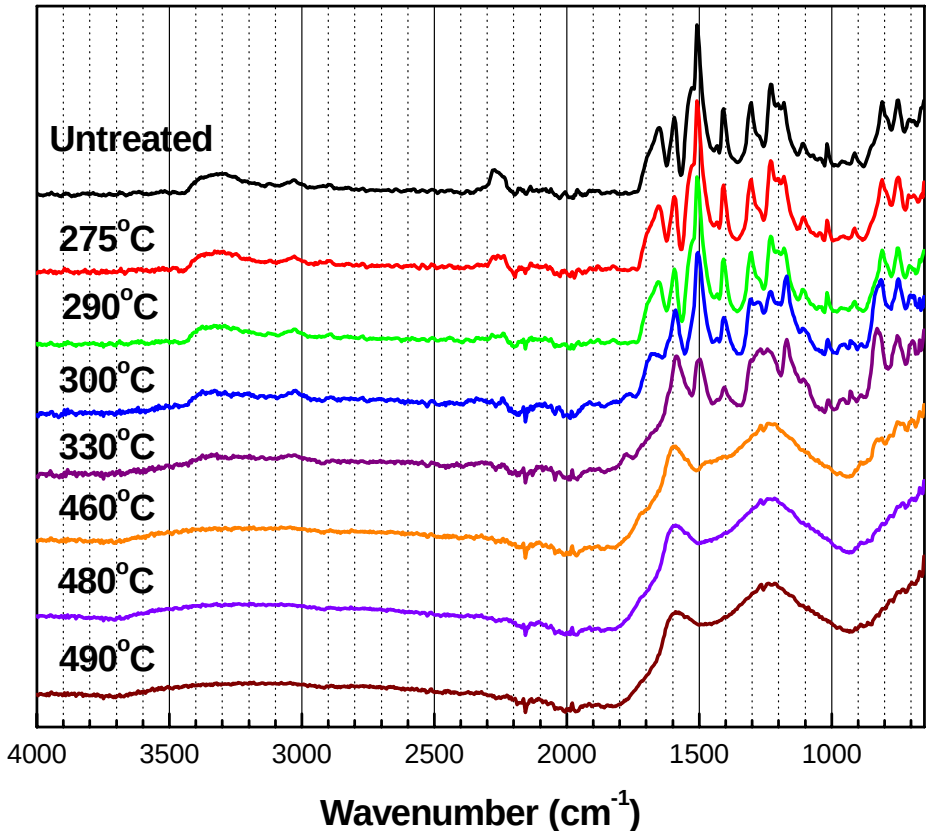

Figure A.6.8.2. Monitoring the thermal degradation of polyurea with IR-spectroscopy (up to 490°C).

The figure shows that the intensity of most of the peaks decreased with increase in temperature until 290°C. From 290° to 300°C, the N-H bending peak (shoulder at 1533 cm^{-1}) disappeared. The intensity of the C-N stretch (1300 cm^{-1}) was also reduced drastically. A drastic change in the spectra was observed from 300° to 330°C, which represented the completion of the first step of the polyurea degradation in air. At 330°C, the following changes in the IR spectra were observed.

- The urea carbonyl stretch peaks (1650 & 1690 cm^{-1}) disappeared.
- The N-H stretch at 3300 cm-1 disappeared.

The only peaks present at 330°C were due to the aromatic ring motions (1592, 1508 & 1400 cm^{-1}). This might suggest that degradation of the urea linkages occurred at 330°C.

From 330° to 460°C, the peak at 1500 cm^{-1} disappeared and the only peak that remained was the broad peaks at 1600 and 1250 cm^{-1}. The spectra did not show any significant changes with further increase in temperature.

References

1. Silverstein, R.M. and F.X. Webster, *Spectrometric Identification of Organic Compounds*. 6th ed. 1998, NY: John Wiley & Sons, Inc.
2. Rosthauser, J.W., et al. in *31st International Particleboard/Composite Materials Symposium*.
3. Smith, B.C., *Infrared Spectral Interpretation: A systamatic approach*. 1999, Boca Raton, FL: CRC Press.

A.6.9. Fitting of Dry Isothermal Creep Data to KWW equation

Table A.6.9.1. KWW fitting parameters for PMDI impregnated Pine wood samples

Temperature (°C)	R^2	τ	*n*
50	0.9996	$6.8\times10^{10} \pm 7.6\times10^{9}$	0.949± 0.003
	0.9995	$8\times10^{10} \pm 1\times10^{10}$	0.942 ± 0.004
	0.9997	$1.7\times10^{10} \pm 1.04\times10^{10}$	0.94 ± 0.003
	0.9998	$2.6\times10^{10} \pm 2.07\times10^{9}$	0.937 ± 0.002
	0.9994	$4.85\times10^{10} \pm 1.31\times10^{10}$	0.929 ± 0.00407
	0.9996	$3.24\times10^{10} \pm 1.96\times10^{9}$	0.94407 ± 0.003
	0.9997	$2.54\times10^{10} \pm 2.53\times10^{9}$	0.934 ± 0.003
90	0.9988	$1.7\times10^{7} \pm 2.8\times10^{6}$	0.805 ± 0.006
	0.999	$2.7\times10^{7} \pm 4.6\times10^{6}$	0.819 ± 0.006
	0.9988	$4.96\times10^{7} \pm 1.04\times10^{7}$	0.834 ± 0.006
	0.9994	$13.6\times10^{7} \pm 2.4\times10^{7}$	0.856 ± 0.004
	0.9984	$2.63\times10^{7} \pm 5.16\times10^{6}$	0.809 ± 0.007
	0.9985	$1.28\times10^{7} \pm 2.11\times10^{6}$	0.797 ± 0.007
	0.9991	$4.95\times10^{7} \pm 8.03\times10^{6}$	0..826 ± 0.005
120	0.999	$5.9\times10^{5} \pm 1.6\times10^{4}$	0.705 ± 0.006
	0.9993	$6.7\times10^{4} \pm 1.6\times10^{3}$	0.706 ± 0.005
	0.999	$9.88\times10^{4} \pm 3.4\times10^{3}$	0.734 ± 0.006
	0.9992	$13.76\times10^{4} \pm 4.7\times10^{3}$	0.757 ± 0.005
	0.9988	$7.23\times10^{4} \pm 1.98\times10^{4}$	0.706 ± 0.007
	0.9988	$5.03\times10^{4} \pm 1.09\times10^{3}$	0.698 ± 0.006
	0.9993	$15.23\times10^{4} \pm 4.76\times10^{3}$	0.741 ± 0.005

Table A.6.9.2.KWW Fitting parameters for Control Poplar Wood Samples

Temperature (°C)	R^2	τ	n
50	0.9992	$1.58 \times 10^5 \pm 4.8 \times 10^3$	0.862 ± 0.001
	0.9998	$7.46 \times 10^7 \pm 1.87 \times 10^6$	0.868 ± 0.0002
	0.9995	$1.83 \times 10^6 \pm 5.4 \times 10^4$	0.834 ± 0.001
	0.9994	$2.55 \times 10^6 \pm 9.1 \times 10^4$	0.831 ± 0.001
	0.9997	$5.2 \times 10^6 \pm 1.5 \times 10^5$	0.858 ± 0.0005
	0.9989	$3.3 \times 10^6 \pm 1.6 \times 10^5$	0.834 ± 0.001
	0.999	$6.9 \times 10^7 \pm 4.3 \times 10^6$	0.844 ± 0.001
	0.9997	$8.5 \times 10^7 \pm 2.9 \times 10^6$	0.864 ± 0.0004
90	0.9992	$1.18 \times 10^6 \pm 4.3 \times 10^4$	0.83 ± 0.001
	0.9985	$1.07 \times 10^8 \pm 8.5 \times 10^6$	0.802 ± 0.001
	0.998	$7.2 \times 10^6 \pm 5.2 \times 10^5$	0.783 ± 0.002
	0.9982	$1.15 \times 10^7 \pm 8.3 \times 10^5$	0.777 ± 0.002
	0.9993	$1.12 \times 10^6 \pm 13.9 \times 10^4$	0.803 ± 0.001
	0.9996	$5.85 \times 10^6 \pm 1.9 \times 10^5$	0.816 ± 0.001
	0.9992	$5.5 \times 10^7 \pm 3.1 \times 10^6$	0.799 ± 0.001
	0.9994	$1.03 \times 10^8 \pm 5.1 \times 10^6$	0.817 ± 0.001
120	0.9998	$1.32 \times 10^5 \pm 1.9 \times 10^3$	0.605 ± 0.001
	0.9993	$5.8 \times 10^4 \pm 1.2 \times 10^3$	0.516 ± 0.003
	0.9991	$5.5 \times 10^4 \pm 1.3 \times 10^3$	0.548 ± 0.003
	0.9998	$5.9 \times 10^5 \pm 1.1 \times 10^4$	0.561 ± 0.002
	0.9997	$3.0 \times 10^5 \pm 5.9 \times 10^3$	0.580 ± 0.002
	0.9997	$1.04 \times 10^5 \pm 1.6 \times 10^3$	0.687 ± 0.001
	0.9988	$1.9 \times 10^5 \pm 6.4 \times 10^3$	0.61 ± 0.003
	0.9995	$1.5 \times 10^6 \pm 4.6 \times 10^4$	0.621 ± 0.002

Table A.6.9.3. KWW fitting parameters for PMDI impregnated poplar wood samples

Temperature (°C)	R^2	τ	*n*
50	0.9998	$1.11 \times 1010 \pm 4.3 \times 10^8$	0.865 ± 0.0004
	0.9997	$5.5 \times 10^6 \pm 1.6 \times 10^5$	0.859 ± 0.0004
	0.9984	$3.6 \times 10^8 \pm 3.2 \times 10^7$	0.822 ± 0.001
	0.9998	$2.9 \times 10^9 \pm 8.5 \times 10^6$	0.864 ± 0.0003
	0.9995	$1.9 \times 10^8 \pm 9.1 \times 10^6$	0.866 ± 0.001
	0.9993	$9.6 \times 10^7 \pm 5.2 \times 10^6$	0.852 ± 0.001
90	0.9993	$6.5 \times 10^7 \pm 4.3 \times 10^5$	0.801 ± 0.001
	0.9989	$9.9 \times 10^7 \pm 6.7 \times 10^6$	0.806 ± 0.001
	0.9988	$1.3 \times 10^8 \pm 9.3 \times 10^6$	0.804 ± 0.001
	0.9982	$2.6 \times 10^7 \pm 2.1 \times 10^6$	0.759 ± 0.002
	0.9964	$3.7 \times 10^7 \pm 4.4 \times 10^6$	0.693 ± 0.004
	0.9992	$7.7 \times 10^7 \pm 4.2 \times 10^6$	0.814 ± 0.001
120	0.9997	$1.01 \times 10^5 \pm 1.5 \times 10^3$	0.631 ± 0.001
	0.9997	$1.8 \times 10^5 \pm 2.9 \times 10^3$	0.602 ± 0.001
	0.9998	$2.3 \times 10^5 \pm 3.2 \times 10^3$	0.599 ± 0.001
	0.9993	$2.0 \times 10^4 \pm 5 \times 10^2$	0.516 ± 0.003
	0.9996	$8.8 \times 10^5 \pm 2.2 \times 10^4$	0.585 ± 0.002
	0.9998	$1.6 \times 10^4 \pm 1.4 \times 10^2$	0.586 ± 0.002

A.6.10. Fitting of Submersion Clamp data to Arrhenius and WLF equation

Table A.6.10.1. Fitting parameters to the Arrhenius equation

Sample	R^2	E_{act} (kJ/mol)
Pine-Control	0.994	213.0 ± 3.7
	0.992	225.6 ± 4.5
	0.994	235.3 ± 4.2
	0.99	223.1 ± 5.0
	0.999	214.8 ± 1.9
Poplar-Control	0.999	239.2 ± 2.4
	0.995	238.0 ± 4.3
	0.985	227.0 ± 6.0
	0.992	212.2 ± 4.3
	0.994	232.6 ± 4.1
Pine-PMDI	0.998	237.0 ± 5.5
	0.992	265.7 ± 2.1
	0.995	236.3 ± 1.9
	0.999	224.7 ± 3.3
	0.994	231.6 ± 2.4
Poplar-PMDI	0.992	253.3 ± 4.4
	0.995	241.3 ± 3.3
	0.993	244.6 ± 3.9
	0.992	241.7 ± 4.1
	0.985	248.9 ± 5.7

Table A.6.10.2. Fitting Parameters to the WLF equation

Sample	R^2	C_1	C_2
Pine-Control	0.999	13.0 ± 1.6	123.1 ± 18.8
	0.999	13.3 ± 2.0	124.9 ± 23.1
	0.999	16.5 ± 1.3	151.7 ± 14.3
	0.999	14.5 ± 0.6	135.8 ± 7.3
	0.997	15.0 ± 4.0	135.7 ± 44.1
Poplar-Control	0.998	18.3 ± 4.7	165.0 ± 50.6
	0.998	15.2 ± 3.0	128.7 ± 31.3
	0.999	16.5 ± 2.1	158.6 ± 24.5
	0.999	16.8 ± 2.3	143.8 ± 24.2
	0.999	17.5 ± 2.8	144.7 ± 28.6
Pine-PMDI	0.999	21.9 ± 3.4	193.9 ± 34.6
	0.998	19.1 ± 4.1	167.7 ± 42.5
	0.999	23.6 ± 5.2	211.9 ± 53.5
	0.999	24.5 ± 1.8	223.6 ± 18.2
	0.999	15.0 ± 0.9	136.2 ± 9.6
Poplar-PMDI	0.999	16.0 ± 1.9	120.8 ± 18.2
	0.999	19.0 ± 1.9	153.0 ± 18.1
	0.998	16.7 ± 1.8	130.3 ± 17.1
	0.999	19.0 ±1.9	154.3 ± 18.2
	0.99	14.2 ± 2.0	108.8 ± 19.3